

# Development of Dissipative Out-of-Equilibrium Materials from Direct Chemical Reaction Cycles

Benedikt Rieß

Vollständiger Abdruck der von der Fakultät für Chemie der Technischen Universität München zur Erlangung des akademischen Grades eines

Doktors der Naturwissenschaften (Dr. rer. nat.)

genehmigten Dissertation.

Vorsitzende: Prof. Dr. Kathrin Lang  
Prüfer der Dissertation: 1. Prof. Dr. Job Boekhoven  
2. Prof. Dr. Angela Casini

Die Dissertation wurde am 27.04.2020 bei der Technischen Universität München eingereicht und durch die Fakultät für Chemie am 09.06.2020 angenommen.



*„We have to confront young students with the frontiers of science and knowledge. And I think you need a playground there to go in unknown territory. Not to be guided too much along the paths we already know. Please! Please! Let universities be a playground for the youth to be creative and let them use their brains and creativity. That will move us forward. .... I treat my students like real talents. They are probably smarter than I am. And I always tell them use your opportunities..... I give my students a lot of freedom, because they are so talented. And I have to encourage them and make them enthusiastic. And then, they will use that university playground with all the beauty you can find there.“*

**Prof. Dr. Ben Feringa**

Interview from the Nobel Banquet on the 10<sup>th</sup> of December 2016

*„Wir müssen junge Studenten mit den Grenzen der Wissenschaft und des Wissens in Berührung bringen. Und ich glaube, man braucht dort einen Spielplatz, um in unbekanntes Gebiet zu vorzudringen. Um nicht zu sehr auf die Wege geführt zu werden, die wir bereits kennen. Bitte! Ich bitte Sie! Lassen Sie die Universitäten eine Spielwiese für die Jugend sein, damit sie kreativ sein können und ihren Verstand und ihre Kreativität nutzen können. Das wird uns vorwärtsbringen. .... Ich behandle meine Studenten wie echte Talente. Sie sind wahrscheinlich klüger als ich. Und ich sage ihnen immer, dass sie ihre Chancen nutzen sollen..... Ich gebe meinen Schülern viel Freiheit, weil sie so talentiert sind. Und ich muss sie ermutigen und sie begeistern. Und dann werden sie diesen Universitätsspielplatz mit all der Schönheit nutzen, die man dort finden kann.“*

**Prof. Dr. Ben Feringa**

Interview vom Nobelpreis Bankett am 10. Dezember 2016

## Abstract

Man-made assemblies exist in- or close to equilibrium. In comparison, biological assemblies exist out-of-equilibrium driven, by constant energy dissipation. To adopt unique properties, like the ability to self-heal or to be controlled in space and time, the dissipative nature of biological assemblies has to be implemented into man-made assemblies, leading to a new class of materials. The aim of thesis is design and study a chemical reaction cycle, which is driven by the consumption of a chemical fuel. This chemical reaction cycle converts a precursor into its corresponding product, which is able to self-assemble into a dissipative supramolecular assembly.

The thesis starts with a short introduction to the field of supramolecular assemblies. Chapter 2 I will give design strategies to construct chemical reaction cycles either driven by chemical fuels or light. The following Chapter 3, couples these artificial reaction cycles to assemblies. I will discuss in detail three different strategies, which can form dissipative assemblies, the abolishment of charges, the combination of two non-assembling precursors, and the conformational change of the precursor.

In the first experimental chapter, *i.e.* Chapter 4, I describe a chemical reaction cycle based on short peptides or amino acids driven by hydrolysis of carbodiimides. This versatile reaction cycle leads to dissipative assemblies, for example, colloids or fiber-forming hydrogels, which can be controlled in space and time and are reusable. The assembled colloids can encapsulate hydrophobic dyes, which could lead to a potential application for drug delivery. With our quantitative understanding of the chemical reaction cycle, we explored the feedback of the colloids on the kinetics of their chemical reaction cycle. Such feedback is crucial for the design of assemblies with biological properties, like oscillations or pattern formation. With this system, we found conditions to tune and also completely switch of this feedback.

After a concluding chapter, I finish the thesis with a list of publications and the reprint of two review articles on the top of dissipative assemblies.

## Zusammenfassung

Von Menschen geschaffene zusammengelagerte Strukturen existieren im oder nahe dem Gleichgewicht. Im Vergleich dazu, existieren biologische Assemblierungen außerhalb des Gleichgewichts, wobei sie kontinuierlich Energie verbrauchen. Um die einzigartigen Eigenschaften, wie die Fähigkeit zur Selbstheilung oder die zeitliche und örtliche Kontrolle, auf künstliche Assemblierungen zu übertragen, muss die dissipative Natur biologischer Baugruppen implementiert werden. Dies führt zu einer neuen Klasse von Materialien. Das Ziel der Arbeit ist die Entwicklung und Untersuchung eines chemischen Reaktionszyklus, der durch den Verbrauch eines chemischen Treibstoffs angetrieben wird. Dieser chemische Reaktionszyklus wandelt einen Präkursor in sein entsprechendes Produkt um, welches in der Lage ist sich zu einer dissipativen, supramolekularen Struktur zusammen zu lagern.

Die Arbeit beginnt mit einer kurzen Einführung in das Gebiet der supramolekularen Assemblierungen. In Kapitel 2 werden Entwurfsstrategien zur Konstruktion chemischer Reaktionskreisläufe gegeben, die entweder durch chemische Brennstoffe oder durch Licht angetrieben werden. Im darauffolgende Kapitel 3, zeige ich auf wie diese Zyklen zu gewünschten Assemblierungen führen können. Ich werde drei verschiedene Strategien im Detail besprechen, die dissipative Assemblierungen bilden können, die Aufhebung von Ladungen, die Kombination von zwei nicht-assemblierenden Bausteinen und die Konformationsänderung des Präkursors.

Im ersten experimentellen Kapitel, d.h. in Kapitel 4, beschreibe ich einen chemischen Reaktionszyklus, der auf kurzen Peptiden oder Aminosäuren basiert und durch die Hydrolyse von Carbodiimiden angetrieben wird. Dieser vielseitige Reaktionszyklus führt zu dissipativen Zusammensetzungen, z.B. Kolloiden oder faserbildenden Hydrogelen, die räumlich und zeitlich kontrolliert werden können und wiederverwendbar sind. Die zusammengelagerten Kolloide können hydrophobe Farbstoffe einkapseln, was zu einer potenziellen Anwendung für die Abgabe von

Medikamenten führen könnte. Mit unserem quantitativen Verständnis des chemischen Reaktionszyklus, haben wir die Rückkopplung der Kolloide auf die Kinetik ihres chemischen Reaktionszyklus untersucht. Eine solche Rückkopplung ist entscheidend für die Gestaltung von Baugruppen mit biologischen Eigenschaften, wie Oszillationen oder Musterbildung. Mit diesem System haben wir Bedingungen gefunden, um diese Rückkopplung einzustellen oder gar vollständig auszuschalten.

Nach einem abschließenden Kapitel schließe ich die Arbeit mit einer Liste der Veröffentlichungen und dem Nachdruck von zwei Übersichtsartikeln über dissipative Assemblierungen ab.

## Abbreviations

ADP	Adenosine diphosphate
ATP	Adenosine triphosphate
CMC	N-Cyclohexyl-N'-(2-morpholinoethyl)carbodiimide
CRC	Chemical reaction cycle
DIC	diisopropylcarbodiimide
DSA	Dissipative self-assembly
EDC	1-Ethyl-3-(3-dimethylaminopropyl)carbodiimide
Fmoc	Fluorenylmethyloxycarbonyl protecting group
P <sub>i</sub>	inorganic phosphor
PKA	protein
γPP	γ-protein phosphatase
MES	2-(N-morpholino)ethanesulfonic acid

---

1. Design of Chemical Reaction Cycles .....	1
1.1 Self-Assembly In- and Out-of-Equilibrium .....	2
1.1.1 Thermodynamics of In- and Out-of-Equilibrium Self-Assembly.....	2
1.1.2 Dissipative Out-of-Equilibrium Self-Assembly of Actin.....	3
1.2 Minimal requirements of chemical reaction cycles for dissipative out-of-equilibrium assemblies .....	5
1.3 Examples of Artificial Chemical Reaction Cycles .....	7
1.3.1 Chemical Reaction Cycles Driven by the Hydrolysis of Fuels .....	7
1.3.2 Chemical Reaction Cycles Driven by the Reduction of Oxidizing Agents.....	10
1.3.3 Light Driven Chemical Reaction Cycles .....	11
1.4 Conclusion and Outlook.....	14
2. Strategies for Coupling Reaction Cycles to Self-Assembly of Molecules.....	16
2.1 Three Strategies to Couple Chemical Reaction Cycles to Dissipative Materials .....	17
2.2 Fuel-Driven Decrease of Electrostatic Repulsion Between Molecules .....	19
2.3 Fuel Driven Combination of Two Non-Assembling Segments.....	22
2.4 Fuel Driven Conformational Change to Induce Self-Assembly .....	24
2.5 Conclusion and Outlook.....	27
3. Aim of the Thesis .....	28
4. Non-equilibrium dissipative supramolecular materials with a tunable lifetime .....	30
5. Dissipative Assemblies that Inhibit Their Deactivation .....	62
6. Conclusion and Outlook .....	81
7. Further Publications .....	83
7.1 List of publications.....	83



---

7.2	Application of Dissipative Supramolecular Materials with a Tunable Lifetime .....	85
7.3	The Design of Dissipative Molecular Assemblies Driven by Chemical Reaction Cycles .....	97
8.	Acknowledgments .....	126
9.	References .....	128

# 1. Design of Chemical Reaction Cycles

## Abstract.

In this chapter, I will give a brief introduction into the field of self-assembled materials in and out-of-equilibrium, how these materials are formed and what are the minimal requirements for man-made supramolecular materials in and out-of-equilibrium. I will end this section with recent examples of man-made chemical reaction cycles driven by the catalyzed hydrolysis of a chemical fuel by the reduction of an oxidizing agent or light.

Parts of this chapter are based on the ideas published in the following manuscripts:

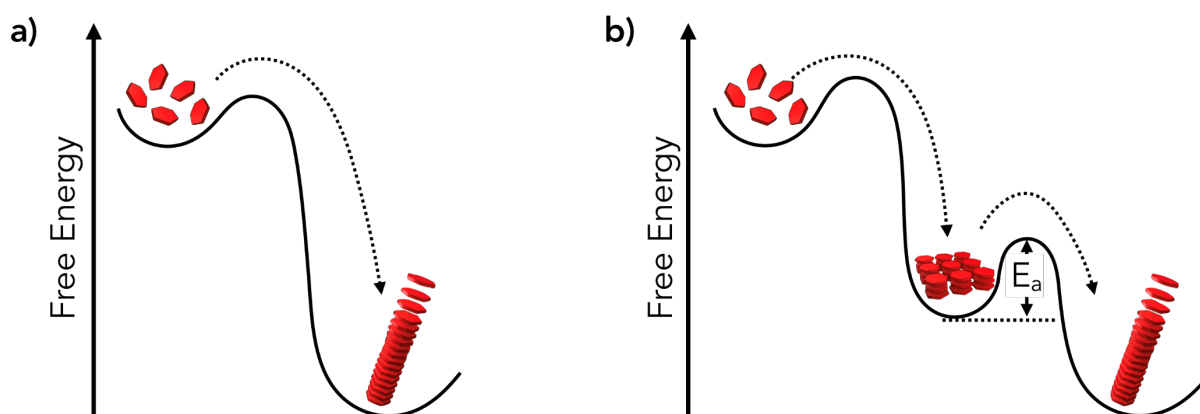
1. **B. Rieß\***; R. K. Grötsch\*; J. Boekhoven, *The Design of Dissipative Molecular Assemblies Driven by Chemical Reaction Cycles*. *Chem* **2019** doi: 10.1016/j.chempr.2019.11.008
2. **B. Rieß**; J. Boekhoven, *Applications of Dissipative Supramolecular Materials with a Tunable Lifetime*. *ChemNanoMat* **2018**, 4 (8), 710-719

## 1.1 Self-Assembly In- and Out-of-Equilibrium

### 1.1.1 Thermodynamics of In- and Out-of-Equilibrium Self-Assembly

Molecules are able to assemble into larger structures driven by non-covalent interactions, like hydrogen bonding, van der Waals interactions,  $\pi$ -Orbital overlap, as well as others.<sup>1-2</sup> From a thermodynamic point of view, these assemblies can be classified in three major categories, in-, out- and dissipative out-of-equilibrium self-assemblies<sup>3-4</sup>.

The first group are assemblies that exist in-equilibrium. This category is the most explored of the three and can result in various structures like fibers<sup>5-8</sup>, tubes<sup>9-12</sup>, weaves<sup>13</sup> or vesicles.<sup>14-15</sup> Some of these assemblies can already be found in everybody's everyday life, for example, liquid crystals in LC-Displays<sup>16-19</sup>, as drug delivery platform with supramolecular vesicles<sup>20</sup> or as peptide assemblies for regenerative medicine.<sup>21-22</sup> In these materials, energy is gained by the self-assembly process as the self-assembled material is in a global minimum on the thermodynamic energy landscape and so thermodynamically more favored (Figure 1 a). The self-assembled structure can exchange building blocks with the surrounding media. In other words, building blocks can leave the assembly and can be replaced immediately by ones from solution, but at equal rates. This means, there is no net flow of energy and matter taking place.<sup>23</sup> Consequently, these assemblies are stable, i.e., over time,



**Figure 1:** Scheme of free energy landscapes of a) *In-equilibrium self-assembly* b) *Out-of-equilibrium self-assembly*

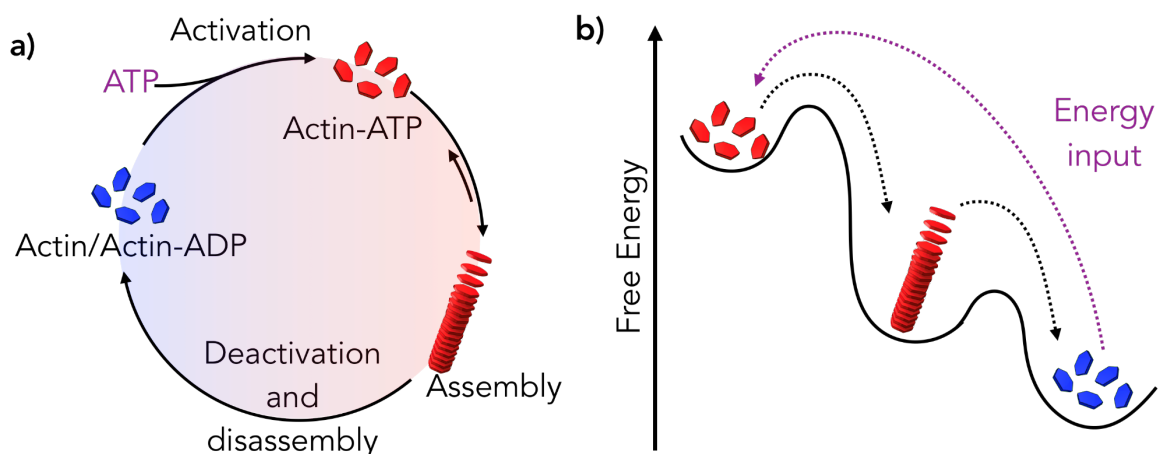
their properties will not change. Because of the exchange, the structures can be changed with an external stimuli like change in pH or solvent change.

In contrast to the in-equilibrium assemblies, the energy state of assemblies out-of-equilibrium does not exist in a global but in a local energy minimum (Figure 1 b).<sup>3, 24</sup> The system, therefore, tries to find the optimal configuration to find the thermodynamically more favored state. In other words, the assemblies are not in equilibrium, as there is a net exchange of matter and energy between the assembly and the rest of the system. Depending on the energy ( $E_a$ ) to overcome this barrier towards a surrounding lower minimum, two scenarios are possible. The energy  $E_a$  can be lower or in the same range than the thermal energy available in the system ( $k_bT$ , Boltzmann constant ( $k_b$ ), and temperature ( $T$ )). In this state, building blocks can leave the assembled state towards the thermodynamically more favored state. This state is called metastable, and the assemblies have a finite lifetime.<sup>25</sup> Compare to in-equilibrium assemblies, the exchange is relatively slow, as the noncovalent interactions are stronger.<sup>26</sup> The energy  $E_a$  can be higher than the thermal energy available, and an exchange of matter and energy is not possible. On experimental timescales, the so-called kinetically trapped assemblies have an infinite lifetime.<sup>3</sup> This kind of assembled-structures can be transferred into a metastable out-of-equilibrium structure by an external energy source, like heat or sonication.<sup>25, 27-28</sup> In the next subsection, I will compare biological out-of-equilibrium materials and discuss the missing third category of man-made self-assembled structures.

### 1.1.2 Dissipative Out-of-Equilibrium Self-Assembly of Actin

In-equilibrium, kinetically trapped, and metastable systems, described in the subsection before, can form the same type of structures like biological materials, which do not exist in or close to equilibrium. However, man-made supramolecular materials lack properties such as adaptivity or self-healing. A further drawback is that they cannot be controlled in space and time. Therefore, supramolecular chemists were highly inspired by the actin network of the cytoskeletal network, which self-assembles

driven by the hydrolysis of ATP to ADP as waste product.<sup>29</sup> The structure of the cell wall, cell locomotion and other functions of the cell are controlled by the actin network.<sup>30</sup> The assembly and disassembly of actin subunits do not occur spontaneously but is driven by a chemical reaction cycle. Each actin subunit can bind one molecule of ATP forming actin-ATP, which can self-assemble with other ATP-bound actin subunits to assemble in a head-to-tail fashion to form a fibril. In the assembled state, ATP-bound actin is autocatalytically converted to actin-ADP and  $P_i$  as waste, which has a lower binding constant compared to ATP-bound actin. Due to the loss in the binding constant, the ADP-bound actin disassembles. As long as ATP is present, ADP of the ADP-bound actin can be replaced by another ATP molecule. The binding constant is, therefore increased again, and actin-ATP can undergo the self-assembly process again. This also means that the building blocks are recycled and can be used for the same or different purposes. The assembly process of actin subunits is controlled by kinetics than by thermodynamics, which allows the cell to adapt the cytoskeleton network rapidly to internal or external stimuli. When the system is running low on ATP, the self-assembled structure will fall apart. This whole process is called dissipative self-assembly and can be schematically represented as reaction cycle (Figure 2 a).<sup>31</sup>



**Figure 2:** Comparison of actin polymerization and dissipative self-assembly. a) *Reaction cycle of the polymerization.* b) *Scheme of the free energy landscape of dissipative out-of-equilibrium assemblies.*

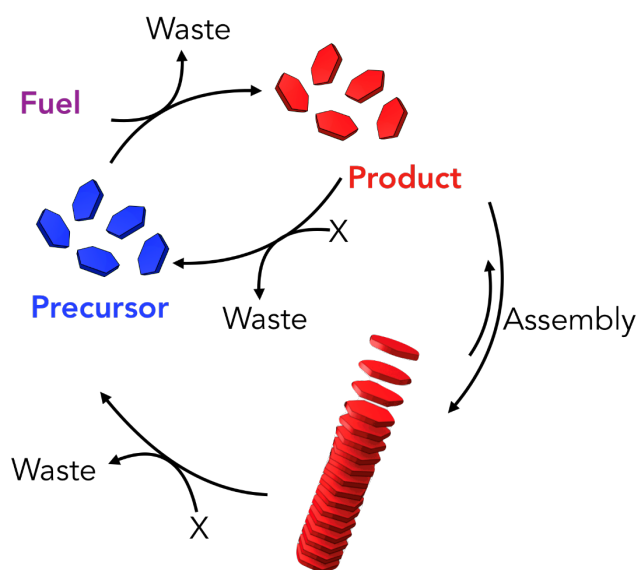
Inspired by this beautiful example of dissipative self-assembly of actin into fibrils by the consumption of fuel, artificial dissipative assemblies were designed. The free energy landscapes of dissipative out-of-equilibrium assemblies is different from the ones of in-equilibrium or non-dissipative out-of-equilibrium self-assembly (Figure 2 b).<sup>4, 32-36</sup> The precursor resides in a thermodynamic minimum and can be activated by a high energy molecule, in the actin example, ATP. In the following sections, I will explain in detail which artificial high energy molecules can be used to fuel man-made chemical reaction cycles. The product formed by the activation reaction, has a higher free energy than the starting state. The system gains free energy by the self-assembly process, and this state is lower in energy, representing a local minimum in the free energy landscape. The deactivation reaction converts the product back to the precursor and brings so the system back to its starting free energy. The deactivation reaction, the autocatalytic hydrolysis of ATP in actin-ATP to actin-ADP, brings the system back to its starting free energy. As long as fuel is present, the precursor can be reactivated by the fuel and undergo the described energy pathway again. The complete system comes back to the global energy minimum when all fuel is hydrolyzed to the corresponding waste product. This process can be restarted by the addition of a new batch of fuel. In the next chapter, I will explain how this theoretical understanding lead to man-made chemical reaction cycles and what minimal requirements are need for the design.

## **1.2 Minimal requirements of chemical reaction cycles for dissipative out-of-equilibrium assemblies**

The understanding of the chemical reaction cycle of actin and also tubulin polymerization<sup>37-38</sup>, raises the question can scientist engineer similar reaction cycles, which lead to man-made dissipative assemblies with exciting properties, like self-healing or the ability to be controlled in space and time? The challenge is to find suitable precursors, which are converted into the metastable product driven by the

addition of a high energy molecule. The product has to be able to self-assemble into the desired structure. The energy barrier from the assembled state to the precursor state has to be lower or in the same range of the free energy of the system (Figure 2b). Otherwise, the assembly is kinetically trapped and will not disassemble.

The chemical reaction cycle comprises at least two chemical reactions, *i.e.*, the activation of the precursor and deactivation of the product. These two reactions regulate the concentrations of the precursor and product. The chemical reaction cycle is driven by an energy source, which can either be a chemical fuel or light (Figure 3). In the activation reaction, the energy source is consumed irreversibly. Chemically fueled reaction cycles are effective catalytic reaction cycles, which means the conversion of fuel to waste is faster than without a reaction cycle present.<sup>32, 39-44</sup> The activation reaction leads to the production of a waste product or to the generation of heat. The deactivation reaction closes the cycle and is, in contrast, a spontaneous reaction. The deactivation reaction happens by a reaction of the product in solvent or by solvolysis and reverts the product to the precursor. By bringing both reactions together, the product is per definition metastable, and its half-life is defined by the rate constant of deactivation. The concentration of the product is regulated by both



**Figure 3:** Scheme of an energy-dissipating chemical reaction cycle driven by chemical fuels.

the activation and deactivation reaction. After the fuel is completely consumed and all product has been deactivated, the only difference between the starting point of the experiment and the end of the cycle is the generation of a waste molecule. In other words, the driving force of the chemical reaction cycles is the conversion of fuel into the corresponding waste. This fact makes the design of artificial chemical reaction cycles even more complicated because the reaction of fuel to waste without precursor has to be drastically slower compared to the reaction of the precursor with fuel to the product and waste. Supramolecular chemists have overcome these challenges by designing artificial chemical reaction cycles. I will give examples for different fuel-driven chemical reaction cycles in the next section.

### 1.3 Examples of Artificial Chemical Reaction Cycles

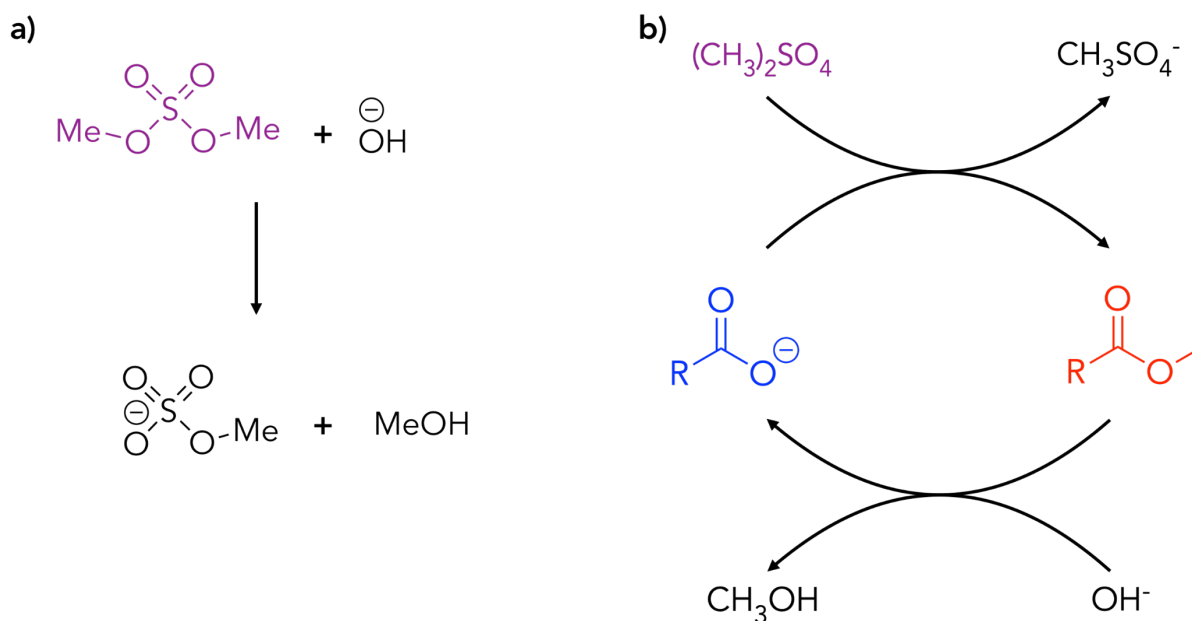
In this section, I will give various examples of chemical reaction cycles driven either by chemical fuels or by light. All these reaction cycles fulfill the basic requirements of the section above. In other words, each cycle I will describe contains an energy-driven activation reaction and a spontaneous deactivation reaction. In most cases, the transient product that is formed can self-assemble. The design rules and challenges associated with the assembly are described in section 2. The reaction cycles driven by chemical fuels can be divided into two classes. The first subclass is driven by the hydrolysis of the fuel to waste. For the second one, the energy to drive the chemical reaction cycle is gained from the reduction of a reducing agent. The section closes with examples of light-driven chemical reaction cycles, which produce heat as waste.

#### 1.3.1 Chemical Reaction Cycles Driven by the Hydrolysis of Fuels

One of the pioneering works on chemical reaction cycles, driven by the hydrolysis of the fuel to the corresponding waste product, was designed by van Esch, Eelkema and co-workers.<sup>45-46</sup> In this work, methylating agents like such as methyl iodide or dimethyl sulfate were used as fuel. The energy for the chemical reaction cycle was produced



by the reaction of a molecule of dimethyl sulfate with a hydroxy ion (net reaction of fuel to waste, Figure 4a) to generate methanol and methyl bisulfate as waste. Under their working conditions and in the absence of the precursor, the degradation of fuel to waste is very slow, and the fuel has a half-life of 41 minutes. Under the same conditions but with precursor present, the reaction rate dramatically increases. The rate increases by a factor of 2.5, if a precursor is present, which forms a metastable ester-based product. The well-soluble carboxylate precursor reacts in the activation reaction with dimethyl sulfate forming its corresponding metastable methyl ester and a waste molecule, methyl bisulfate (Figure 4 b). In the deactivation reaction, the product reacts with a hydroxide ion to form the original precursor and releasing methanol, as a second waste product. As the transient product is able to self-assemble into fibers, the chemical reaction cycle yields a dissipative hydrogel. I will discuss the exact properties and design strategies in Chapter 2. This specific chemical reaction cycle is highly pH dependent, which allows a fine-tuning of the reaction rates of the hydrolysis reaction. But this chemical reaction cycle shows also some drawbacks. For example, the fuel, dimethyl sulfate, is toxic for living organisms, because it can methylate parts of the DNA. Therefore, the chemical reaction cycle cannot be used for biological or medical materials. The reaction rates are also slow compared to examples of dissipative out-of-equilibrium materials from biology.

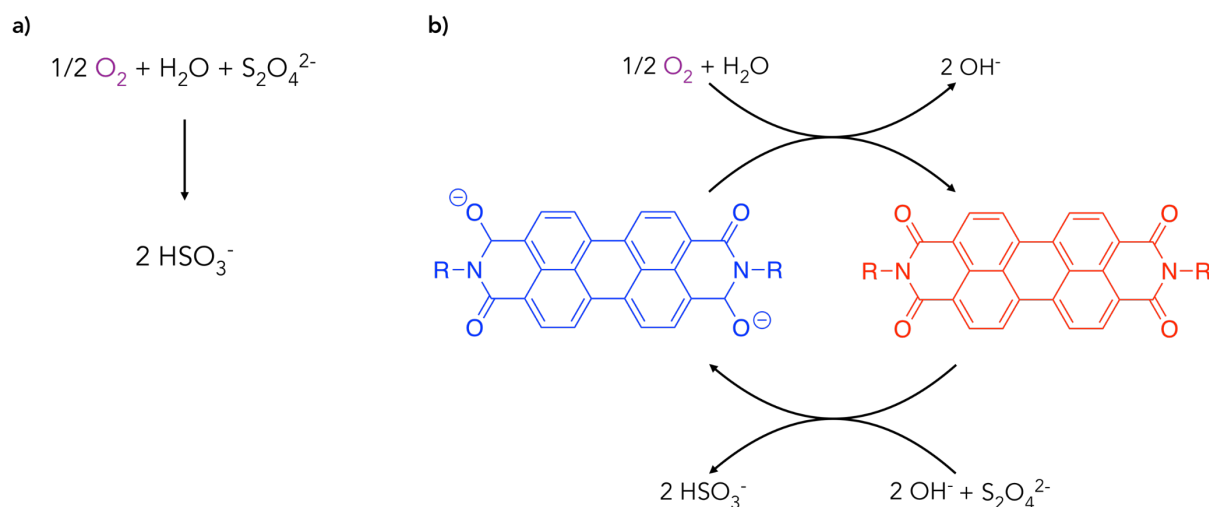


**Figure 4:** Chemical reaction cycle driven by the hydrolysis of dimethyl sulfide a) The energy is gained from the reaction of fuel with hydroxy ions from solution. b) Increased hydrolysis of the fuel by the chemical reaction cycle.

In biology, ATP is frequently used as an energy source.<sup>47-48</sup> Also, there are countless examples of enzymes driven by the hydrolysis of ATP to ADP or AMP, which convert different precursors to their corresponding products, like helicase, ATPase domains on dynein and DNase.<sup>49-51</sup> Based on this variety, new man-made chemical ATP-driven chemical reaction cycles can be designed. For example, Hermans and co-worker designed a chemical reaction cycle, that transiently phosphorylates the side chain of serine by the protein kinase A (PKA) with the energy of the hydrolysis of ATP to ADP.<sup>52</sup> The phosphorylated peptide sequence (LRRASL) is metastable as the second enzyme  $\gamma$ -protein phosphatase ( $\gamma$ -PP) removes the phosphate group. The inorganic phosphate, generated by the deactivation reaction, is a potent inhibitor of the enzyme  $\gamma$ -PP. In other words, the chemical reaction cycle can just be refueled once, because the waste accumulation is slowing down or even completely inhibiting the deactivation reaction. To overcome this downside, the authors designed a new setup with a membrane, allowing constant addition of fuel and removal of the waste.

### 1.3.2 Chemical Reaction Cycles Driven by the Reduction of Oxidizing Agents

Besides the Chemical reaction cycles driven by the hydrolysis of fuel, chemical reaction cycles based on carefully balancing redox chemistry have been explored. In this strategy, oxidizing agents are used as chemical fuels in reducing environments, which results in the reduction of these agents. In a recent example, the Hermans group designed a chemical reaction cycle, which is driven by the oxidation of dithionite ions into hydrogen sulfite by oxygen (Figure 5).<sup>53</sup> A perylene diimide derivative (PDI<sup>2-</sup>) was oxidized in the activation reaction by oxygen from the surrounding air to form the product (PDI). In the presence of dithionite, the deactivation reaction reverts PDI to the precursor state, while releasing hydrogen sulfite as waste. The net equation of the redox reaction between oxygen and dithionite yields two molecules of hydrogen sulfite and leads to the transient activation of the precursor (Figure 5b). The properties of the material formed by this chemical reaction cycle will be discussed in section 2.



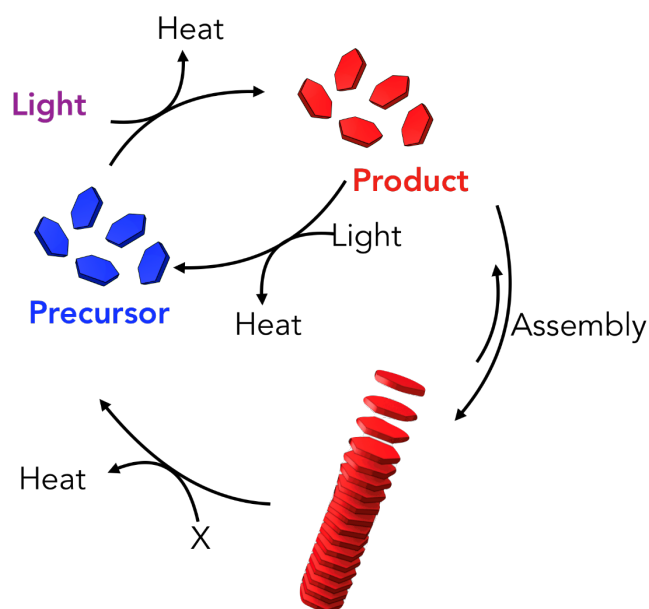
**Figure 5:** Chemical reaction cycle driven by the oxidation of dithionite a) The net reaction of the redox reaction, which drives the chemical reaction cycle. b) The uncharged product is formed by the oxidation of the precursor.

In the recent work of Fletcher and co-workers, two non-assembling precursors are combined in a chemical reaction cycle to form a transient amphiphilic product. The energy to drive this chemical reaction cycle was harvested by the oxidation of two thiol derivatives into their corresponding disulfide by the fuel hydrogen peroxide.<sup>54</sup> In

the activation reaction, the product is formed by the precursor, 2-nitro-5-sulfidobenzoate, and 1-octanethiol in a two-step reaction. The disulfide product is deactivated in a second thiol-disulfide exchange into the precursor, while simultaneously, the waste product, octyl disulfide, is formed. The net equation of the redox reaction between one molecule of hydrogen peroxide and two molecules of 1-octanethiol leading to the corresponding disulfide and water is the driving force of the chemical reaction cycle. The self-assembling of the transient product and the unique characteristics of this particular chemical reaction cycle will be discussed in section 2.

### 1.3.3 Light Driven Chemical Reaction Cycles

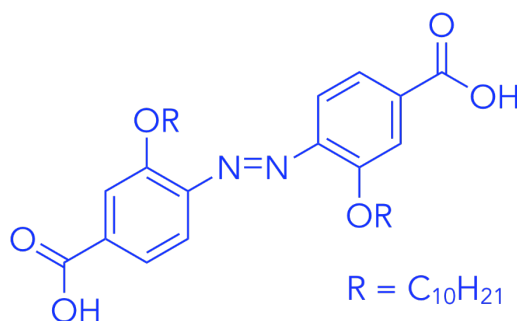
Besides using high energy molecules, the energy source for man-made chemical reaction cycle can also come from the absorption of light.<sup>55-58</sup> The precursor gets activated by absorbing a photon and can, therefore, undergo a photochemical reaction, for example, photoisomerization (Figure 6).<sup>59-61</sup>



**Figure 6:** General scheme of a light driven chemical reaction cycle: The precursor is activated by light to form a metastable product, which can either be deactivated, spontaneously or by another light source, or is able to self-assemble into a nanostructure.

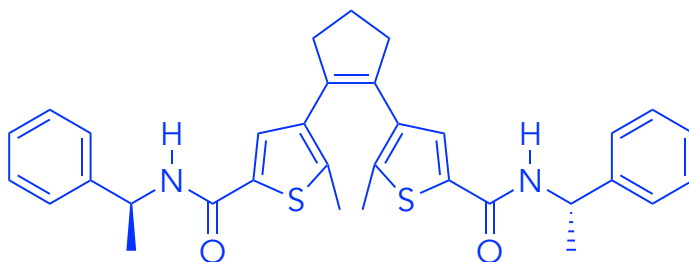
The deactivation reaction of the product back to the precursor typically occurs spontaneously or by the adsorption of a second photon. In comparison to the chemical fueled chemical reaction cycle, the light-driven reaction cycles show two differences. One, the light-driven chemical reaction cycles do not produce a waste molecule. This fact can be a major advantage, as the chemical fueled reaction cycles can be poisoned by the accumulation of waste products. Second, light-driven reaction cycles are not catalytic reaction cycles as chemical fueled ones are. In other words, the conversion of the energy of a photon into heat occurs at the same rates if a precursor is present or not.

In an early example by Sleiman and co-workers azobenzene derivatives were used in a chemical reaction cycle.<sup>55</sup> Upon UV-light irradiation, the precursor (Figure 7) is able to photo-isomerize from its thermodynamically favored *trans*- to its *cis*-conformation. This state is thermodynamically not favored and will, therefore, lead to a spontaneous back isomerization to the *trans*-state. Both the precursor and the product are able to self-assemble. The *trans*-conformation of the precursor is leading to linear tapes, which can subsequently organize into larger ordered structures. Upon continuous irradiation of the sample, a morphological transition takes place, where the product is formed, and cyclic structures are formed. After the light irradiation is stopped, the cycle reverts back to the original precursor state.



**Figure 7:** Azobenzene derivate, which can undergo a photoisomerization reaction upon UV-light irradiation.

In another example of light-driven reaction cycle by van Esch and co-workers diarylethene based molecular switches are used as precursors (Figure 8).<sup>62</sup> In the precursor state, the molecule is relatively flexible, soluble in toluene, and barriers an open ring motive. After irradiation with UV-light of 313 nm a ring closure reaction takes place, and therefore the molecule is more rigid.<sup>63-64</sup> The product is able to self-assemble into fibers due to hydrogen bonding between the amide groups and decreased solubility due to the increased rigidity. The deactivation reaction takes place by irradiation of the sample with green light of 520 nm. Irradiating the sample with both wavelengths, the light-driven chemical reaction cycles takes place. In other words, the molecular switch is converted to the product back and forth.



**Figure 8:** Diarylethene based molecular switch, which can undergo a ring closure reaction upon irradiation with UV-light of 313 nm.

## 1.4 Conclusion and Outlook

Over the past years, the field of dissipative out-of-equilibrium self-assembled materials has gained much attention because of their unique properties like the ability to self-heal. Supramolecular chemists were able to adopt the biological principles to artificial chemical reaction cycles, which led to an impressive number of man-made catalytic reaction cycles, as shown in this section. The accumulation of waste materials is still a big problem because it can interfere with the cycle or completely inhibits one of the reactions. This problem has to be overcome, not just theoretically but also experimentally, to design and create man-made dissipative out-of-equilibrium materials with unique properties. Possible ways to overcome that problem could be that the waste molecule is not interfering at all with the chemistry, somehow reactivated to form a new molecule of fuel or that the waste is precipitating out or leaving the sample as gas. It is also conceivable that computer-based discovery helps in the future to overcome this problem. This method could also lead to new reaction cycles based on completely new activation or deactivation reactions.<sup>65-66</sup> The deactivation of most chemical reaction cycles reported so far is based on the metastability of the product in its surrounding media. This fact makes it very complicated to tune the rate of this reaction. This can be overcome by implementing an enzyme or chemical driven deactivation reaction, which is not interfering with the activation reaction.<sup>39</sup> Besides these facts, fuels used so far are toxic to living organisms, which makes the assembled material unsuitable for the application as biomaterials, like transiently covering of wounds. Enzyme driven chemical reaction cycles have the downside that they are hard to analyze with typical analytical methods like HPLC. The kinetic rates of the reaction of these chemical reaction cycles can, therefore, also not be extracted that easily, which makes it hard to set up a mathematic model to predict the outcome, like the lifetime or half-life of the product, of these cycles. Another downside of the reported examples is that the chemical reaction cycles are relatively slow, which means the assembled materials have relative long

lifetimes, and the exchange of material in the assembly is also slow compared to the biological. This downside prevents most unique properties, like self-healing or self-division, because the system cannot adjust the assembly fast enough to overcome the external stress onto the assembly. To overcome this, downside the kinetics of the chemical reaction cycle have to be tuned to be much faster. Theoretical calculations have already shown that oil droplets can spontaneously self-divide if the chemical fluxes of the building blocks are fast enough and carefully balanced.<sup>67</sup>



## 2. Strategies for Coupling Reaction Cycles to Self-Assembly of Molecules

### Abstract.

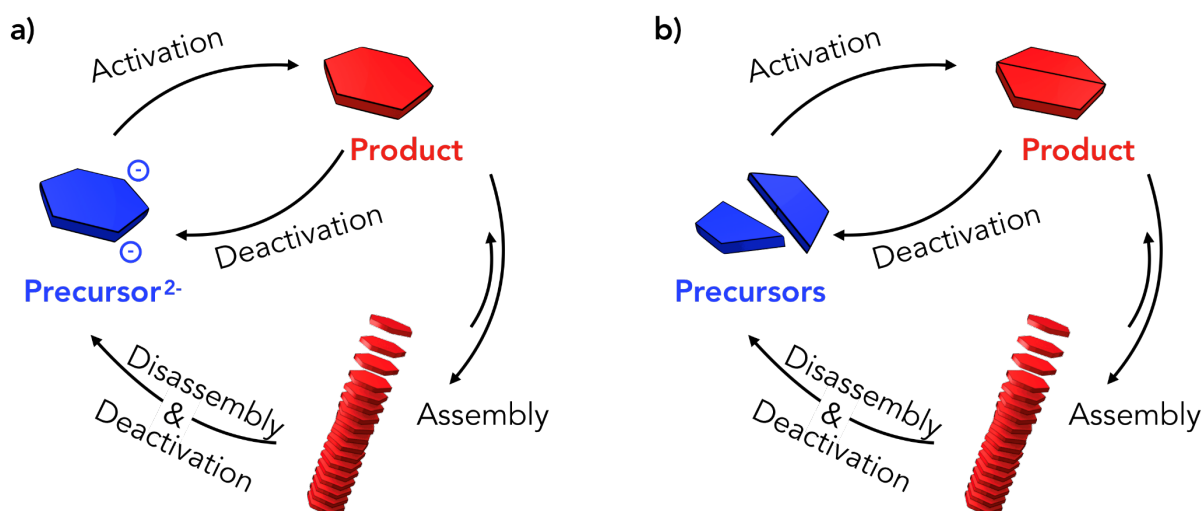
In the previous chapter, I discussed how chemical reaction cycles can be designed that harvest energy from chemical fuels or light and transform this energy into transient products. In this chapter, I will show how these energy chemical reaction cycles are used to create molecules assemblies. I have identified three different strategies. In the first strategy, the chemical reaction cycle abolishes the charges of the precursor. In these examples, the activation reactions convert the precursors to the corresponding uncharged or less charged products, which is, therefore, able to self-assemble. The second group of examples is based on the combination of two non-assembling precursors. There the activation reaction combines the two precursors to form the product, which is able to self-assemble due to intermolecular interactions. The last group consists of examples in which the precursor undergoes a conformational change. The isomerized product can self-assemble to the dissipative material, due to the increased non-covalent interactions. From these design rules, I will distill three major design rules for the precursor molecules in chemical reaction cycles.

Parts of this chapter are based on the ideas published in the following manuscripts:

1. **B. Rieß\***; R. K. Grötsch\*; J. Boekhoven, *The Design of Dissipative Molecular Assemblies Driven by Chemical Reaction Cycles*. *Chem* **2019** doi: 10.1016/j.chempr.2019.11.008
2. **B. Rieß**; J. Boekhoven, *Applications of Dissipative Supramolecular Materials with a Tunable Lifetime*. *ChemNanoMat* **2018**, 4 (8), 710-719

## 2.1 Three Strategies to Couple Chemical Reaction Cycles to Dissipative Materials

In the previous section, I described minimal requirements for chemical reaction cycles and three examples of how these cycles can be powered by different high energy molecules or light. The energy from the fuel is stored temporally in the metastable product, which is able to self-assemble. The thermodynamic minimum is reached after all fuel has been depleted and all product is hydrolyzed. In other words, all of the energy from the fuel is catalytically depleted by the chemical reaction cycle by forming the corresponding waste molecules. In this section now, I describe three main design strategies how these energy dissipating cycles can be coupled to dissipative out-of-equilibrium materials. The main goal is to find a precursor that is well-soluble and, after activation to the product, is able to self-assemble into the dissipative material. The properties of the molecular assemblies are determined by the kinetics of the reaction cycle, for example, reaction rates of the activation and deactivation reaction, which is completely different from the materials in-equilibrium, which are determined by the thermodynamics of the system, like the features of the free energy landscape or the temperature of the system.



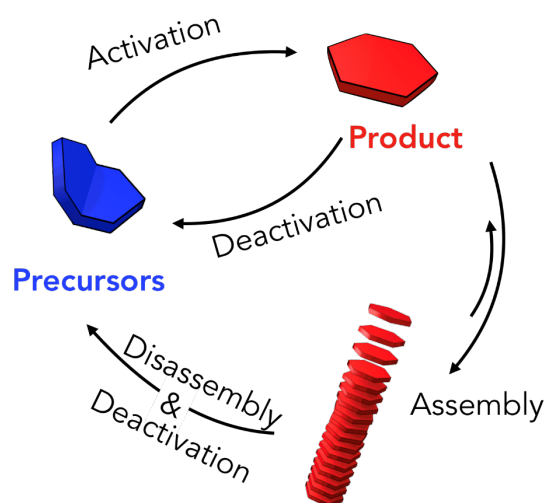
**Figure 9:** Schemes of chemical reaction cycles, where the product is able to self-assemble. a) The charged precursor gets converted into its corresponding non-charged product, which reduces electrostatic repulsions. b) Two non-assembling precursors are combined to one product by the activation reaction.

In the first strategy to design dissipative materials, the precursor is ionically charged and, therefore, well soluble in the reaction medium (Figure 9a). In other words, due to the electrostatic repulsion between the precursor molecules, the precursor is not able to self-assemble. The activation reaction converts the precursor into an uncharged or less charged product, which can subsequently undergo a self-assembly process due to the decreased electrostatic interactions.

The second strategy makes use of transiently combining two non-assembling molecules to form an assembling transient product (Figure 9b). In the activation reaction, two non-assembling precursors are combined into the transient product. That product has the ability to form more non-covalent interactions than the individual precursor components and is thus able to self-assemble.

The last strategy is based on a conformational change in the precursor molecule. The precursor is well soluble and is not able to self-assemble due to the missing intermolecular interactions (Figure 10). After activating the precursor with fuel, the precursor changes conformation, for example, from trans- to cis- configuration of a

double bond. Due to this change, the intermolecular interactions are increased, and the product is able to self-assemble.



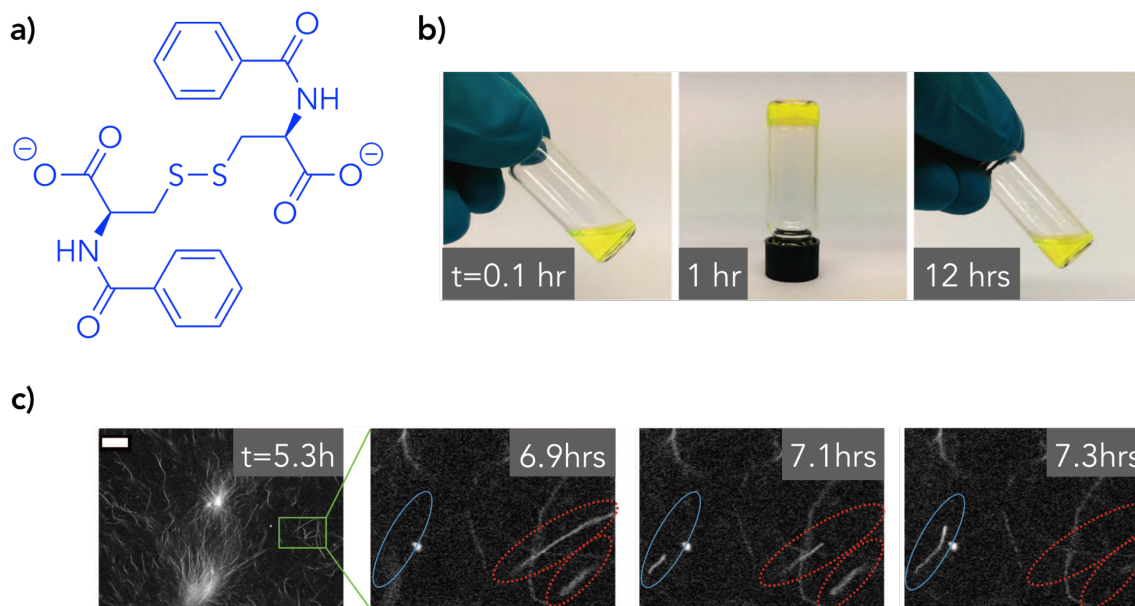
**Figure 10:** Schemes of chemical reaction cycles, where the product undergoes conformational change upon activation.

## 2.2 Fuel-Driven Decrease of Electrostatic Repulsion Between Molecules

A frequently used strategy to induce self-assembly with a chemical reaction cycle is by abolishing the charges of the precursor by the activation with chemical fuel. The activation reaction is converting a charged precursor into an uncharged or less charged product. The loss of the charges is able to induce self-assembly due to the decreased electrostatic repulsion. In the deactivation reaction, the charges of the precursor are reestablished. This strategy is relatively well explored because the design principles are similar to the pH-triggered self-assembly of molecules. Upon a change in pH the charges of a molecule are removed, for example, by protonating a carboxylate group.<sup>68-70</sup> The material can be redissolved by reverting the pH back to starting value. I have identified several examples based on the abolishing of charges by chemical reaction cycles, which will be discussed below. Even though this is a frequently applied method of inducing dissipative self-assembly, these examples are the most far away from biological examples, like the GTP-fueled

microtubules, because in biological systems, this type of dissipative material is hard to realize. It is worth mentioning, that this method has also been explored for fuel driven chemical reaction cycles which are indirectly responsible for the self-assembly of molecules. For example, a fuel-driven chemical reaction cycle can change transiently the pH of the surrounding, which induces self-assembly of the precursor.<sup>71-73</sup> In the indirect chemical reaction cycles the fuel does not react with the precursor and is thus not catalyzing the fuel conversion.

The first example of a dissipative out-of-equilibrium material I want to highlight is the hydrogel developed by van Esch, Eelkema and co-workers.<sup>45-46</sup> In this reaction cycle, the well soluble precursor dibenzoyl-L-cysteine is used as a precursor, which can self-assemble into hydrogel-forming fibers if the pH is lowered below the two pKas.<sup>74</sup> Instead of changing the pH of the environment, the authors used methylating agents to transiently decrease the charges of the precursor by forming the corresponding methyl esters (Figure 4). The product can assemble into bundles of fibers after reaching a threshold concentration. The fiber formation leads to a self-standing hydrogel, which collapses if all product is hydrolyzed to the precursor. The lifetime of the hydrogel can be tuned by kinetic parameters like the initial amount of fuel or the pH of the system. Dynamic growth and collapse of the fibers, almost like microtubule fibers, could be observed at the tips of the fibers. The constant activation and deactivation of the precursor to the product by the chemical reaction cycle as long as fuel is present in the cycle is leading to this phenomenon.



**Figure 11:** Dissipative self-assembly of dibenzoyl-L-cysteine into fibers. **a)** Molecular structure of the precursor, which is transformed into its uncharged product after methylation. **b)** Photographs of the transient formation of the hydrogel formed by the chemical reaction cycle. **c)** Confocal micrographs showing the dynamics of the assemblies (scale bar 10  $\mu\text{m}$ ).

In the second example by Hermans and co-workers, the double negatively charged perylene diimide derivate precursor ( $\text{PDI}^{2-}$ ) is oxidized to the uncharged product PDI (Figure 5).<sup>53, 75</sup> In other words, the negative charges are abolished by the activation reaction. The uncharged product is able to self-assemble into stacks, which subsequently organize side-by-side into colloids. The product is metastable due to the reducing environment, which reduces PDI back to the precursor. The lifetime of the colloids depends on the amount of fuel, in this case, the oxidizing agent, added. By a continuous supply of oxidizing and reduction agent, the system shows complex behavior, which is reflected by a periodical change of the morphology of the assemblies, caused by the different oxidation states. The self-assembly process occurs through a nucleation-elongation-fragmentation mechanism leading to a lag phase, which is then followed by an autocatalytic growth. The self-assembly process is non-linear and also the disassembly process as it is size-dependent. With low fuel amounts

continuously added to the system, steady-states with constant product-, fuel- and precursor concentrations could be obtained. An increase in the fuel flux leads to the oscillator behavior described above. By increasing the flux even further, the product precipitates out of the solution. Or in other words, the oscillatory behavior of the system was tunable by the fuel flux into the system before it collapses.

### 2.3 Fuel Driven Combination of Two Non-Assembling Segments

The second design strategy to couple reaction cycles to the self-assembly of molecules is based on chemical reaction cycles in which two soluble non-assembling precursor molecules are combined by the activation reaction.<sup>76-78</sup> The product formed by these chemical reaction cycles is then able to self-assemble into the desired structure, due to increased intermolecular interactions. After the product is deactivated and all the fuel is depleted, the material will dissipate again into the two soluble precursor molecules, which can undergo another fueling round.

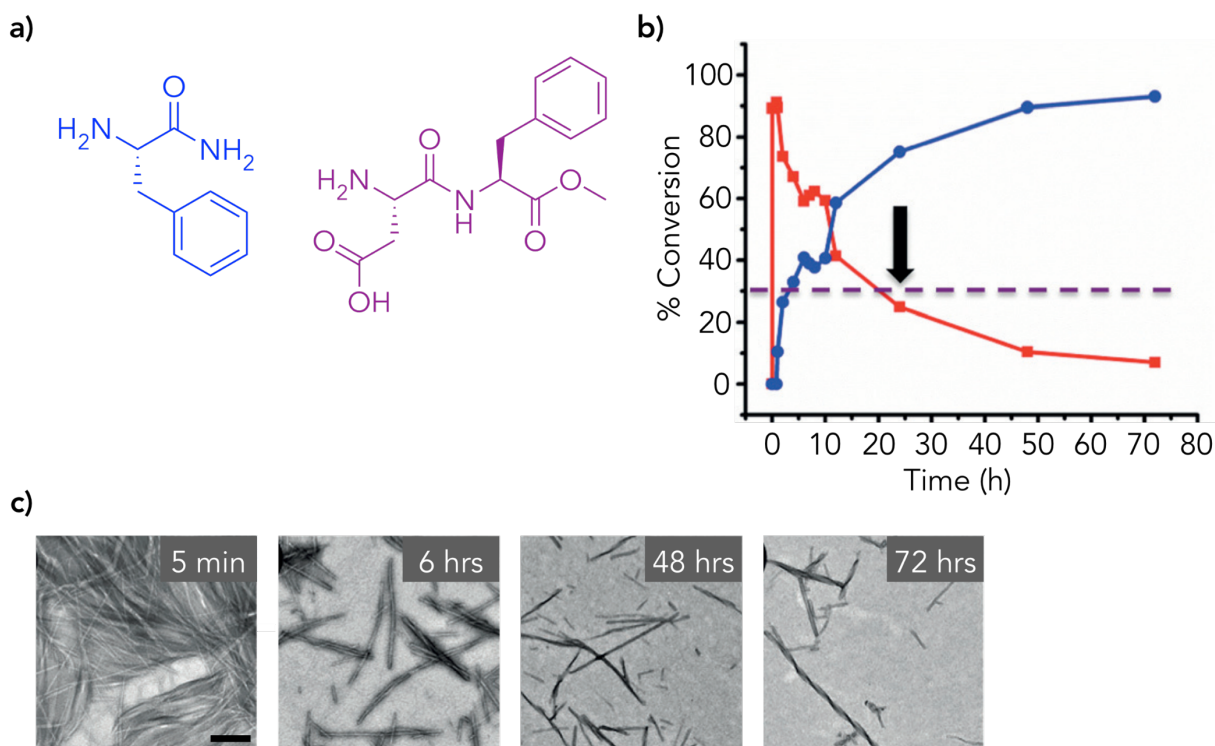
In a very nice example, Fletcher and co-workers designed a chemical reaction cycle based on the assembly of two non-assembling precursors into an amphiphilic product.<sup>54</sup> They used two thiol derivatives, which are oxidized by the added fuel, hydrogen peroxide. The disulfide product is formed out of the well-soluble precursor 2-nitro-5-sulfidobenzoate and the barely soluble second precursor 1-octanethiol into a two-step reaction. The product, with its well-soluble and less-soluble group, has an amphiphilic character. Indeed, if the product concentration exceeds 0.2 mM the disulfide product is able to self-assemble into micelles due to its amphiphilic character. In the deactivation reaction, a second thiol-disulfide exchange between the product and 1-octanethiol takes place, which reforms the precursor and octyl-disulfide as waste product. The net reaction of fuel to waste can be written as follows. Two molecules of 1-octanethiol react with hydrogen peroxide to form one molecule of waste, octyl-disulfide, and one molecule of water. The interesting feature of this chemical reaction cycle is its autocatalytic behavior, which arises under the right

circumstances from the self-assembled process. The micelles help to solubilize 1-octanthiol and therefore help to increase the rate of the activation reaction. As a consequence, the precursor concentration decreases faster, and therefore, the product is formed faster, compared to a reaction cycle without assemblies present. The design of the chemical reaction cycle is outstanding, as the assemblies and kinetics are directly influenced by each other, meaning they exert feedback on one another.

The second chemical reaction cycle example from Ulijn and co-workers is based on the combination of two water-soluble segments to form a product which is able to self-assemble into fibers, which subsequently form a hydrogel.<sup>79-80</sup> The energy to drive this chemical reaction cycle is obtained from the hydrolysis of the methyl ester of aspartame. This reaction is catalyzed by the enzyme chymotrypsin and forms aspartate as fuel and methanol as waste (Figure 10a). In the activation reaction, the N terminus of the phenylalanine amid precursor reacts with the methylated C terminus of the fuel, the peptide aspartame, to form the corresponding tripeptide (Figure 12). The tripeptide is deactivated by hydrolysis into the original precursor and demethylated aspartame as waste product. The deactivation reaction is catalyzed by the same enzyme, chymotrypsin. The tripeptide can assemble into fibers, which form a hydrogel based on the interactions in the extended peptide backbone. The maximal concentration of tripeptide is measured by HPLC after 30 minutes, but the hydrogel for this specific sample has a lifetime of 24 hours due to the slow hydrolysis of the product. The system can be refueled up to three times, with a loss in conversion of the product, due to the accumulation of waste products. Despite this fact, this



example cleverly uses just one enzyme for both the activation and deactivation reaction, which negates the need for orthogonal conditions, like buffer or pH.



**Figure 12:** Transient formation of a hydrogel driven by the hydrolysis of aspartame. a) Molecular structure of the precursor and the fuel, which are combined by the activation reaction leading to the product and methanol as waste. b) Conversion profile of the product shows transient formation of the hydrogel (curve above the dotted line). c) TEM images of the gel formed by DFF-NH<sub>2</sub> show the dissolution of the hydrogel (scale bar 500 nm).

## 2.4 Fuel Driven Conformational Change to Induce Self-Assembly

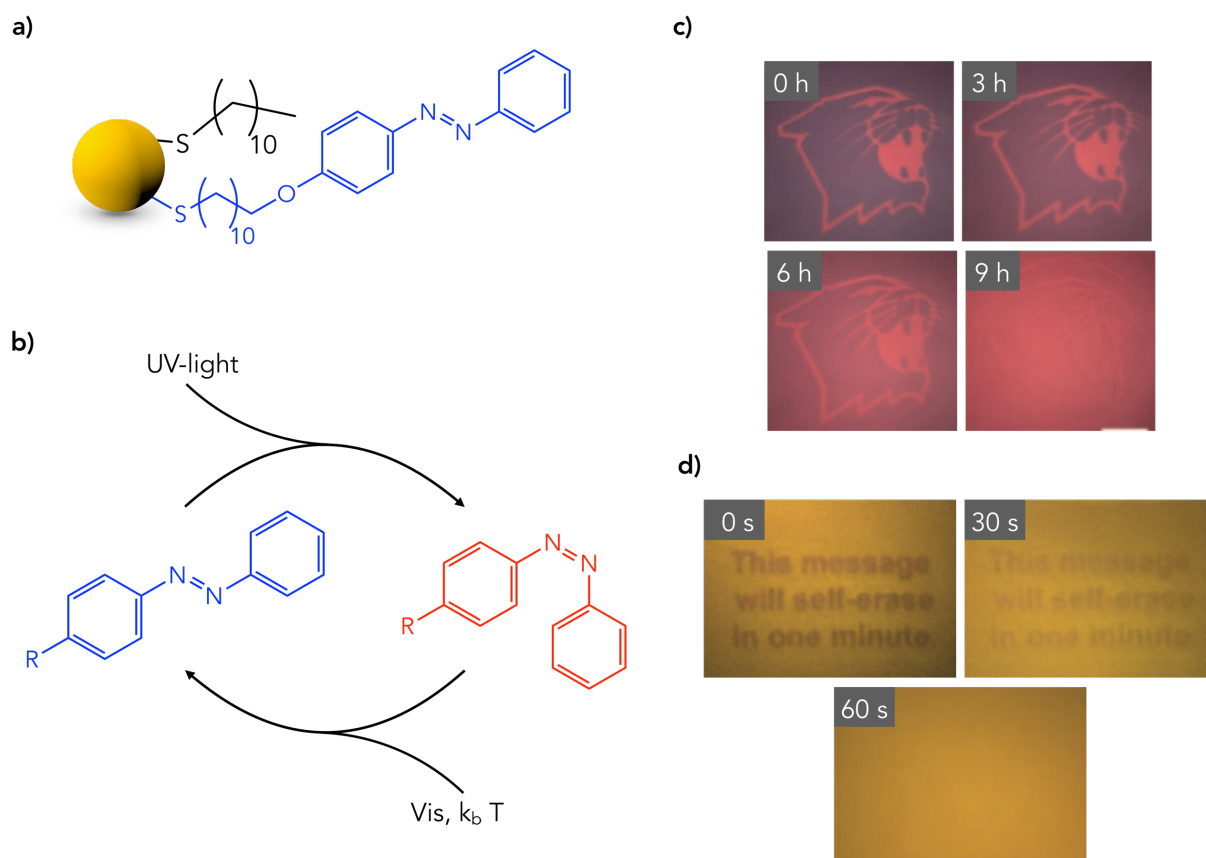
In the last strategy I discuss, the self-assembly of the product is induced by a conformational change of the precursor molecule of dissipative self-assembled materials are based on a change of the conformation of the precursor. The generated product can self-assemble. Fundamentally, this strategy is similar to the ATP-driven self-assembly of actin.<sup>81</sup> The binding of ATP to actin changes the conformation of the actin-subunit and activates it to self-assemble with another product. Nevertheless, it

is hard to design such chemical reaction networks, which limits the explored examples to just a few.<sup>82-83</sup> The method of changing the conformation of a molecule can also be used the other way around to trigger disassembly of the assembled structure.<sup>82, 84</sup>

The work on chemical reaction cycles by Hartley et al. is based on the hydrolysis of carbodiimides where a dicarboxylic acid precursor is condensed in its corresponding anhydride.<sup>85</sup> The oligo(ethylene glycol) precursor is functionalized with two carboxylic moieties, one at each end of the molecule. The fuel condenses these two groups to form the cyclic anhydride. The fuel-induced change in conformation is leading to an increased affinity to bind metal ions, lithium, sodium, potassium, and cesium. In their study, two different precursors, which are based on the design of crown ethers (18-crown-6 and 21-crown-7) are used.<sup>86-87</sup> Counterintuitively, the metastable products of both precursors showed decreased binding affinity to the metal ions, which match the size of the cavity of the macrocycle and *visa versa*. This negative templating effect led to lower concentration of the product compared to reaction cycles without mismatched ions present.

In the work of Grzybowski and co-workers, the dissipative self-assembly of gold or silver-nanoparticles is driven by UV-light.<sup>88</sup> Both types of nanoparticles are functionalized with an azobenzene derivative. The azobenzene unit can isomerize by the irradiation with UV-light from the thermodynamically favored *trans*- to the *cis*-conformation of the azobenzene (Figure 13). This unfavored state quickly reverts to the initial *trans*-precursor. The change in conformation induces a change of the dipole moment of the precursor. This change is sufficient to induce the self-assembly of the nanoparticles into larger clusters. The clusters started disassembling when the fuel source, light, was switched off. The assembly of the gold nanoparticles caused a color change of the sample from red to blue. The silver nanoparticles changed from yellow to blue. This fact makes both chemical reaction cycles interesting for an application as temporal inks. Therefore, the chemical reaction cycle was embedded in a polymer gel and irradiated with UV-light through a photomask. Where the light activated the nanoparticles, they started to self-assemble into clusters and changed the color of the

polymer gel, respectively. It was so possible to write messages with a UV-laser pen or created complex patterns via the photomasks. After removing the light source, the clusters disassembled over time, and the messages or patterns disappeared completely. The polymer gel with the embedded nanoparticles could be used over and over again, as the chemical reaction cycle does not produce any waste molecule except heat. The time the messages or patterns were visible could be tuned from seconds to hours. The lifetime of the messages or patterns was depending on the precursor used for the chemical reaction network. The message created from silver nanoparticles was erased after sixty seconds. In contrast, the pattern created from embedded gold nanoparticles disappeared completely after 9 hours.



**Figure 13:** Conformational change induced by UV-light irradiation. a) Gold and silver nanoparticles are functionalized with an azobenzene derivative. b) Isomerization of the precursor driven by the irradiation with UV-light. c) The gold nanoparticles can be used to temporally show patterns. d) Temporal ink used to write messages with a lifetime of 60 seconds.

## 2.5 Conclusion and Outlook

The past decades showed a tremendous increase in the development of chemical reaction cycles leading to dissipative out-of-equilibrium materials. Biological examples of dissipative self-assembled materials show unique features like the ability to self-heal<sup>89</sup>, and the ability to regulate the kinetics of the reaction by exerting feedback between the material and the chemical reaction cycle. For example, the assembly of microtubules catalyzes its building block deactivation, which is a crucial element of the complex behavior of the emerging structure.<sup>90</sup> Complex behavior is leading to self-replication<sup>91</sup>, self-selection<sup>92</sup>, motion<sup>93-94</sup>, molecular evolution<sup>95-96</sup> and exertion of forces.<sup>97</sup> In the discussed examples, these complex behaviors are still missing. Robustness and feedback of the assemblies onto the kinetics of the chemical reaction cycle are still hard to design. A few examples, like the work of Walther and co-workers, shows already a nice starting point of these complex behaviors<sup>72</sup>. Nevertheless, the kinetics of the chemical reaction cycle and the assemblies are not reciprocally coupled. The deactivation reaction in this example is influenced by a reagent, which slowly changes the pH back to the original value. So, it remains a big challenge for the field of dissipative out-of-equilibrium chemistry to include such feedback and robustness between the self-assembled materials and the chemical reaction cycles.

Another downside of the listed examples is that the materials are not biocompatible or bio-orthogonal. The gap between living matter and man-made materials could be bridged by materials that interfacing with each other.<sup>67</sup> In other words, the properties of the materials would be able to dynamically adapt to the stress of their surrounding living matter or visa versa.<sup>39</sup>

### 3. Aim of the Thesis

Synthetic dissipative materials have drawn much attention in the last years because they offer unique properties compared to their in-equilibrium counterparts. Because these materials are under kinetic control, as opposed to thermodynamic control, these materials can be regulated in space and time by gradients of reactants. As mentioned in Chapter 1, most examples discussed so far involve toxic chemicals or enzymes, which makes the materials incompatible for healthcare application and hard to analyze quantitatively. Besides that, for unique biological properties, like self-healing or adaptivity, the reaction rates of the chemical reaction cycles and turnover rates are generally too slow. As concluded from Chapter 2, dissipative out-of-equilibrium materials do not have reciprocal coupling between the assembled structures and the kinetics of the chemical reaction cycle either. In other words, the assemblies do not show real feedback on the kinetics of the chemical reaction cycle like biology typically does.

The first aim of the thesis is thus to develop a chemical reaction cycle which does not operate that toxic chemicals and could, therefore, be used in or close to physiological conditions. The second aim is to increase the reaction rates in the chemical reaction cycle compared to the current state of the art. In Chapter 4, I describe such a chemical reaction cycle, which comprises mild reagents and takes place in water, making it therefore extremely versatile and scalable. This chemical reaction cycle can be driven by several non-toxic fuels and can be coupled to numerous precursors. The transient products are able to self-assemble into a wide range of dissipative out-of-equilibrium structures. We showed that these materials emerge and decay in response to chemical fuel. Moreover, it was possible to tune the lifetimes of these materials from minutes to hours. Finally, we demonstrate that, after the materials had decayed, we could reuse this precursor many times without interference of the waste. With our quantitative understanding of the chemical reaction cycle, we set out to develop new strategies to implement feedback into the chemical reaction cycle. It was possible to

include and study the robustness of the assemblies. The feedback of the assembled colloids is reciprocally coupled to their kinetics. The tuneability of the robustness of assemblies is shown in Chapter 5.

In conclusion, the aim of the thesis is to develop new chemical reaction cycles that induce the dissipative self-assembly of different water-soluble precursors, like Fmoc-protected amino acids or short peptides. With these newly developed chemical reaction cycles I aim to design feedback of the assemblies on their chemical reaction network.

## 4. Non-equilibrium dissipative supramolecular materials with a tunable lifetime

### **Abstract.**

Over the past decades, a huge number of supramolecular assemblies, for example supramolecular polymers, fiber forming hydrogels or vesicles have been developed. Such assemblies consist of molecular building blocks, the precursors, which are able to self-assemble due to their intermolecular interactions. The development of this kind of assemblies already led to materials which can be found in everyone's everyday life, for example liquid crystals in LC-displays or as application as drug delivery platform. These assemblies and materials remain in stark contrast with biological non-equilibrium supramolecular assemblies, which are driven by a chemical reaction cycle. Biological supramolecular assemblies show unique features like adaptivity and the ability to be controlled in space and time and are controlled by kinetics rather than by thermodynamics. As these systems are challenging to design, the already developed examples remain limited and the unique material properties are hardly explored.

In this work, we describe a new chemical reaction cycle that can drive the self-assembly of different Fmoc-protected short peptides and amino acids. In the chemical reaction cycle, a precursor that carries two carboxylate groups is converted into its corresponding anhydride after the addition of fuel. This anhydride product is metastable and rapidly hydrolyzes back to its initial precursor state. The loss of electrostatic repulsion induces the assembly of the product. Depending on the molecular design of the precursor, we found different types of assemblies in response to the chemical fuels. For example, fiber-forming hydrogels, hydrophobic colloids, and spherulites. We could demonstrate that these assemblies are transient, that the lifetime could be tuned from minutes to hours and that the chemical reaction cycles can be restarted with a new batch of fuel without any change in the lifetime or the property of the assembly.

This work has been published:

Title: Non-equilibrium dissipative supramolecular materials with a tunable lifetime

Authors: Dr. Marta Tena-Solsona\*, Benedikt Rieß\*, Dr. Raphael K. Grötsch, Franziska C. Löhner, Caren Wanzke, Dr. Benjamin Käsdorf, Prof. Dr. Andreas R. Bausch, Prof. Dr. Peter Müller-Buschbaum, Prof. Dr. Oliver Lieleg, Prof. Dr. Job Boekhoven

First published: 08. July 2017

Journal: *NatCommun* **2017**, 8, 15895.

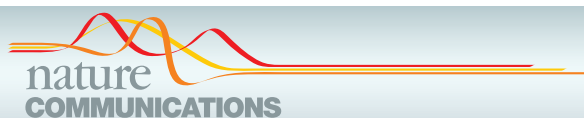
Publisher: Nature Publishing Group

DOI: 10.1038/ncomms1589

Reprinted with permission of Nature Publishing Group.

This section states the individual work of each author in the publication above. M. Tena-Solsona and B. Rieß designed and conducted all experiments. C. Wanzke imaged Fmoc-AVE and Fmoc-AVD with a cryogenic transmission electron microscope. R. K. Grötsch studied Fmoc-E with DLS. F. C. Löhner and P. Müller-Buschbaum carried out the experiments and helped to use Fmoc-D as temporary ink. B. Käsdorf and O. Lieleg carried out and helped analyzing the gel properties of Fmoc-AVE, Fmoc-AVD, Fmoc-AAE and Fmoc-AAD with top-plate rheology. M. Tena-Solsona, B. Rieß and J. Boekhoven wrote the manuscript. The work was performed under the supervision and guidance of J. Boekhoven.





## ARTICLE

Received 19 Jan 2017 | Accepted 10 May 2017 | Published 18 Jul 2017

DOI: 10.1038/ncomms15895

OPEN

# Non-equilibrium dissipative supramolecular materials with a tunable lifetime

Marta Tena-Solsona<sup>1,2,\*</sup>, Benedikt Rieß<sup>1,\*</sup>, Raphael K. Grötsch<sup>1</sup>, Franziska C. Löhner<sup>3</sup>, Caren Wanzke<sup>1</sup>, Benjamin Käsdorf<sup>4</sup>, Andreas R. Bausch<sup>5</sup>, Peter Müller-Buschbaum<sup>3</sup>, Oliver Lieleg<sup>4</sup> & Job Boekhoven<sup>1,2</sup>

Many biological materials exist in non-equilibrium states driven by the irreversible consumption of high-energy molecules like ATP or GTP. These energy-dissipating structures are governed by kinetics and are thus endowed with unique properties including spatio-temporal control over their presence. Here we show man-made equivalents of materials driven by the consumption of high-energy molecules and explore their unique properties. A chemical reaction network converts dicarboxylates into metastable anhydrides driven by the irreversible consumption of carbodiimide fuels. The anhydrides hydrolyse rapidly to the original dicarboxylates and are designed to assemble into hydrophobic colloids, hydrogels or inks. The spatiotemporal control over the formation and degradation of materials allows for the development of colloids that release hydrophobic contents in a predictable fashion, temporary self-erasing inks and transient hydrogels. Moreover, we show that each material can be re-used for several cycles.

<sup>1</sup>Department of Chemistry, Technische Universität München, Lichtenbergstrasse 4, 85748 Garching, Germany. <sup>2</sup>Institute for Advanced Study, Technische Universität München, Lichtenbergstrasse 2a, 85748 Garching, Germany. <sup>3</sup>Lehrstuhl für Funktionelle Materialien, Physik-Department, Technische Universität München, James-Frank-Strasse 1, 85748 Garching, Germany. <sup>4</sup>Department of Mechanical Engineering and Munich School of Bioengineering, Technische Universität München, Boltzmannstrasse 11, Garching 85748, Germany. <sup>5</sup>Lehrstuhl für Biophysik E27, Physik-Department, Technische Universität München, James-Frank-Strasse 1, 85748 Garching, Germany. \* These authors contributed equally to this work. Correspondence and requests for materials should be addressed to J.B. (email: job.boekhoven@tum.de).

Supramolecular materials consist of molecular building blocks that are assembled via non-covalent interactions such as hydrogen bonding and ionic interactions<sup>1</sup>. Examples include supramolecular polymers<sup>2</sup>, bioactive hydrogels<sup>3</sup>, photocatalytic fibre that can produce hydrogen<sup>4</sup> as well as macroscopic actuators assembled from small molecules<sup>5</sup>. The past decades have seen tremendous development in the field, and as a result of combined efforts, supramolecular materials are now found in healthcare<sup>6</sup>, opto-electronics<sup>7</sup> and others areas. More recent advances have led to supramolecular materials that change their function in response to externally applied stimuli such as light<sup>8</sup>, oscillations in pH<sup>9,10</sup>, enzymes<sup>11</sup> or even cellular activity<sup>12</sup>. Despite this progress, these materials remain in stark contrast with biological non-equilibrium supramolecular structures especially when it comes to their autonomy and adaptivity<sup>13</sup>. Biological materials typically exist in states far-from-equilibrium, for example, driven by chemical reaction networks that consume chemical fuels like ATP (adenosine triphosphate) or GTP (guanosine triphosphate). As a result, these materials are kinetically controlled, in contrast to man-made materials that are governed by thermodynamic parameters, like free energy landscapes and temperature. This kinetic control endows biological materials with unique properties including a tunable lifetime, robustness, adaptivity and the capacity to self-heal<sup>14</sup>. Inspired by biology, molecular assemblies coupled to chemical reaction networks that involve enzymes have recently been developed to drive man-made molecular assemblers out-of-equilibrium<sup>15,16</sup>. As these systems remain challenging to design, the number of molecular assemblies driven by chemical reaction networks based on exclusively non-biological entities remain limited<sup>17,18</sup>, and their use as supramolecular materials with unique properties is largely unexplored terrain.

Here we show a class of autonomously forming and disappearing supramolecular materials. The transient, non-equilibrium materials are produced by a chemical reaction network that can be fully rationalized by a set of kinetic equations. The network comprises mild, man-made reagents and takes place in water making it extremely versatile and scalable. It can be driven by several fuels and coupled to numerous precursors, which allows for the exploration of a wide range of autonomous forming and degrading aqueous supramolecular materials. We demonstrate that these materials are transient, that their lifetimes can be tuned from minutes to hours and that they can be reused by application of another batch of fuel.

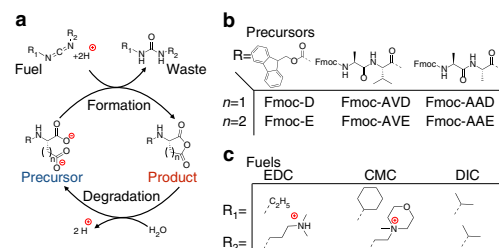
## Results

**Characterization of the chemical reaction network.** The chemical reaction network we describe takes place in buffered water at pH 6 at room temperature and consists of a dicarboxylate (precursor) that is converted into an anhydride (product) by consumption of a carbodiimide (fuel; Fig. 1a). The aqueous anhydride product is unstable and rapidly hydrolyses back to the corresponding dicarboxylate. While the dicarboxylate precursor carries two negative charges under the described conditions, the anhydride product is uncharged. We used this hydrophobization, driven by our chemical reaction network, to decrease the solubility of the precursor and thus induce self-assembly. We explored precursors based on aspartate (D) and glutamate (E) because their corresponding cyclic anhydrides were formed with high relative yields. Moreover, being natural amino acids, these precursors were commercially available in numerous variations or could be incorporated in peptide-based supramolecular materials. We tested three fuels and six precursors (Fig. 1b,c). The precursors all bear a relatively large hydrophobic protecting group (fluoren-9-ylmethoxycarbonyl, Fmoc) that aids assembly driven

by  $\pi$ -orbital overlap and hydrophobic collapse. Indeed, we found that the anhydrides of Fmoc-D and Fmoc-E assembled in spherulites and colloids, respectively (*vide infra*). We introduced the amino acids alanine and valine (A and V, respectively) with a high propensity to form  $\beta$ -sheets with neighboring peptides to increase the anisotropy of the assemblies. Indeed, we found that the anhydrides of Fmoc-AAD, Fmoc-AVD, Fmoc-AAE and Fmoc-AVE assembled into anisotropic fibres (*vide infra*).

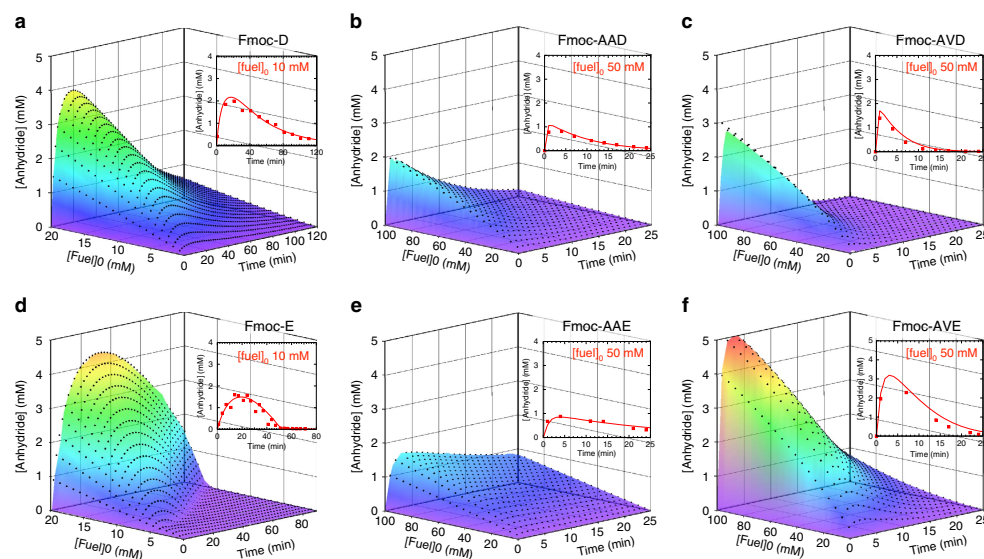
By means of high-pressure liquid chromatography (HPLC) and electrospray ionization mass spectroscopy, the evolution of the concentration of fuel, precursor and product was followed. In all experiments, a batch of carbodiimide fuel was added to a buffered solution of 10 mM precursor. At a concentration of 10 mM, we did not find any evidence of assemblies for any of the precursors (Supplementary Fig. 1a,b). We monitored the pH during a cycle to confirm that under these conditions the buffer has sufficient capacity (Supplementary Fig. 1c). The highest anhydride yields were found for the fuel based on ethyl-3-(3-dimethylaminopropyl) carbodiimide (EDC) as it was relatively stable in our buffer (Supplementary Fig. 1d), yet reactive towards our precursors. Although the other carbodiimide fuels also formed anhydrides and were able to induce self-assembly (*vide infra*), their yields were drastically lower (Supplementary Fig. 1e). We therefore focused most of our studies on EDC. Each precursor-EDC combination resulted in the transient formation of the anhydride product with a cycle time in the range of tens of minutes to several hours (Fig. 2; Supplementary Figs 2–4). It was found that the chemical reaction networks that used derivatives based on glutamic acid (E) as a precursor were prone to the unwanted *N*-acylisourea formation as a side reaction, a reaction which yields a stable product of the carbodiimide attached to the precursor. The yields of this unwanted side reaction were not >2% as expressed in amount of fuel added (Supplementary Note 1; Supplementary Table 4), and it is unlikely that these concentrations affect material properties.

A kinetic model was used to describe all relevant reactions in our chemical reaction networks (Supplementary Note 2). These reactions are the direct hydrolysis of EDC, the formation of *O*-acylisourea by reaction of fuel with precursor, the conversion of the *O*-acylisourea to the anhydride, the direct hydrolysis of the *O*-acylisourea to the original precursor, and the hydrolysis of the anhydride to the precursor. The rate-determining step in the anhydride formation was the formation of the *O*-acylisourea. This reaction had a second-order rate constant which was in the same order of magnitude for each dicarboxylate we tested (Supplementary Table 1). In contrast, the first-order rate constant for anhydride hydrolysis differed up to two orders of magnitude,



**Figure 1 | Transient anhydride formation by carbodiimide fuels.**

(a) Scheme of the chemical reaction network for the fuel driven formation of a transient anhydride bond. (b) Molecular structures of the dicarboxylates precursors used in this study. (c) Molecular structures of the fuels used in this study.



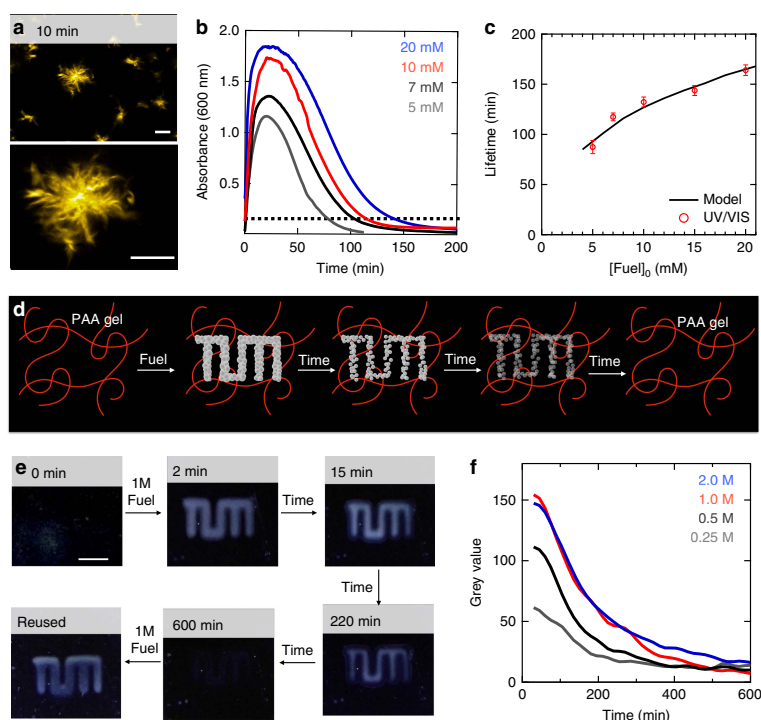
**Figure 2 | Evolution of anhydride concentrations through fuel driven cycles calculated by kinetic models. (a–f)** 3D plots of the anhydride concentration against time in a dissipative cycle for different initial EDC concentrations for Fmoc-D, Fmoc-AAD, Fmoc-AVD, Fmoc-E, Fmoc-AAE and Fmoc-AVE. The black markers represent the calculated concentration using the kinetic model, the planes represent interpolations between the model data. Note the different x (time) and y (fuel) axis for **a,d** compared to the Fmoc-AA and Fmoc-AV series. The insets show a 2D graph of the concentration anhydride against time for one batch of fuel (10 or 50 mM) as determined by HPLC (markers) and the kinetic model (solid line).

ranging from  $3.8 \times 10^{-2} \text{ s}^{-1}$  for Fmoc-AVD to  $3.8 \times 10^{-4} \text{ s}^{-1}$  for Fmoc-D corresponding to an anhydride half-life of 0.3 and 30 min, respectively (Supplementary Table 1). For all precursors except Fmoc-E and Fmoc-D, the model was straightforward and the rate constants for the above-mentioned reactions were sufficient to fit our data, whether assemblies were present or not (Supplementary Figs 2–4). To our surprise, for Fmoc-E and Fmoc-D, the anhydride hydrolysis rate constant was found to be significantly lower in the presence of assemblies. In effect, the large three dimensional assemblies that these products formed exerted negative feedback on their own hydrolysis rate by protecting the anhydrides from water, thereby increasing the lifetime of the materials (*vide infra*). The feedback was implemented into the kinetic model by introducing a second  $k$ -value for hydrolysis above a threshold concentration. This threshold concentration was determined such that the model fitted the HPLC data best (see Supplementary Note 2 for a discussion on the feedback and threshold concentration). Using our kinetic models, the evolution of the relevant chemical species through the cycle could be calculated for each precursor (Fig. 2).

**Characterization of self-erasing inks.** We found that application of 10 mM EDC as a fuel to a solution of 10 mM Fmoc-D turned the clear solution into a turbid one, pointing to assemblies formed by the Fmoc-D anhydride with sizes of at least hundreds of nanometers. The assembly process can be explained by the conversion of the two negatively charged carboxylates into a relatively hydrophobic anhydride. The hydrophobization renders the molecules insoluble and induces self-assembly, likely driven by  $\pi$ -orbital overlap and hydrophobic collapse. Confocal microscopy images of these samples revealed the presence of spherulites with diameters of tens of micrometres 10 min after fuel addition

(Fig. 3a). The turbid solutions turned transparent over time and a lack of assemblies was verified by confocal microscopy (Supplementary Fig. 5a–c). The transient turbidity was quantified by UV/Vis spectroscopy and we found that the greater the batch of fuel, the longer the solutions remained turbid (Fig. 3b). An arbitrary threshold of 0.1 absorbance units was chosen to define the turbidity of the samples. We found that 10 mM of fuel kept the samples turbid for  $132 \pm 5$  min corresponding to a threshold concentration of  $0.3 \pm 0.1$  mM of Fmoc-D anhydride according to the introduced kinetic model. This threshold concentration was used to calculate the lifetime of turbid solutions for other initial fuel concentrations. Indeed, the calculations corresponded well to the experimentally determined lifetimes of turbidity and our active solutions could be kept turbid for  $87$  to  $164 \pm 5$  min for 5 to 20 mM of EDC (Fig. 3c). Finally, the reusability of our system was tested by adding 5 mM of EDC as fuel and measuring the turbidity for 100 min for five cycles. No significant differences between the cycles were observed (Supplementary Fig. 5d).

We sought out the applicability of our the Fmoc-D solutions with transient turbidity as a carrier for temporary messages with a tunable lifetime, that is, as a self-erasing medium (Fig. 3d). Dynamic self-assembled structures have been demonstrated before in the context of self-erasing ink using nanoparticle self-assembly driven by light, which makes tuning the lifetime by amount of energy applied challenging<sup>19</sup>. We immobilized 10 mM Fmoc-D in a polyacrylamide polymer hydrogel and applied high concentrations of fuel as ink with a spray coater through a three-dimensional (3D) printed mask. The transparent gels rapidly turned turbid, but only where the fuel had been applied. Over time the messages auto-erased allowing the reuse of the message carrier. Different EDC concentrations ranging from 0.25 to 2 M were used as ink and all concentrations showed the messages (Supplementary Fig. 5e–h). Using time-lapse photography and



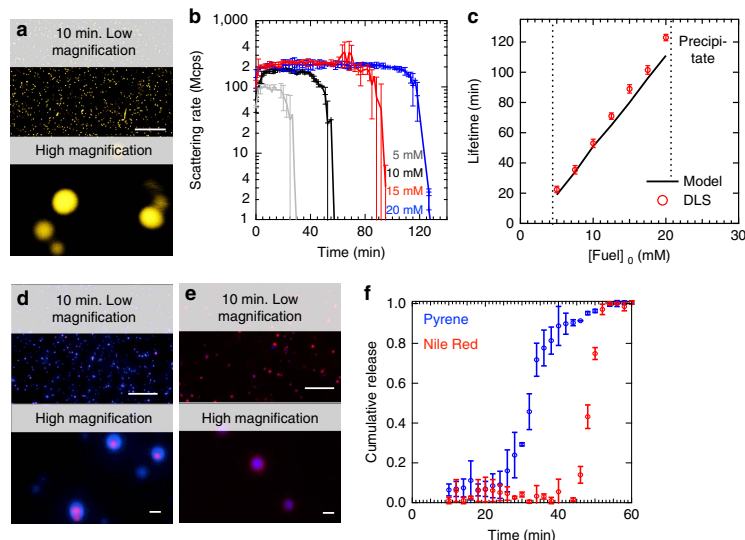
**Figure 3 | Self-erasing inks with a tunable lifetime formed by Fmoc-D.** (a) Confocal micrographs of a solution of 10 mM Fmoc-D anhydride 10 min after addition of 10 mM EDC in the presence of 2.5  $\mu$ M Nile Red (scale bars represent 10  $\mu$ m). (b) Absorbance at 600 nm as a measure for turbidity for solutions of 10 mM Fmoc-D against time after addition of a batch of fuel. The dotted black line represents the selected threshold of 0.1 absorbance units. (c) The lifetime of the turbidity of the samples as determined by data from **b** (markers) and calculated by the kinetic model (solid lines) against initial fuel concentration. Error bars represent the s.d. ( $n=3$ ). (d) Schematic representation of self-erasing medium. Fmoc-D is dissolved in a 30% polyacrylamide hydrogel. Only where fuel is applied turbidity appears. (e) Photographs of gels over time. The polyacrylamide gels were placed on a black surface and side-lit with white light to improve contrast. After 600 min, no evidence of the original image was found and the material was rinsed and reused (scale bar represents 1 cm). (f) Average grey values of photographs of inked areas over time.

image analysis software, we quantified the visibility over time. The initial visibility increased with increasing concentration of fuel, but this trend did not hold beyond 1 M of fuel. At this moment, it is not clear why this trend fails at high fuel concentrations. The visibility of the prints decreased over time and was fully erased after roughly 10 h. Crucially, the lifetimes of the visible prints could be tuned from roughly 200 to 500 min by altering the concentration of fuel (Fig. 3f).

**Colloids with a tunable lifetime.** Next, we studied the behaviour of Fmoc-E in response to fuel. While 10 mM of this precursor yielded clear solutions, application of 5 mM or more EDC formed transient turbid solutions. Confocal microscopy showed, to our surprise, uniform colloids 10 min after application of the fuel (Fig. 4a). Dynamic light scattering (DLS) confirmed the transient presence of particles and showed that their radii initially rapidly grew to a plateau value of 0.6  $\mu$ m. After the plateau, the particles decreased their size until all had disappeared (Fig. 4b; Supplementary Fig. 6a). This plateau value was independent of the amount of fuel added. Above 20 mM of EDC, the particles precipitated, while below 5 mM EDC no particles were found. Within this window of fuel concentrations, particles were

transiently present. The DLS scattering intensity data was used to find the time where no more particles were found. For instance, in the case of 10 mM of fuel, the scattering intensity reached its original level after  $53 \pm 2$  min, corresponding to an Fmoc-E anhydride concentration of  $0.07 \pm 0.02$  mM according to the model. This threshold concentration was used in combination with the kinetic model to predict the lifetime of the particles for other initial fuel concentrations. With the model, we found that the lifetime increased linearly from 20 to 120 min for 5 to 20 mM of EDC, and DLS verified that the model predicted these lifetimes correctly. Moreover, application of a second batch of fuel resulted in the reformation of the transient particles with similar radii and lifetimes demonstrating the reusability of these systems (Supplementary Fig. 6b). Even after 15 cycles, the particles still transiently formed with similar radii, albeit with a somewhat shorter lifetime.

For Fmoc-E, the assembly process drastically affected the anhydride hydrolysis kinetics. When small batches of fuel were applied, for instance below 5 mM, no assemblies were formed. In the absence of assemblies, hydrolysis was first order in anhydride concentration. However, in the presence of assemblies, hydrolysis followed 0th order kinetics with a rate constant of

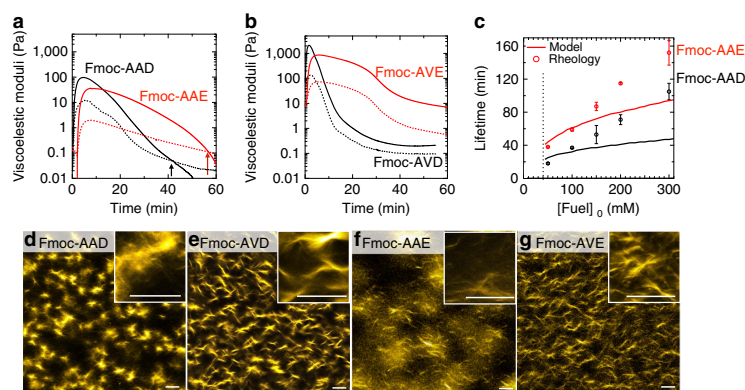


**Figure 4 | Transient colloids formed by Fmoc-E.** (a) Confocal micrographs of 10 mM Fmoc-E with 10 mM EDC after 10 min shows the formation of colloids in the presence of 2.5  $\mu\text{M}$  Nile. The scale bars represent 25  $\mu\text{m}$  and 1  $\mu\text{m}$  for the lower and higher magnification, respectively. (b) DLS scattering intensity against time for 10 mM Fmoc-E with varying concentration of fuel. (c) The lifetimes of the colloids as a function of concentration of initial fuel as determined by DLS and the kinetic model. The two dotted lines indicate the window where particles were found. (d) Micrographs of 10 mM Fmoc-E with 10 mM EDC after 10 min that were prepared in the presence of 250 nM Nile Red while 2.5  $\mu\text{M}$  pyrene was added after 5 min. The red (Nile Red) and blue (pyrene) channels were overlaid. Scale bar, 25 (lower magnification); 1  $\mu\text{m}$  (higher magnification). (e) Micrographs of 10 mM Fmoc-E with 10 mM EDC after 10 min that were prepared in the presence of 250 nM pyrene while 2.5  $\mu\text{M}$  Nile Red was added after 5 min. The red (Nile Red) and blue (pyrene) channels were overlaid. The scale bars represent 25  $\mu\text{m}$  and 1  $\mu\text{m}$  for the lower and higher magnification, respectively. (f) Release profiles of pyrene (blue markers) and Nile Red (red markers) of the particle described in d. Data collection was started 10 min after addition of EDC. All error bars represent the s.d. ( $n = 2$ ).

$1.5 \times 10^{-6} \text{ M s}^{-1}$ , drastically slowing down the hydrolysis upon self-assembly. In other words, the assembly of the Fmoc-E anhydride into colloids has a negative feedback on its own hydrolysis. Because the Fmoc-E anhydride assembles into large colloids driven by hydrophobic collapse, they likely shield the anhydride from water, effectively excluding it from the chemical reaction network. As a result, anhydride hydrolysis mostly happens on free anhydride in solution and is thus limited by its solubility. The pool of soluble anhydride is replenished by the particles until all particles have disassembled. This finding implies that particles should first collectively grow until the system runs out of fuel and then collectively shrink by surface erosion, that is, degradation from the particle's surface that is limited by the solubility of the anhydride. Such a mechanism contrasts a dynamic mechanism where individual particles grow while others collapse. To confirm the proposed mechanism, we prepared particles in the presence of 250 nM Nile Red. After 5 min, 2.5  $\mu\text{M}$  of the hydrophobic dye pyrene was added, and the particles were imaged after 10 min (Fig. 4d). While Nile Red had mostly incorporated into the core of the particles, pyrene was primarily found in their shell. When the addition of dyes was carried out in the opposite order, the cores had encapsulated Pyrene, while the shell was emitting in the Nile Red channel (Fig. 4e). In contrast, when both dyes were present from the beginning of the cycle, particles were found that had incorporated both dyes homogeneously (Supplementary Fig. 6d). These observations confirm the above-proposed mechanism of sequential growth and collapse steps. It is worth to note that also the other two fuels (CMC and DIC) were able to induce the formation of colloids when added to solutions of Fmoc-E (Supplementary Fig. 6d,e).

We used the mechanism of sequential growth and collapse to develop particles that can release hydrophobic agents sequentially. As described above, we prepared particles with Nile Red in their interior and a shell with pyrene incorporated into it. Using a fluorescence spectrophotometer, the release of both dyes from the particles into solution was measured. From the release profiles (Fig. 4f) it can be observed that pyrene release commences after 30 min in the cycle, and most dye has been released after 40 min. In contrast, Nile Red was only released after 50 min. Moreover, when the dyes had Pyrene in their interior and Nile Red in their shell, an opposite release pattern was found (Supplementary Fig. 6f).

**Hydrogels with a predictable lifetime.** When 100 mM EDC was added to solutions of either 10 mM Fmoc-AAD or Fmoc-AAE, each of them rapidly turned into gels. Fmoc-AAD formed weak gels that did not pass the inverted tube test (Supplementary Fig. 7a). Crucially, the gels collapsed within an hour. We confirmed these observations by macrorheology, and found that both precursors formed viscoelastic gels ( $G' > G''$ ) if at least 50 mM EDC was added (Fig. 5a; Supplementary Fig. 7b,c). The maximum gel elasticity for Fmoc-AAD with 100 mM of fuel was obtained after 4 min and was in the range of 100–300 Pa, while the maximum elasticity obtained for Fmoc-AAE was between 40 and 100 Pa and observed after 10 min. Then, the gel stiffness decreased and eventually a solution was found ( $G'' > G'$ ). For 100 mM of fuel, this point occurred at  $37 \pm 1$  and  $59 \pm 2$  min for Fmoc-AAD and Fmoc-AAE, respectively (Fig. 5c). According to our kinetic model, the concentration of anhydride at these times



**Figure 5 | Temporary hydrogels formed by Fmoc-tripeptides.** (a,b) Rheological time sweeps of gels formed by 10 mM Fmoc-AAD and Fmoc-AAE, or Fmoc-AVD and Fmoc-AVE precursor combined with 100 mM EDC. Solid line represents the storage modulus ( $G'$ ), dashed line represents the loss modulus ( $G''$ ). (c) The lifetimes of the gels described in a, as measured by rheology (markers) or calculated by the kinetic model (solid lines). Error bars represent the s.d. ( $n=3$ ). (d-g) Confocal microscopy of 100 mM EDC combined with 10 mM Fmoc-AAD, Fmoc-AVD, Fmoc-AAE and Fmoc-AVE after 10 min. Scale bar, 10  $\mu\text{m}$ .

is  $100 \pm 50$  and  $180 \pm 80 \mu\text{M}$  for Fmoc-AAD and Fmoc-AAE, respectively. These concentrations were then used to predict the lifetimes of our gels for other initial concentrations of fuels (Fig. 5c). To our surprise, whereas the prediction made by the model seemed to agree for lower concentrations of fuel, it deviated far from the rheology data for higher concentrations of fuel. For example, for 200 mM of EDC added to Fmoc-AAE, the anhydride concentration falls below  $180 \mu\text{M}$  after 80 min while the gel sustained for roughly 2 h. Although both the experimentally determined lifetime of the gel and the crossing through the threshold concentration of anhydride scaled linearly with the amount of fuel added, their slopes were not equal (Fig. 5c). In other words, we can predict and tune the lifetimes of the transient gels ranging from 18 to 152 min for 50 to 300 mM of fuel, but the moment the gel becomes a liquid does not correspond to one critical threshold concentration of anhydride. These observations could be justified by the complex behaviour of hydrogels that not only rely on the gelator concentration, but also on the type and number of crosslinks, and the length and mechanical properties of the fibres it comprises<sup>20</sup>. To test the reusability of our fuel driven hydrogels, a second batch of fuel was added to the solution after the cycle had finished. Similar gel stiffnesses and lifetimes were found for the first four cycles driven by 50 mM of fuel (Supplementary Fig. 7d).

For both Fmoc-AA precursors, confocal microscopy showed no assemblies before addition of fuel (Supplementary Fig. 8a,c), while addition of 100 mM of fuel rapidly induced the transient formation of fibrillar assemblies (Fig. 5d,f; Supplementary Fig. 8a,c). With this amount of fuel, we found a relatively dense network of fibres for both gelators. Crucially, all fibres of the Fmoc-AA series had completely disappeared after 4 h (Supplementary Fig. 8a,c). We followed the gel formation with circular dichroism spectroscopy at 305 nm, where the signal of the Fmoc-groups is typically recorded<sup>21</sup>. Before initiating the cycle, we found a small positive signal at 305 nm for the Fmoc-AA precursors (Supplementary Fig. 9a). After addition of fuel, the signal rapidly grew, but, over time, returned to its original value pointing to full disassembly after roughly 80 and 200 min for Fmoc-AAD and Fmoc-AAE, respectively. We also followed the Fmoc-fluorescence emission over time during a

cycle as a direct indication for  $\pi$ -orbital overlap between the Fmoc-moieties (Supplementary Fig. 9c-e). Before starting the cycle, a relatively sharp peak at 318 nm was found, indicative for fluorenyl-groups that are not engaged in  $\pi$ - $\pi$  interactions. Upon addition of fuel, the 318 nm signal rapidly decreased, while a broad peak at 460 nm appeared. Both observations point to  $\pi$ - $\pi$  stacking of the Fmoc-groups<sup>11</sup>. Over time the 318 nm peak grew back to its original level, while the 460 nm peak disappeared, pointing to loss of the  $\pi$ - $\pi$  interactions.

#### Kinetic trapping of assemblies via dissipative pathways.

When 100 mM of EDC was added to solutions of Fmoc-AVD or Fmoc-AVE, each of them rapidly turned into gels (Supplementary Fig. 7a). To our surprise, these gels did not revert to their original solutions, even after 4 h when no significant amounts of anhydride were present according to our model or HPLC. These surprising observations were confirmed by rheology that showed a decrease in gel-stiffness as the overall anhydride concentration decreased to zero, but never a full recovery to a liquid state (Fig. 5b). The lack of recovery was not a result of the accumulating waste (EDU), as addition of 100 mM or more EDU to solutions of precursor did not change their rheological behaviour (data not shown). Confocal microscopy on the Fmoc-AV systems showed no assemblies before, and dense networks of fibres after addition of fuel (Fig. 5e,g; Supplementary Fig. 8b and d). In contrast to the Fmoc-AA series, the fibres did not disappear, even after 24 h. The longer presence of these fibres allowed us to study them with cryo-transmission electron microscopy (TEM), which confirmed the presence of fibres for both Fmoc-AVD and Fmoc-AVE, with diameters of  $6.9 \pm 0.6$  and  $4.8 \pm 0.6$  nm, respectively. Finally, circular dichroism showed a small peak at 305 nm before initiating the chemical reaction network that decreased to negative values during the cycle. Although the negative signal decreased in magnitude as the system had run out of fuel, it never returned to the small peak found before initiating the cycle. The original spectrum, as observed before fuel addition, could only be regenerated by heating the sample to 80 degrees and subsequently cooling it down to room temperature (Supplementary Fig. 9a).

We can conclude that all the Fmoc-tripeptides studied in this work assembled into fibres in their anhydride state that subsequently formed viscoelastic gels. The assembly into fibres was driven by  $\beta$ -sheet formation between molecules as evidenced by a Thioflavin-T (THT) assay, and  $\pi$ -orbital overlap between the Fmoc-groups as evidenced by fluorescence-spectroscopy (Supplementary Fig. 9). For the Fmoc-AA series, as the system was running out of fuel, the hydrolyzed anhydrides fibres became unstable which resulted in full disassembly of the fibres and a transition to a liquid. Whether the dicarboxylates left the fibres instantaneously, or a co-assembly of pure anhydride and precursors could exist is not clear at this moment. However, it is evident that when all anhydride had hydrolyzed, all fibres had disappeared. Thus, we conclude that fibres comprising exclusively Fmoc-AAD or Fmoc-AAE dicarboxylates could not exist. In contrast, when all Fmoc-AVE or Fmoc-AVD anhydride had hydrolysed towards their corresponding carboxylates, fibres were still observed. These observations imply that hydrolysis towards the dicarboxylates did not induce (full) disassembly and fibres comprising exclusively the dicarboxylate could exist for the Fmoc-AV series. Only heating and cooling the sample resulted in full disassembly of the dicarboxylate fibres, which demonstrates that the dicarboxylates' thermodynamic minimum is a disassembled state. From the overall results, we conclude that the dissipative cycle, initiated by addition of fuel, kinetically trapped the dicarboxylates into fibres by temporarily converting them into their corresponding anhydrides. The existence of such a kinetically trapped state implies that the molecules did not have sufficient free energy to break out of the fibres, but can only be brought to their thermodynamic minimum by application of heat. The ability to kinetically trap Fmoc-AV, but not Fmoc-AA, likely has to do with the increased  $\beta$ -sheet forming propensity of V versus A<sup>22</sup>. Kinetically trapping molecules in fibres by  $\beta$ -sheet formation and hydrophobic interactions is frequently observed for assemblies in, or close to, equilibrium<sup>23</sup>, but are rare in the context of chemically driven out-of-equilibrium cycles<sup>8</sup>. Our observations demonstrate that the balance between assembly and disassembly is crucial in the design of assemblers for materials driven by chemical reactions; when the driving force for assembly is too weak, no assembly will take place, but in contrast, when the driving force is too strong, assemblies can be kinetically trapped in non-favourable states.

## Discussion

We have described a chemical reaction network that drives an anionic dicarboxylate out-of-equilibrium by forming its corresponding metastable non-charged anhydride. Because of the versatility of the network, it can easily be incorporated into peptide-based self-assembling structures, which we showcase with hydrophobic colloids, supramolecular inks and self-assembled hydrogels. Unlike the more classical supramolecular materials, the behaviour of these non-equilibrium materials is dictated by kinetics rather than thermodynamics. This allows us to tune their lifetimes and their decomposition pathway, and we can use them for several cycles. We found that some of the assemblies exert feedback on their own degradation by excluding their building blocks from the chemical reaction network, which we used to our advantage to increase the lifetime of their corresponding materials. Such feedback of assemblies is also one of the crucial ingredients to study more complex life-like behaviour of non-equilibrium assemblies, including robustness, adaptive and oscillatory behaviour of the assemblies.

## Methods

**Materials.** All reagents were purchased from Sigma-Aldrich and Alfa-Aesar and used without any further purification unless otherwise indicated.

**Peptide synthesis and purification.** All peptides were synthesized by solid phase synthesis. Their purity was determined by analytical HPLC as well as electrospray ionization mass spectrometry in positive mode. See Supplementary Methods and Supplementary Tables 2–3 for more details.

**Sample preparation.** Stock solutions of the precursor were prepared by dissolving the peptide in 200 mM MES buffer, after which the pH was adjusted to pH 6.0. Stock solutions of EDC were prepared by dissolving the EDC powder in MQ water and used freshly. Reaction networks were started by addition of the high concentration EDC to the precursor solution.

**Kinetics.** The kinetics of the chemical reaction networks were monitored over time by means of analytical HPLC. A 750  $\mu$ l sample was prepared as described above and placed into a screw cap HPLC vial. Every 10 min, samples of these solutions were directly injected and all compounds involved were separated and quantified. To avoid aggregation during the injection, samples of Fmoc-D were continuously stirred. In the case of the gelators, the gels were slightly broken manually before injection into the HPLC. See Supplementary Methods and Supplementary Figs 10–15 for more details.

**Kinetic model.** A kinetic model was written using Matlab in which all reactions were described. The concentrations of each reactant were calculated for every 1 s in the cycle and  $k$ -values were fitted to the HPLC data. See Supplementary Methods for more details.

**UV/Vis.** The UV/Vis measurements were carried out using a UV/VIS spectrophotometer to monitor turbidity. See Supplementary Methods for more details.

**Dynamic light scattering.** DLS measurements on Fmoc-E solutions were performed using a DynaPro NanoStar from Wyatt following a literature procedure. See Supplementary Methods for more details.

**Rheology.** Rheological measurements were carried out on a Anton Paar Modular Compact Rheometer using steel parallel plate-plate geometry. See Supplementary Methods for more details.

**Spray coating set-up.** The fuel deposition via spray coating was performed using a spray gun set up. Applying a constant nitrogen pressure of 2 bar, the flow rate of the solution was set to about 15  $\mu$ l s<sup>-1</sup> by tuning the nozzle diameter accordingly. About 300  $\mu$ l of the respective solution were deposited on the substrate using 2 spray shots of 10 s duration with a short pause. 3D-printed masks were placed onto the substrates in order to create reproducible, detailed images. After the completed spray deposition, the substrates were immediately transferred to an imaging station. See Supplementary Methods for more details.

**Fluorescence spectroscopy.** Fluorescence spectroscopy was performed on a Jasco (Jasco FP-8300) spectrofluorimeter with an external temperature control (Jasco MCB-100). See Supplementary Methods for more details about Fmoc-, THT fluorescence and release assays.

**Cryo-TEM.** Cryo-TEM was performed on a Jeol JEM-1400 plus operating at 120 kV. See Supplementary Methods for more details.

**Circular dichroism spectroscopy.** Circular dichroism measurements were performed on a Jasco (Jasco J750) equipped with a Peltier temperature Control. See Supplementary Methods for more details.

**Confocal microscopy.** Confocal fluorescence microscopy was performed on a Leica SP5 confocal microscope using a  $\times 63$  oil immersion objective. Samples were prepared as described above, but with 2.5  $\mu$ M Nile Red as dye. Twenty microlitre of the sample was deposited on the glass slide and covered with a 12 mm diameter coverslip. Samples were excited with 543 nm laser and imaged at 580–700 nm.

**Data availability.** The data that support the findings of this study are available from the corresponding author upon reasonable request.

## References

1. Stupp, S. I. *et al.* Supramolecular materials: Self-organized nanostructures. *Science* **276**, 384–389 (1997).
2. Aida, T., Meijer, E. W. & Stupp, S. I. Functional supramolecular polymers. *Science* **335**, 813–817 (2012).

3. Silva, G. A. *et al.* Selective differentiation of neural progenitor cells by high-epitope density nanofibers. *Science* **303**, 1352–1355 (2004).
4. Weingarten, A. S. *et al.* Self-assembling hydrogel scaffolds for photocatalytic hydrogen production. *Nat. Chem.* **6**, 964–970 (2014).
5. Arazoe, H. *et al.* An autonomous actuator driven by fluctuations in ambient humidity. *Nat. Mater.* **15**, 1084–1089 (2016).
6. Boekhoven, J. & Stupp, S. I. Supramolecular materials for regenerative medicine. *Adv. Mater.* **26**, 1642–1659 (2014).
7. Hirst, A. R., Escuder, B., Miravet, J. F. & Smith, D. K. High-tech applications of self-assembling supramolecular nanostructured gel-phase materials: from regenerative medicine to electronic devices. *Angew. Chem. Int. Ed.* **47**, 8002–8018 (2008).
8. Balkenende, D. W., Monnier, C. A., Fiore, G. L. & Weder, C. Optically responsive supramolecular polymer glasses. *Nat. Commun.* **7**, 10995–11003 (2016).
9. Zhang, S. *et al.* A pH-responsive supramolecular polymer gel as an enteric elastomer for use in gastric devices. *Nat. Mater.* **14**, 1065–1071 (2015).
10. Heuser, T., Steppert, A.-K., Molano Lopez, C., Zhu, B. & Walther, A. Generic concept to program the time domain of self-assemblies with a self-regulation mechanism. *Nano Lett.* **15**, 2213–2219 (2014).
11. Williams, R. J. *et al.* Enzyme-assisted self-assembly under thermodynamic control. in *Nat. Nanotechnol.* **4**, 19–24 (2009).
12. Zhou, J., Du, X. & Xu, B. Regulating the rate of molecular self-assembly for targeting cancer cells. *Angew. Chem. Int. Ed.* **55**, 5770–5775 (2016).
13. Grzybowski, B. A., Wilmer, C. E., Kim, J., Browne, K. P. & Bishop, K. J. M. Self-assembly: from crystals to cells. *Soft Matter* **5**, 1110–1128 (2009).
14. Fialkowski, M. *et al.* Principles and implementations of dissipative (dynamic) self-assembly. *J. Phys. Chem. B* **110**, 2482–2496 (2006).
15. Pappas, C. G., Sasselli, I. R. & Ulijn, R. V. Biocatalytic pathway selection in transient tripeptide nanostructures. *Angew. Chem. Int. Ed.* **54**, 8119–8123 (2015).
16. Maiti, S., Fortunati, L., Ferrante, C., Scrimin, P. & Prins, L. J. Dissipative self-assembly of vesicular nanoreactors. *Nat. Chem.* **8**, 725–731 (2016).
17. Boekhoven, J., Hendriksen, W. E., Koper, G. J., Eelkema, R. & van Esch, J. H. Transient assembly of active materials fueled by a chemical reaction. *Science* **349**, 1075–1079 (2015).
18. Leira-Iglesias, J., Sorrenti, A., Sato, A., Dunne, P. A. & Hermans, T. M. Supramolecular pathway selection of peryleneimides mediated by chemical fuels. *Chem. Commun.* **52**, 9009–9012 (2016).
19. Klajn, R., Wesson, P. J., Bishop, K. J. & Grzybowski, B. A. Writing self-erasing images using metastable nanoparticle 'inks'. *Angew. Chem. Int. Ed.* **48**, 7035–7039 (2009).
20. Terech, P. & Weiss, R. G. *Molecular Gels, Materials with Self-Assembled Fibrillar Networks of Gels* (Springer, 2006).
21. Roy, S., Javid, N., Sečik, J., Halling, P. J. & Ulijn, R. V. Salt-induced control of supramolecular order in biocatalytic hydrogelation. *Langmuir* **28**, 16664–16670 (2012).
22. Newcomb, C. J. *et al.* Cell death versus cell survival instructed by supramolecular cohesion of nanostructures. *Nat. Commun.* **5**, 3321–3330 (2014).
23. Tantakitti, F. *et al.* Energy landscapes and functions of supramolecular systems. *Nat. Mater.* **15**, 469–476 (2016).

### Acknowledgements

This work was supported by the Technische Universität München – Institute for Advanced Study, funded by the German Excellence Initiative and the European Union Seventh Framework Programme under grant agreement n° 291763 and the International Research Training Group ATUMS (IRTG 2022). A.R.B., P.M.B. and F.C.L. acknowledge funding by the Nanosystems Initiative Munich (NIM). A.R.B. and O.L. acknowledge funding by Deutsche Forschungsgemeinschaft within the SFB No. 863. M.T.S. acknowledges the European Union's Horizon 2020 Research and Innovation program for the Marie Skłodowska Curie Fellowship under grant agreement n° 747007.

### Author contributions

M.T.S., B.R. and J.B. designed and performed experiments, analysed the data and wrote the manuscript. R.G., F.C.L., C.W., B.K., performed experiments, analysed the data and provided discussion. O.L., A.R.B. and P.M.B. provided discussion. J.B. supervised the research.

### Additional information

**Supplementary Information** accompanies this paper at <http://www.nature.com/naturecommunications>

**Competing interests:** The authors declare no competing financial interests.

**Reprints and permission** information is available online at <http://npg.nature.com/reprintsandpermissions/>

**How to cite this article:** Tena-Solsona, M. *et al.* Non-equilibrium dissipative supramolecular materials with a tunable lifetime. *Nat. Commun.* **8**, 15895 doi: 10.1038/ncomms15895 (2017).

**Publisher's note:** Springer Nature remains neutral with regard to jurisdictional claims in published maps and institutional affiliations.



**Open Access** This article is licensed under a Creative Commons Attribution 4.0 International License, which permits use, sharing, adaptation, distribution and reproduction in any medium or format, as long as you give appropriate credit to the original author(s) and the source, provide a link to the Creative Commons license, and indicate if changes were made. The images or other third party material in this article are included in the article's Creative Commons license, unless indicated otherwise in a credit line to the material. If material is not included in the article's Creative Commons license and your intended use is not permitted by statutory regulation or exceeds the permitted use, you will need to obtain permission directly from the copyright holder. To view a copy of this license, visit <http://creativecommons.org/licenses/by/4.0/>

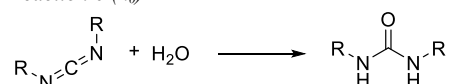
© The Author(s) 2017



**Supplementary Note 1.** In chemical reaction networks that use E (glutamic acid) as a precursor, we found significant N-acyl urea side product. Although that did not affect material properties, it did accumulate as the cycle progressed. The amount of N-Acyl urea we found was never greater than 2% of the amount of EDC added. For instance, after the addition of 10 mM fuel to 10 mM solution of precursor the N-acyl urea detected for Fmoc-E was 2%. The percentage of N-acyl urea was less than 0.5% for Fmoc-AAE and less than 0.1% for Fmoc-AVE.

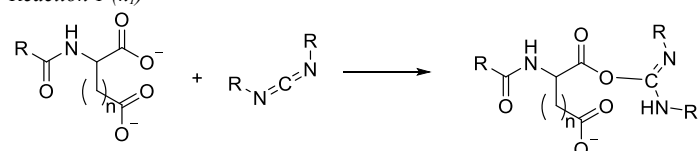
**Supplementary Note 2.** A kinetic model was written using Matlab in which the reactions below were described. The concentrations of each reactant were calculated for every 1 second in the cycle.

*Reaction 0 ( $k_0$ )*



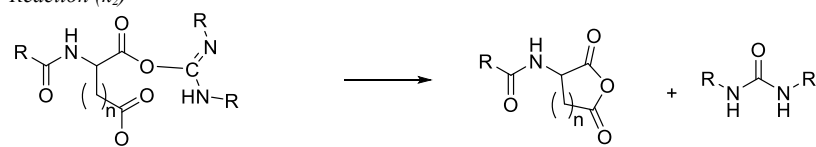
Direct hydrolysis of carbodiimide with a first order rate constant of  $1.3 \times 10^{-5} \text{ sec}^{-1}$  as determined by HPLC (See Supplementary Figure 1c) and implies that in most experiments, this reaction is irrelevant.

*Reaction 1 ( $k_1$ )*



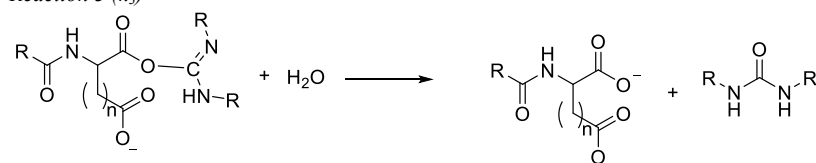
Formation of O-acylisourea by reaction with EDC. This second order rate constant was dependent on the nature of the precursor. The rate constant was determined for each precursor by HPLC, by monitoring the EDC consumption.

*Reaction ( $k_2$ )*



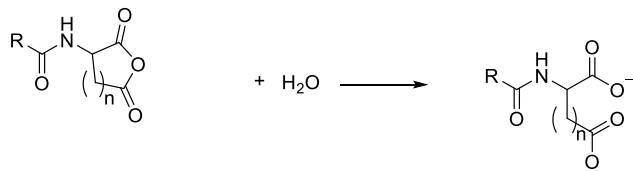
Formation of anhydride with a first order rate constant. This rate constant could not be determined because the O-acylisourea was never observed. It was therefore set to be twice the rate of  $k_1$ . As a result, the O-acylisourea did never reach concentrations over 1  $\mu\text{M}$  in the model.

*Reaction 3 ( $k_3$ )*



Direct hydrolysis of O-acylisourea (unwanted side reaction). This reaction rate could not be obtained because the O-acylisourea was not observed. The ratio of  $k_2$  and  $k_3$  (anhydride formation and competing direct hydrolysis of O-acylisourea) was varied to fit the HPLC data for several concentration of  $[\text{fuel}]_0$  and  $[\text{di-acid}]_0$ .

Reaction 4 ( $k_4$  and  $k_5$ )



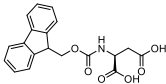
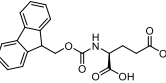
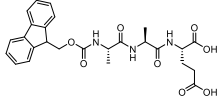
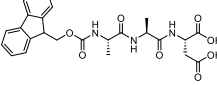
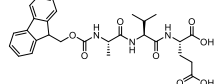
Hydrolysis of anhydride proceeded with a (pseudo)-first order rate as determined by HPLC. We found that for Fmoc-D, this rate was slowed down two orders of magnitude if assemblies were formed. When small amounts of fuel were added and no assemblies were formed, the HPLC data could be fitted with  $k_4$ . However, when a greater batch of fuel was added (3mM or more), we could not fit the data and had to implement a 1<sup>st</sup> order  $k_5$  for the hydrolysis reaction in the models that acts when the concentration anhydride was  $>0.08$  mM. In other words, the assemblies exerted negative feedback on their own degradation (they slowed down hydrolysis).

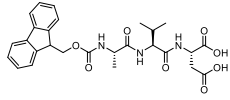
For Fmoc-E, similar behavior was found. At low fuel concentrations, the model could fit the data well with  $k_4$ . As soon as we added 5 mM or more fuel, the concentration anhydride reached values higher than 0.13 mM and the data could not be fit. Here, the behavior was somewhat different than for Fmoc-D. We needed to implement a 0<sup>th</sup> order  $k_5$  that only acted when the concentration anhydride was  $> 0.13$  mM in order to fit the data well. This can be rationalized by a mechanism where the assemblies exclude water from the anhydrides, protecting them from degradation. They do that such that hydrolysis is limited by the solubility of the anhydride.

Supplementary Table 1: Table of k values used in kinetic model

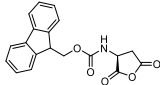
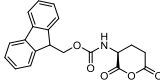
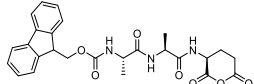
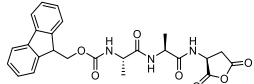
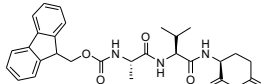
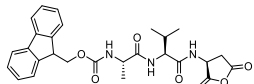
	$k_1$ ( $M^{-1} \times \text{sec}^{-1}$ )	$k_2$	$k_3$	$k_4$ ( $\text{sec}^{-1}$ )	Half-life of anhydride (calculated by: $\ln(2)/k_4$ )	$k_5$ ( $M \times \text{sec}^{-1}$ )	Half-life of anhydride (calculated by: $\ln(2)/k_5$ )
<i>Order</i>	2 <sup>nd</sup>	1 <sup>st</sup>	1 <sup>st</sup>	1 <sup>st</sup>		0 <sup>th</sup> or 1 <sup>st</sup>	
Fmoc-D	$1.2 \times 10^{-1}$	$2 * k_1$	$4.0 * k_1$	$1.4 \times 10^{-2}$	$t_{1/2} = 0.8$ min	$3.8 \times 10^{-4}$ (1 <sup>st</sup> order)	$t_{1/2} = 30$ min
Fmoc-AVD	$2.0 \times 10^{-1}$	$2 * k_1$	$2.5 * k_1$	$3.8 \times 10^{-2}$	$t_{1/2} = 0.3$ min	NA	NA
Fmoc-AAD	$0.95 \times 10^{-1}$	$2 * k_1$	$2.5 * k_1$	$2.8 \times 10^{-2}$	$t_{1/2} = 0.4$ min	NA	NA
Fmoc-E	$0.50 \times 10^{-1}$	$2 * k_1$	$2.0 * k_1$	$0.75 \times 10^{-2}$	$t_{1/2} = 1.5$ min	$1.5 \times 10^{-6}$ (0 <sup>th</sup> order)	NA Depends on [anhydride]
Fmoc-AVE	$1.5 \times 10^{-1}$	$2 * k_1$	$2.5 * k_1$	$1.1 \times 10^{-2}$	$t_{1/2} = 1.1$ min	NA	NA
Fmoc-AAE	$0.40 \times 10^{-1}$	$2 * k_1$	$2.9 * k_1$	$1.3 \times 10^{-2}$	$t_{1/2} = 0.9$ min	NA	NA

Supplementary Table 2: Characterization of precursors

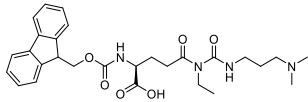
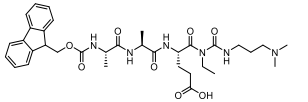
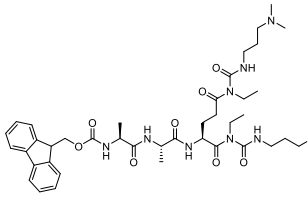
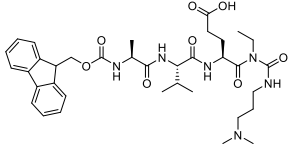
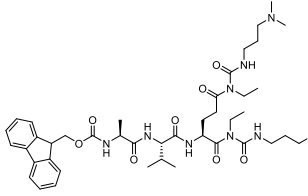
name	purity [%]	structure	mass calculated [g/mol]	mass found [g/mol]	retention time [min]
Fmoc-D	Commercial: 95%		Mw = 355.11 C <sub>19</sub> H <sub>17</sub> NO <sub>6</sub>	378.1 [Mw+Na] <sup>+</sup>	6.13
Fmoc-E	Commercial: 95%		Mw = 369.12 C <sub>20</sub> H <sub>19</sub> NO <sub>6</sub>	392.1 [Mw+Na] <sup>+</sup>	6.14
Fmoc-AAE	97		Mw = 511.20 C <sub>26</sub> H <sub>29</sub> N <sub>3</sub> O <sub>8</sub>	534.2 [Mw+Na] <sup>+</sup>	5.64
Fmoc-AAD	98		Mw = 497.18 C <sub>25</sub> H <sub>27</sub> N <sub>3</sub> O <sub>8</sub>	520.3 [Mw+Na] <sup>+</sup>	5.62
Fmoc-AVE	98		Mw = 539.23 C <sub>28</sub> H <sub>33</sub> N <sub>3</sub> O <sub>8</sub>	562.2 [Mw+Na] <sup>+</sup>	6.21

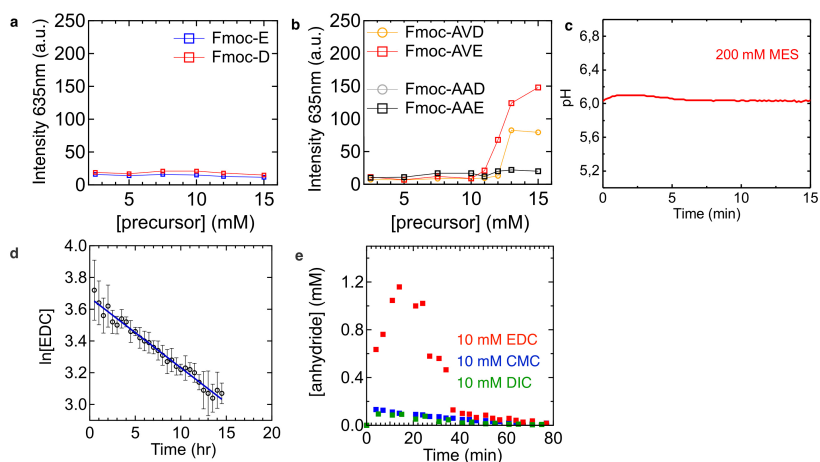
name	purity [%]	structure	mass calculated [g/mol]	mass found [g/mol]	retention time [min]
Fmoc-AVD	99		Mw = 525.21 C <sub>27</sub> H <sub>31</sub> N <sub>3</sub> O <sub>8</sub>	548.2 [Mw+Na] <sup>+</sup>	6.21

**Supplementary Table 3: Characterization of main products of the chemical reaction network**

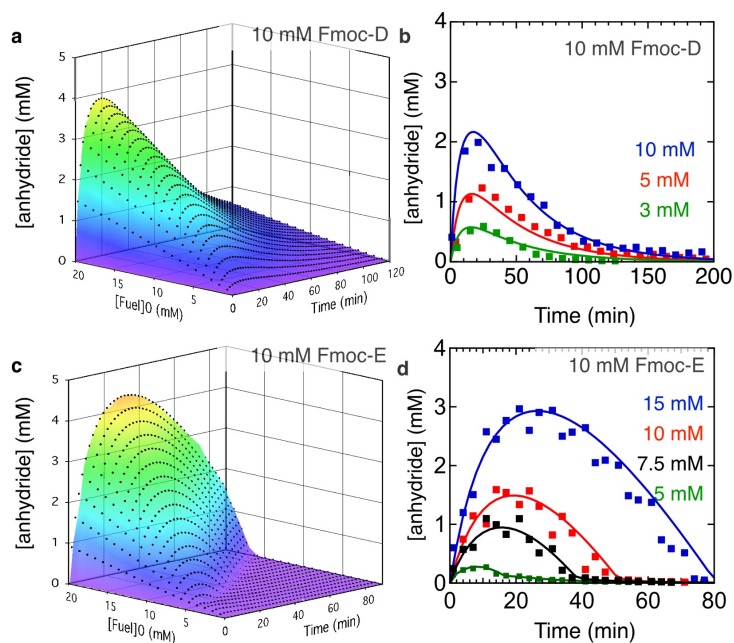
name	structure	mass calculated [g/mol]	mass found [g/mol]	retention time [min]
Fmoc-D-anhydride		Mw = 337.10 C <sub>19</sub> H <sub>15</sub> NO <sub>5</sub>	360.0 [Mw+Na] <sup>+</sup>	7.88
Fmoc-E-anhydride		Mw = 351.11 C <sub>20</sub> H <sub>17</sub> NO <sub>5</sub>	373.9 [Mw+Na] <sup>+</sup>	7.68
Fmoc-AAE-anhydride		Mw = 493.18 C <sub>26</sub> H <sub>27</sub> N <sub>3</sub> O <sub>7</sub>	516.2 [Mw+Na] <sup>+</sup>	6.68
Fmoc-AAD-anhydride		Mw = 479.17 C <sub>25</sub> H <sub>25</sub> N <sub>3</sub> O <sub>7</sub>	502.1 [Mw+Na] <sup>+</sup>	6.93
Fmoc-AVE-anhydride		Mw = 521.22 C <sub>25</sub> H <sub>25</sub> N <sub>3</sub> O <sub>7</sub>	544.3 [Mw+Na] <sup>+</sup>	7.32
Fmoc-AVD-anhydride		Mw = 507.20 C <sub>27</sub> H <sub>29</sub> N <sub>3</sub> O <sub>7</sub>	530.2 [Mw+Na] <sup>+</sup>	7.54

Supplementary Table 4: Characterization of the side products of the chemical reaction network

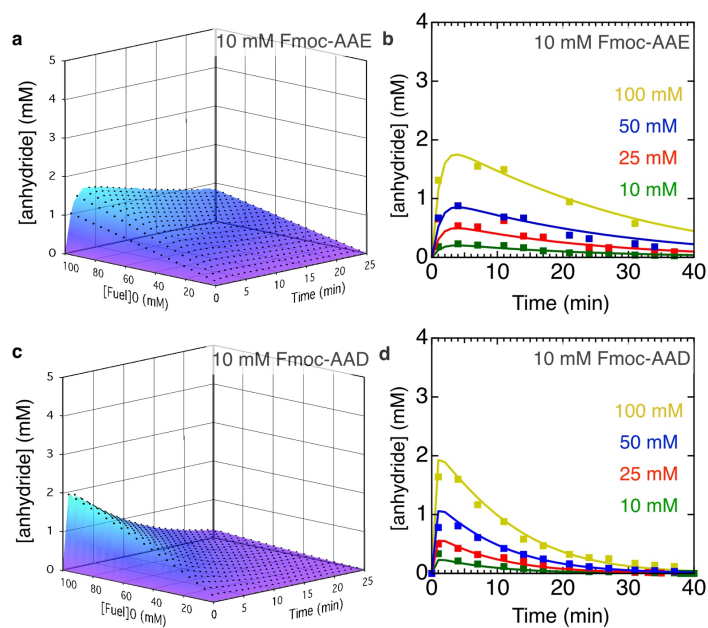
Name	side product	mass calculated [g/mol]	mass found [g/mol]	retention time [min]
Fmoc-E-N-acyl-urea		Mw = 524.26 C <sub>28</sub> H <sub>36</sub> N <sub>4</sub> O <sub>6</sub>	525.5 [Mw+H]	6.97
Fmoc-AAE-N-acyl-urea-1		Mw = 666.33 C <sub>34</sub> H <sub>46</sub> N <sub>6</sub> O <sub>8</sub>	667.4 [Mw+H]	6.52
Fmoc-AAE-N-acyl-urea-2		Mw = 821.48 C <sub>42</sub> H <sub>63</sub> N <sub>9</sub> O <sub>8</sub>	822.2 [Mw+H]	6.60
Fmoc-AVE-N-acyl-urea-1		Mw = 694.37 C <sub>36</sub> H <sub>50</sub> N <sub>6</sub> O <sub>8</sub>	695.5 [Mw+H] <sup>+</sup>	6.84
Fmoc-AVE-N-acyl-urea-2		Mw = 849.51 C <sub>44</sub> H <sub>67</sub> N <sub>9</sub> O <sub>8</sub>	850.6 [Mw+H] <sup>+</sup>	7.12



**Supplementary Figure 1. Buffer stability, background hydrolysis of fuel and responses of Fmoc-E to different fuels.** **a, b,** Nile Red fluorescence intensity at 635 nm against concentration precursor. The intensity of the solvatochromic dye serves as an indication for self-assembly and was not observed for concentrations below 15 mM Fmoc-D or Fmoc-E (**a**), or below a concentration of 12 mM for Fmoc-AVD, Fmoc-AVE, Fmoc-AAD or Fmoc-AAE (**b**). **c,** pH against time of a solution of 10 mM Fmoc-AVE as precursor in response to 50 mM EDC. **d,** Natural logarithm of concentration profiles of 40 mM EDC in MES buffer. A linear fit (black line) gave a  $k_0$ -value  $1.3 \times 10^{-5} \text{ sec}^{-1}$ . Error bars represent the standard deviation ( $n=3$ ). **e,** Concentration profiles of chemical reaction networks with 10 mM Fmoc-E as precursor and 10 mM of fuel (EDC, CMC or DIC). All fuels yielded the Fmoc-E anhydride transiently. EDC gave the highest relative yield and our studies therefore focus on this fuel.

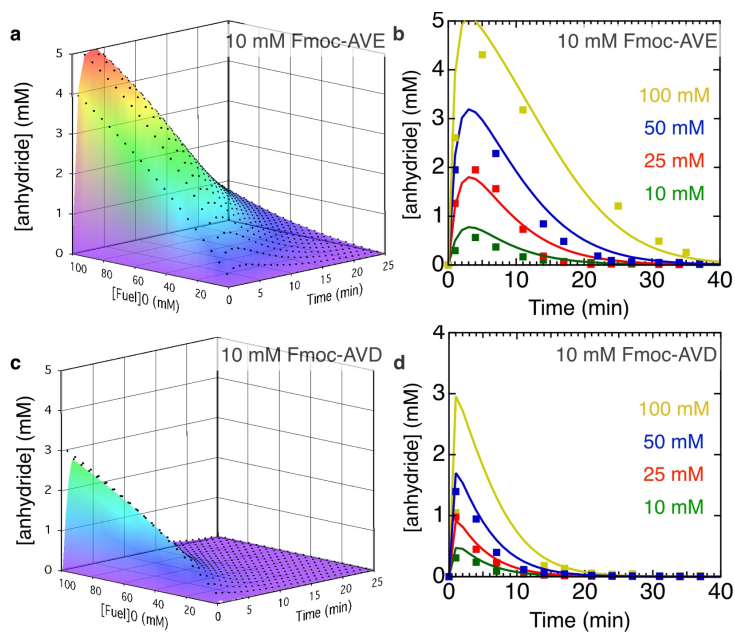


**Supplementary Figure 2: Kinetic traces of Fmoc-D and Fmoc-E with EDC.** *a*, Concentration profiles of chemical reaction network with 10 mM Fmoc-D as precursor and varying concentrations of fuel. The black markers represent the calculated concentration using the kinetic model, the planes represent interpolations between the model data. *b*, 2D plot of the data shown in *a* for 3, 5 and 10 mM of fuel with corresponding HPLC data. *c*, Concentration profiles of chemical reaction network with 10 mM Fmoc-E as precursor and varying concentrations of fuel in 3D plot. Colored plane is the data from the kinetic model. *d*, 2D plot of the data shown in *c* for 5, 7.5, 10 and 15 mM of fuel with corresponding HPLC data. All experiments were performed at 25°C with 10 mM precursor in 200 mM MES at pH6.

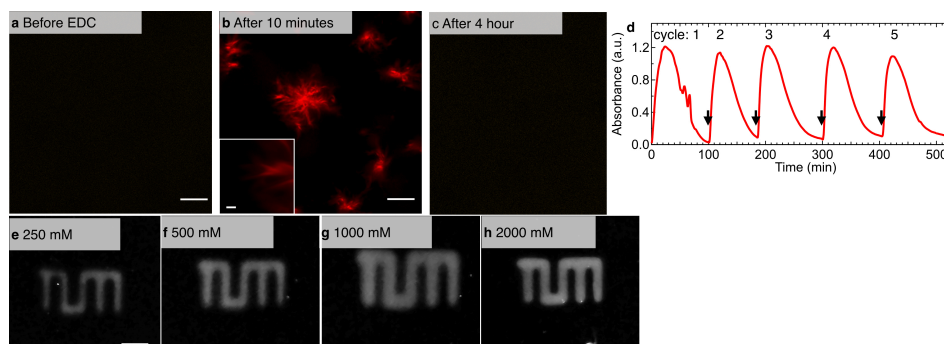


**Supplementary Figure 3: Kinetic traces of Fmoc-AAE and Fmoc-AAD with EDC.** *a*, Concentration profiles of chemical reaction network with 10 mM Fmoc-AAE as precursor and varying concentrations of fuel. The black markers represent the calculated concentration using the kinetic model, the planes represent interpolations between the model data. *b*, 2D plot of the data shown in *a* for 10, 25, 50 and 100 mM of fuel with corresponding HPLC data. *c*, Concentration profiles of chemical reaction network with 10 mM Fmoc-AAD as precursor and varying concentrations of fuel in 3D plot. Colored plane is the data from the kinetic model. *d*, 2D plot of the data shown in *c* for 10, 25, 50 and 100 mM of fuel with corresponding HPLC data. All experiments were performed at 25°C with 10 mM precursor in 200 mM MES at pH6.

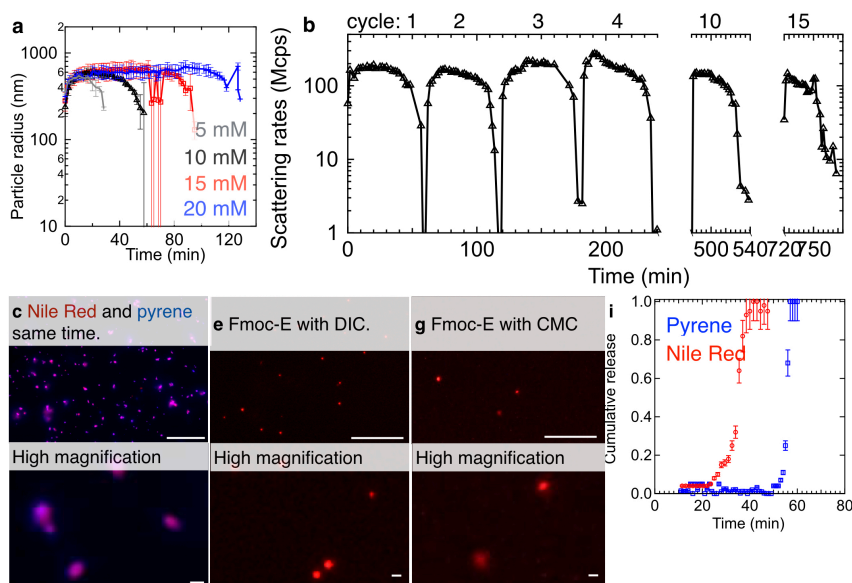




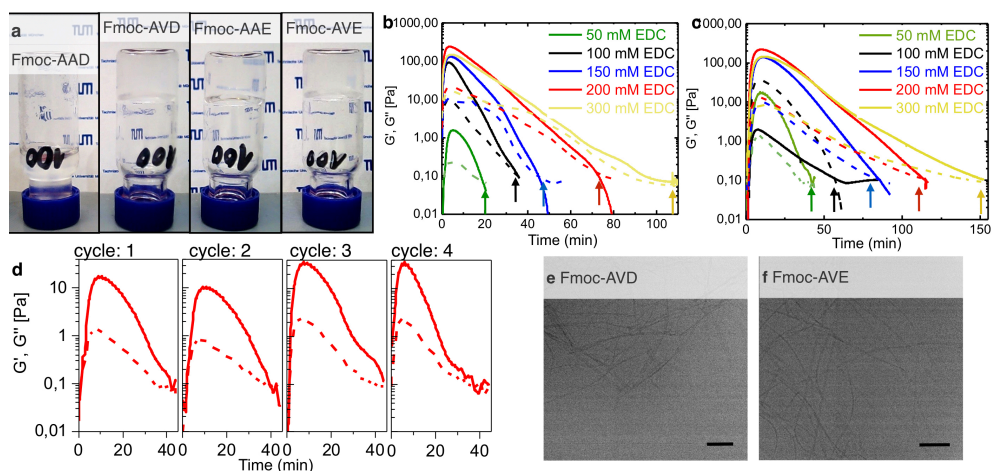
**Supplementary Figure 4: Kinetic traces of Fmoc-AVE and Fmoc-AVD with EDC.** *a*, Concentration profiles of chemical reaction network with 10 mM Fmoc-AVE as precursor and varying concentrations of fuel. The black markers represent the calculated concentration using the kinetic model, the planes represent interpolations between the model data. *b*, 2D plot of the data shown in *a* for 10, 25, 50 and 100 mM of fuel with corresponding HPLC data. *c*, Concentration profiles of chemical reaction network with 10 mM Fmoc-AVD as precursor and varying concentrations of fuel in 3D plot. Colored plane is the data from the kinetic model. *d*, 2D plot of the data shown in *c* for 10, 25, 50 and 100 mM of fuel with corresponding HPLC data. Note the missing HPLC data for 100 mM of fuel between 3 and 12 minutes. Data acquisition was not possible for these time points as a result of the stiff gels formed. All experiments were performed at 25°C with 10 mM precursor in 200 mM MES at pH6.



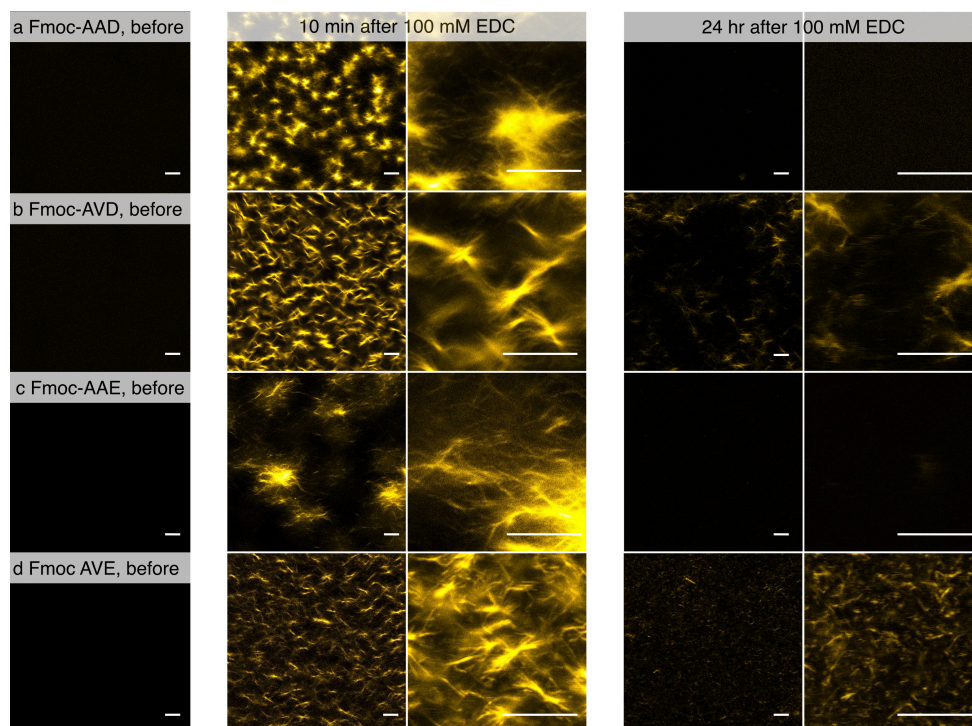
**Supplementary Figure 5: Characterization of Fmoc-D in response to EDC.** Micrographs of solutions of 10 mM Fmoc-D combined with 10 mM EDC and 2.5  $\mu$ M Nile Red, **a**, before addition of EDC, **b**, after 10 minutes, and **c**, after 4 hours (scale bars represent 10  $\mu$ m, 1  $\mu$ m for the inset). **d**, Absorbance at 600 nm as an indication of turbidity against time. 5 mM of fuel was added at each step indicated by arrows. **e-h**, Photographs of sprayed solutions with varying concentrations of fuel (scale bar represents 1 cm).



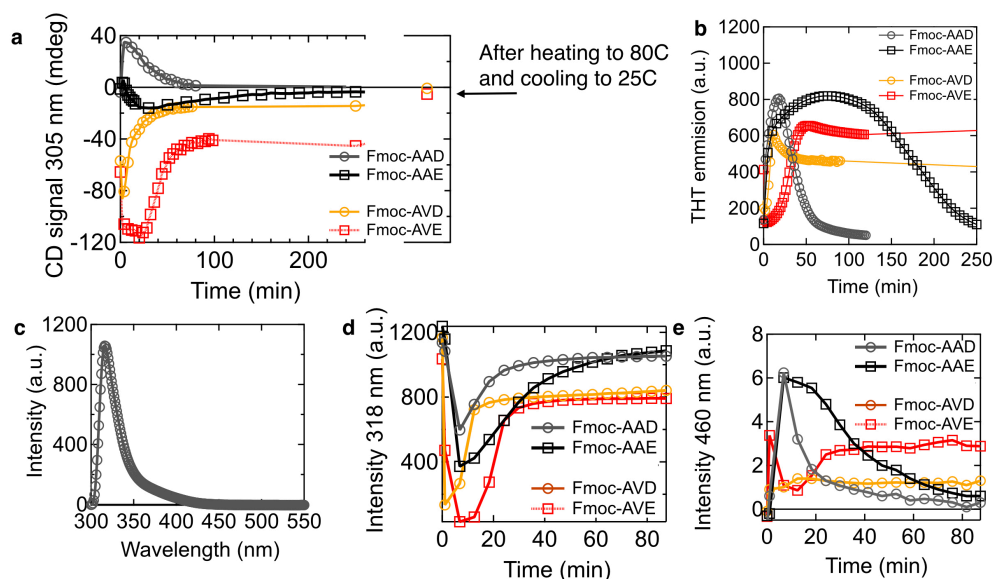
**Supplementary Figure 6: Characterization of Fmoc-E in response to fuels.** **a**, Hydrodynamic radii as determined by DLS as a function of time for various initial fuel concentration. The error bars represent the standard deviation ( $n=2$ ). **b**, DLS scattering intensity against time for four repetitive cycles of 10 mM EDC against time. New fuel was added every 60 minutes. **c**, Micrographs of solutions of 10 mM Fmoc-E with 10 mM EDC and 2.5  $\mu$ M Nile Red and 2.5  $\mu$ M pyrene as dyes. Both pyrene and Nile Red were present from the beginning of the cycle. The scale bars represent 25  $\mu$ m and 1  $\mu$ m for the lower and higher magnification respectively. **d**, **e**, Micrographs of solutions of 10 mM Fmoc-E with 50 mM DIC (**d**) or with 50 mM CMC (**e**) and 25  $\mu$ M Nile Red. The scale bars represent 25  $\mu$ m and 1  $\mu$ m for the lower and higher magnification respectively. **f**, Release profiles of pyrene (blue markers) and Nile Red (red markers) of the particle described in Figure 4e. Data collection was started 10 minutes after addition of EDC. All error bars represent the standard deviation ( $n=2$ ).



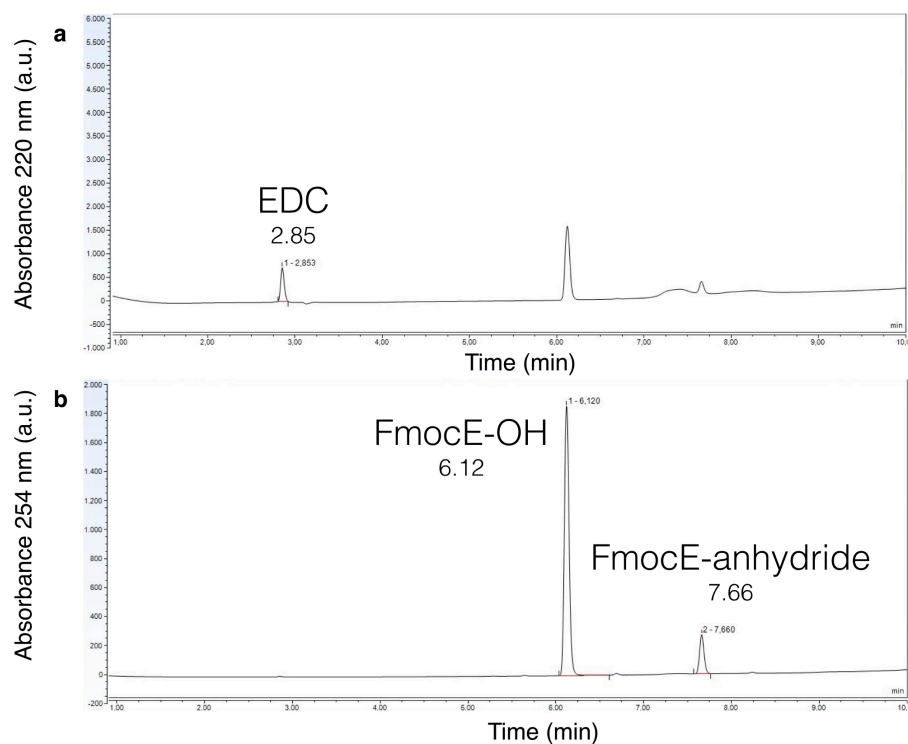
**Supplementary Figure 7: Characterization of self-assembly of Fmoc-tripeptides in response to EDC.** *a*, Photographs of gels of tripeptides 10 minutes after addition of 100 mM of fuel. *b*, *c*, Representative rheology time sweeps of gels formed by 10 mM Fmoc-AAD and Fmoc-AAE respectively using different EDC concentrations ranging from 50 to 300 mM. Solid lines represent the storage modulus ( $G'$ ), dashed line represents the loss modulus ( $G''$ ), arrows indicated the crossover point. *d*, Rheology time sweeps of gels formed by 10 mM of Fmoc-AAE and 4 cycles of 50 mM EDC addition. Gels were prepared in a separate container and placed between the two plates immediately after a new fuel addition. Fuel addition was performed every 12 hours. *e*, *f*, Cryo-TEM images for Fmoc-AVD and Fmoc-AVE 24 hour after addition of fuel (scale bars represent 100 nm).



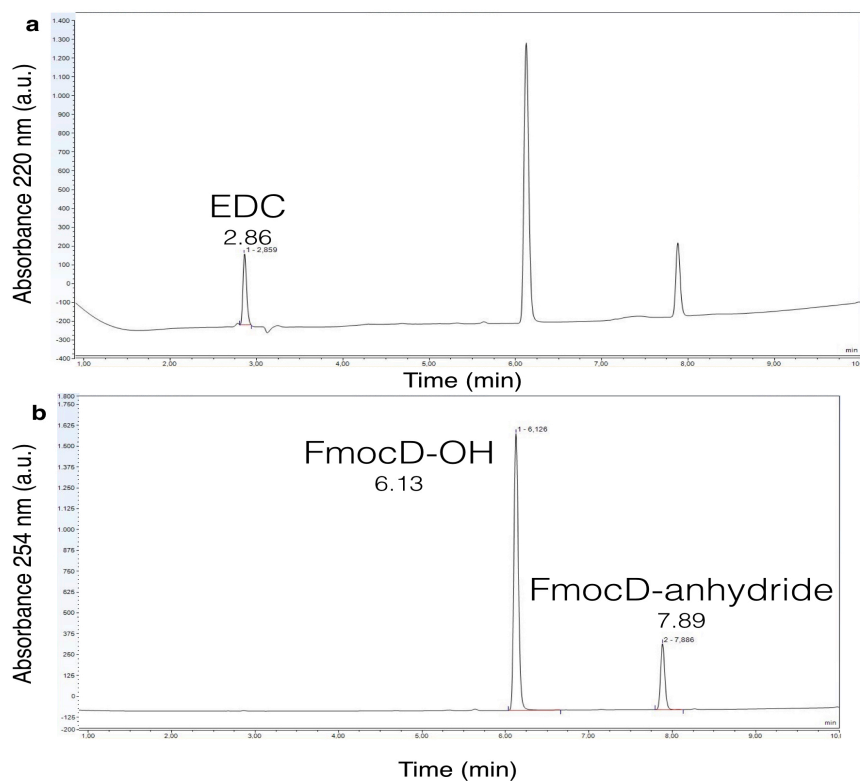
**Supplementary Figure 8: Confocal micrographs of Fmoc-AA and Fmoc-AV series in response to EDC. a, Fmoc-AAD, b, Fmoc-AVD, c, Fmoc-AAE and d, Fmoc-AVE before, 10 minutes and 24 hours after addition of 100 mM EDC. All scale bars are 10  $\mu$ m.**



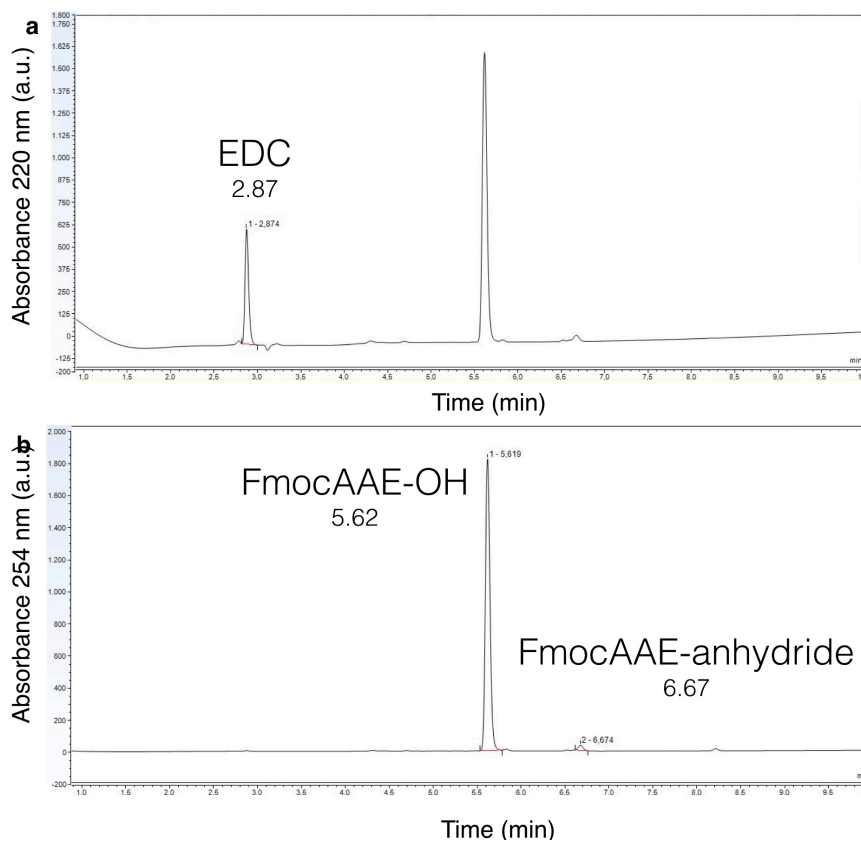
**Supplementary Figure 9: Spectroscopic characterization of self-assembly of Fmoc-tripeptides in response to EDC.** **a**, CD spectroscopy signal at 305 nm as an indication of self-assembly (pathlength is 1 mm). Note that the Fmoc-AV series remains in an assembled state, due to kinetic trapping within the assemblies. Only after heating and cooling is the original level obtained. **b**, THT intensity at 485 nm against time as a measure for the presence of  $\beta$ -sheets in the self-assembled fibers. **c**, Fluorescence emission spectrum of the Fmoc-AAD at 10 mM (excitation wavelength 285 nm). **d**, **e**, Fluorescence emission intensity at 318 nm and 460 nm respectively against time (excitation wavelength 285 nm). Note that the signal at 318 nm (corresponding to the monomeric fluorenyl group) initially decreases while the signal at 460 nm (corresponding to fluorenyl excimer) increases upon the self-assembly. Both trends demonstrate the aromatic interaction in the assembly process. Again, the Fmoc-AAX recovers to values at similar to those at the beginning of the cycle, while the Fmoc-AVX tripeptides remain trapped.



**Supplementary Figure 10: Representative HPLC traces of Fmoc-E after EDC addition.** HPLC traces of 10 mM Fmoc-E after 11 minutes of EDC addition (10 mM). EDC consumption was monitored at 220 nm (a) while changes in precursor and anhydride concentration were monitored at 254 nm (b). Chromatogram represents a linear gradient water: ACN from 40:60 to 2:98.

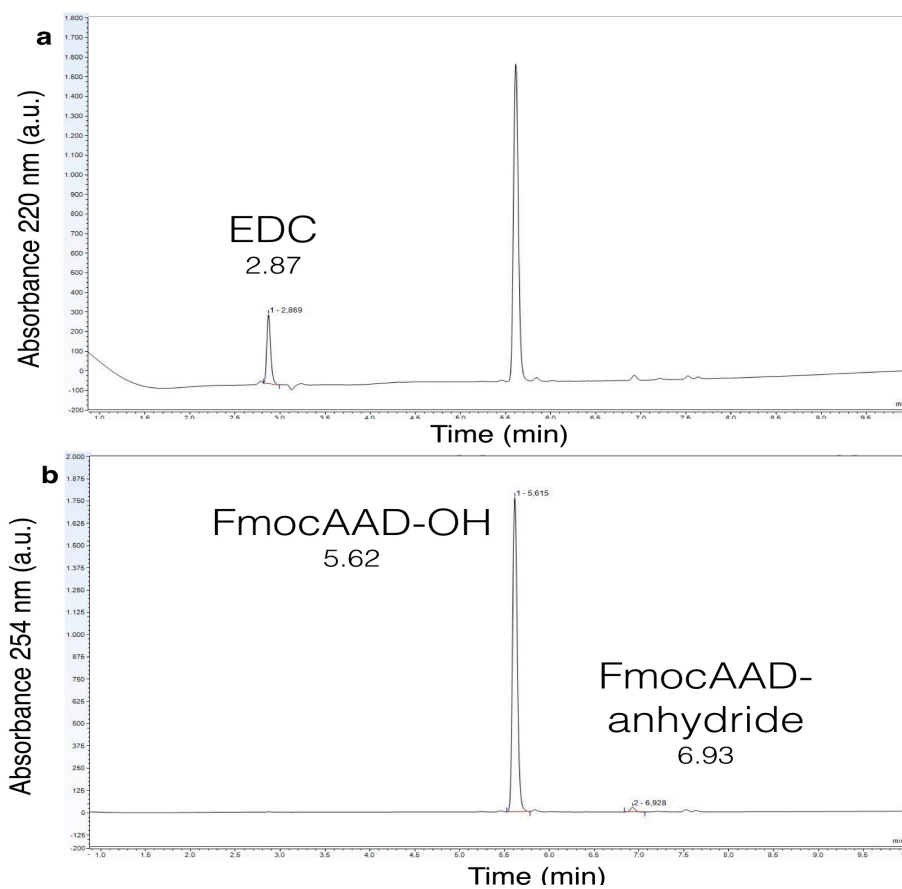


**Supplementary Figure 11: Representative HPLC traces of Fmoc-D after EDC addition.** HPLC traces of 10 mM Fmoc-D after 11 minutes of EDC addition (10 mM). EDC consumption was monitored at 220 nm (a) while changes in precursor and anhydride concentration were monitored at 254 nm (b). Chromatogram represents a linear gradient water: ACN from 40:60 to 2:98.

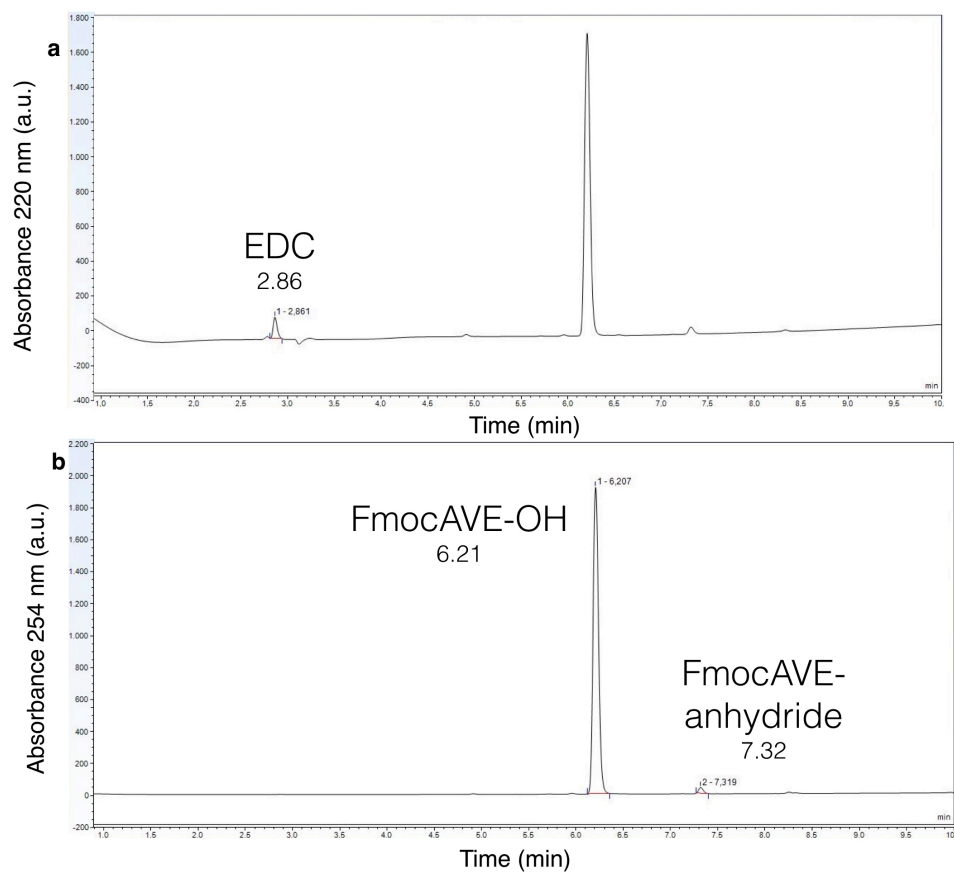


**Supplementary Figure 12: Representative HPLC traces of Fmoc-AAE after EDC addition.** HPLC traces of 10 mM Fmoc-AAE after 11 minutes of EDC addition (10 mM). EDC consumption was monitored at 220 nm (a) while changes in precursor and anhydride concentration were monitored at 254 nm (b). Chromatogram represents a linear gradient water: ACN from 40:60 to 2:98.

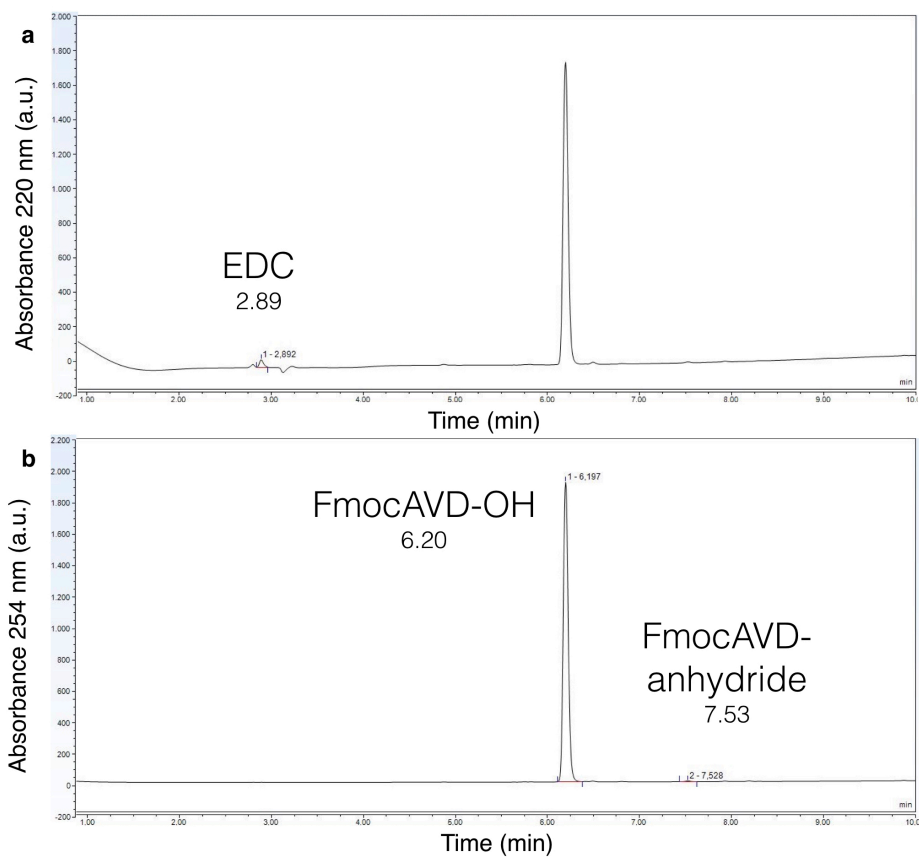




**Supplementary Figure 13: Representative HPLC traces of Fmoc-AAD after EDC addition.** HPLC traces of 10 mM Fmoc-AAD after 11 minutes of EDC addition (10 mM). EDC consumption was monitored at 220 nm (a) while changes in precursor and anhydride concentration were monitored at 254 nm (b). Chromatogram represents a linear gradient water: ACN from 40:60 to 2:98.



**Supplementary Figure 14: Representative HPLC traces of Fmoc-AVE after EDC addition.** HPLC traces of 10 mM Fmoc-AVE after 11 minutes of EDC addition (10 mM). EDC consumption was monitored at 220 nm (**a**) while changes in precursor and anhydride concentration were monitored at 254 nm (**b**). Chromatogram represents a linear gradient water: ACN from 40:60 to 2:98.



**Supplementary Figure 15: Representative HPLC traces of Fmoc-AVD after EDC addition.** HPLC traces of 10 mM Fmoc-AVD after 11 minutes of EDC addition (10 mM). EDC consumption was monitored at 220 nm (a) while changes in precursor and anhydride concentration were monitored at 254 nm (b). Chromatogram represents a linear gradient water: ACN from 40:60 to 2:98.

## Supplementary Methods

**Peptide synthesis and purification.** All peptides were synthesized using standard fluoren-9-ylmethoxycarbonyl (Fmoc) solid-phase peptide synthesis on Wang resin (100-200 mesh, 1.1 mmol/g loading). Synthesis was performed on a CEM Liberty microwave-assisted peptide synthesizer. The first amino acid coupling to the resin was accomplished by using symmetrical anhydride methodology. Briefly, a 0.2 M solution of the Fmoc-amino acid symmetrical anhydride was prepared by allowing the corresponding Fmoc-protected amino acid (FmocE(OtBu)OH or FmocD(OtBu)OH, 12 mmol) and N,N'-diisopropylcarbodiimide (DIC, 6 mmol) to react in 30 mL N,N-dimethylformamide (DMF) for 40 min. The solution was placed in the freezer for 15 min and the solid urea formed was filtered out before next step. Loading of the resin was performed using the automated peptide synthesizer. The symmetrical anhydride solution (0.2 M, 12 mL) and 4-(dimethylamino)pyridine (DMAP) solution in DMF (20 mM, 2.5 mL) were added to the pre-swollen Wang resin (0.5 mmol, 1.1 mmol/g) and heated in the microwave (30 min, 75 °C). The coupling was repeated twice. The resin was then washed with DMF (2x10 mL). Following couplings were achieved using 4 equivalents (eq.) of Fmoc-protected amino acid in DMF, 4 eq. of DIC and 4 eq. of ethyl (hydroxyimino)cynoacetate (Oxyma). The resin solution was then heated in the microwave (1x2 min, 90°C). Fmoc removal was accomplished using a solution of 20% piperidine in DMF (1x2 min, 90°C). The resin was washed with DMF (3x7 mL) between different steps. Tripeptides were cleaved from the resin using a mixture of 95% trifluoroacetic acid (TFA), 2.5% water, and 2.5% triisopropylsilane (TIPS). The solvent was removed by co-distillation with ether by rotary evaporation and dried under reduced pressure. The product was purified using reversed-phase high-performance liquid chromatography (HPLC, Thermofisher Dionex Ultimate 3000, Hypersil Gold 250x4.8 mm) in a linear gradient of acetonitrile (ACN, 40% to 98%) and water with 0.1% TFA. Purified product was lyophilized and stored at -20 °C until further use. The purity of the tripeptides was analysed by electrospray ionization mass spectrometry in positive mode (ESI-MS) as well as analytical HPLC (Thermofisher Dionex Ultimate 3000, eluted with a gradient of 0.1% TFA in water: ACN from 40:60 to 2:98 in 10 min, see below for results).

**Sample preparation.** Stock solutions of the precursor were prepared by dissolving the precursor in 200 mM MES buffer, after which the pH was adjusted to pH 6.0. Stock solutions of EDC were prepared by dissolving the EDC powder in MQ water. Typically, stock solutions of 1.0 M EDC were used freshly. Reaction networks were started by addition of the high concentration EDC to the peptide solution.

**HPLC.** The kinetics of the chemical reaction networks were monitored over time by means of analytical HPLC (HPLC, Thermofisher Dionex Ultimate 3000, Hypersil Gold 250 x 4.8 mm). A 750  $\mu$ L sample was prepared as described above and placed into a screw cap HPLC vial. Every 10 minutes, samples of these solutions were directly injected without further dilution, and all compounds involved were separated using a linear gradient water: ACN from 40:60 to 2:98. In order to avoid aggregation problems during the injection, samples of Fmoc-D were continuously stirred. In the case of the gelators, gels were just slightly broken manually by shaking the vial before the injection took place.

Calibration curves for fuels ( $\lambda = 220$  nm) and precursors ( $\lambda = 254$  nm) were performed in triplicate in order to quantify the compounds over time. Calibration was not possible for the anhydrides due to their intrinsic instability. Instead, the absorption coefficient of their corresponding precursor was used. Measurements were performed at 25 °C.

**UV/Vis Spectroscopy.** The UV/Vis measurements were carried out using a Genesys 10S (ThermoFisher) UV-VIS spectrophotometer. Samples were prepared as described above and placed in a 10 mm quartz cell (HellmaAnalytics) and stirred while acquiring data. Data was measured at 600 nm with an interval of 7 seconds.

**DLS.** DLS measurements on Fmoc-E solutions were performed using a DynaPro NanoStar from Wyatt with a laser wavelength of 658 nm. The MES buffered samples were measured using the disposable cuvette for DLS from Wyatt. Each measurement consisted of 5 acquisitions with an acquisition time of 10 s. For measurements and analysis the software Dynamics V7 was used. Measurements were performed at 25 °C.

**Rheology.** Rheological measurements were carried out on a stress controlled rheometer (MCR 302, Anton Paar, Graz, Austria) using a plate-plate geometry (PP25, Anton Paar, Graz, Austria) and a plate separation of 0.3 mm. Samples were prepared as previously mentioned and placed between the two plates. Frequency and strain values were fixed to 1 Hz and 10 % respectively. A solvent trap was placed around the sample holder to avoid evaporation. Data was recorded at 25 °C. The reusability experiments were performed by first preparing gels in an Eppendorf tube and, after at least 24 hours, the second, third or fourth gel was prepared in the rheometer using the above described procedure.

**Confocal Fluorescence Microscopy.** Confocal fluorescence microscopy was performed on a Leica SP5 confocal microscope using a 63x oil immersion objective. Samples were prepared as described above, but with 25  $\mu$ M Nile Red as dye. 20  $\mu$ L of the sample was deposited on the glass slide and covered with a 12mm diameter coverslip. Samples were excited with 543 nm laser and imaged at 580-700 nm.

**Fluorescence Microscopy.** For samples that used both Nile Red and Pyrene as dye, we used conventional fluorescence microscopy. Sample preparation was performed as described above and micrographs were acquired on a Leica DMi8 microscope using a 100x oil immersion objective.

**Fluorescence Spectroscopy.** Fluorescence spectroscopy was performed on a Jasco (Jasco FP-8300) spectrofluorimeter with an external temperature control (Jasco MCB-100).

In order to measure the cumulative release of Nile Red and pyrene, we used the solvatochromic properties of these dyes when free in water. Over time, as the particles hydrolysed, the Nile Red and pyrene signal decreased as it was expelled into the water phase. The signal was normalized as a measured for release of dye. Nile Red was excited at 550 nm and its emission was traced over time at 630 nm, while pyrene was excited at 330 nm and its emission traced at 384 nm. Measurements were performed at 25 °C.

The Nile Red assay was performed on the same spectrofluorimeter as described above. Samples were directly prepared in the 10 mm quartz cuvette (Precision Cells Inc.) by mixing different concentrations of precursor (from 2.5 to 15 mM in MES 0.2 M) with Nile Red (5  $\mu$ M). The fluorescence intensities were measured at 635 nm with and excitation at 550 nm.

The THT assay was performed on the same spectrofluorimeter as described above. Samples were directly prepared in the 10 mm quartz cuvette (Precision Cells Inc.) by mixing precursor (10 mM in MES 0.2M) with EDC (100 mM) and THT (5  $\mu$ M). The fluorescence intensities were measured over time, every 2 minutes, at 485 nm with excitation at 450 nm.

The Fmoc assay was performed on the same spectrofluorimeter as described above. Samples were directly prepared in the 10 mm quartz cuvette (Precision Cells Inc.) by mixing precursor (10 mM in MES 0.2M) with EDC (100 mM). The fluorescence intensities were measured over time, every 5.8 minutes, from 300 to 600 nm with excitation at 285 nm.

**Circular Dichroism Spectroscopy.** Circular dichroism measurements were performed on a Jasco (Jasco J750) equipped with a Peltier temperature Control. Samples were prepared as described above and placed into a 1 mm quartz cell (Hellma Analytics) cuvette. Spectra were recorded from 325 to 280 nm with 0.2 nm step, 1 nm bandwidth. For single measurements, final spectra are the average of 10 accumulations at scan speed of 50 nm/min. For kinetic measurements spectra were recorded every 2 minutes with no accumulation at scan speed of 100 nm/min. Measurements were performed at 25 °C.

**Spray Coating.** For the preparation of the self-erasing medium, Fmoc-D was immobilized in a 30% polyacrylamide hydrogel. Briefly, a solution of 30% (29:1) acrylamide: bisacrylamide was prepared. In this solution, 10 mM Fmoc-D and 200 mM MES was dissolved. To prepare a gel, 4 mL of this stock solution was deposited in a petridish and 8  $\mu$ L tetramethylethylenediamine (TEMED) was added. The gelation was started by addition of 60  $\mu$ L 10w/w/% ammonium persulfate in water. The reaction was allowed to proceed for at least 2 hours, before EDC was spray coated or painted.

The fuel deposition via spray coating was performed using a spray gun (Harder & Steenbeck GmbH & Co. KG, Grafo T3) and oil-free nitrogen as carrier gas. The spray gun was fastened on a mount above a vertically adjustable sample stage to fixate the nozzle-to-sample distance at 15 cm. Applying a constant nitrogen pressure of 2 bar, the flow rate of the solution was set to about 15  $\mu$ L s<sup>-1</sup> by tuning the nozzle diameter accordingly. The spray time and thereby the amount of deposited material was defined by an electronic controller. About 300  $\mu$ L of the respective solution were deposited on the substrate using 2 spray shots of 10 s duration with a short pause. 3D-printed masks were placed onto the substrates in order to create reproducible, detailed images. After the completed spray deposition, the substrates were immediately transferred to an imaging station for further analysis.

**ESI.** ESI-MS measurements were performed using a Varian 500 MS LC ion trap spectrometer. The samples were diluted in acetonitrile and injected into an acetonitrile carrier flow (20  $\mu$ L/min).

**Cryogenic-Transmission Electron Microscopy (cryo-TEM).** Samples for TEM were prepared as described above. Shortly before imaging the samples were diluted a 10-fold to decrease the density of fibers in the micrographs. Cryo-TEM imaging was performed on a Jeol JEM-1400 plus operating at 120 kV. The images were recorded in a low-dose mode on a CCD camera. Quantifoil R2/2 on Cu-grid 400 mesh were used. The grids were freshly glow-discharged for 30 seconds prior to use. Preparation of the grids was performed in a FEI Vitrobot at 21 °C with the relative humidity set to 100% and the blotting force was set to -5. The sample (5  $\mu$ L) was incubated for 30 seconds, blotted twice for 3.5 seconds and then directly plunged into liquid ethane that was pre-cooled by liquid nitrogen. The cryo-EM grids were transferred and stored in liquid nitrogen, and when needed, placed into a Gatan 625 cryo-specimen holder to insert into the microscope. The specimen temperature was maintained at -170 °C during the data collection.

## 5. Dissipative Assemblies that Inhibit Their Deactivation

### **Abstract.**

Supramolecular dissipative examples from biology, like the GTP-fueled polymerization of microtubules and ATP driven actin assembly, led to the development of artificial supramolecular dissipative assemblies driven by chemical reaction cycles. These examples from biology show unique properties of the emerging assemblies, like pattern formation or oscillatory behavior. Until now such complex responses could not be implemented into assemblies, because of the lack of feedback mechanisms of the assemblies on their chemical reaction network.

The focus of this Chapter is to generalize and explore the mechanism of inhibition for other building blocks. The chemical reaction cycle, which was developed and characterized in Chapter 4 is used to study the mechanism of the inhibition of the hydrolysis reaction in the presence of colloids. These precursors are designed to self-assemble after the addition of fuel and are able to self-assemble exclusively into colloids. The activation reaction converts the two carboxylic acids of the precursor into the corresponding anhydride. Due to their metastability in the MES buffered media, the product rapidly hydrolyzes back to the initial precursors. By decreasing the intermolecular interactions between the product molecules, the formation of colloids can be switched off. In the presence of colloids, just the rate of the deactivation reaction changed. The colloids inhibit the hydrolysis of the product, due to their structure and hydrophobic character. By the addition of a surfactant or by changing the buffer concentration, the feedback of the assemblies on the chemical reaction cycle can be switched off completely or fine-tuned in a desired way. With this mechanism in hand, it was possible to show that colloids with a high rate of inhibition survive a period without fuel much longer compared to colloids with low rate of inhibition. In other words, increasing the inhibition of the hydrolysis reaction by the colloids leads to high robustness of the assemblies towards starvation periods.

This work has been published:

Title: Dissipative Assemblies that Inhibit Their Deactivation  
Authors: Benedikt Rieß,\* Caren Wanzke,\* Dr. Marta Tena-Solsona, Dr. Raphael K. Grötsch, Dr. Chandan Maity, Prof. Dr. Job Boekhoven  
First published: 23. May 2018  
Journal: Soft Matter **2018**, 14, 4852.  
Publisher: Royal Society of Chemistry  
DOI: 10.1039/C8SM00822A

Reprinted with permission of The Royal Society of Chemistry, License Number 1021100-1.

This section states the individual work of each author in the publication above. B. Rieß and C. Wanzke designed and conducted all experiments. C. Wanzke synthesized and analyzed Fmoc-GD as well as Cbz-D. Furthermore, C. Wanzke imaged Fmoc-E and Fmoc-GD with a cryogenic transmission electron microscope. B. Rieß analyzed Fmoc-E and Cbz-E, studied the robustness of Fmoc-E and provided images from the fluorescence microscope. R. K. Grötsch studied Fmoc-E with DLS. M. Tena-Solsona and C. Maity helped with scientific problems. C. Wanzke, B. Rieß und J. Boekhoven wrote the manuscript. The work was performed under the supervision and guidance of J. Boekhoven.





Cite this: *Soft Matter*, 2018, 14, 4852

Received 20th April 2018,  
Accepted 22nd May 2018

DOI: 10.1039/c8sm00822a

rsc.li/soft-matter-journal

## Dissipative assemblies that inhibit their deactivation†

Benedikt Rieß,<sup>‡a</sup> Caren Wanzke,<sup>‡a</sup> Marta Tena-Solsona,<sup>ab</sup> Raphael K. Grötsch,<sup>a</sup> Chandan Maity<sup>a</sup> and Job Boekhoven<sup>†</sup> <sup>\*ab</sup>

Dissipative self-assembly is a process in which energy-consuming chemical reaction networks drive the assembly of molecules. Prominent examples from biology include the GTP-fueled microtubule and ATP-driven actin assembly. Pattern formation and oscillatory behavior are some of the unique properties of the emerging assemblies. While artificial counterparts exist, researchers have not observed such complex responses. One reason for the missing complexity is the lack of feedback mechanisms of the assemblies on their chemical reaction network. In this work, we describe the dissipative self-assembly of colloids that protect the hydrolysis of their building blocks. The mechanism of inhibition is generalized and explored for other building blocks. We show that we can tune the level of inhibition by the assemblies. Finally, we show that the robustness of the assemblies towards starvation is affected by the degree of inhibition.

### Introduction

Molecular self-assembly into various structures has received widespread attention over the past decades<sup>1–5</sup> and has resulted in biomaterials,<sup>6,7</sup> catalysts,<sup>8</sup> molecular electronics,<sup>9</sup> and many other supramolecular materials.<sup>10</sup> Inspired by biological assemblies such as the GTP-driven assembly of microtubules,<sup>11</sup> or the ATP-fueled crosslinking of actin filaments,<sup>12</sup> the dissipative self-assembly of non-biological molecules has been pioneered.<sup>13</sup> In dissipative assembly, the assembly process is induced by a chemical reaction network that consists of at least two chemical reactions.<sup>14–18</sup> First, a precursor is activated for self-assembly by the irreversible consumption of a high-energy molecule (fuel) or photon (light). We refer to this reaction as the activation reaction. A second reaction reverts the activated product spontaneously to its initial precursor state. We refer to this reaction as the deactivation. The activated product, in its limited lifetime, can self-assemble. Researchers have described both light-driven<sup>19</sup> and fuel-driven<sup>13,20</sup> dissipative assembly.

The kinetics of the activation and deactivation control the material properties of dissipative assemblies, which makes them intrinsically different than their in-equilibrium counterparts. For example, these materials can be controlled over space

and time which opens the door to temporary materials with a predefined lifetime. To that end, researchers have developed self-erasing inks,<sup>21,22</sup> hydrogels that disappear after a predefined lifetime<sup>22–25</sup> colloids that can release hydrophobic molecules after a tunable time,<sup>22</sup> and others.<sup>26–29</sup> Other unique material properties of dissipative assemblies, include adaptivity and autonomous self-healing.<sup>23</sup>

Until now, the complex behavior we find in dissipative biological assemblies, like oscillations or pattern formation,<sup>30</sup> have not been observed in artificial analogs. A reason for the discrepancy in complex behavior in dissipative assemblies is the lack of feedback mechanisms of dissipative assemblies on their chemical reaction network. For example, the assembly of tubulin into microtubules catalyzes its own deactivation.<sup>31</sup> One of the goals for the field of dissipative self-assembly is thus to implement mechanisms by which the assemblies exert feedback on their activation and deactivation reaction.

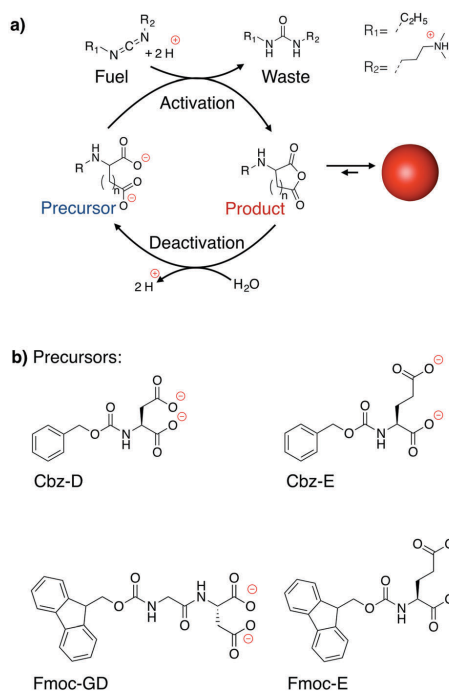
We recently introduced a new chemical reaction network that takes place in buffered water at pH 6.<sup>22</sup> The chemical reaction network converts a dicarboxylate precursor into a transient anhydride at the expense of a carbodiimide (Scheme 1a). In the activation reaction, derivatives of aspartic (D) or glutamic (E) acid reacted with a carbodiimide to form their corresponding *O*-acylisourea. This *O*-acylisourea further reacted to form its corresponding anhydride. The reaction released one molecule of urea. We called the urea waste, as it had no further function in the cycle. Our previous study has shown that the waste does not affect the assemblies or kinetics significantly.<sup>22</sup> In the deactivation reaction, the anhydride hydrolyzed back to the original dicarboxylate precursor. Upon addition of a finite amount of

<sup>a</sup> Department of Chemistry, Technical University of Munich, Lichtenbergstrasse 4, 85748 Garching, Germany. E-mail: job.boekhoven@tum.de

<sup>b</sup> Institute for Advanced Study, Technical University of Munich, Lichtenbergstrasse 2a, 85748 Garching, Germany

† Electronic supplementary information (ESI) available. See DOI: 10.1039/c8sm00822a

‡ These authors contributed equally to this work.



**Scheme 1** (a) The chemical reaction network employed to drive self-assembly of anhydrides. The dicarboxylate precursor is converted into the metastable product (anhydride) by a high energy condensing agent (EDC). For Fmoc-E or Fmoc-GD as a precursor, this product is able to self-assemble into colloids. In the aqueous environment, the product is hydrolyzed back to the precursor. (b) The molecular structure of precursors used in this study.

carbodiimide fuel, the anhydride was temporarily present at the expense of the carbodiimide. Work by others demonstrated the generality of the carbodiimide induced transient anhydride formation.<sup>32</sup>

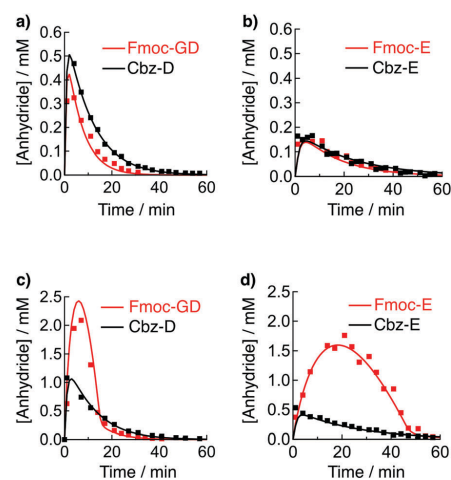
While the dicarboxylate precursor carried two anions, the anhydride was charge-neutral. This hydrophobization converted soluble precursors into assembling anhydride products. We found that one specific precursor, *N*-fluorenylmethyloxycarbonyl glutamic acid (Fmoc-E), formed colloids. These colloids significantly decreased the rate of hydrolysis of its anhydride building blocks.

In the current work, we study the underlying mechanism of the inhibition of the hydrolysis reaction in the presence of colloids. We show that the mechanism is a result of the assemblies protecting its anhydride product from deactivation and that the mechanism can be generalized for other colloid-forming anhydrides. We demonstrate that we can tune the level of the inhibition of the hydrolysis. With that control, we can manipulate the survival time of the colloids and their robustness towards periods of starvation from their energy source.

## Results and discussion

### Chemical reaction network

We studied the kinetics of the chemical reaction network using four different dicarboxylate precursors (Scheme 1b). Two precursors were derivatives of aspartic acid (D), while the other two were derivatives of glutamic acid (E). Of the aspartic acid derivatives, we used the *N*-carboxybenzyl protected amino acid (Cbz-D), and an *N*-fluorenylmethyloxycarbonyl protected-glycine derivative (Fmoc-GD). Of the glutamic acid derivatives, we investigated Cbz-E and Fmoc-E. The anhydrides of the Cbz-amino acids were well soluble under all experimental conditions, whereas the anhydrides of Fmoc-E and Fmoc-GD assembled into colloids (*vide infra*). In all experiments, we used 10 mM solutions of the precursor in water buffered at pH 6 with MES. We added finite amounts of carbodiimide as fuel (1-ethyl-3-(3-dimethylaminopropyl)carbodiimide, EDC) to these solutions and measured the response of the chemical reaction network by high-pressure liquid chromatography and electrospray ionization mass spectroscopy (HPLC, ESI-MS, Fig. 1 and Tables S1–S3, ESI†). It should be noted that the reactions between fuel and Fmoc-E or Cbz-E resulted in a small amount of the *N*-acylurea (Table S3, ESI†) which did not interfere with the other reactions or the assemblies. Finally, we should note that our HPLC method was optimized and verified to ensure that all anhydride, be it in an assembly or not, was injected. In other words, the assembling species was not filtered out by the analysis method neither did it sediment during the experiment.



**Fig. 1** Concentration anhydride against time in response to addition of EDC as determined by HPLC (markers) or the kinetic model (solid line) for (a) 10 mM Fmoc-GD (red) or Cbz-D (black) with 10 mM EDC, (b) 10 mM Fmoc-E (red) or Cbz-E (black) with 3 mM EDC, (c) 10 mM Fmoc-GD (red) or Cbz-D (black) with 25 mM EDC, (d) 10 mM Fmoc-E (red) and Cbz-E (black) with 10 mM EDC.

We recorded the concentration of the fuel, the precursor, and the product over time (Fig. 1a and b). These concentrations were used to fit a previously described kinetic model.<sup>22</sup> The model could be used to predict the concentrations accurately when the chemical reaction network did not produce any assemblies (Fig. 1a and b, the rate constants can be found in Table S4, see Supplementary Notes 1 for a description of the kinetic model, ESI†). We found similar yields, reaction times and  $k$ -values for precursors based on the same terminal amino acid demonstrating that the reactivity was not drastically affected by the protecting group. For example, adding 3 mM of EDC to Cbz-E or Fmoc-E resulted in a maximum concentration of anhydride of 0.15 mM after 5 minutes.

When we added relatively large batches of fuel, differences between the evolution of the concentration product of Cbz-D and Fmoc-GD, as well as Cbz-E and Fmoc-E were evident (Fig. 1c and d). For instance, when we added 10 mM of EDC to 10 mM of Cbz-E, a maximum concentration of anhydride was found after 5 minutes at 0.42 mM whereas, for the same experiment with Fmoc-E, the maximum anhydride was a four-fold higher at 1.6 mM after 18 minutes. Similar higher anhydride concentrations and delays of the maxima were found for Fmoc-GD when compared to Cbz-D. The apparent change in the kinetics was not a result of a change in the activation kinetics as the EDC consumption showed a similar profile for Cbz-E compared to Fmoc-E as well as Cbz-D compared to Fmoc-GD (Fig. S1a and b, ESI†).

#### Morphological assessment of the assemblies

We used dynamic light scattering (DLS) to assess the nature of the assemblies of the anhydrides of Fmoc-E and Fmoc-GD. We initiated the cycle by addition of 10 mM EDC to 10 mM Fmoc-E, or 25 mM EDC to 10 mM Fmoc-GD which rapidly turned the transparent precursor solutions turbid. We measured an increase in the DLS scattering rate of at least an order of magnitude compared to before addition of fuel for both Fmoc-GD and Fmoc-E (Fig. 2a and b). The radii calculated by the fitted DLS data peaked after roughly 7 minutes at 390 nm, and after 20 minutes at 550 nm for Fmoc-GD and Fmoc-E, respectively (Fig. 2c and d). It is worth to note that these times correspond to the time of maximum anhydride concentration. The increased turbidity was temporary, and the scattering rates decreased to their original values after roughly 15 and 50 minutes, respectively. We found no evidence for assemblies when adding 10 mM or 3 mM of EDC to Fmoc-GD or Fmoc-E, respectively (Fig. 2a and b).

We utilized fluorescence microscopy with Nile Red as a hydrophobic dye to further assess the assemblies. Microscopy showed no assemblies before addition of the fuel. In contrast, minutes after addition of fuel, colloids were found for both Fmoc-GD and Fmoc-E (Fig. 3a–d). Using image analysis software on micrographs taken around 7 minutes for Fmoc-GD and 20 minutes for Fmoc-E, the radii of at least 2500 colloids were measured. The radii of the colloids were found to be in line with those found by DLS: 0.35  $\mu\text{m}$  for Fmoc-GD and 0.4  $\mu\text{m}$  for Fmoc-E (Fig. 3e and f). Finally, cryo-TEM microscopy further confirmed

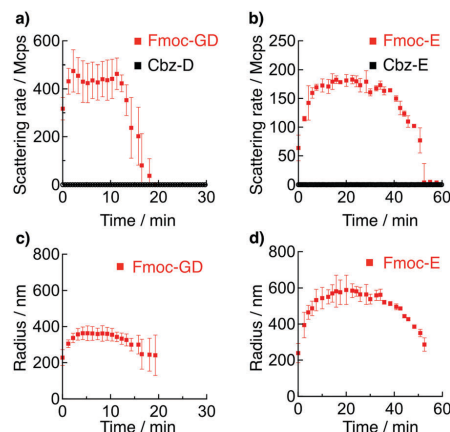


Fig. 2 Scattering rates against time as measured by DLS (a) Fmoc-GD (red) or Cbz-D (black) and 25 mM EDC, and (b) Fmoc-E (red) or Cbz-E (black) with 10 mM EDC. Note that the Cbz-based experiments did not increase the turbidity and their scattering rate thus remains around 0. (c and d) Hydrodynamic radii against time for the experiments described in a and b, respectively. We obtained no reliable data for the Cbz-based precursors because of the limited scattering. All error bars represent the standard deviation of the mean for a sample size  $n = 3$ .

that the colloids were already present within the first minutes of the chemical reaction network with a radius in the range of 300 to 400 nm (Fig. 3g and h). From all of the above observations, we concluded that the increased anhydride concentrations were a result of the presence of the colloids.

#### Mechanism of inhibition of the deactivation

In the following, we explain the mechanism of inhibition. In the presence of colloids, the activation of the anhydride remained unchanged (Fig. S1a and b, ESI†). The difference in the kinetics in the presence of colloids must thus be a result of the deactivation reaction. To that end, we hypothesized that the assemblies protect the anhydride from hydrolysis, *via* a simple mechanism. The colloids are relatively large and hydrophobic, which means that any anhydride in these colloids is effectively separated from the aqueous environment. In other words, the colloids protect their anhydrides from hydrolysis, but only the fraction that is found in the colloids. The anhydride that remained in solution thus remained susceptible to hydrolysis. The protection from hydrolysis explained the relatively high concentration of anhydride when colloids were formed.

To confirm our hypothesis, we adjusted the kinetic model to exclude from hydrolysis the fraction of the anhydride above the critical aggregation concentration (CAC). In other words, hydrolysis of the anhydride only occurred on the fraction that remained in solution, and hydrolysis was thus limited to a rate of  $v_4 = k_4 \times \text{CAC}$ . In that equation,  $k_4$  is the first order rate constant for hydrolysis in solution. Empirically determining the CAC was challenging, given the metastability of the anhydride.

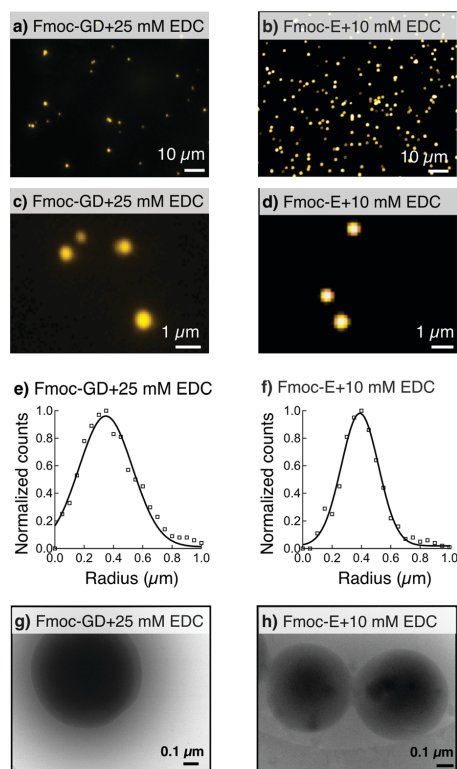


Fig. 3 Fluorescence microscopy micrographs of (a) Fmoc-GD with 25 mM EDC after roughly 7 minutes and (b) Fmoc-E with 10 mM EDC after roughly 20 minutes. Fluorescence microscopy micrographs of (c) Fmoc-GD with 25 mM EDC after roughly 7 minutes and (d) Fmoc-E with 10 mM EDC after roughly 20 minutes, with high magnification. (e and f) Histograms of the normalized colloid's radii distribution ( $n > 2500$ ) of the micrographs of (c) and (d), respectively. Cryo-TEM of colloids under the same conditions in the first minute for (g) Fmoc-E and (h) Fmoc-GD.

Instead, we used the updated kinetic model and adjusted the CAC to fit the HPLC data (Table S4, ESI†). Since both  $k_4$  and the CAC are both constants, the resulting rate is also a constant, *i.e.*, the hydrolysis followed 0th order kinetics. This rather simple addition to the kinetic model allowed us to fit all HPLC data for cycles that did or did not form assemblies (Fig. 1a–d).

Fig. 4 depicts a tentative mechanism of the evolution of the dissipative cycle. At the beginning of the cycle, the rate of building block activation was high, because the amount of fuel was at its highest. Within the first minute, the solution reached supersaturation and excess anhydride self-assembled into colloids. When these first colloids were present, we hypothesized that any activated anhydride was deposited on the existing colloids. This deposition was confirmed by the increase in radius as observed by DLS (Fig. 2). After 7 minutes

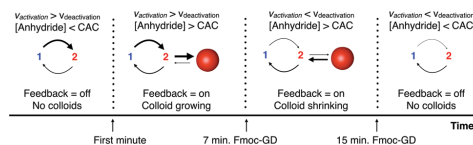


Fig. 4 Mechanism of kinetically controlled assembly into colloids during a dissipative cycle. The assemblies inhibit deactivation of anhydride (2) to carboxylate (1).

for Fmoc-GD and 20 minutes for Fmoc-E, the fuel level had decreased such that the activation rate is lower than hydrolysis rate. The net anhydride formation was thus negative, and the concentration of anhydride in the system decreased. As the hydrolysis happened in solution, the solution became undersaturated. The undersaturated solution could now accept anhydride from the colloids, resulting in a decrease of the colloids radii. Here, we assumed that anhydride disassembly from the colloids is faster than hydrolysis.<sup>33</sup> The colloids kept on supplying the undersaturated solution with anhydride until they had disappeared. At this point, the inhibition is switched off, and hydrolysis proceeded with first order kinetics.

While we understood the above mechanism qualitatively for Fmoc-E, we confirmed the mechanism for other colloid-forming assemblies and could quantitatively express the level of inhibition with our kinetic model. The quantitative understanding allows us to set some preliminary design rules for this type of inhibition in dissipative assemblies. First, the deactivation reaction of the assembling species needs to be driven either by reaction with the solvent or a reagent in the solvent. The assembly needs to be sufficiently large compared to its building blocks in all three dimensions, and it needs to exclude the building blocks from the solvent. We mention large in three dimensions, as we have not seen this effect in large one-dimensional fibers.<sup>22</sup> Under these conditions, the assemblies protected their anhydride building blocks from hydrolysis. Finally, the disassembly rate is required to be faster than the hydrolysis rate, such that the rate determining step is the hydrolysis and not the exchange of building blocks between assemblies and solution.

#### Tuning the deactivation inhibition

We wondered if we could control the level of inhibition of the assemblies on the anhydride hydrolysis rate. We first performed experiments under conditions that prevent the self-assembly of the anhydride of Fmoc-E into the observed colloids. To do so, we added 1.0 mM of cetyltrimethylammonium bromide<sup>34</sup> (CTAB). CTAB is a common cationic surfactant with a critical micelle concentration of 0.1 mM under the employed conditions (Fig. S2, ESI†). We reasoned that CTAB micelles would solubilize the anhydride of Fmoc-E, thus inhibiting its self-assembly into colloids. Indeed, with CTAB, no increased turbidity was found after addition of 10 mM EDC to 10 mM Fmoc-E. HPLC analysis showed that the EDC consumption rate was similar compared to without CTAB (Fig. S1c, ESI†). However, the

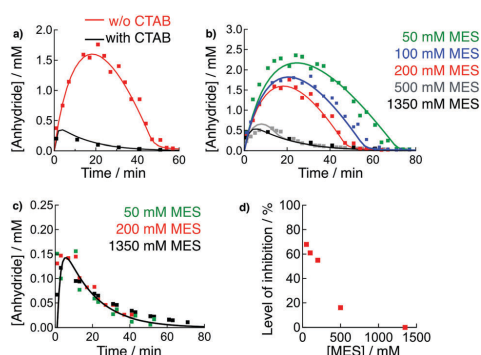


Fig. 5 (a) The concentration of Fmoc-E anhydride in response to 10 mM EDC with (black) or without (red) 1 mM of CTAB. (b) The concentration of Fmoc-E anhydride in response to 10 mM EDC with varying MES concentration. (c) The same experiment at b, but with only 3 mM of EDC. (d) Level of inhibition against the concentration of MES buffer. The inhibition level scaled between 0 and 100% where 0% is no inhibition, and 100% is complete inhibition of the hydrolysis.

anhydride concentration remained much lower compared to without CTAB (Fig. 5a). The HPLC data was fitted using the kinetic model, and we obtained a good fit by removing the inhibition mechanism (Table S4, ESI<sup>†</sup>). In summary, the addition of the surfactant increased the anhydride solubility and prevented the formation of colloids required for the inhibition of the deactivation.

In the next experiments, we aimed at tuning the level of inhibition by the colloids. To do so, the CAC is to be altered by minimal amounts. We found that the concentration MES buffer could tune the solubility of the precursor, *i.e.*, the more MES we added, the higher the solubility (Fig. S3, ESI<sup>†</sup>). Such an effect is referred to as “salting in.”<sup>35</sup> We assumed a similar trend for the anhydride of Fmoc-E. We also verified that at the relatively low buffer concentration of 50 mM MES, the buffer still had sufficient capacity to diminish fluctuations in pH (Fig. S4, ESI<sup>†</sup>). Addition of 10 mM EDC to 10 mM Fmoc-E in 50 mM MES buffer at pH 6 resulted in a maximum anhydride concentration around 2.5 mM (Fig. 5b). In contrast, when we performed the same experiment in 1350 mM MES, the maximum anhydride concentration was only 0.5 mM, and the evolution of the anhydride concentration resembled the one without the inhibition mechanism. To our surprise, the drastically different evolution of the chemical reaction network could be fitted by only adjusting the CAC in the kinetic model (Fig. 5b). The CAC in 200 mM MES was previously fitted to be 0.24 mM. For 50 mM MES, a good fit was obtained by decreasing the CAC to 0.17 mM. In contrast, for 1350 mM, we removed the inhibition mechanism to obtain a good fit (Fig. 5b).

As a control, we carried out a similar experiment but added only 3 mM of EDC to ensure the absence of assemblies under any of the conditions. Under these control conditions, the evolution of the anhydride concentration was similar for each

buffer concentration (Fig. 5c). We quantified the level of inhibition by calculating the 0th order hydrolysis rate as a fraction of the maximum hydrolysis rate without inhibition (Fig. 5d and Supplementary Notes 2, ESI<sup>†</sup> for calculations). In this calculation, 0% equals no inhibition, and 100% implies a complete inhibition of the hydrolysis.

#### Inhibition of deactivation makes the assemblies more robust

Finally, we set out to test the robustness of our assemblies towards periods of starvation. We fueled our assemblies with a batch of 10 mM EDC. After the fueling, we starved them from fuel for 50 minutes after which we gave them another batch of 10 mM EDC. We performed this fueling-starvation sequence for three rounds. We tested the response of two levels of inhibition: a system with an intermediate amount of inhibition ( $\pm 50\%$  at 200 mM MES) and a system with a high amount of inhibition ( $\pm 70\%$  at 50 mM MES). The model showed that for a low amount of inhibition, the concentration anhydride would fall below the CAC in the starvation period (Fig. 6a). In contrast, in the high inhibition experiment, the concentration would remain above the CAC throughout the experiment. In other words, in the high inhibition experiments, colloids can “survive” the entire experiment, whereas a colloid in the intermediate inhibition experiment will likely disassemble.

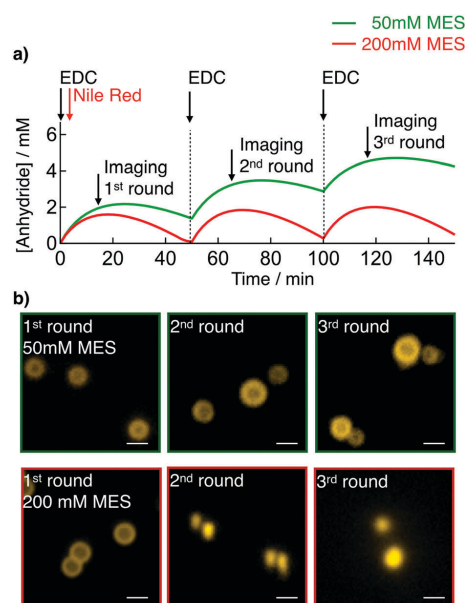


Fig. 6 (a) The concentration of anhydride against time as calculated by the kinetic model. Every 50 minutes a new batch of 10 mM EDC is added. 15 minutes after addition of EDC the solutions were imaged. (b) Micrographs of the samples as described in Fig. 4d. Scale bar corresponds to 1  $\mu\text{m}$ . The left micrographs correspond to 50 mM MES and the right ones to 200 mM MES.

To confirm the survival or disassembly of the colloids, we had to mark them with a dye that could distinguish colloids that had disassembled from colloids that had remained assembled. To do so, 5 minutes after initiating the first cycle, 2.5  $\mu\text{M}$  Nile Red was added. In the first 5 minutes, the colloids had grown to roughly 400 nm in radius. That means that the hydrophobic dye could only incorporate into a layer around the core of the particles, which looked like a ring under the microscope (Fig. 6b). If the colloids disassembled and reassembled later, they lost that unique dye distribution, which allowed us to distinguish them from colloids that had survived the experiment (*vide infra*). The samples were imaged 20 minutes after each fuel addition. In the first fueling round, microscopy revealed colloids of roughly 1  $\mu\text{m}$  with the characteristic ring (Fig. 6b). After the 50 minute-starvation period, the second batch of fuel was added. In the second fueling round, both solutions showed particles of roughly 1  $\mu\text{m}$ . In the high inhibition-experiment, microscopy showed particles, that maintained the characteristic ring, serving as a strong indication that they had survived the starvation period. In contrast, the colloids with intermediate inhibition showed a homogeneous distribution of the dye through the core of the particle (Fig. 6b). After the second starvation period, the system was refueled for the third time. The final imaging round showed similar particles as the second round.

The layered dye distribution throughout the colloids rendered them unique, and only a colloid that “survived” the entire experiment could carry the unique color code. In contrast, a particle that had disassembled would have released its dye into the solution and subsequently reincorporated it into the core of new colloids upon addition of new fuel. The coding allowed us to discriminate particles that had “survived” the starvation from particles that had “died.” These last experiments show that our colloids with a high level of inhibition all “survived” the starvation periods of 50 minutes. In contrast, the particles with low inhibition did not show the color coding and had thus fully disassembled during the starvation period.

## Conclusions

Our work shows a method of incorporating a feedback mechanism into dissipative non-equilibrium assemblies. The understanding of the molecular mechanisms at play allows us to switch on or off the inhibition or to tune it. We show that increasing inhibition gives the inherently unstable assemblies increased robustness towards starvation periods.

## Experimental

### Materials

Fmoc-E, Cbz-E, Cbz-D, EDC, urea, MES were purchased from Sigma-Aldrich and Alfa-Aesar and used without any further purification unless otherwise indicated. Fmoc-GD was synthesized using standard fluoren-9-ylmethoxycarbonyl (Fmoc) solid-phase

peptide synthesis on Wang resin (100–200 mesh, 1.1 mmol  $\text{g}^{-1}$  loading). Peptides were synthesized on a CEM Liberty microwave-assisted peptide synthesizer. The ESI<sup>†</sup> gives a detailed description of the synthesis.

**Kinetic model.** We used a kinetic model to predict the evolution of the anhydride concentration over time. In brief, the kinetic model uses rate constant for six reactions in the chemical reaction network. Each second, the kinetic model calculates the concentrations of the reactants and product. The kinetic model and MatLab code are described in detail Supplementary Notes 1 (ESI<sup>†</sup>). Table S4 (ESI<sup>†</sup>) gives the rate constants.

**Dynamic light scattering.** We carried out DLS measurements on all solutions with a DynaPro NanoStar from Wyatt with a laser wavelength of 658 nm in disposable cuvette for DLS from Wyatt. The measurements for Fmoc-E with 10 mM EDC and Fmoc-GD with 25 mM EDC consisted of 5 acquisitions with an acquisition time of 10 seconds. The remaining experiments consisted of 1 acquisition with an acquisition time of 5 seconds. For measurements and analysis, we used the software Dynamics V7.

**HPLC.** We monitored the kinetics of the chemical reaction networks over time by using analytical HPLC (HPLC, Thermo-fisher Dionex Ultimate 3000, Hypersil Gold 250  $\times$  4.8 mm). A 750  $\mu\text{L}$  sample was prepared as described above and placed into a screw cap HPLC vial. We injected samples of the solutions directly, without further dilution. The HPLC separated all compounds involved using a linear gradient of water with 0.1% TFA:ACN with 0.1% TFA from 40:60 to 2:98.

We performed calibration curves for the EDC ( $\lambda_{\text{abs}} = 220 \text{ nm}$ ) and precursors ( $\lambda_{\text{abs}} = 254 \text{ nm}$ ) in triplicate. Calibration was not possible for the anhydrides due to their intrinsic instability. Instead, we used the absorption coefficient of their corresponding precursor.

**Fluorescence microscopy.** Fluorescence microscopy was performed on a Leica DMI8 microscope using a 63 $\times$  oil immersion objective. We prepared samples as described above but with 25  $\mu\text{M}$  Nile Red as a dye. We deposited 20  $\mu\text{L}$  of the sample on the glass slide and covered with a 12 mm diameter coverslip. Samples were excited with 543 nm laser and imaged at 580–700 nm. Particle diameters were counted using ImageJ cell counting package.

**ESI.** ESI-MS measurements were performed using a Varian 500 MS LC ion trap spectrometer. The samples were diluted in acetonitrile and injected into an acetonitrile carrier flow (20  $\mu\text{L min}^{-1}$ ).

**Cryogenic-transmission electron microscopy (cryo-TEM).** Samples for TEM were prepared as described above. The grids (Quantifoil R2/2 on Cu-grid 400 mesh) were freshly glow-discharged for 30 (Fmoc-GD) or 90 seconds (Fmoc-E) before use. Preparation of the grids was performed in an FEI/Thermo Fisher Vitrobot at 25  $^{\circ}\text{C}$  with the relative humidity set to 100%. Fmoc-GD (5  $\mu\text{L}$ ) was incubated for 30 seconds, blotted twice for 3.5 seconds (blotting force set to  $-5$ ) and then directly plunged into liquid ethane that was pre-cooled by liquid nitrogen. Fmoc-E (5  $\mu\text{L}$ ) was incubated for 15 seconds, blotted for 2 seconds (blotting force set to  $-1$ ) and then also directly plunged into liquid ethane.

The cryo-EM grids were transferred and stored in liquid nitrogen, and when needed, placed into a Gatan cryo-transfer-specimen holder to insert into the microscope. The specimen temperature was maintained at  $-170\text{ }^{\circ}\text{C}$  during the data collection. Cryo-TEM imaging of Fmoc-GD was performed on a Jeol JEM-1400 plus operating at 120 kV, and Cryo-TEM imaging of Fmoc-E was performed on a Tecnai Spirit microscope (FEI/Thermo Fisher) operating at 120 kV. The images were recorded in a low-dose mode on a CCD camera.

**Solubility determination of precursors.** The samples of Fmoc-E (10 mM) were prepared as described above in different buffer concentrations (50, 100, 200, 500 and 1350 mM MES). After the pH was adjusted to 1, the precipitate was filtered off with a 200 nm syringe filter. HPLC analysis was carried out like described above to determine the remaining Fmoc-E in solution.

**Sample preparation.** Stock solutions of the precursor were prepared by dissolving the precursor in MES buffer, after which the pH was adjusted to pH 6.0. Stock solutions of EDC were prepared by dissolving the EDC powder in MQ water. Typically, stock solutions of 1.0 M EDC were used freshly. Reaction networks were started by addition of the high concentration EDC to the peptide solution. All analysis was carried out at  $25\text{ }^{\circ}\text{C}$ .

## Conflicts of interest

There are no conflicts to declare.

## Acknowledgements

J. B. is grateful for funding by the Technical University of Munich – Institute for Advanced Study, funded by the German Excellence Initiative and the European Union Seventh Framework Programme under grant agreement no. 291763. B. R. acknowledges the Deutsche Forschungsgemeinschaft within the SFB No. 863. R. G. is grateful for funding by the International Research Training Group ATUMS (IRTG 2022). M. T. S. acknowledges the European Union's Horizon 2020 Research and Innovation program for the Marie Skłodowska Curie Fellowship under grant agreement no. 747007.

## References

- 1 J. D. Hartgerink, E. Beniash and S. I. Stupp, *Science*, 2001, **294**, 1684–1688.
- 2 J. P. Hill, W. Jin, A. Kosaka, T. Fukushima, H. Ichihara, T. Shimomura, K. Ito, T. Hashizume, N. Ishii and T. Aida, *Science*, 2004, **304**, 1481–1483.
- 3 P. A. Korevaar, S. J. George, A. J. Markvoort, M. M. Smulders, P. A. Hilbers, A. P. Schenning, T. F. De Greef and E. W. Meijer, *Nature*, 2012, **481**, 492–496.
- 4 A. Lampel, S. A. McPhee, H. A. Park, G. G. Scott, S. Humagain, D. R. Hekstra, B. Yoo, P. W. J. M. Frederix, T. D. Li, R. R. Abzalimov, S. G. Greenbaum, T. Tuttle, C. Hu, C. J. Bettinger and R. V. Ulijn, *Science*, 2017, **356**, 1064–1068.
- 5 P. W. Rothemund, *Nature*, 2006, **440**, 297–302.
- 6 G. A. Silva, C. Czeisler, K. L. Niece, E. Beniash, D. A. Harrington, J. A. Kessler and S. I. Stupp, *Science*, 2004, **303**, 1352–1355.
- 7 F. Tantakitti, J. Boekhoven, X. Wang, R. V. Kazantsev, T. Yu, J. Li, E. Zhuang, R. Zandi, J. H. Ortony, C. J. Newcomb, L. C. Palmer, G. S. Shekhawat, M. O. de la Cruz, G. C. Schatz and S. I. Stupp, *Nat. Mater.*, 2016, **15**, 469.
- 8 M. D. Pluth, R. G. Bergman and K. N. Raymond, *Science*, 2007, **316**, 85–88.
- 9 Y. Yamamoto, T. Fukushima, Y. Suna, N. Ishii, A. Saeki, S. Seki, S. Tagawa, M. Taniguchi, T. Kawai and T. Aida, *Science*, 2006, **314**, 1761–1764.
- 10 J. Boekhoven and S. I. Stupp, *Adv. Mater.*, 2014, **26**, 1642–1659; D. B. Amabilino, D. K. Smith and J. W. Steed, *Chem. Soc. Rev.*, 2017, **46**, 2404–2420.
- 11 A. Desai and T. J. Mitchison, *Annu. Rev. Cell Dev. Biol.*, 1997, **13**, 83–117.
- 12 S. Köhler, V. Schaller and A. R. Bausch, *Nat. Mater.*, 2011, **10**, 462–468.
- 13 J. Boekhoven, A. M. Brizard, K. N. Kowligi, G. J. Koper, R. Eelkema and J. H. van Esch, *Angew. Chem., Int. Ed.*, 2010, **49**, 4825.
- 14 S. A. P. van Rossum, M. Tena-Solsona, J. H. van Esch, R. Eelkema and J. Boekhoven, *Chem. Soc. Rev.*, 2017, **46**, 5519–5535.
- 15 A. Sorrenti, J. Leira-Iglesias, A. J. Markvoort, T. F. de Greef and T. M. Hermans, *Chem. Soc. Rev.*, 2017, **46**, 5476–5490.
- 16 L. Heinen and A. Walther, *Soft Matter*, 2015, **11**, 7857–7866.
- 17 F. Della Sala, S. Neri, S. Maiti, J. L. Chen and L. J. Prins, *Curr. Opin. Biotechnol.*, 2017, **46**, 27–33.
- 18 R. Merindol and A. Walther, *Chem. Soc. Rev.*, 2017, **46**, 5588–5619.
- 19 J. J. de Jong, P. R. Hania, A. Puzgyls, L. N. Lucas, M. de Loos, R. M. Kellogg, B. L. Feringa, K. Duppen and J. H. van Esch, *Angew. Chem., Int. Ed.*, 2005, **44**, 2373–2376.
- 20 C. G. Pappas, I. R. Sasselli and R. V. Ulijn, *Angew. Chem., Int. Ed.*, 2015, **54**, 8119–8123.
- 21 R. Klajn, P. J. Wesson, K. J. Bishop and B. A. Grzybowski, *Angew. Chem., Int. Ed.*, 2009, **48**, 7035–7039.
- 22 M. Tena-Solsona, B. Rieß, R. K. Grötsch, F. C. Löhrer, C. Wanzke, B. Käs Dorf, A. R. Bausch, P. Müller-Buschbaum, O. Lieleg and J. Boekhoven, *Nat. Commun.*, 2017, **8**, 15895.
- 23 T. Heuser, A.-K. Steppert, C. Molano Lopez, B. Zhu and A. Walther, *Nano Lett.*, 2014, **15**, 2213–2219.
- 24 C. G. Pappas, I. R. Sasselli and R. V. Ulijn, *Angew. Chem., Int. Ed.*, 2015, **54**, 8119–8123.
- 25 J. Boekhoven, W. E. Hendriksen, G. J. Koper, R. Eelkema and J. H. van Esch, *Science*, 2015, **349**, 1075–1079.
- 26 S. Maiti, I. Fortunati, C. Ferrante, P. Scrimin and L. J. Prins, *Nat. Chem.*, 2016, **8**, 725–731.
- 27 T. Heuser, A.-K. Steppert, C. Molano Lopez, B. Zhu and A. Walther, *Nano Lett.*, 2014, **15**, 2213–2219.

- 28 J. Leira-Iglesias, A. Sorrenti, A. Sato, P. A. Dunne and T. M. Hermans, *Chem. Commun.*, 2016, **52**, 9009–9012.
- 29 A. Sorrenti, J. Leira-Iglesias, A. Sato and T. M. Hermans, *Nat. Commun.*, 2017, **8**, 15899.
- 30 F. J. Ndlec, T. Surrey, A. C. Maggs and S. Leibler, *Nature*, 1997, **389**, 305–308.
- 31 S. Roychowdhury and M. M. Rasenick, *Biochemistry*, 1994, **33**, 9800–9805.
- 32 L. S. Kariyawasam and C. S. Hartley, *J. Am. Chem. Soc.*, 2017, **139**, 11949–11955.
- 33 We can make this hypothesis because we find no delay between the kinetic of the chemical reaction network and the size or presence of the colloids. For example, the maximum size of the colloids is obtained at the same time as the maximum anhydride concentration, and the colloids disappear at exactly the moment the anhydride concentration falls below its solubility.
- 34 J. M. Neugebauer, *Methods Enzymol.*, 1990, **182**, 239–253.
- 35 P. Lo Nostro and B. W. Ninham, *Chem. Rev.*, 2012, **112**, 2286–2322.



Electronic Supplementary Material (ESI) for Soft Matter.  
This journal is © The Royal Society of Chemistry 2018

### Dissipative assemblies that inhibit their deactivation

Benedikt Rieß,<sup>a</sup> Caren Wanzke,<sup>a</sup> Marta Tena-Solsona,<sup>a,b</sup> Raphael K. Grötsch,<sup>a</sup> Chandan Maity,<sup>a</sup> Job Boekhoven<sup>a,b</sup>

**Fmoc-GD synthesis.** Fmoc-GD was synthesized using standard fluoren-9-ylmethoxycarbonyl (Fmoc) solid-phase peptide synthesis on Wang resin (100-200 mesh, 1.1 mmol/g loading). Synthesis was performed on a CEM Liberty microwave-assisted peptide synthesizer. The first amino acid coupling to the resin was accomplished by using symmetrical anhydride methodology. Briefly, a 0.2 M solution of the Fmoc-FmocD(OtBu)OH symmetrical anhydride was prepared by allowing the corresponding Fmoc-protected amino acid (FmocD(OtBu)OH, 12 mmol) and *N,N'*-diisopropylcarbodiimide (DIC, 6 mmol) to react in 30 mL *N,N*-dimethylformamide (DMF) for 40 minutes. The solution was placed in the freezer for 15 minutes and the solid urea formed was filtered out before next step. Loading of the resin was performed using the automated peptide synthesizer. The symmetrical anhydride solution (0.2 M, 12 mL) and 4-(dimethylamino)pyridine (DMAP) solution in DMF (20 mM, 2.5 mL) were added to the pre-swollen Wang resin (0.5 mmol, 1.1 mmol/g) and heated in the microwave (30 minutes, 75 °C). The coupling was repeated twice in order to increase the yield. The resin was then washed with DMF (2x10 mL). Before the following coupling the Fmoc protecting group was removed using a 20% solution of piperidine in DMF. The reaction mixture was heated in the microwave (1x1 minutes, 90 °C) and then washed with DMF (2x10 mL). The coupling was achieved by using 4 equivalents (eq.) of Fmoc-glycine in DMF, 4 eq. of DIC and 4 eq. of ethyl (hydroxyimino)cynoacetate (Oxyma). The resin solution was then heated in the microwave (1x2 minutes, 90 °C). This coupling was also repeated twice to increase the yield. The peptide was then cleaved from the resin using a mixture (10 mL) of 50% DCM, 47.5% trifluoroacetic acid (TFA), 1.25% water, and 1.25% triisopropylsilane (TIPS). The solvent was removed by co-distillation with ether by rotary evaporation and dried under reduced pressure. The product was purified using reversed-phase high-performance liquid chromatography (HPLC, Thermofisher Dionex Ultimate 3000, Hypersil Gold 250x4.8 mm) in a linear gradient of acetonitrile (ACN with 0.1% TFA, 40% to 98%) and water with 0.1% TFA. Purified product was lyophilized and stored at -20 °C until further use. The purity of the peptide was analysed by electrospray ionization mass spectrometry in positive mode (ESI-MS) as well as analytical HPLC (Thermofisher *Dionex* Ultimate 3000, eluted with a gradient of 0.1% TFA in water: 0.1% TFA in ACN from 40:60 to 2:98 in 10 minutes, see below for results).

### Supplementary Methods

**Sample preparation.** Stock solutions of the precursor were prepared by dissolving the precursor in MES buffer, after which the pH was adjusted to pH 6.0. Stock solutions of EDC were prepared by dissolving the EDC powder in MQ water. Typically, stock solutions of 1.0 M EDC were used freshly. Reaction networks were started by addition of the high concentration EDC to the peptide solution. All analysis was carried out at 25°C.

## Supporting Figures

Supporting Table 1: Assessment of the used materials and their purity

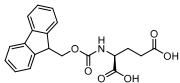
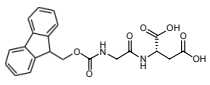
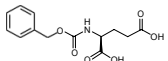
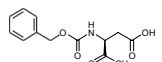
name	purity [%]	structure	mass calculated [g/mol]	mass observed [g/mol]	retention time [min]
Fmoc-E	Commercial: 95%		Mw = 369.12 C <sub>20</sub> H <sub>19</sub> NO <sub>6</sub>	392.1 [Mw+Na] <sup>+</sup>	6.14
Fmoc-GD	Synthesized (see methods) 97%		Mw = 412.13 C <sub>21</sub> H <sub>20</sub> N <sub>2</sub> O <sub>7</sub>	435.0 [Mw+Na] <sup>+</sup>	5.61
Cbz-E	Commercial: 97%		Mw = 281.09 C <sub>13</sub> H <sub>15</sub> NO <sub>6</sub>	304.1 [Mw+Na] <sup>+</sup>	4.51
Cbz-D	Commercial: 99%		Mw = 267.07 C <sub>12</sub> H <sub>13</sub> NO <sub>6</sub>	290.9 [Mw+Na] <sup>+</sup>	4.47

Table S1. Characterization of precursors.

Supporting Table 2: Assessment of the products

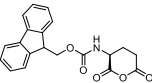
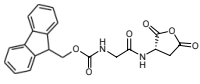
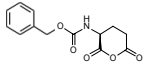
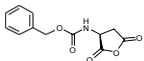
name	structure	mass calculated [g/mol]	mass observed [g/mol]	retention time [min]
Fmoc-E anhydride		Mw = 351.11 C <sub>20</sub> H <sub>17</sub> NO <sub>5</sub>	373.9 [Mw+Na] <sup>+</sup>	7.68
Fmoc-GD anhydride		Mw = 394.12 C <sub>21</sub> H <sub>18</sub> N <sub>2</sub> O <sub>6</sub>	417.2 [Mw+Na] <sup>+</sup>	7.02
Cbz-E anhydride		Mw = 263.08 C <sub>13</sub> H <sub>13</sub> NO <sub>5</sub>	286.1 [Mw+Na] <sup>+</sup>	6.14
Cbz-D anhydride		Mw = 249.06 C <sub>12</sub> H <sub>11</sub> NO <sub>5</sub>	272.22 [Mw+Na] <sup>+</sup>	6.36

Table S2. Characterization of main products of the chemical reaction network.

Supporting Table 3

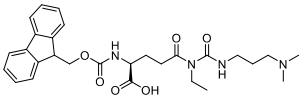
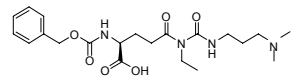
name	structure	mass calculated [g/mol]	mass observed [g/mol]	retention time [min]
Fmoc-E N-acylurea		Mw = 524.26 C <sub>28</sub> H <sub>36</sub> N <sub>4</sub> O <sub>6</sub>	525.5 [Mw+H]	6.97
Cbz-E N-acylurea		Mw = 436.23 C <sub>21</sub> H <sub>32</sub> N <sub>4</sub> O <sub>6</sub>	459.4 [Mw+Na] <sup>+</sup>	4.82

Table S3. Characterization of the side products of the chemical reaction network.

Supporting Table 4

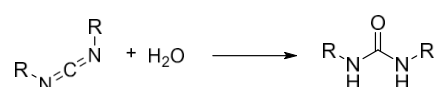
Precursor	k <sub>1</sub> (M <sup>-1</sup> x sec <sup>-1</sup> )	k <sub>2</sub> (sec <sup>-1</sup> )	k <sub>3</sub> (sec <sup>-1</sup> )	k <sub>4</sub> (sec <sup>-1</sup> )	CAC (mM)
Cbz-D	8.0*10 <sup>-2</sup>	2xk <sub>1</sub>	1.5xk <sub>1</sub>	1.5*10 <sup>-2</sup>	N/A
Fmoc-GD	11*10 <sup>-2</sup>	2xk <sub>1</sub>	1.5xk <sub>1</sub>	2.0*10 <sup>-2</sup>	0.60 (200 mM MES)
Cbz-E	3.5*10 <sup>-2</sup>	2xk <sub>1</sub>	0.5xk <sub>1</sub>	1.0*10 <sup>-2</sup>	N/A
Fmoc-E	5.0*10 <sup>-2</sup>	2xk <sub>1</sub>	1.5xk <sub>1</sub>	0.75*10 <sup>-2</sup>	N/A (1350 mM MES)
Fmoc-E	5.0*10 <sup>-2</sup>	2xk <sub>1</sub>	1.5xk <sub>1</sub>	0.75*10 <sup>-2</sup>	0.45 (500 mM MES)
Fmoc-E	5.0*10 <sup>-2</sup>	2xk <sub>1</sub>	1.5xk <sub>1</sub>	0.75*10 <sup>-2</sup>	0.24 (200 mM MES)
Fmoc-E	5.0*10 <sup>-2</sup>	2xk <sub>1</sub>	1.5xk <sub>1</sub>	0.75*10 <sup>-2</sup>	0.21 (100 mM MES)
Fmoc-E	5.0*10 <sup>-2</sup>	2xk <sub>1</sub>	1.5xk <sub>1</sub>	0.75*10 <sup>-2</sup>	0.17 (50 mM MES)
Fmoc-E	5.0*10 <sup>-2</sup>	2xk <sub>1</sub>	1.5xk <sub>1</sub>	0.75*10 <sup>-2</sup>	N/A (200 mM MES+1 mM CTAB)

Table S4. Rate constant used in the kinetic model.

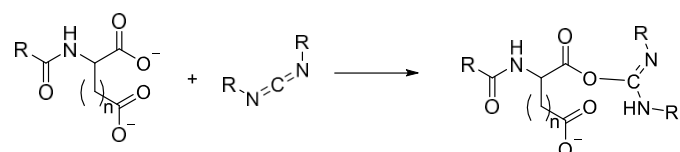
**Supporting notes 1: Description of model**

A kinetic model was written in MATLAB that described five reactions involved in the chemical reaction network except. It did not include minor side reaction that formed the N-acylurea. The concentrations of each reactant were calculated for every 1 second in the cycle. The model was used to fit the obtained HPLC data that described the evolution of the concentration of anhydride, EDC and acid over time. In all experiments, the concentration of the precursor was 10 mM. For all precursor/product combinations, at least three different batch sizes of fuel were used to obtain an accurate fit (e.g. 10 mM Cbz-D + 10, 25 and 50 mM of EDC).

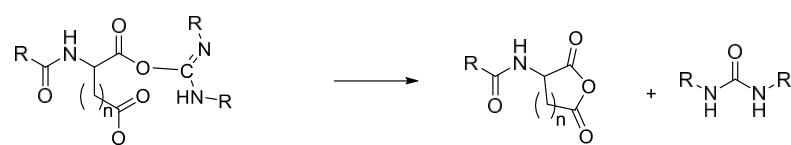
In the model, the following reactions were taken into account:

*Reaction 0 ( $k_0$ )*


The direct hydrolysis of carbodiimide with a first order rate constant of  $1.3 \times 10^{-5} \text{ sec}^{-1}$  as determined by HPLC in previous work.<sup>22</sup> In the experiments, this reaction is irrelevant as it is so slow.

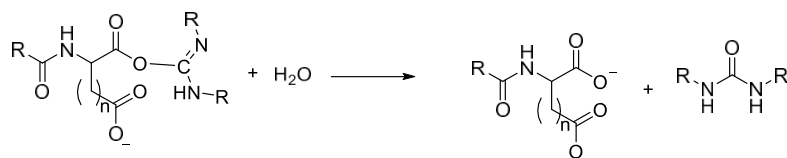
*Reaction 1 ( $k_1$ )*


The formation of O-acylisourea by reaction with EDC with a second order rate constant that was dependent on the nature of the precursor (Table S4). The rate constant was determined for all precursors by HPLC, by monitoring the EDC consumption.

*Reaction ( $k_2$ )*


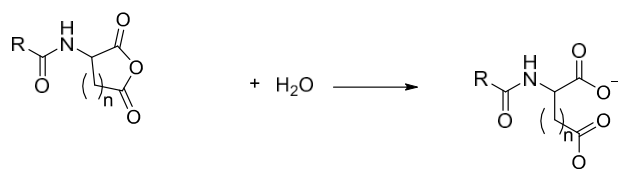
The formation of anhydride with a first order rate constant (Table S4). This rate constant could not be determined because the O-acylisourea was never observed. It was therefore set to be twice the rate of  $k_1$ . As a result, the O-acylisourea did never reach concentrations over  $1 \mu\text{M}$  in the model.

**Reaction 3 ( $k_3$ )**



The direct hydrolysis of O-acylisourea with a first order rate constant (Table S4). This reaction rate could not be obtained because the O-acylisourea was not observed. The ratio of  $k_2$  and  $k_3$  (anhydride formation and competing direct hydrolysis of O-acylisourea) was varied to fit the HPLC data for several concentrations of  $[\text{fuel}]_0$  and  $[\text{di-acid}]_0$ .

**Reaction 4 ( $k_4$ )**



The hydrolysis of anhydride proceeded with a (pseudo)-first order rate as determined by HPLC (Table S4). This reaction describes the hydrolysis on the fraction of anhydride in solution. When the concentration was greater than the solubility of the anhydride, only the fraction that remained in solution was taken into account. In other words, above the solubility the rates was calculation by  $k_4 \cdot \text{CAC}$ .

The model that takes into account all these equations in MATLAB code:

```

%//// SETUP ////
clf, clear
hr = 3600; %amount of seconds per hour
t = 1*hr; %amount of hours to be calculated
plot_EDC = 0; %Plot the [EDC]? (0 or 1 for yes or no)
plot_ANH = 1; %Plot the [anhydride]? (0 or 1 for yes or no)

%///// SET THE INITIAL CONCENTRATIONS/////
COOH(1) = 0.02; %Concentration COOH groups in M (i.e. 0.020 mM for 10 mM fmoc-GD)
EDC(1) = 25/1000; %concentration EDC in M
COOEDC(1) = 0; %concentration O-acylurea in M
COOOC(1) = 0; %concentration O-acylurea in M

%///// SET THE RATE CONSTANTS/////
CAC = 0.65/1000; %CAC in M
k0 = 1.35E-5;
k1 = 1.1E-1;
k2 = 2*k1;
k3 = 1.5*k1;
k4 = 2E-2;

%///// CALCULATIONS OF THE RATES/////
for i=1:t
    r0(i) = k0*EDC(i); %EDC => EDU (direct hydrolysis)
    r1(i) = k1*EDC(i)*COOH(i); %COO + EDC => COOEDC
    r2(i) = k2*COOEDC(i); %COO + COOEDC => COOOC + EDU
    r3(i) = k3*COOEDC(i); %COOEDC => COO + EDCU
    if COOOC(i) > CAC %test if concentration anhydride is greater than its solubility
        r4(i) = CAC*k4; %COOOC => 2COO
    else
        r4(i) = k4*COOOC(i); %COOOC => 2COO
    end

    EDC(i+1) = EDC(i)-r1(i)-r0(i); %Calculation of all the new concentrations.
    COOH(i+1) = COOH(i)-r1(i)-r2(i)+2*r4(i)+r3(i);
    COOEDC(i+1) = COOEDC(i)+r1(i)-r2(i)-r3(i);
    COOOC(i+1) = COOOC(i)+r2(i)-r4(i);
end

%///// PLOTTING ////
if plot_EDC == 1
    plot((1:t)/60,EDC(1:t)*1000,'-m'); %plots [EDC] in mM and a data point per minute in magenta
    hold on
end

if plot_ANH == 1
    plot((1:t)/60,COOOC(1:t)*1000,'-b'); %plots [Anhydride] in mM and a data point per minute in blue
    hold on
end

```

### Supporting notes 2: Description of the quantification of feedback.

According to the above described model, when 10 mM of EDC was added to 10 mM of Fmoc-E and no feedback was in place, the maximum hydrolysis rate was found after 5.1 minutes at a rate of 4.02  $\mu\text{M}/\text{sec}$ . When feedback was in place, the maximum hydrolysis rate was limited to  $k_4 \cdot \text{CAC}$ , where  $k_4$  is the 1<sup>st</sup> order rate constant for hydrolysis and CAC is the critical aggregation concentration. This relation implied that the  $r_4$  decreased with decreasing CAC. In order to quantify the feedback, the decreased  $r_4$  as a result of the feedback was divided by the maximum rate (4.02  $\mu\text{M}/\text{sec}$ ). This fraction was normalized between 0 and 100%, where 100% implied full inhibition of the hydrolysis ( $r_4 = 0 \mu\text{M}/\text{sec}$ ) and 0% meant no inhibition of the hydrolysis ( $r_4 = 4.02 \mu\text{M}/\text{sec}$ ).

Supporting Figure 1

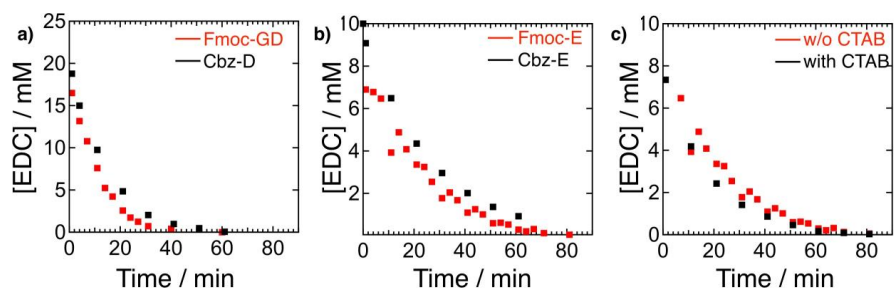


Fig. S1. Concentration EDC against time in response determined by HPLC (markers) for a) 10 mM Fmoc-GD (red) or Cbz-D (black) with 25mM EDC, b) 10 mM Fmoc-E (red) or Cbz-E (black) with 10 mM EDC, c) 10 mM Fmoc-E with (red) or without (black) CTAB and 10 mM EDC.

Supporting Figure 2

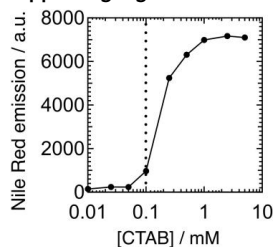


Fig. S2. Nile Red emission intensity at 635 nm against concentration of CTAB. A drastic increase intensity was observed around 0.1 mM, indicative of the critical micelle concentration of CTAB.

Supporting Figure 3

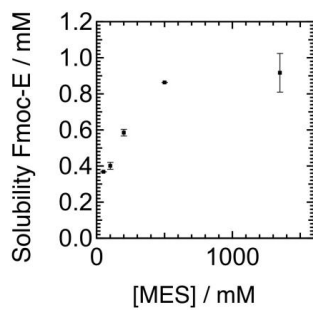




Fig. S3. Solubility of Fmoc-E at pH 1 at different MES concentrations. The error bars depict the standard deviation ( $n=3$ ).

Supporting Figure 4

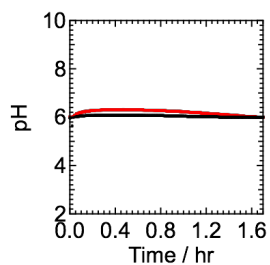


Fig. S4. pH against time for a solution of 10 mM Fmoc-E in response to 10 mM EDC for 200 mM MES buffer (black) and 50 mM MES (red).

## 6. Conclusion and Outlook

The overarching goal of this thesis was to develop a new chemical reaction cycle that can be used to form dissipative assemblies. Up until the start of my Ph.D. work, chemical reaction cycle had been slow, and relied on toxic chemical fuels. The further aims of this work were to use the network to control the assemblies, and to find mechanism by which the assemblies can control the reaction cycles (i.e., feedback mechanisms).

In the first chapter, I describe general design rules for chemical reaction cycles and how they can drive the self-assembly of molecules. The energy to drive dissipative self-assembly can be harvested from the conversion of a fuel into waste or from the conversion of light into heat. The second chapter describes how these chemical reaction cycle can be coupled to the assembly of molecules. We identified three strategies: the reaction cycle can be used to transiently abolish ionic charges, transiently combine two non-assembling precursors, or to induce a conformational change of the precursors.

In Chapter 4, I demonstrate the development and design of a versatile chemical reaction cycle, which operates close to physiological conditions. The Fmoc-protected precursors react to the corresponding metastable product by the consumption of the carbodiimide. The products are designed such that they are able to self-assemble into different dissipative structures. The products rapidly hydrolyze back to the precursor state and can be reactivated as long as fuel is present. It was possible to encapsulate hydrophobic dyes into the dissipative colloids formed by Fmoc-glutamic acid. These colloids could be further explored to encapsulate and release hydrophobic drugs. It could also be possible that these colloids help to increase reaction rates of reactions taking place in or close to the assemblies. Further, it was possible to have control of the assemblies in space and time. In contrast to biological examples, like the microtubule networks, the fibers of the self-standing hydrogels do not show dynamic formation and degradation, which would be an important element for the ability to

self-heal. The dynamics of the fibers can be enhanced by either decreasing the precursor concentration to create a pseudo steady-state in precursor, fuel and product concentration. Other experimental setups, like continuous fueling through a membrane, could also help to increase the dynamics of the fibers.

In Chapter 5, I describe how the robustness of assemblies based on the newly developed chemical reaction cycle can be fine-tuned or switched off completely. The colloidal assemblies inhibit the deactivation reaction of the chemical reaction cycle by shielding the anhydride from hydrolysis. It was possible to show that assemblies with high inhibition rates survive starvation periods without fuel compared to assemblies with low inhibition properties. It is crucial to understand the underlying mechanism of the inhibition to further implement this property into other types of assembly. Further, true complex behavior can arise from such feedback, like adaptivity or oscillatory behavior of the assemblies. In the future, true feedback of the assemblies on either the activation or deactivation reaction has to be implemented to lead to assemblies closer to biological examples. This could be done by including histidine into the precursor molecule or designing a catalyst, which is able to co-assemble with the product. The histidine moiety can act as a proton shuttle in the assembled state. This catalytic behavior would then lead to an increased rate of the deactivation reaction, which could be tuned by the histidine concentration.

In conclusion, this work describes the development and analysis of a newly developed chemical reaction cycle, which is versatile, scalable, and operates under close to physiological conditions. The assemblies show life-like properties, like reusability, and can be controlled in space and time. Furthermore, I could show how the assemblies affect the deactivation reaction of a chemical reaction cycle. The development of such a versatile chemical reaction cycle and the design of assemblies with robustness against their degradation opens the door for new man-made dissipative supramolecular assemblies and applications with unique properties.

## 7. Further Publications

Besides the two publications reprinted in sections 4 and 5 with the focus on dissipative materials ranging from fibers to colloidal structures I contributed to five more publications. One manuscript is in preparation.

### 7.1 List of publications

1. C. Wanzke; M. Tena-Solsona; **B. Rieß**; L. Tebcharani; J. Boekhoven, *Active Droplets In A Hydrogel Release Drugs With A Constant And Tunable Rate*. *Materials Horizons* **2020**  
doi: 10.1039/C9MH01822K
2. **B. Rieß\***; R. K. Grötsch\*; J. Boekhoven, *The Design of Dissipative Molecular Assemblies Driven by Chemical Reaction Cycles*. *Chem* **2020**, 6 (3), 552-578.
3. M. Tena-Solsona; J. Janssen; C. Wanzke; F. Schnitter; H. Park; **B. Rieß**; J. M. Gibbs; C. A. Weber; J. Boekhoven, *Kinetic Control over Droplet Ripening in Fuel-Driven Active Emulsions*. *ChemRxiv* **2019**.  
doi: 10.26434/chemrxiv.9978539.v1
4. **B. Rieß**; J. Boekhoven, *Applications of Dissipative Supramolecular Materials with a Tunable Lifetime*. *ChemNanoMat* **2018**, 4 (8), 710-719.
5. M. Tena-Solsona; C. Wanzke; **B. Rieß**; A. R. Bausch; J. Boekhoven, *Self-Selection of Dissipative Assemblies Driven by Primitive Chemical Reaction Networks*. *Nat Commun.* **2018**, 9 (1), 2044.

- 
6. **B. Rieß\***; C. Wanzke\*; M. Tena-Solsona; R. K. Grötsch; C. Maity; J. Boekhoven, *Dissipative Assemblies That Inhibit Their Deactivation. Soft Matter* **2018**, 14 (23), 4852-4859.
  7. S. Pomplun; C. Sippel; A. Hähle; D. Tay; K. Shima; A. Klages; C. M. Unal; **B. Rieß**; H. T. Toh; G. Hansen; H. S. Yoon; A. Bracher; P. Preiser; J. Rupp; M. Steinert; F. Hausch, *Chemogenomic Profiling of Human and Microbial Fk506-Binding Proteins. J Med Chem* **2018**, 61 (8), 3660-3673.
  8. M. Tena-Solsona; **B. Rieß**; R. K. Grötsch; F. C. Löhner; C. Wanzke; B. Käsdorf; A. R. Bausch; P. Müller-Buschbaum; O. Lieleg; J. Boekhoven, *Non-Equilibrium Dissipative Supramolecular Materials with a Tunable Lifetime. Nat Commun* **2017**, 8, 15895.

\* These Authors contributed equally to this work.

## 7.2 Application of Dissipative Supramolecular Materials with a Tunable Lifetime

### Abstract.

The research and application of supramolecular materials have grown rapidly over the past years. But in comparison to biological materials, these man-made supramolecular materials exist in equilibrium. Biological materials, in contrast, exist out-of-equilibrium and have, therefore, outstanding properties. Properties like a tunable lifetime, the ability to self-heal, or even to self-replicate. Inspired by biology, researchers have developed analogs of dissipative supramolecular materials, which can be controlled in space and time. In this review article, we introduce the crucial difference between in-equilibrium and dissipative out-of-equilibrium materials. Furthermore, we focus on materials that have a tunable lifetime. A facial way to tune the lifetime is by the initial amount of fuel added to the chemical reaction cycle. We extracted other methods, which also lead to tunable lifetimes, like adjusting the precursor concentration or the concentration of reactants, which are involved in the deactivation reaction. Besides this key property, we list materials which can have application in everyone's everyday life. So, dissipative out-of-equilibrium materials can be used as temporary inks or as reusable paper. Another type of assemblies is self-standing hydrogels, which can find its application as drug delivery platforms or as biofilm, to help in the body to regenerate tissue. The last type of dissipative assemblies discussed are assemblies which can help to control rates of reactions. The biological property of spatio-temporal control has been successfully implemented into man-made dissipative supramolecular assemblies. But true complex behavior of the assembly on the chemical reaction cycle is still missing.

This work has been published:

Title: Application of Dissipative Supramolecular Materials with a Tunable Lifetime

Authors: Benedikt Rieß, Prof. Dr. Job Boekhoven

First published: 04. June 2018

Journal: ChemNanoMat **2018**, 4, 710-719.

Publisher: Wiley-VCH

DOI: 10.1002/cnma.201800169

Reprinted with permission of John Wiley and Sons; License Number: 4780840275614.

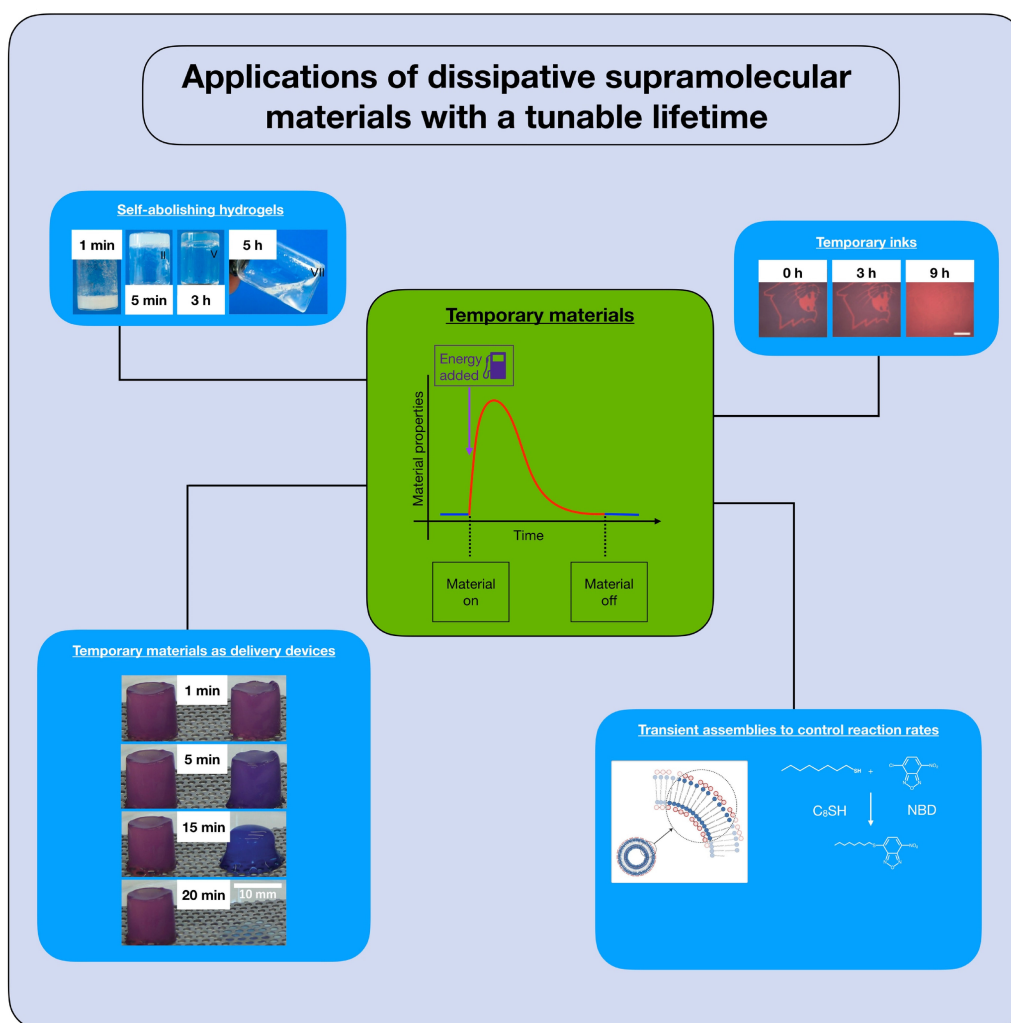
This section states the individual work of each author in the publication above. B. Rieß and J. Boekhoven both wrote paragraphs in the review article. The figures were primarily designed by B. Rieß.

Self-Assembly

SPECIAL  
ISSUE

Applications of Dissipative Supramolecular Materials with a Tunable Lifetime

Benedikt Rieß<sup>[a]</sup> and Job Boekhoven<sup>\*,[a, b]</sup>





**Abstract:** Supramolecular materials are materials in which molecular building blocks are held together by non-covalent interactions. These materials exist in equilibrium with their environment. In contrast, most biological materials exist out of equilibrium. They require constant dissipation of energy and consumption of nutrients to be sustained. As a result of their non-equilibrium nature, biological materials have superior properties compared to their in-equilibrium counterparts. These properties include spatial and temporal control over

their presence, the ability to self-heal and even the ability to self-replicate. Inspired by biology, researchers have developed analogs of such dissipative supramolecular materials. This Focus Review introduces the crucial differences between in-equilibrium and dissipative supramolecular materials. We focus on one unique property of the emerging materials: their tunable lifetime. With recent examples, we show the principles involved and how these materials can be applied in the future.


## 1. Introduction

Supramolecular materials are materials in which molecular building blocks are held together by non-covalent interactions, like hydrogen bonding or  $\pi$ -orbital overlap.<sup>[1]</sup> Over the past decades, the field of supramolecular materials has seen explosive growth, in part because of design rules<sup>[2-8]</sup> new synthetic methods and prominent applications.<sup>[9-11]</sup> Successful examples include block copolymer micelles<sup>[12]</sup> that can be used to deliver drugs at diseased sites<sup>[13,14]</sup> or supramolecular polymers<sup>[15]</sup> that help the body to regenerate lost tissue.<sup>[16,17]</sup> Despite their success, man-made supramolecular materials remain rather basic compared to supramolecular materials as found in biology. Biological supramolecular materials, like skin, bone or even cells, demonstrate some remarkable features, including self-replication, the ability to make decisions and the ability to self-heal.<sup>[18]</sup> Although many of these processes in biological supramolecular materials are ill-understood, one concept recurs in all of these materials: supramolecular biological materials almost always exist out of equilibrium with their environment.<sup>[18]</sup> That means that biological materials can only exist by constant dissipation of energy taken from their surrounding.<sup>[19,20]</sup> Irreversible (photo-)chemical reactions deliver the source of energy. A prime example is the dissipative self-assembly of microtubules driven by GTP.<sup>[21]</sup> Due to their energy-dissipating nature, these materials have several unique properties that we do not observe in in-equilibrium materials.

In this review, we will explain the difference between equilibrium and dissipative supramolecular materials. We will highlight the unique properties of the dissipative materials, and we will focus on one of their specific features: the ability to be controlled over time. We will review strategies to manage the lifetimes of these materials, their possible applications and we close with an outlook.

[a] B. Rieß, Prof. Dr. J. Boekhoven  
Technical University of Munich, Chemistry Department, Lichtenbergstr. 4,  
80895, Garching, Germany  
E-mail: job.boekhoven@tum.de

[b] Prof. Dr. J. Boekhoven  
Technical University of Munich, Institute for Advanced Study, Lichtenbergstr.  
2a, 80895, Garching, Germany

 This manuscript is part of a Special Issue on Supramolecular Nanostructures.  
Click here to see the Table of Contents of the special issue.

## 2. Chemical Reactions to form Unique Materials Supramolecular Materials

### 2.1 Chemical Reaction Networks to Induce Dissipative Self-assembly

In dissipative supramolecular materials, materials are formed by the self-assembly of molecules. Crucially, the formation of these assemblies is coupled to a chemical reaction network of at least two chemical reactions.<sup>[22-26]</sup> In the activation reaction, a non-assembling molecule (precursor) reacts with a sacrificial high-energy molecule (fuel) or with light (photon) to form a metastable product (Figure 1a). It is essential that this activation reaction is irreversible and that the fuel is thus irreversibly “burned.” The second reaction brings the product back to the precursor. Also for this deactivation reaction, it is crucial that the reaction is irreversible and the reaction has to occur spontaneously. Under these set of conditions, a product is formed by the dissipation of energy (fuel or photon), and it remains transiently present. In its limited lifetime, the product can act as a building block to form assemblies which constitute the supramolecular material.

We clarify the above definition with a recently introduced chemical reaction network by our group.<sup>[27]</sup> The precursors are derivatives of aspartic acid (Figure 1b). The two carboxylates of aspartic acid render the molecule well soluble in aqueous buffer. In the activation reaction, the two carboxylates react with a carbodiimide fuel to irreversibly transform it into an cyclic anhydride (product). The product, in the aqueous environment, is metastable and hydrolyzes to its original precursor state. The half-life of the anhydride is in the range of several minutes to several seconds at pH 6, depending on its nature. Hartley and coworkers described that the chemical reaction network could also be applied to larger macrocycles.<sup>[28]</sup> In essence, the chemical reaction networks entail the transient anhydride formation driven by carbodiimide hydrolysis.

The conversion of the precursor’s two anionic carboxylates into non-charged anhydride makes the product more hydrophobic than its precursor. The hydrophobization can be used to induce self-assembly into a supramolecular material, which we will discuss in detail in the sections below. In contrast to equilibrium materials, the properties of the emerging supramolecular material are determined by the governing

reaction rates and lifetimes of the product, which is the focus of this review.

## 2.2 Unique Properties of Dissipative Supramolecular Materials

Because of their non-equilibrium nature, dissipative supramolecular materials have unique properties compared to their in-equilibrium counterparts.<sup>[19]</sup> Due to the dynamic product activation and deactivation, the emerging materials can be intrinsically self-healing. To that end, researchers have shown that supramolecular hydrogels that are typically not self-healing, can regenerate after damage when formed via dissipative self-assembly.<sup>[29]</sup> Another unique property of dissipative assemblies is that patterns of the assemblies can emerge on much greater length-scales than the molecules or assemblies themselves. This phenomenon, referred to as self-organization, has so far only been demonstrated for biological dissipative assemblies, like microtubules<sup>[21]</sup> that form asters and vortices on millimeter length scales.<sup>[30,31]</sup> Other properties of dissipative assemblies include the ability to self-replicate and the ability to be controlled over space and time. The temporal control has been the most studied unique property of dissipative materials and is the focus of this review.

## 3. Supramolecular Materials with a Tunable Lifetime

In this section, we will discuss examples of dissipative supramolecular materials, in which the researchers focused on controlling the lifetime of the emerging materials.<sup>[32]</sup> The general strategy in these studies involves the application of a finite amount of energy to the chemical reaction network (Figure 2). The energy in these examples is added in the form of a chemical fuel or by irradiation with light. In response, the chemical reaction network activates some of its precursors to their product state. The product can then self-assemble into the supramolecular material. With the formation of the product, deactivation commences. As the reaction network is running out of fuel, the rate of deactivation will be higher than the activation rate, and, consequently, the supramolecular material starts to decay. Equilibrium is reinstated when all fuel has been consumed, and the material has entirely decayed. We demonstrate the success of dissipative supramolecular materials with self-erasing inks, self-abolishing hydrogels, assemblies that release molecules after a predetermined time, and materials that can enhance or inhibit reactions for specific times.

### 3.1 Self-erasing Inks

In dissipative supramolecular inks, the self-assembly of building blocks results in a change in color or turbidity of the material. In these systems, a polymeric matrix traps the precursors and

their solvent such that energy can be applied locally. Thus, a pattern, image or message appears only where the energy is applied. During the reinstatement of equilibrium, the message self-erases after which the material can be reused. As such, dissipative supramolecular inks, offer an exciting platform for the development of a reusable paper.

To that end, Grzybowski and coworkers introduced a first self-erasing ink based on the dissipative self-assembly of gold- or silver-nanoparticles driven by UV-light (Figure 3).<sup>[33]</sup> They functionalized nanoparticles with a trans-azobenzene derivative which served as the precursor in the chemical reaction network (Figure 3a). The precursor can isomerize to cis-azobenzene in response to UV-light as the energy source (Figure 3b). Importantly, the isomerized cis-azobenzene state was not the thermodynamically favored state but reverted to the trans-state spontaneously. The UV-induced isomerization caused a change in the dipole moment of the azobenzene-functionalized particles. That dipole moment-shift was sufficient to induce the self-assembly of the nanoparticles into large clusters (Figure 3c). As the cis-azobenzene groups spontaneously isomerized back to their thermodynamically more favored trans-state, the cluster started disassembling over time, when the energy source (UV-light) was taken away. Taken together, UV-light can convert precursor into an activated product state that can self-assemble, but the thermal energy spontaneously brings the activated state back to the disassembled precursor.

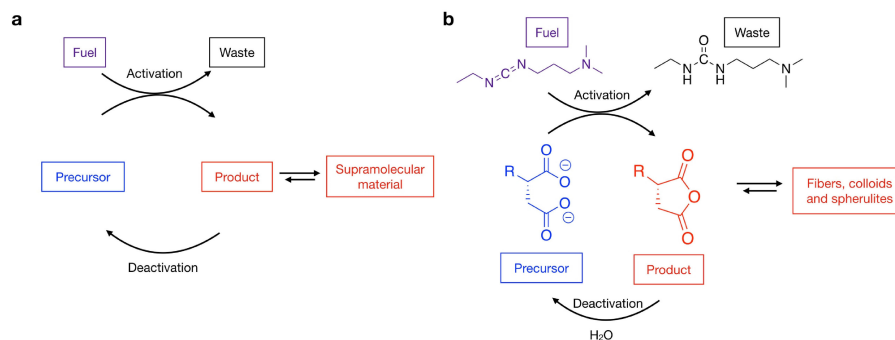
The dissipative assembly of these nanoparticles induced a color-shift of the sample from red to blue. The researchers embedded the chemical reaction network in a polymer gel and

*Benedikt Rieß studied Chemistry at the Technical University of Munich (2013). After obtaining his M.Sc. in Organic and Polymer Chemistry (2015) under the guidance of Prof. Felix Henschel, he joined the group of Prof. Job Boekhoven as a Ph.D. researcher in 2016. His research focuses on the development of man-made dissipative materials driven by chemical reaction networks.*

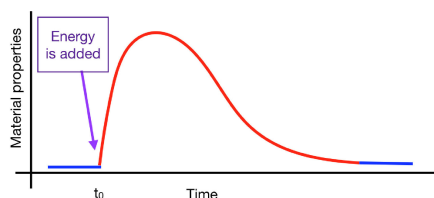


*Job Boekhoven is a Rudolf Mößbauer assistant professor at the Department of Chemistry of the Technical University of Munich. He received his M.Sc. degree in Chemistry in 2008 from the University of Groningen. In 2012, he got his Ph.D. for his work in the group of Prof. Jan van Esch and Prof. Rienk Eelkema at Delft University of Technology. He pursued his academic career as a Rubicon postdoctoral fellow in the group of Prof. Sam Stupp at Northwestern University from 2012 to 2015. Boekhoven's current work focusses on the development of supramolecular materials via non-equilibrium self-assembly.*





**Figure 1.** a) General chemical reaction network for dissipative self-assembly. A precursor (blue) reacts irreversibly with a fuel (purple) to form a product (red) in the activation reaction. The metastable product reverts spontaneously to the original precursor in the deactivation reaction. In its limited lifetime, the product can self-assemble into a supramolecular material. b) In the depicted chemical reaction network, a dicarboxylate precursor converts into a metastable anhydride driven by the hydrolysis of carbodiimides.



**Figure 2.** Generalized profile of material properties against time for dissipative supramolecular materials. At  $t_0$ , a finite amount of energy is added. Consequently, the supramolecular material (red line) emerges. When the system runs out of energy, equilibrium (blue line) is reinstated. The lifetime of the material can be controlled by parameters like the amount of fuel applied or the concentration of precursor.

irradiated the gel with UV-light through a photomask. Upon irradiation, the color of the gel changed from red to blue for the gold nanoparticles. For the silver nanoparticles, the color-shift was from yellow to blue (Figure 3d). The researchers showed that a UV-laser pen could also be used induce the color-shift. Moreover, they were able to write messages on the material. Crucially, all the patterns and messages erased over time as soon as the researchers removed the source of UV-light. The self-erasure time could be tuned from seconds to hours.

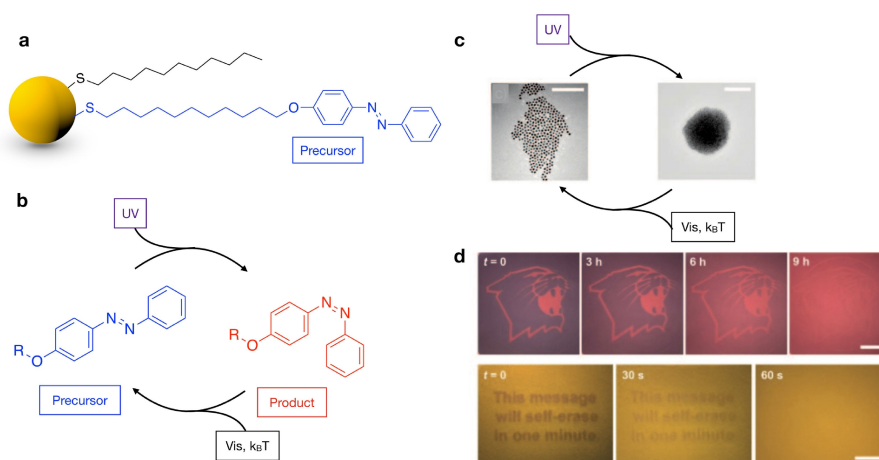
Our group recently demonstrated that self-erasing inks could also be based on chemical fuels, as opposed to UV-light, to deliver the required energy. The chemical reaction network is similar to the one described in Figure 1b. The precursor in this reaction network consisted of fluorenylmethyloxycarbonyl protected aspartic acid (Fmoc-D, Figure 4a). The precursor converted into its corresponding anhydride by addition of carbodiimide condensing agent as a fuel (Figure 4b). Upon conversion from precursor to product, the molecule lost two of its negatively charged carboxylates which made it less soluble. As a consequence, the anhydride product self-assembled into spherulites which transformed an initially clear solution into a turbid one (Figure 4c). Because of the anhydride's transient

nature, the spherulites were temporary present, and the turbid solution reverted to a clear one when the system ran out of fuel. A solution of the precursor was trapped in a polyacrylamide hydrogel, and the fuel was applied onto the gel, either with a paint-brush or using a spray-coating setup. As a result, the turbidity of the gel increased where fuel was applied, and messages could be written (Figure 4d). Due to their non-equilibrium nature, the hydrogels lost their increased turbidity over the course of hours. Moreover, the self-erasure time could be tuned from one to several hours by the concentration of the applied fuel solution.

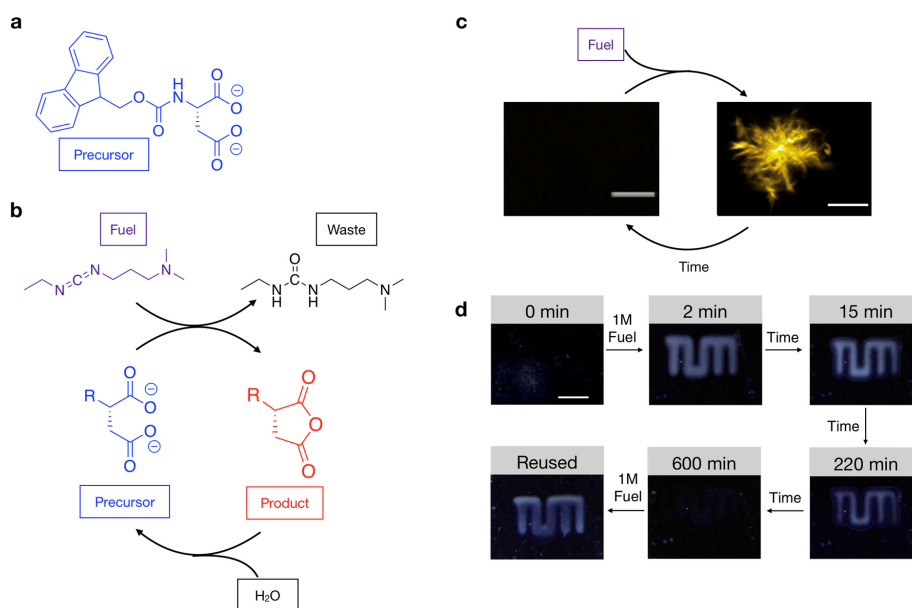
### 3.2 Self-abolishing Hydrogels

In supramolecular hydrogels, molecules assemble into fibers that subsequently form a network that traps its solvent.<sup>[34–36]</sup> Consequently, the self-assembly of molecules can convert an aqueous buffer into a material with solid-like properties.<sup>[37]</sup> For biomedical purposes, hydrogels have proven extremely powerful, ranging from applications as scaffolds for cells<sup>[38–41]</sup> to reservoirs that control the release of drugs.<sup>[42–45]</sup> Coupling these useful features of hydrogels to the unique properties dissipative self-assembly can thus result in self-abolishing hydrogels with a finite lifetime which is the focus of this section.

Van Esch and Eelkema introduced the first example of chemically driven dissipative self-assembly of fibers.<sup>[46,29]</sup> The chemical reaction network involved a well-soluble precursor, *N,N'*-dibenzoyl-L-cystine, that has two carboxylates (Figure 5a). When a methylating agent like methyl iodide or dimethyl sulfate was added, it reacted with the precursor to form the corresponding methyl ester (Figure 5b). Under the employed conditions, the methyl-ester product deactivated to the original precursor via hydrolysis. The reaction network thus formed metastable methyl-esters at the expense of methylating agent. The methyl ester, due to its loss of anionic carboxylates, was less soluble and self-assembled into fibers. The ensemble was



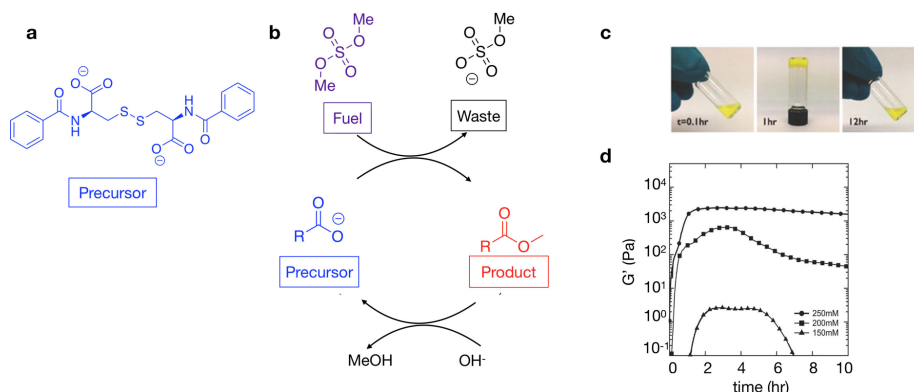
**Figure 3.** a) Schematic depiction of the precursor used in the study. b) In the depicted chemical reaction network, the azobenzene precursor (blue) absorbs a UV-photon (fuel, purple) and is isomerized to the metastable product (red). The product reverts spontaneously to the original precursor. c) TEM images of the precursor in solution (left) and the aggregates (right). The scale bar measures 100 nm. d) Photographs of self-erasing images or text using gold nanoparticles (first row) and silver nanoparticles (second row). The scale bars measure 1 cm. Reproduced with permission from Ref. 32. Copyright 2009 Wiley-VCH.



**Figure 4.** a) Chemical structure of the precursor Fmoc-D. b) In the depicted chemical reaction network, the dicarboxylate precursor (blue) reacts irreversibly with a carbodiimide fuel (purple) to form a metastable anhydride product (red). Hydrolysis deactivates the anhydride to the precursor. c) Confocal micrograph of the transiently arising spherulites of Fmoc-D in response to carbodiimide as fuel. The scale bar measures 10  $\mu\text{m}$ . d) Photographs of the self-erasing inks at different times during the cycles. The scale bar measures 1 cm. Reproduced with permission from Ref. 26. Copyright 2017 Nature Publishing Group.

thus able to transform a solution of the precursor into a temporary hydrogel at the expense of methylating agent as

fuel (Figure 5c). The lifetime of the hydrogels could be tuned from several hours to days by the pH of the solution or the

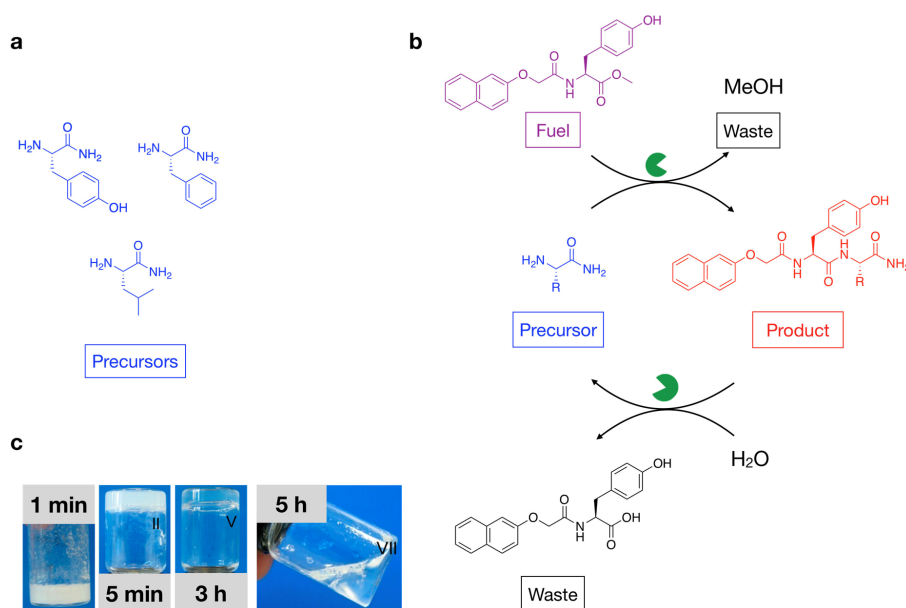


**Figure 5.** a) The molecular structure of the N,N-dibenzoyl cysteine precursor. b) The depicted chemical reaction network converts the precursor into its corresponding methyl ester product at the expense of dimethylsulfate as fuel. The methyl ester hydrolyzes back to the precursor over time. c) Photographs of the transient hydrogel at different times after addition of fuel. d) The viscoelastic response against time of the samples as measured by plate-plate rheology in response to various amounts of fuel. When more fuel was added, gels were stronger and persisted for longer times. Reproduced with permission from Ref. 28. Copyright 2015 American Association for the Advancement of Science.

amount and nature of the methylating agent as fuel added (Figure 5d).

Work by Ulijn and coworkers showed that the formation of dissipative hydrogels was not limited to methylating agents,

but could also be induced by enzymes.<sup>[48,49]</sup> The study described a tyrosine-based precursor (Figure 6a). The precursor that was activated by reaction with a second amino acid as fuel, specifically the methyl ester of tyrosine with its N-terminus



**Figure 6.** a) The molecular structures of the tyrosine-based precursors. b) The depicted chemical reaction network converts the precursor into a dipeptide product at the expense of the tyrosine methyl ester as fuel. The network requires chymotrypsin (green) for both the activation and deactivation reaction. c) Photographs of the transient hydrogel taken at different times after addition of fuel. Reproduced with permission from Ref. 47. Copyright 2015 Wiley-VCH.

protected by a naphthoxyacetyl group (Figure 6b). The activation reaction did not occur spontaneously, but the enzyme  $\alpha$ -chymotrypsin was used to catalyze it. Crucially, the same enzyme catalyzed the hydrolysis of the dipeptide product to the precursor, which rendered the dipeptide metastable. The dipeptide was designed to assemble into a hydrogel-forming fiber network (Figure 6c). With the enzyme concentration and the nature of the precursor, the authors could tune the lifetime of the hydrogel from minutes to several hours.

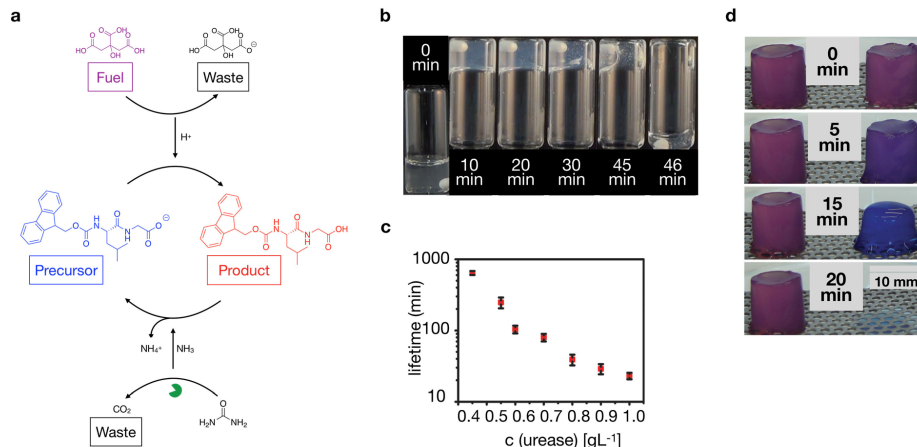
The self-abolishing hydrogels and supramolecular polymers we highlighted above, as well as work by others,<sup>[50–57]</sup> are an exciting development for the field of biomaterials. Specifically, in regenerative medicine, the creation of a hydrogel with embedded cells that changes its function over time has been a long-standing challenge.<sup>[58]</sup>

### 3.3 Temporary Materials as Delivery Devices

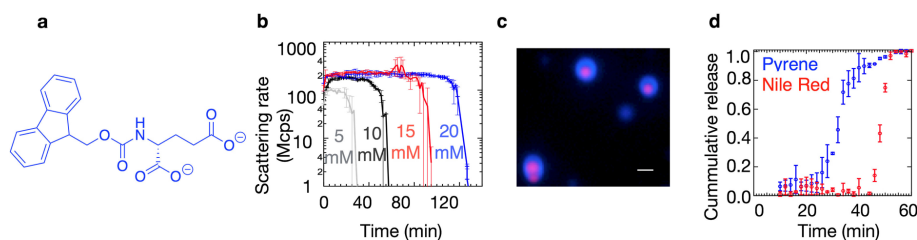
Another promising biomedical application for materials with a tunable lifetime is as a delivery vehicle for drugs. To that end, Walther and coworkers demonstrated the burst release of a product from a dissipative hydrogel.<sup>[59]</sup> The chemical reaction network was described in earlier work and based on the addition of the enzyme urease and citric acid as fuel (Figure 7a).<sup>[60]</sup> The acid addition induced a decrease in the pH. In parallel, the urease hydrolyzed urea to form ammonia as a product. The released ammonia raised the pH back to alkaline. As a result, the pH was only temporary brought to acidic values and reverted to the starting pH.

The unique approach allowed the researchers to couple pH-responsive assemblies to the chemical reaction network. Indeed, when the chemical reaction cycle was carried out in the presence of a pH-responsive hydrogelator, the decrease in pH resulted in the formation of a transient gel (Figure 7b). The researchers demonstrated that the lifetime of the hydrogel could be tuned from minutes to hours by the amount of urease in the system (Figure 7c). Moreover, it was also demonstrated that their temporary hydrogels could release hydrophilic dye after a preprogrammed time (Figure 7d). Because of the generality of the principle, several other assemblies have been formed via this principle including DNA i-motifs<sup>[61]</sup> and photonic devices.<sup>[62]</sup>

To demonstrate the use of dissipative materials as delivery vehicles, we recently described the release of hydrophobic dyes from a dissipative supramolecular material. We used Fmoc-protected glutamic acid (Fmoc-E, Figure 8a) as a precursor in the carbodiimide-fueled chemical reaction network described in Figure 3a. The activated building block self-assembled into colloids driven by hydrophobic collapse. Due to the transient nature of the activated anhydride building block, the colloids had a finite lifetime that could be tuned from 30 to 120 minutes by the amount of fuel added to the system (Figure 8b). We found that hydrophobic dyes could be incorporated into these colloids. Moreover, the time point in the cycle when the dye was added determined where it was incorporated. For example, when Nile Red was added from the beginning of the cycle, i.e., with the fuel, it was incorporated in the core of the colloid (Figure 8c). When pyrene was added 10 minutes after initiating the cycle, it was built into the outer layers of the colloids. The inhomogeneous distribution of the dyes could be used to



**Figure 7.** a) In the depicted chemical reaction network, citric acid is used as a fuel to release protons. The decrease in pH-activated the enzyme urease which releases ammonia and resets the pH to the original value. If the cycle was carried out in the presence of a dipeptide as a precursor, it was temporarily protonated and self-assembled into fibers. b) Photographs of the gel at different time points. c) A plot of the lifetime against concentration urease. The amount of enzyme can tune the lifetime of the hydrogel. d) Photographs of a static (left) and a transient (right) hydrogel at different times. The transient hydrogel decayed after a preprogrammed time and released the encapsulated dye Resazurin. The scale bar measures 1 cm. Reproduced with permission from Ref. 58. Copyright 2015 Wiley-VCH.



**Figure 8.** a) Chemical structure of Fmoc-E used as a precursor molecule for the dissipative chemical reaction network based on carbodiimide hydrolysis. b) DLS measurement of the dissipative network against time showed the transient nature of the assemblies. c) Confocal images of colloids coded with Nile red and pyrene. The scale bar measures 1  $\mu\text{m}$ . d) Release profile obtained from the collapse of the colloids. Reproduced with permission from Ref. 26. Copyright 2017 Nature Publishing Group.

control the order of the release of the hydrophobic molecules from the colloids. Because the colloids were deactivated from their outer shells, the blue pyrene was released first (Figure 8d). Near the end of the lifetime of the colloids, also the Nile Red in the core was released. Consequently, the sequence of release of hydrophobic dyes could be controlled by order of incorporation of the dyes during the preparation of the colloids. Moreover, the amount of fuel could be used to tune the point at which the molecules were released.

The examples described above demonstrate the ability to release both hydrophobic and hydrophilic dyes from dissipative assemblies. Moreover, both the time when the material is released as well as the sequence of the released dyes can be predetermined by the users. These studies, as well as other from the field,<sup>[63]</sup> show the exciting possibilities of dissipative supramolecular materials as drug delivery vehicles or other biomaterials in the future.

### 3.4 Transient Assemblies to Control Reaction Rates

Besides the application of dissipative assemblies as delivery devices, researchers have used dissipative supramolecular materials to control reaction rates. A recent study of Prins and coworkers explored that principle. In their work, a cationic surfactant,  $\text{C}_{16}\text{TACN}^+\text{Zn}^{2+}$  (Figure 9a), served as a precursor.<sup>[64]</sup> The precursor was electrostatically complexed by the anionic fuel ATP (Figure 9b). The complexation screened the charges of the surfactant and induced its assembly into vesicles (Figure 9c) as evidenced by confocal and electron microscopy (Figure 9d). However, under the employed conditions, the ATP was unstable and hydrolyzed to AMP, which induced the disassembly of the vesicles. Addition of the enzyme potato apyrase increased the hydrolysis rate, which allowed the researchers to control the lifetime of the transient vesicles.

The researchers hypothesized that the bilayer of the vesicles could serve as a hydrophobic container that hosts reactants. Following that idea, they were able to tune the kinetics of an aromatic nucleophilic substitution reaction between two hydrophobic compounds (Figure 9e). The amount of ATP added to

the system increase the number of vesicles in the solution and, consequently, it increased the yield of the aromatic nucleophilic substitution (Figure 9f).

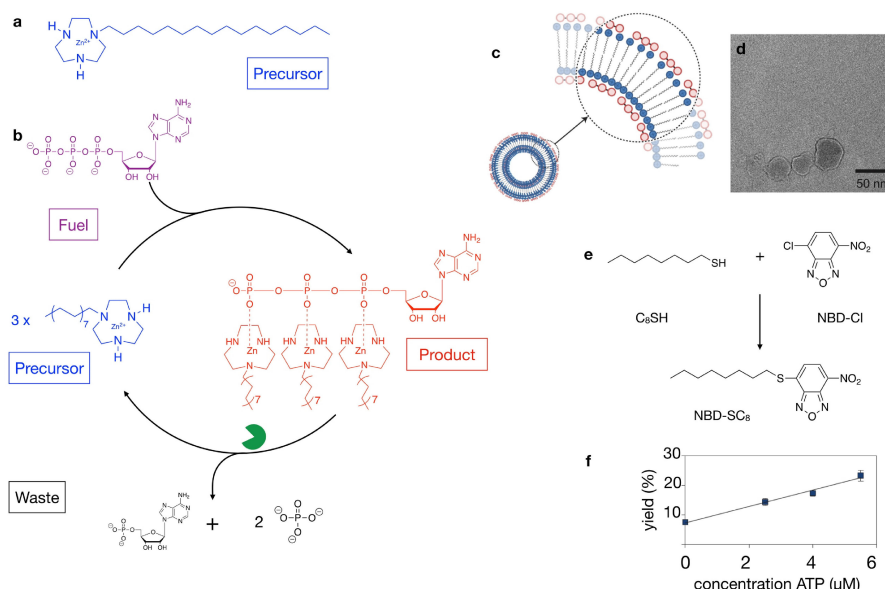
Examples of the dissipative assembly of nanoparticles have also been reported. The systems make use of nanoparticles but with different roles. In a first example, the surface of the nanoparticles acted as a catalyst, and their transient assembly thus decreased the reaction rate.<sup>[65]</sup> Klajn *et al.* described a system in which the assembly helped concentrating the reactants, thus serving as a temporary “nano flask.”<sup>[66]</sup> As a result, reaction rates accelerated upon assembly.

## 4. Conclusions

In this Focus Review, we described recent examples of dissipative self-assembly that researchers developed with the intention to tune the lifetime of the emerging materials. In these dissipative supramolecular materials, energy-dissipating chemical reaction networks are coupled directly or indirectly to the self-assembly of molecules into supramolecular materials. The emerging materials have properties that are determined by the kinetics of the chemical reaction networks. In this Focus Review, we chose to focus on the finite lifetime of the material. A facile way to tune the lifetime is by the initial amount of fuel added. Other methods include adjusting the precursor concentration or the concentration of reactants that are involved in the deactivation.

Preliminary studies have shown that the emerging dissipative supramolecular materials can be used as self-erasing inks or as a reusable paper. Another application includes self-abolishing hydrogels. Such gels could find application as a biomaterial that aids the body to regenerate lost tissue, and, after its function has been carried out, self-abolish. Alternatively, these materials can be used to deliver pharmaceuticals at a predetermined time or following a specific sequence. A final application of dissipative supramolecular materials we discussed is as a material that can control reaction rates over time.

In biological dissipative materials, we can find, besides a finite lifetime also other exciting, unique properties, which include the ability to self-heal, self-replicate and to sponta-



**Figure 9.** a) Molecular structure of the amphiphilic  $C_{16}TACNZn^{2+}$  precursor. b) Chemical reaction network that forms vesicles under ATP usage by coordinating the precursor. The enzyme potato pyruvate kinase (green) hydrolyzes ATP to AMP and two-times  $P_i$ . c) Schematic representation of the vesicle bilayer. d) Cryo-TEM of the dissipative vesicle. The scale bar measures 50 nm. e) Scheme of the aromatic nucleophilic substitution reaction carried out in the vesicular system. f) The yield of NBD- $C_6$  as a function of ATP concentration after a reaction time of 30 minutes. Reproduced with permission from Ref. 63. Copyright 2016 Nature Publishing Group.

neously form patterns. Engineering such behavior in artificial supramolecular materials is one of the primary goals for the field of supramolecular chemistry. A step towards that objective is implementing feedback of the assemblies on their chemical reaction network. For example, the assembly of microtubules catalyzes its building block deactivation, which is a crucial element of the complex behavior of the emerging structures.<sup>[21]</sup> Very recent work by our group has shown that feedback of the assemblies on their network can indeed initiate new behavior that includes self-selection<sup>[67]</sup> or an increased robustness of the assemblies.<sup>[68]</sup> However, true complex behavior of the resulting materials, like self-replication or pattern formation is still missing. With these unique properties, we foresee a significant role of dissipative self-assembly in the materials of the future.

### Acknowledgments

J.B. is grateful for funding of his position by the Institute for Advanced Study through the German Excellence Initiative and the European Union Seventh Framework Programme under grant agreement n° 291763. B.R. is grateful for funding by the Deutsche Forschungsgemeinschaft (DFG) via the collaborative research centre SFB 863 project B11.

### Conflict of Interest

The authors declare no conflict of interest.

**Keywords:** dissipative self-assembly · lifetime · self-assembly · supramolecular materials · temporary material

- [1] S. I. Stupp, V. LeBonheur, K. Walker, L. S. Li, K. E. Huggins, M. Keser, A. Amstutz, *Science* **1997**, *276*, 384.
- [2] D. B. Amabilino, D. K. Smith, J. W. Steed, *Chem. Soc. Rev.* **2017**, *46*, 2404–2420.
- [3] R. N. Shah, N. A. Shah, M. M. Del Rosario Lim, C. Hsieh, G. Nuber, S. I. Stupp, *Proc. Natl. Acad. Sci. USA* **2010**, *107*, 3293–8.
- [4] M. de Loos, B. L. Feringa, J. H. van Esch, *Eur. J. Org. Chem.* **2005**, *17*, 3615–3631.
- [5] J. H. van Esch, *Langmuir* **2009**, *25*, 8392–4.
- [6] R. J. Macfarlane, B. Lee, M. R. Jones, N. Harris, G. C. Schatz, C. A. Mirkin, *Science* **2011**, *334*, 204–8.
- [7] P. W. Rothemund, *Nature* **2006**, *440*, 297–302.
- [8] P. Yin, H. M. Choi, C. R. Calvert, N. A. Pierce, *Nature* **2008**, *451*, 318–22.
- [9] M. J. Webber, E. A. Appel, E. W. Meijer, R. Langer, *Nat. Mater.* **2015**, *15*, 13–26.
- [10] A. R. Hirst, B. Escuder, J. F. Miravet, D. K. Smith, *Angew. Chem. Int. Ed. Engl.* **2008**, *47*, 8002–18.
- [11] M. Zelzer, R. V. Uljin, *Chem. Soc. Rev.* **2010**, *39*, 3351–7.
- [12] L. Zhang, A. Eisenberg, *Science* **1995**, *268*, 1728–31.
- [13] B. Jeong, Y. H. Bae, D. S. Lee, S. W. Kim, *Nature* **1997**, *388*, 860.
- [14] K. T. Oh, T. K. Bronich, A. V. Kabanov, *J. of Control. Rel.* **2004**, *94*, 411–422.
- [15] T. Aida, E. W. Meijer, S. I. Stupp, *Science* **2012**, *335*, 813–817.



- [16] F. Tantakitti, J. Boekhoven, X. Wang, R. V. Kazantsev, T. Yu, J. Li, E. Zhuang, R. Zandi, J. H. Ortony, C. J. Newcomb, L. C. Palmer, G. S. Shekhawat, M. O. de la Cruz, G. C. Schatz, S. I. Stupp, *Nature Mater.* **2016**, *15*, 469–476.
- [17] G. A. Silva, C. Czeisler, K. L. Niece, E. Beniash, D. A. Harrington, J. A. Kessler, S. I. Stupp, *Science* **2004**, *303*, 1352–5.
- [18] B. Alberts, A. Johnson, J. Lewis, et al. *Molecular Biology of the Cell*, Vol. 4, Garland Science, New York, **2002**.
- [19] M. Fialkowski, K. J. Bishop, R. Klajn, S. K. Smoukov, C. J. Campbell, B. A. Grzybowski, *J. Phys. Chem. B* **2006**, *110*, 2482–96.
- [20] B. A. Grzybowski, C. E. Wilmer, J. Kim, K. P. Browne, K. J. M. Bishop, *Soft Matter* **2009**, *5*, 1110–1128.
- [21] H. Hess, J. L. Ross, *Chem. Soc. Rev.* **2017**, *46*, 5570–5587.
- [22] A. Sorrenti, J. Leira-Iglesias, A. J. Markvoort, T. F. de Greef, T. M. Hermans, *Chem. Soc. Rev.* **2017**, *46*, 5476–5490.
- [23] S. A. P. van Rossum, M. Tena-Solsona, J. H. van Esch, R. Eelkema, J. Boekhoven, *Chem. Soc. Rev.* **2017**, *46*, 5519–5535.
- [24] S. De, R. Klajn, *Adv. Mater.* **2018**, *30*, 1706750, 1–6.
- [25] S. Dhiman, S. J. George, *Bull. Chem. Soc. Jpn.* **2018**, *91*, 687–699.
- [26] R. K. Grötsch, J. Boekhoven, **2018**, Unique properties of supramolecular biomaterials through nonequilibrium self-assembly. In: *Self-Assembling in Self-assembling biomaterials* (ed. H. S. Azevedo, R. da Silva), 235–250. Woodhead Publishing
- [27] M. Tena-Solsona, B. Rieß, R. K. Grötsch, F. C. Löhner, C. Wanzke, B. Käs Dorf, A. R. Bausch, P. Müller-Buschbaum, O. Lieleg, J. Boekhoven, *Nat. Commun.* **2017**, *8*, 15895.
- [28] L. S. Kariyawasam, C. S. Hartley, *J. Am. Chem. Soc.* **2017**, *139*, 11949–11955.
- [29] J. Boekhoven, W. E. Hendriksen, G. J. Koper, R. Eelkema, J. H. van Esch, *Science* **2015**, *349*, 1075–1079.
- [30] F. J. Ndlec, T. Surrey, A. C. Maggs, S. Leibler, *Nature* **1997**, *389*, 305–308.
- [31] T. Surrey, F. Nédélec, S. Leibler, E. Karsenti, *Science* **2001**, *292*, 1167.
- [32] F. d. Sala, S. Neri, S. Maiti, J. L.-Y. Chen, L. J. Prins, *Curr. Opin. Biotechnol.* **2017**, *46*, 27–33.
- [33] R. Klajn, P. J. Wesson, K. J. Bishop, B. A. Grzybowski, *Angew. Chem. Int. Ed.* **2009**, *48*, 7035–7039; *Angew. Chem.* **2009**, *121*, 7169–7173.
- [34] S. Zhang, *Nature Biotech.* **2003**, *21*, 1171–8.
- [35] J. Kopeček, *J. Polym. Sci. Part A* **2009**, *47*, 5929–5946.
- [36] H. Yokoi, T. Kinoshita, S. Zhang, *P. Nat. Acad. Sci. U.S.A.* **2005**, *102*, 8414–8419.
- [37] P. Terech, R. G. Weiss, *Chem. Rev.* **1997**, *97*, 3133–3160.
- [38] J. D. Hartgerink, E. Beniash, S. I. Stupp, *Science* **2001**, *294*, 1684–8.
- [39] E. Beniash, J. D. Hartgerink, H. Storrer, J. C. Stendahl, S. I. Stupp, *Acta Biomater.* **2005**, *1*, 387–97.
- [40] S. Zhang, *Nature Biotech.* **2003**, *21*, 1171–1178.
- [41] P. Y. Dankers, M. C. Harmsen, L. A. Brouwer, M. J. van Luyn, E. W. Meijer, *Nature Mater.* **2005**, *4*, 568–74.
- [42] M. J. Webber, J. B. Matson, V. K. Tamboli, S. I. Stupp, *Biomaterials* **2012**, *33*, 6823–6832.
- [43] J. Li, X. Li, X. Ni, X. Wang, H. Li, K. W. Leong, *Biomaterials* **2006**, *27*, 4132–4140.
- [44] Y. Gao, Y. Kuang, Z. F. Guo, Z. Guo, I. J. Krauss, B. Xu, *J. Am. Chem. Soc.* **2009**, *131*, 13576–13577.
- [45] B. Jeong, Y. H. Bae, D. S. Lee, S. W. Kim, *Nature* **1997**, *388*, 860.
- [46] J. Boekhoven, A. M. Brizard, K. N. Kowligi, G. J. Koper, R. Eelkema, J. H. van Esch, *Angew. Chem. Int. Ed.* **2010**, *49*, 4825.
- [47] C. G. L. Wolf, E. K. Rideal, *Biochem. J.* **1922**, *16*, 548–55.
- [48] S. Debnath, S. Roy, R. V. Ulijn, *J. Am. Chem. Soc.* **2013**, *135*, 16789–16792.
- [49] C. G. Pappas, I. R. Sasselli, R. V. Ulijn, *Angew. Chem. Int. Ed. Engl.* **2015**, *54*, 8119–23.
- [50] C. Angula, J. Miravet, *Chem. Commun.* **2016**, *52*, 5398–5401.
- [51] J. Leira-Iglesias, A. Sorrenti, A. Sato, P. A. Dunne, T. M. Hermans, *Chem. Commun.* **2016**, *52*, 9009–12.
- [52] A. Sorrenti, J. Leira-Iglesias, A. Sato, T. M. Hermans, *Nat. Commun.* **2017**, *8*, 15899.
- [53] M. Araujo, B. Escuder, *ChemistrySelect* **2017**, *2*, 854–862
- [54] A. Mishra, D. B. Korlepara, M. Kumar, A. Jain, N. Jonnalagadda, K. K. Bejagam, S. Balasubramanian, S. J. George, *Nat. Commun.* **2018**, *9*, 1295.
- [55] S. Dhiman, A. Jain, S. J. George, *Angew. Chem. Int. Ed.* **2017**, *56*, 1329–1333; *Angew. Chem.* **2017**, *129*, 1349–1353.
- [56] S. Dhiman, A. Jain, M. Kumar, S. J. George, *J. Am. Chem. Soc.* **2017**, *139*, 16568–16575
- [57] D. Spitzer, L. L. Rodrigues, D. Straßburger, M. Mezger, P. Besenius, *Angew. Chem. Int. Ed.* **2017**, *56*, 15461–15465; *Angew. Chem.* **2017**, *129*, 15664–15669.
- [58] M. J. Webber, E. A. Appel, E. W. Meijer, R. Langer, *Nat. Mater.* **2015**, *15*, 13–26.
- [59] T. Heuser, E. Weyandt, A. Walther, *Angew. Chem. Int. Ed.* **2015**, *54*, 13258–13262; *Angew. Chem.* **2015**, *127*, 13456–13460.
- [60] T. Heuser, A. -K. Steppert, C. Molano Lopez, B. Zhu, A. Walther, *Nano Lett.* **2014**, *15*, 2213–2219.
- [61] L. Heinen, A. Walther, *Chem. Sci.* **2017**, *8*, 4100–4107.
- [62] T. Heuser, R. Merindol, S. Loescher, A. Klaus, A. Walther, *Adv. Mater.* **2017**, *29*, 1606842.
- [63] X. Hao, L. Chen, W. Sang, Q. Yan, *ACS Macro Lett.* **2018**, *5*, 1700591.
- [64] S. Maiti, I. Fortunati, C. Ferrante, P. Scrimin, L. J. Prins, *Nat. Chem.* **2016**, *8*, 725–731.
- [65] H. Zhao, S. Sen, T. Udayabhaskararao, M. Sawczyk, K. Kučanda, D. Manna, P. K. Kundu, J. W. Lee, P. Král, R. Klajn, *Nat. Nanotechnol.* **2016**, *11*, 82–8.
- [66] Y. Wei, S. Han, J. Kim, S. Soh, B. A. Grzybowski, *J. Am. Chem. Soc.* **2010**, *132*, 11018–20.
- [67] M. Tena-Solsona, C. Wanzke, B. Riess, A. R. Bausch, J. Boekhoven, *Nat. Commun.* **2018**, *9*, 2044
- [68] B. Riess, C. Wanzke, M. Tena-Solsona, R. K. Grötsch, C. Maity, J. Boekhoven, *Soft Matter* **2018**, Advance Article DOI: 10.1039/C8SM00822A.

Manuscript received: April 17, 2018  
Version of record online: June 13, 2018

### 7.3 The Design of Dissipative Molecular Assemblies Driven by Chemical Reaction Cycles

#### **Abstract.**

The field of supramolecular materials has undergone a change in the last years. The field first focused on assemblies and materials, which are formed in equilibrium. These materials already have a widespread application like liquid crystals in LC-screens. In the last couple of years, the focus of the field moved towards assemblies, which are formed out-of-equilibrium by a constant energy dissipation by a chemical reaction cycle. These assemblies are closer to biological examples like microtubule networks. Both man-made and biological examples can be controlled in time and space. But biological examples show more complex properties, like self-healing or self-division. With this review article, we explain clear design rules how chemical reaction cycles can be developed to obtain dissipative supramolecular assemblies. First, we clarify minimal requirements for the chemical reaction cycles and show how complex cycles can be designed. We extracted three major categories based on what kind of fuel is used to drive the chemical reaction cycles. The energy can come from the hydrolysis of the fuel, the reduction of oxidizing agents, or light. The first two are catalytic reaction cycles. In other words, the activation and deactivation of the chemical reaction cycle lead to faster conversion of the fuel to its waste product. Based on the extracted reactions, we found three major design strategies, how reaction cycles can be coupled to the self-assembly of molecules. We end with examples for the abolishment of electrostatic charges, the combination of two non-assembling precursors, and the change of the molecular conformation.

This work has been published:

Title: The Design of Dissipative Molecular Assemblies Driven by  
Chemical Reaction Cycles

Authors: Benedikt Rieß\*, Dr. Raphael K. Grötsch\*, Prof. Dr. Job Boekhoven

First published: 09. December 2019

Journal: Chem **2020**, 6 (3), 552-578.

Publisher: Elsevier

DOI: 10.1016/j.chempr.2019.11.008

Reprinted with permission of Elsevier Group.

This section states the individual work of each author in the publication above. B. Rieß, R. K. Grötsch and J. Boekhoven both wrote paragraphs in the review article. The figures were primarily designed by B. Rieß

## Review

## The Design of Dissipative Molecular Assemblies Driven by Chemical Reaction Cycles

Benedikt Rieß,<sup>1,3</sup> Raphael Kurt Grötsch,<sup>1,3</sup> and Job Boekhoven<sup>1,2,\*</sup>

The field of supramolecular chemistry and molecular self-assembly has entered a new phase in which the use of chemical reactions to create out-of-equilibrium molecular assemblies is becoming more common. These dynamic assemblies have vastly different properties than their in-equilibrium counterparts, which include the ability to be controlled over space and time or the ability to self-replicate. Such behaviors would set significant steps toward the synthesis of artificial life. However, a limiting factor toward the revolution of the field is the lack of clear definitions and design rules for such systems. In this review, we explain the core principles that help to design energy-dissipating chemical reaction cycles that can drive molecular assemblies. We discuss strategies for coupling these reaction cycles to building blocks for the materials. We conclude with an outlook for the field of dissipative self-assembly and its potential role as a material or model for life.

## INTRODUCTION

In supramolecular materials, molecules self-assemble into large structures driven by non-covalent interactions yielding functional assemblies.<sup>1</sup> Such non-covalent interactions include hydrogen bonding, van der Waals interactions, the hydrophobic effect, electrostatic attraction, as well as others. When these forces are tailored to balance repulsive interactions, such as ion-ion repulsion,<sup>2,3</sup> molecules can self-assemble into well-ordered structures, which include fibers,<sup>4–7</sup> tubes,<sup>8–11</sup> weaves,<sup>12</sup> or vesicles.<sup>13,14</sup> Complex structures such as cages,<sup>15</sup> coordination complexes,<sup>16</sup> assembled peptides,<sup>2,17,18</sup> and DNA-based assemblies<sup>19</sup> can also be designed and produced. Such molecular assemblies have attracted significant attention over the last decades partly because of emerging design rules<sup>20,21</sup> and their wide range of applications. Prominent examples of applications include liquid crystals in liquid-crystal displays,<sup>22–25</sup> vesicles used to deliver drugs,<sup>26</sup> or peptide assemblies used for regenerative medicine.<sup>27,28</sup>

Molecular self-assembly is typically an in- or close-to-equilibrium process.<sup>29,30</sup> That means that the molecular assembly can exchange building blocks with its surrounding environment. However, the exchange of building blocks is, on average, balanced. No energy or matter is injected into or released from the system.<sup>31</sup> The in-equilibrium nature of self-assembly of synthetic structures starkly contrasts molecular self-assembly in biology. Like synthetic supramolecular materials, living systems comprise self-assembled molecules, such as fiber- or vesicle-forming building blocks. However, the assemblies in living systems do not exist in or close to equilibrium. In life, most molecular assemblies exist out of equilibrium, driven by energy harvested from reaction cycles.<sup>32,33</sup>

## The Bigger Picture

If we want to create materials as sophisticated as biological ones, we should use strategies similar to those used in biology. Living biological materials, like skin or bone, are made through the self-assembly of molecules and exist far out of chemical equilibrium, which means that these molecular assemblies require the constant input and dissipation of energy in order to be sustained. Because of their dissipative nature, living materials possess properties that we typically associate with life and do not find in classical materials: properties such as spontaneous emergence, the ability to self-heal, or the ability to adapt to a change in environment. Inspired by biology, researchers have been coupling energy-dissipative chemical reaction cycles to the creation of supramolecular materials. Indeed, the emerging materials are endowed with some of the unique properties we typically associate with life. The design strategies are the focus of this review.





We explain the out-of-equilibrium nature of biological assemblies with a reasonably well-understood example, i.e., the self-assembly of the actin network driven by the hydrolysis of ATP.<sup>34</sup> The actin network is a cytoskeletal network that is responsible for the structure of the cell wall and cell locomotion as well as other functions.<sup>35</sup> The building blocks for the actin network are actin subunits that can assemble in a head-to-tail fashion to form a filament. The process of assembly and disassembly does not occur spontaneously but is driven by a chemical reaction cycle that hydrolyzes ATP. Each actin subunit can bind a molecule of ATP, which activates the actin subunit for self-assembly with other activated actin monomers. Consequently, in the presence of ATP, actin monomers rapidly assemble into fibrils. However, the ATP bound to the actin hydrolyzes into ADP upon self-assembly. The binding strength to other actin subunits decreases upon hydrolysis of ATP-bound to ADP-bound actin. Therefore, upon self-assembly, the actin hydrolyzes and disassembles, after which it can bind a new molecule of ATP and repeat the cycle. The consequence is a dynamic assembly, with its building blocks' assembly and disassembly tightly regulated by the kinetics of the reaction cycle. That kinetic control allows the cell to adapt its cytoskeleton to internal or external stimuli rapidly. It also means that building blocks are recycled and can be used for different purposes. And finally, using kinetics to regulate molecular assemblies can give rise to materials with unique features that are unimaginable in equilibrium. For example, the process of treadmilling, in which an actin fiber grows on one end and collapses on the other.<sup>36</sup>

From the example above, it is clear that the dissipative assembly of molecules endows the emerging structures with exciting properties, which raises the question: can we engineer similar principles into synthetic self-assembled systems? With the unique features that dissipative self-assembly offers us and the scalability of synthetic chemistry, we can envision exciting materials for the future.<sup>37,38</sup> For example, a supramolecular polymer that heals itself after externally applied damage, as our skin does. Alternatively, the dynamic nature of these materials can be exploited as a self-erasing paper that can be reused over and over,<sup>39</sup> similar to how the building blocks of our cells are reused.

This review will discuss strategies by which dissipative assemblies have been developed synthetically. We divide the review into the two essential components of dissipative self-assembly, i.e., the chemical reaction cycle that consumes energy as it is proceeding and the self-assembly of one of the metastable products in the chemical reaction cycle. In The Chemical Reaction Cycle, we explain the minimal requirements for the chemical reaction cycle, which we clarify with recent examples. We end the section with design rules for energy-dissipating cycles. In Strategies for Coupling Reaction Cycles to Self-Assembly of Molecules, we clarify the requirements from the self-assembly part of dissipative self-assembly. We discuss three design strategies to couple the chemical reaction cycle to the self-assembly of molecules. We close the review with an outlook on the future of the field.

## THE CHEMICAL REACTION CYCLE

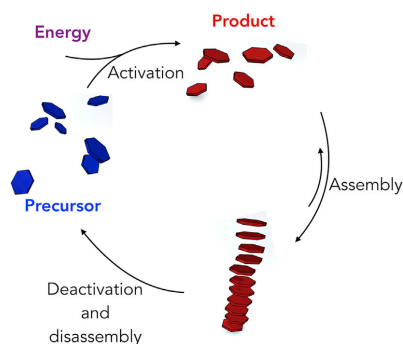
In this section, we focus on the design of the chemical reaction to drive dissipative self-assembly. We will first explain the minimal requirements for the chemical reaction cycle, after which, we provide examples of successfully applied reaction cycles. We divide the latter into two parts according to the nature of the source of energy that drives the chemical reaction cycle, that is, dissipative reaction cycles driven by the conversion of chemical fuels into waste and cycles driven by the conversion of light into heat.

<sup>1</sup>Department of Chemistry, Technical University of Munich, Lichtenbergstrasse 4, Garching 85748, Germany

<sup>2</sup>Institute for Advanced Study, Technical University of Munich, Lichtenbergstrasse 2a, Garching 85748, Germany

<sup>3</sup>These authors contributed equally

\*Correspondence: [job.boekhoven@tum.de](mailto:job.boekhoven@tum.de)  
<https://doi.org/10.1016/j.chempr.2019.11.008>



**Figure 1. Schematic Representation of Dissipative Self-Assembly**

A chemical reaction cycle transiently activates molecules driven by the conversion of energy. The energy can come from photons or chemical fuels and is irreversibly converted into heat and/or waste (data not shown).

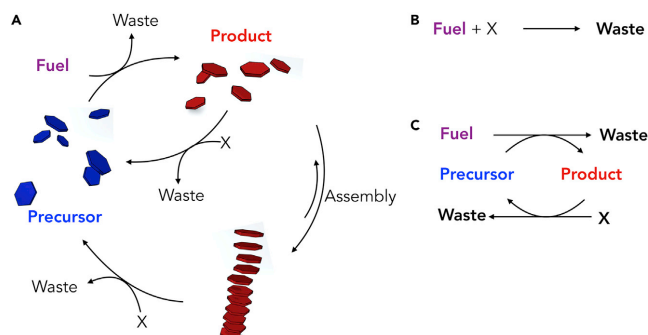
#### Minimal Requirements for the Chemical Reaction Cycle

The chemical reaction cycles we discuss in this section follow the minimal requirements to drive dissipative self-assembly. The chemical reaction cycle comprises at least two chemical reactions, an activation and a deactivation, that regulate the concentrations of a minimum of two species, a precursor and a product (Figure 1). The activation is a reaction that converts a precursor into a product that is driven by the irreversible consumption of an energy source. In other words, the reaction is driven by the consumption of a chemical fuel (Fuel-Driven Reaction Cycles Are, Effectively, Catalytic Reaction Cycles) or by the absorption of light (Chemical Reaction Cycles Driven by the Conversion of Light into Heat). The activation reaction has to be irreversible. That means that the fuel is irreversibly “burned” or the photon is absorbed to convert the precursor into a product, and the energy cannot be regained. In contrast, the deactivation is a spontaneous reaction that reverts the product to the precursor. The ensemble means that the product molecule is by definition metastable, and its half-life is defined by the rate constant of deactivation, while its concentration is regulated by both the rate of activation and deactivation. In its finite lifetime, the product can either assemble, which is the topic of Strategies for Coupling Reaction Cycles to Self-Assembly of Molecules.

#### Fuel-Driven Reaction Cycles Are, Effectively, Catalytic Reaction Cycles

We discuss chemical reaction cycles that are driven by the conversion of a chemical fuel (Figure 2A). In fuel-driven reaction cycles, the activation converts the precursor into a metastable product at the expense of chemical fuel. That metastable product spontaneously reverts to the precursor state in the deactivation reaction. The latter reaction typically occurs by reaction with a ubiquitous species in the reaction solution (indicated by X in Figure 2A). For example, we will describe reaction cycles in which X is a molecule of water or a reducing agent. Because the product is eventually reverted to the precursor, the cycle, per definition, has to generate molecules of waste. Therefore, we treat this class of reaction cycles separately from the light-driven reaction cycles where the energy is converted into heat, but no waste is generated.

After the fuel is depleted and all product has been deactivated, the only difference between the starting point of the experiment is the conversion of fuel into waste. We can thus consider that the net reaction that drives the formation of the transient product is the reaction of fuel with the ubiquitous molecule in solution (e.g.,  $\text{H}_2\text{O}$



**Figure 2. Dissipative Self-Assembly Driven by the Conversion of Chemical Fuels**

(A) The generic design of an energy-dissipating chemical reaction cycle driven by chemical fuels.

(B) The energy is obtained from the conversion of fuel into waste by reaction with a species in solution (X).

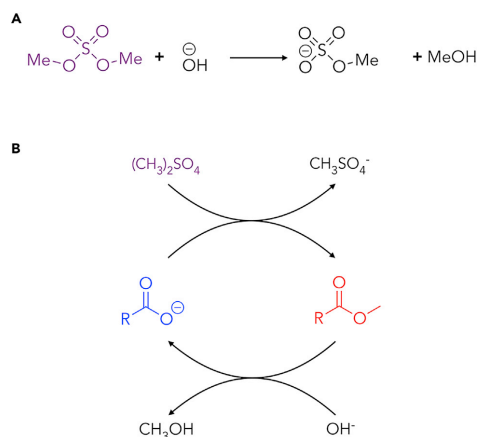
(C) The dissipative reaction cycle catalyzes the conversion of fuel into waste.

or reducing agent). In other words, these reaction cycles are effectively driven by the conversion of fuel into waste (Figure 2B). A challenge in the design of dissipative reaction cycles is to choose the chemistry such that the direct conversion of fuel into waste (e.g., direct hydrolysis of ATP) is drastically slower than the reaction of fuel with the precursor. When these requirements are fulfilled, the reaction cycles are, effectively, catalysts for the conversion of fuel into waste products (Figure 2C). As an analogy, a car engine is effectively a catalyst for the conversion of fuel into exhaust gases, and as it does so, it produces work and heat. Similarly, the chemical reaction cycles we discuss are catalysts that convert fuel into waste while producing transient building blocks for self-assembly. While doing so, the reaction cycle reroutes the flow of energy from fuel to waste and temporarily stores energy into the metastable product. That temporary energy storage in a metastable product can subsequently induce assembly into dynamic structures, as we will discuss in Strategies for Coupling Reaction Cycles to Self-Assembly of Molecules.

#### Chemical Reaction Cycles Driven by the Hydrolysis of Fuels

In the following, we will describe examples of catalytic reaction cycles that catalyze the hydrolysis of a fuel. In pioneering work, van Esch, Eelkema, and co-workers developed a chemical reaction cycle that catalyzes the hydrolysis of methylating agents such as methyl iodide or dimethyl sulfate.<sup>40,41</sup> In the case of dimethyl sulfate, the energy to drive the reaction cycle is extracted from the reaction of a molecule of dimethyl sulfate (fuel) with a hydroxide ion (X) to generate methanol and methyl bisulfate (waste) (Figure 3A). In the absence of precursor, the hydrolysis of the dimethyl sulfate fuel is slow, i.e., the fuel has a half-life of 41 min. We refer to that reaction as the direct fuel conversion. In contrast, in the presence of the precursor, the conversion of the fuel occurs at a 2.5-fold faster rate. In other words, the presence of the precursor catalyzes the conversion of the dimethyl sulfate into methanol and methyl bisulfate while forming a transient, metastable ester-based product.

In the activation reaction, a molecule of carboxylate reacts with the dimethyl sulfate to form its corresponding methyl ester and a waste molecule of methyl bisulfate (Figure 3B). In other words, part of the waste (methyl bisulfate) is generated in the



**Figure 3. A Chemical Reaction Cycle Driven by the Hydrolysis of Dimethyl Sulfate**

(A) The energy to drive the chemical reaction cycle is obtained from the hydrolysis of dimethylsulfate.

(B) The addition of a carboxylate-based precursor (blue) increases the rate of dimethyl sulfate hydrolysis by forming the transient ester product (red).

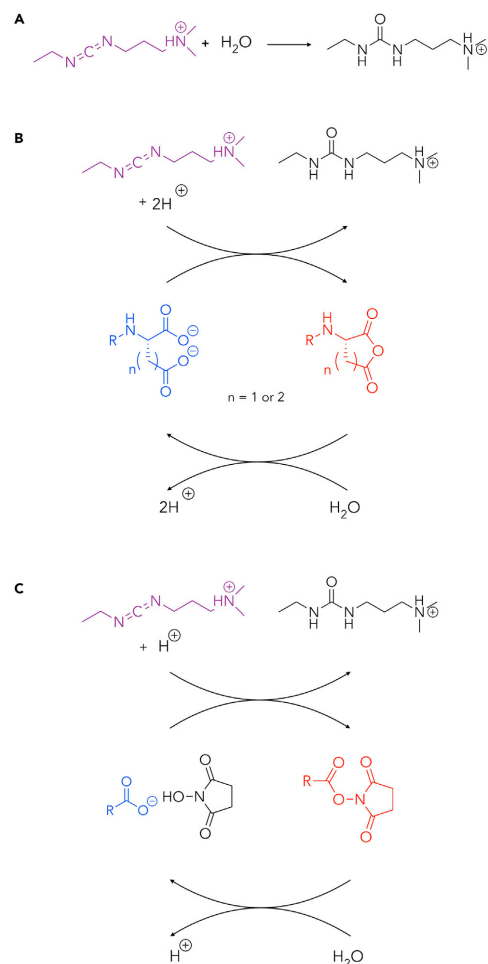
The reaction cycle is adapted from Boekhoven et al.<sup>40</sup>

activation step. In the deactivation reaction, the metastable methyl ester reacts with a hydroxide ion to form the original precursor and releasing methanol (waste). In this specific study, the precursors are chosen such that they are well soluble in the precursor state but self-assemble into fibers upon conversion into the product state. The result is a hydrogel that comprises dynamically growing and shrinking fibers. We discuss the design considerations for the self-assembly in Strategies for Coupling Reaction Cycles to Self-Assembly of Molecules.

The rate constants of each reaction in the chemical reaction cycle are determined experimentally, and kinetic models are used to quantitatively predict the evolution of concentration in response to a batch of fuel or the continuous addition of fuel. Another feature of the reaction cycle is its sensitivity to pH, which allows tuning the reaction rates of the hydrolysis reaction. The cycle also has some shortcomings. For example, the rates of the reaction cycle are relatively slow, particularly in comparison with the rates of biological reaction cycles. To put that in perspective, under the fastest conditions described (pH 11), the cycle lasted 8 h when fueled with 200 mM dimethyl sulfate.

To increase the rates in the chemical reaction cycles, our group and the Hartley group developed a reaction cycle that is driven by the energy obtained by the hydrolysis of carbodiimides (Figure 4A).<sup>42–46</sup> The precursor in the cycle is a dicarboxylate that converts into its corresponding anhydride in the activation reaction (Figure 4B). The anhydride reacts with water in the deactivation reaction in a first-order reaction with a half-life of roughly 30 s at pH 6. Given the short half-life of the anhydride, the overall cycle is also fast. The cycle lasts under 1 h when 200 mM EDC is added to 10 mM of the aspartic acid-based peptides. Under the employed conditions, carbodiimides such as EDC (1-ethyl-3-(3-dimethylaminopropyl)carbodiimide) are relatively stable with a half-life in the range of 14 h. In contrast, with the aspartic acid





**Figure 4. Chemical Reaction Cycles Driven by the Hydrolysis of Carbodiimides**

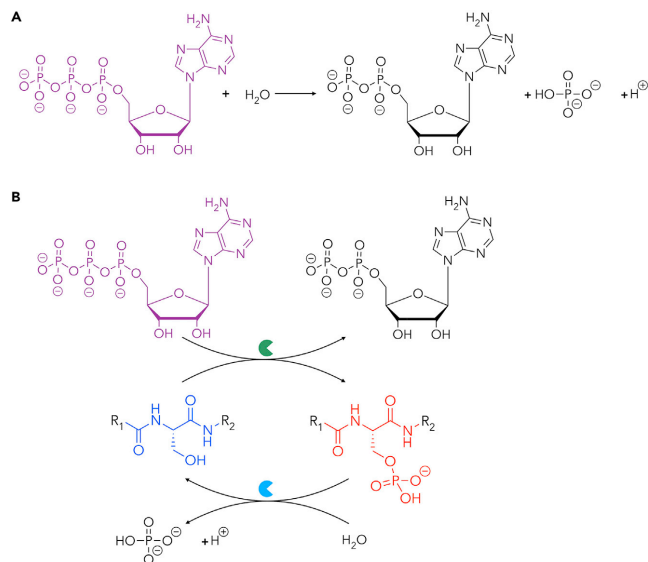
(A) The energy to drive the chemical reaction cycle is obtained from the hydrolysis of carbodiimide.

(B) The addition of a dicarboxylate-based precursor (blue) increases the rate of carbodiimide hydrolysis by forming the transient product (red).

(C) Similarly, the use of a carboxylate-based precursor combined with NHS increased the rate of carbodiimide hydrolysis by forming the transient NHS-ester.

The reaction cycles are adapted from Tena-Solsona et al.,<sup>42</sup> Rieß et al.,<sup>43</sup> and Tena-Solsona et al.<sup>44</sup>

derivatives as a precursor, the half-life of EDC decreases to roughly 14 min (with 10 mM precursor). In other words, under these specific conditions, the catalytic cycle accelerates the hydrolysis of EDC by a factor of 60 while producing transient building blocks for dissipative assemblies. Using the same energy source, we also developed a chemical reaction cycle that forms active esters based on N-hydroxysuccinimide



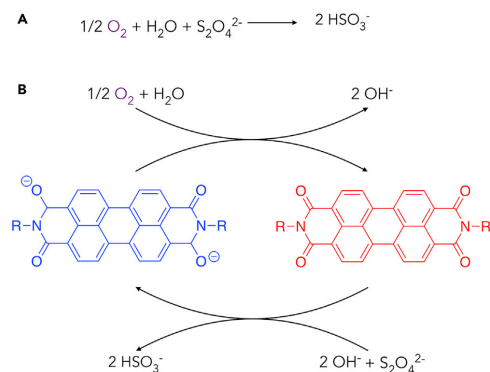
**Figure 5. A Chemical Reaction Cycle Driven by the Hydrolysis of ATP**

(A) The energy to drive the chemical reaction cycle is obtained from the hydrolysis of ATP into ADP and phosphate.

(B) The precursor in the cycle carries a serine amino acid that can be transiently phosphorylated. The reaction cycle is adapted from Sorrenti et al.<sup>50</sup>

(NHS) (Figure 4C).<sup>47,48</sup> Given the increased stability of the NHS-ester, the overall cycle lasts roughly 15 h, roughly seven times longer when compared to the anhydride-based cycle. Other nucleophiles, including 4-nitrophenol, have also been used to form the transient active ester product.<sup>49</sup>

A final reaction cycle we discuss in this section is a cycle driven by the energy obtained from hydrolyzing adenosine triphosphate (ATP) to adenosine diphosphate (ADP) (Figure 5A). As ATP is biology's frequently used energy current, the number of ATP-driven enzymes is virtually countless, as is the number of precursors and products that can be used in these reaction cycles. The broad range of ATP-driven cycles gives researchers a large toolbox to choose reactions and enzymes. As an example, Hermans and co-workers<sup>50</sup> used the combination of protein kinase A (PKA) that phosphorylates the side-chain of serine driven by the hydrolysis of ATP into ADP and a  $\gamma$ -protein phosphatase ( $\gamma$ PP) that simultaneously removes the phosphate group (Figure 5B). The precursor in the reaction cycle contains a peptide sequence (LRRASL) that is easily phosphorylated by the kinase into the product. Subsequently, the product is dephosphorylated by the phosphatase. The inhibition of the phosphatase by accumulating waste products limits the chemical reaction cycle to a few repetitions. However, the authors cleverly overcome that problem by engineering an experimental setup that simultaneously fuels a reactor and removes waste products.



**Figure 6. A Chemical Reaction Cycle Driven by the Oxidation of Dithionite**

(A) The net reaction of the redox reaction, which drives the chemical reaction cycle.  
 (B) The cycle can be used to generate the non-charged product PDI temporarily.  
 The reaction cycle is adapted from Leira-Iglesias et al.<sup>51</sup>

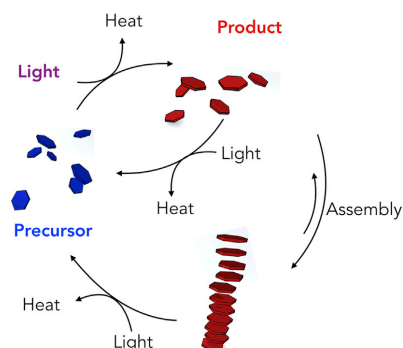
#### Chemical Reaction Cycles Driven by the Reduction of Oxidizing Agents

The use of cycles driven by redox chemistry has also been explored. In these cycles, an oxidizing agent is used in a reducing environment resulting in the reduction of the oxidizing agent as the driving force for the reaction. We demonstrate the design with a recent example by the Hermans group, who used a chemical reaction cycle that is driven by the oxidation of dithionite ions into hydrogen sulfite by oxygen (Figure 6A).<sup>51</sup> In the activation reaction, the precursor, a perylene diimide derivative (PDI<sup>2-</sup>), is oxidized by oxygen from the surrounding air and converted to the uncharged PDI. In the deactivation reaction, the oxidized PDI product can react with a molecule of dithionite to the original precursor state while releasing hydrogen sulfite as waste (Figure 6B). As a consequence, the net reaction occurs between oxygen and dithionite to yield two molecules of hydrogen sulfite, while transiently activating a PDI-based molecule for assembly. We will discuss the self-assembly in more detail in Strategies for Coupling Reaction Cycles to Self-Assembly of Molecules.

#### Chemical Reaction Cycles Driven by the Conversion of Light into Heat

In this subsection, we discuss chemical reaction cycles that are designed to induce dissipative self-assembly and are driven by the energy consumed from absorbing a photon, i.e., reaction cycles driven by the conversion of light into heat.<sup>39,52–55</sup> In the activation reaction of these cycles, a precursor molecule absorbs a photon and undergoes a photochemical reaction, e.g., photoisomerization. The deactivation, where isomerization is reverted, typically occurs spontaneously or by the absorption of a second photon (Figure 7).

These reaction cycles are different from the reaction cycles driven by the consumption of a chemical fuel in two ways. The first difference is that light-driven reaction cycles do not create (chemical) waste, while the fuel-driven reaction cycles do. That difference can be advantageous, considering that the waste can accumulate and interfere with the reaction cycle or assembly process. Second, while the chemical fuel-driven reaction cycles are catalytic reaction cycles that catalyze the conversion of fuel in waste, light-driven reaction cycles are not. That means that with or



**Figure 7. Schematic Representation of Dissipative Self-Assembly Driven by the Conversion of Light into Heat**

The energy to drive the chemical reaction cycle is harvested from the conversion of light into heat.

without the presence of the precursor, the energy is not converted into heat significantly faster.

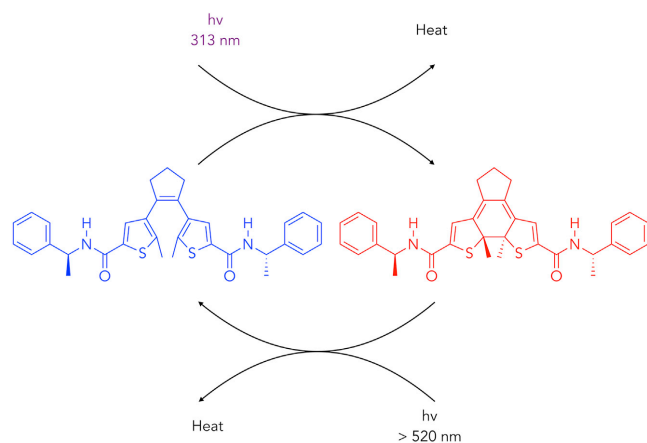
A particularly illustrative example has been described that uses a diarylethene-based molecular switch as a precursor in a chemical reaction cycle.<sup>56</sup> This type of molecular switch converts from a ring-open, relatively flexible molecule to a ring-closed rigid molecule upon irradiation with UV light of 313 nm in wavelength (Figure 8).<sup>57,58</sup> The ring-closed state is photochemically reverted to the open state by irradiation with green light with a wavelength of 520 nm. Interestingly, when the diarylethene-based precursor is irradiated with both wavelengths simultaneously, a photostationary state emerges in which the precursor and product rapidly switch back and forth.

The authors designed the specific molecular variation of the diarylethene-based molecular switch such that it is well soluble in toluene due to the relatively flexible nature of the ring-opened photoisomer. However, upon ring-closing the cycle, the molecules self-assemble into fibers due to hydrogen bonding between the amide groups and increased rigidity of the molecule. The assembly is driven by the photostationary state and thus rapidly exchanges precursors and products between the fibers and solution.

#### Design Considerations for the Chemical Reaction Cycle

The chemical reaction cycle is the motor of dissipative self-assembly: it converts energy into transient building blocks for dynamic self-assembly. When designing such reaction cycles, it is important to consider the type of energy source, i.e., energy from fuel or energy from light, as they operate on independent design principles. Chemical reaction cycles based on the conversion of fuel into waste should follow the design stipulated in Figure 3. These cycles are effectively catalytic reaction cycles that convert fuel into waste. Chemical reaction cycles driven by light should follow the design as stipulated in Figure 7.

In the general design of fuel-driven reaction cycles, it is important to consider the half-life of the product species in this reaction cycle. If the deactivation of this product is fast and its half-life thus short, it becomes challenging to reach sufficient concentrations of product required to induce self-assembly. The activation reaction is



**Figure 8. A Photochemical Reaction Cycle Driven by Irradiation with UV Light**

The precursor is based on a diarylethene switch that can switch to its closed form by UV light. The reaction cycle is adapted from de Jong et al.<sup>56</sup>

typically a second-order reaction in precursor and fuel, so the rapid loss of the product can be overcome by increasing the fuel and precursor concentration.

In most designs, the deactivation reaction is based on the reaction of the product with an abundant species in solution. For example, the product reacts with water or a hydroxide ion in the hydrolysis reactions (Chemical Reaction Cycles Driven by the Hydrolysis of Fuels) or it reacts with a reducing agent (Chemical Reaction Cycles Driven by the Reduction of Oxidizing Agents). Consequently, the reaction follows pseudo-first-order kinetics and can be tuned to some degree by the pH or amount of reducing agent, respectively. Interestingly, because the chemical reaction requires a reagent from the solvent, the assembly process can “protect” its product from the deactivation reaction. For example, when the assembly is sufficiently large, it can change the order of deactivation reaction from pseudo first order to zeroth order<sup>43,44</sup> or to a surface erosion mechanism.<sup>51</sup> Such design rules (i.e., large assemblies combined with deactivation occurring in solution can change the deactivation pathway) lead to an increased crosstalk between the assembly and its reaction kinetics, which results in complex behavior including selection of assembling species or even oscillations in the morphology of the assemblies.<sup>51</sup>

In these reaction cycles, one should also consider the effect of waste, as it may interfere with the reaction cycle or the assembly process. A trick used to avoid the build-up of waste exploited by Hermans and co-workers is the use of continuously fueled reactors that allow the in- and outflow of precursor, fuel, and waste, thus creating a steady state in waste.<sup>51</sup>

A final design consideration involves both chemically and light-fueled reaction cycles: the possibility of side reactions. The precursor in the reaction cycle is activated and deactivated tens or even hundreds of times. (The actual number for chemically fueled cycles can be calculated by dividing the concentration precursor by the total

concentration of fuel added.) At these numbers, even a minor side reaction becomes a major problem.

### Analysis of Chemical Reaction Cycles

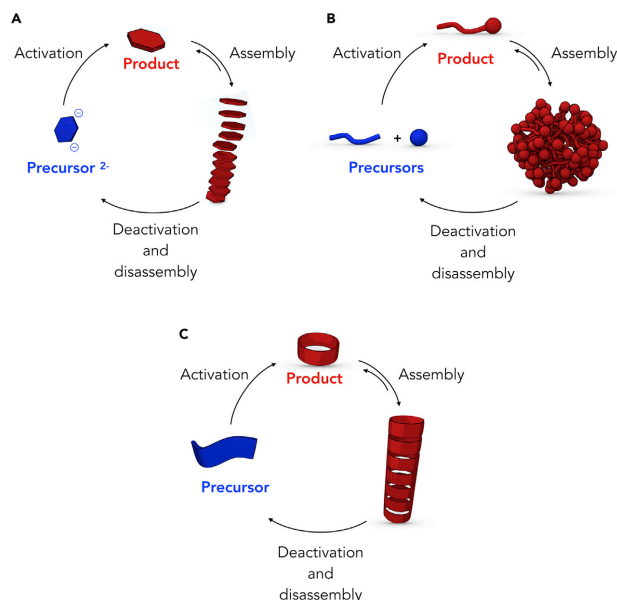
A thorough understanding of the kinetics in the chemical reaction cycle can be important to relate kinetic parameters to material properties. Typically, the concentrations of the components in the reaction cycle are experimentally determined with techniques such as HPLC (high-performance liquid chromatography), NMR, fluorescence, or UV-visible (UV-vis) spectroscopy. An important consideration here is that the technique offers an accurate measure of the concentration within a time window. Depending on the rates of the chemical reactions in the reaction cycle, that window can be seconds or minutes. For example, HPLC is accurate and also offers direct insights in the formation of side products because reactants are separated, but it is a rather “slow” technique. When the reaction rates are fast and lifetimes are in the order of seconds, HPLC may fail as an experimental technique (e.g., because chemical reactions occur on the HPLC column). In other words, for fast chemistry, it may be better to use stopped-flow spectroscopy techniques. Alternatively, a trick that we are currently exploring is to “quench” the chemistry such that activation and deactivation are effectively stopped, and the concentration can be analyzed in detail with the right method. “Quenching” in this context can be a rapid dilution, snap-freezing, or the addition of reagent that stops all reactions.

When an appropriate technique is found, we typically measure the concentrations of reactants and side products during the evolution of batch-fueled cycles. Typically, we vary the amount of fuel added to initiate the cycle. It is particularly powerful to fit the gathered data with kinetic models that describe the chemical reactions that are operating in the chemical reaction cycle. These kinetic models allow finding rate constants of reactions that are difficult to measure empirically. For example, the concentration product is governed by both the activation and deactivation rate simultaneously. It can thus be challenging to measure the “pure” deactivation rate from the product concentration. In contrast, a kinetic model allows fitting the deactivation rate when the activation rate is known. Finding the rate constant of the “pure” deactivation then allows calculating the half-life of the product.

We usually find the rate constants of the reaction cycle at fuel concentrations where assemblies are observed and no assemblies are found. These experiments allow calculation of what is roughly the threshold concentration of product above which one can expect assemblies by extrapolation. More importantly, these experiments can rapidly identify whether the assemblies change the kinetics of the cycle and thus exert feedback on their reaction cycle which is a strong indication of feedback mechanisms playing a role.<sup>43,51,59</sup>

### STRATEGIES FOR COUPLING REACTION CYCLES TO SELF-ASSEMBLY OF MOLECULES

In the previous section, we described two types of reaction cycles that can drive dissipative self-assembly. In this section, we describe three molecular design strategies to ensure the transient product of the reaction cycle self-assembles. The overall goal is to design a reaction cycle precursor that is well soluble while being able to self-assemble in its product state. In that case, kinetic properties, such as reaction rates, regulate the properties of the molecular assemblies, which is fundamentally different from that of in-equilibrium self-assembly.



**Figure 9. Strategies to Induce Dissipative Self-Assembly with Chemical Reaction Cycles**

(A) The chemical reaction cycle abolishes an electrostatic charge of the precursor, thereby inducing self-assembly.

(B) The chemical reaction network forms a bond between two non-assembling building blocks.

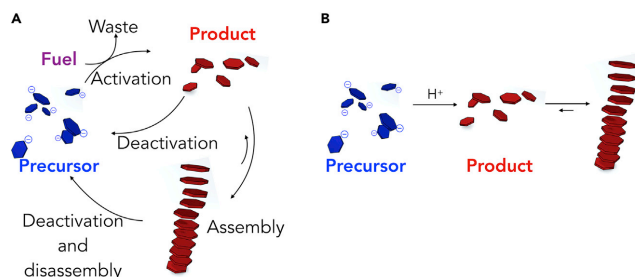
(C) The product undergoes a conformational change to the product and can therefore self-assemble.

In the first design strategy, the precursor molecule is charged, and the deactivation reaction negates or decreases the charges on the molecule (Figure 9A). As a result of electrostatic repulsion, the precursor is not able to self-assemble. In contrast, upon conversion to the product, the electrostatic repulsion is decreased, allowing product molecules to self-assemble. In the second strategy, the self-assembly is induced by combining two non-assembling molecular components such that the product is able to self-assemble (Figure 9B). In a final strategy, the catalytic reaction cycle induces a conformational change of the precursor such that the product can form intermolecular non-covalent interactions and subsequent self-assembly (Figure 9C).

#### The Activation Decreases Electrostatic Repulsion to Induce Self-Assembly

In this section, we describe the design strategy that uses the chemical reaction cycle to transiently remove a charge on a precursor, thereby decreasing intermolecular electrostatic repulsion and thus inducing self-assembly (Figure 10A). This strategy has been relatively well explored, in part, because the design principles are similar to the pH-triggered self-assembly of molecules, i.e., in pH-triggered self-assembly, a charge is removed by an increase or decrease in pH, e.g., by protonating a carboxylate group (Figure 10B).<sup>60–62</sup>

In the examples of dissipative self-assembly that uses the abolishment of a charge, we focus on reaction cycles where the fuel reacts directly with the precursor to form a



**Figure 10. The Use of Charge Abolishment to Induce Self-Assembly**

(A) Chemically fueled dissipative self-assembly based on charge abolishment driven by the reaction cycle.

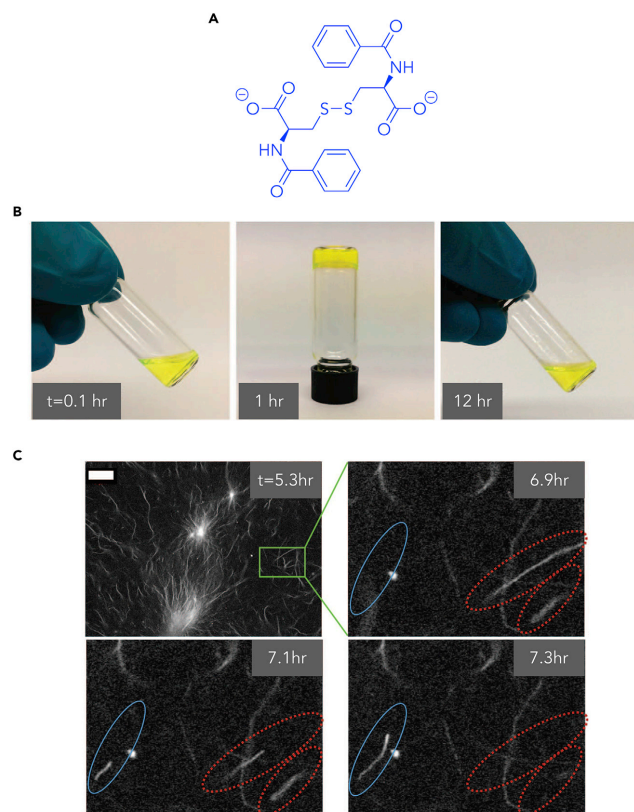
(B) Self-assembly of building blocks induced by a decrease in pH.

transient product, which self-assembles following the reaction cycles discussed in The Chemical Reaction Cycle. We should point out that another strategy has been explored successfully in which a fuel-driven chemical reaction cycle is *indirectly* responsible for the self-assembly of molecules. As an example, a fuel-driven chemical reaction cycle can transiently change the pH of a solution, which induces self-assembly.<sup>63–65</sup> The crucial difference between dissipative self-assembly and the indirectly coupled self-assembly is that the self-assembling building block does not directly react with the fuel and is thus not catalyzing the fuel conversion.

In an early example of chemically fueled negation of charges, the precursor is based on dibenzoyl-L-cystine (Figure 11A), a molecule that is well soluble in water because of its two carboxylate groups. When the pH is lowered to below its two pK<sub>a</sub>s, dibenzoyl-L-cystine is charge neutral and self-assembles into hydrogel-forming fibers.<sup>66</sup> Van Esch, Eelkema, and co-workers used the pH-responsive nature of this molecule to drive the self-assembly process. However, rather than protonating the precursor, they used the chemical reaction cycle that transiently methylates the carboxylates as fuel described in Chemical Reaction Cycles Driven by the Hydrolysis of Fuels (Figure 3). Thus, the chemical reaction cycle converts the anionic carboxylates into their corresponding uncharged methyl esters to drive the self-assembly of dibenzoyl-L-cystine.<sup>40,41</sup> Upon methylation, the product assembles into bundles of fibers that form a self-supporting hydrogel (Figure 11B). When a finite amount of fuel is added, the emerging hydrogels are transient, and their lifetime is regulated by kinetic parameters like the pH or the initial amount of added fuel. Over time, all product hydrolyzes to the precursor, which results in complete dissolution of the gel. More excitingly, as a result of the dynamics of the reaction cycle, which transiently activates and deactivates molecules for self-assembly, dynamic growth and collapse of the fibers could be observed at the tips of the fibers (Figure 11C).

We recently used the design strategy that uses a chemical reaction cycle to negate charges and induce the dissipative self-assembly of fluorenylmethyloxycarbonyl (Fmoc)-protected amino acids and peptides (see Figure 12A) driven by the reaction cycle depicted in Figure 4B.<sup>44</sup> The hydrophobic and aromatic Fmoc protecting group in these peptides is widely used as a peptide modification to drive their self-assembly.<sup>67,68</sup> In our design strategy, we used the anionic amino acids aspartic (D) or glutamic (E) acid on the peptide's C terminus in order to balance the driving force for assembly of the Fmoc group which yielded well-soluble precursors. The





**Figure 11. Dissipative Self-Assembly of Dibenzoyl-L-Cystine into Fibers**

(A) The molecular structure of the precursor dibenzoyl-L-cystine-based precursor forming dissipative fibers. Upon methylation, the charges on the precursor are abolished, which induces its self-assembly.

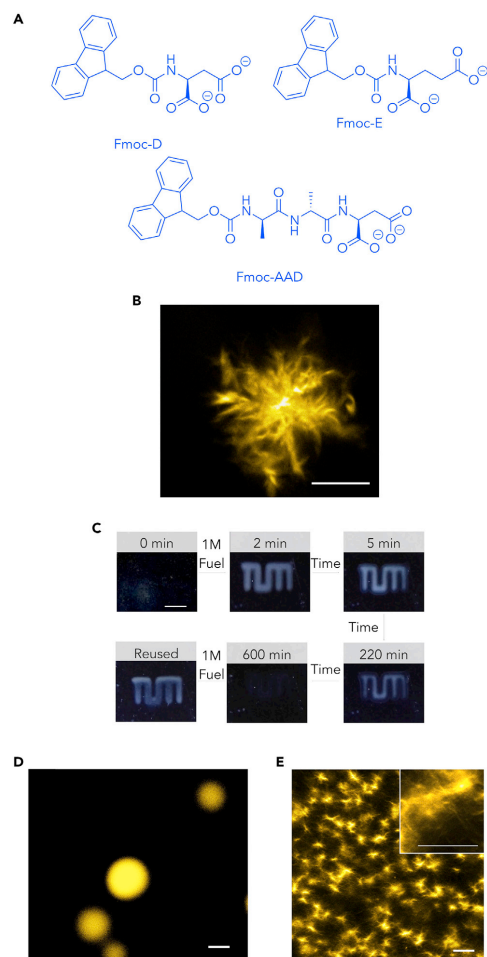
(B) Photographs of the transient hydrogel that forms in response to the addition of a methylating agent as fuel.

(C) Dynamic confocal micrographs of the fibers over time (scale bars: 10  $\mu\text{m}$ ). The blue ellipses highlight the growth of fibers, which occurs in the proximity of collapsing fibers (red ellipses).

Reprinted with permission from Boekhoven et al.<sup>40</sup> Copyright 2015 AAAS.

reaction cycle converts the two carboxylates of the C-terminal aspartic (D) or glutamic (E) acid into their corresponding anhydride driven by the hydrolysis of a condensing agent (carbodiimide, EDC). Consequently, all precursors carry two anionic carboxylate groups that convert into an uncharged product. The loss of the two anions upon activation drives the self-assembly of the product.

Depending on the molecular design of the precursor, the product self-assembles into spherulites, colloids, or hydrogel-forming fibers. For example, Fmoc-protected aspartic acid (Fmoc-D) is soluble at concentrations over 10 mM, but upon activation



**Figure 12. Dissipative Self-Assembly Driven by Carbodiimides**

(A) List of precursors forming various supramolecular structures.

(B) Confocal micrograph of spherulites by Fmoc-D fueled with EDC (scale bar: 10  $\mu\text{m}$ ).

(C) Application of the self-assembled spherulites as self-erasing ink.

(D) A confocal micrograph of colloids formed by Fmoc-E fueled with EDC (scale bar: 1  $\mu\text{m}$ ).

(E) Confocal micrographs of the fibers formed by the tripeptide precursor Fmoc-AAD fueled with EDC (scale bar: 10  $\mu\text{m}$ ).

Reprinted with permission from Tena-Solsona et al.<sup>44</sup> Copyright 2017 Springer Nature.

into its corresponding cyclic anhydride product, it self-assembles into spherulites (Figure 12B). These spherulites disassemble over time as the deactivation reaction reverses the cyclic anhydride product to the charged precursor. Because the spherulites are sufficiently large to scatter light, they convert transparent solutions into



turbid ones. When the precursor is embedded into a polyacrylamide hydrogel and the fuel applied through a mask by spray coating, the spherulites appear only where the fuel reacts with the precursor. Consequently, the transient spherulites can be used as a platform to write temporary messages, i.e., a self-erasing ink (Figure 12C).

Similarly, Fmoc-protected glutamic acid (Fmoc-E) is well soluble, but self-assembles into colloids upon carbodiimide-driven activation into its corresponding cycle anhydride (Figure 12D). We used these colloids to encapsulate and release various hydrophobic dyes. Excitingly, the colloids show a self-protection behavior against the deactivation reaction.<sup>43</sup> Because the deactivation of the anhydride occurs via hydrolysis, it requires water. Since the colloids are hydrophobic and expel water, the hydrolysis reaction cannot take place in the colloids, but exclusively at the surface of the colloids and on the fraction that remains in solution. Consequently, the hydrolysis occurs at much lower rates compared to a similar precursor that does not assemble.

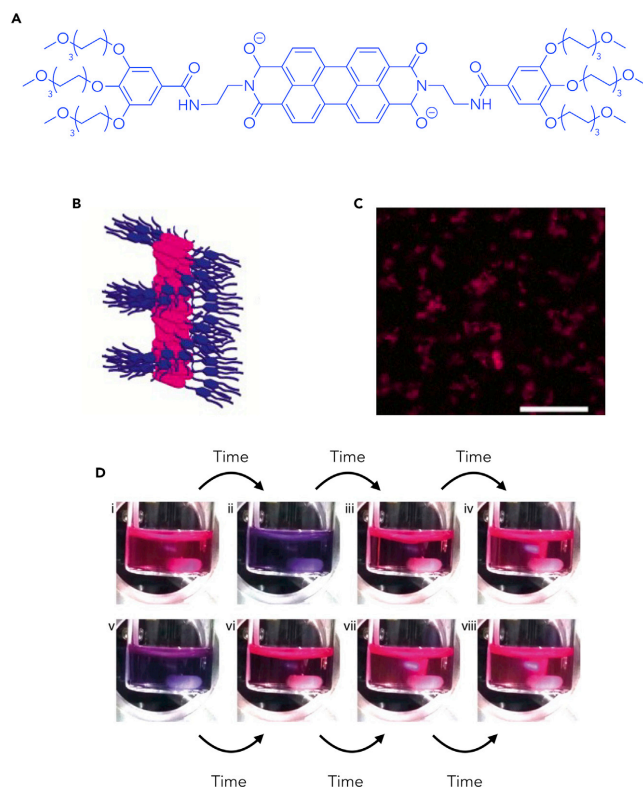
Finally, the strategy of negating negative charges is used to induce the self-assembly of tripeptides into fibers such as Fmoc-AAD, in which A stands for alanine and D stands for aspartic acids. In the precursor state, this tripeptide is well soluble in water. Upon activation of the precursor into the product, this tripeptide assembles into fibers that consecutively entangle and form hydrogels (Figure 12E).

Hermans and co-workers<sup>51,69</sup> used the strategy of negating charges by a chemical reaction cycle to induce the dissipative self-assembly of a perylene diimide derivate (PDI) (Figure 13A). In the activation reaction, the negatively charged  $\text{PDI}^{2-}$  is oxidized to yield the uncharged PDI (Figure 6). Due to its loss of charges, the uncharged PDI self-assembles into stacks that subsequently organize side-by-side into colloids (Figures 13B and 13C). The reaction is performed in a reducing environment, and the PDI thus reduces back to its charged precursor state,  $\text{PDI}^{2-}$ . Consequently, the colloids are transient, and their presence depends on the presence of the oxidizing agent as fuel.

The authors observe complex oscillatory behavior when the solutions are continuously fueled with an oxidizing and reducing agent: the morphology of the assemblies periodically changes, which is reflected in the color of the solution (Figure 13D). The oscillatory behavior is a result of non-linear relations in the self-assembly behavior of the PDI. For example, self-assembly occurs through a nucleation-elongation-fragmentation mechanism, which results in a lag phase followed by an autocatalytic growth. Similarly, the disassembly mechanism follows a size-dependent pathway resulting in further non-linearity in the process. The oscillatory behavior was tunable by the amount of fuel flowing through the systems. For example, with low fuel fluxes, the system reaches a steady state, where the product, fuel, and precursor concentrations stay constant and dynamically exchange. By increasing the fuel flux, the reaction mixture starts oscillating (Figure 13D). Further increasing the fuel flux results in precipitation of the product.

### The Activation Combines Non-assembling Molecular Segments to Form a Building Block

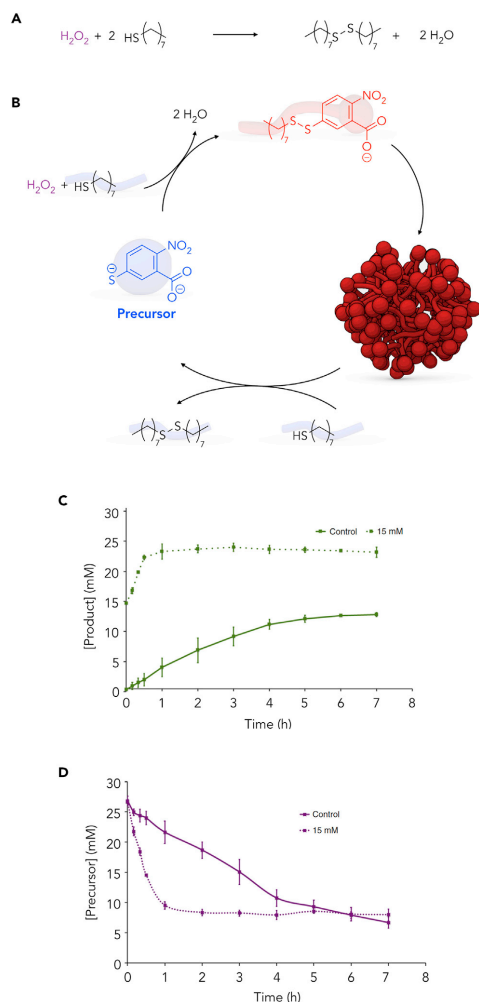
In this section, we focus on the design strategy that uses two non-assembling segments that are combined in the activation reaction to yield a product that can self-assemble (Figure 9B).<sup>70,71</sup>



**Figure 13. Oscillations in Supramolecular Structure Driven by the Conversion of Dithionite**

(A) The precursor used for the chemical reaction cycle.  
 (B) Schematic representation of the assembly formed upon fueling the reaction cycle.  
 (C) Confocal image of 100 μM perylene diimide assemblies (scale bar: 50 μm).  
 (D) Vials with PDI oscillations of different oxidations states.  
 Reprinted with permission from Leira-Iglesias et al.<sup>51</sup> Copyright 2018 Springer Nature.

A particularly illustrative example of this design strategy was recently described by Fletcher and co-workers. In their work, two non-assembling precursors are combined in a chemical reaction cycle to form an amphiphilic product (Figure 14A).<sup>59</sup> The reaction cycle is driven by the oxidation of two thiol derivatives into their corresponding disulfide at the expense of hydrogen peroxide as fuel.<sup>59</sup> The well-soluble precursor 2-nitro-5-sulfidobenzoate is conjugated with the marginally soluble 1-octanethiol in a two-step reaction (Figure 14B). The disulfide product has an amphiphilic character and assembles into micelles once the product concentration is greater than 0.2 mM. The deactivation reaction comprises a second thiol-disulfide exchange between 1-octanethiol and the product deactivates into the precursor and form octyl disulfide as waste. Overall, one molecule of hydrogen peroxide and two molecules of 1-octanethiol are combined to form the corresponding disulfide and water.



**Figure 14. Autocatalytic Formation of Micelles Driven by the Conversion of Hydrogen Peroxide**

(A) The energy to drive the reaction cycles is harvested from the oxidation of 1-octanethiol.

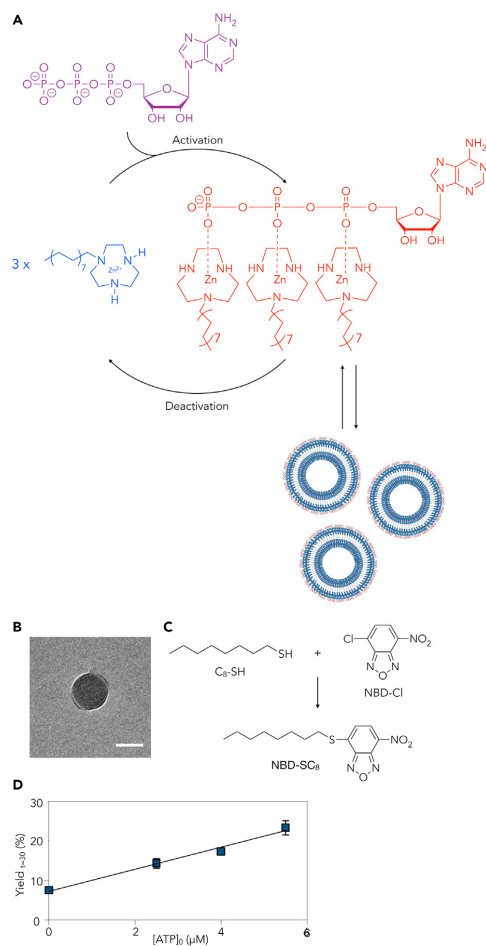
(B) The catalytic reaction cycle that transiently forms an amphiphilic product (red).

(C) The autocatalytic behavior of the micelles increases the concentration of product over time (dashed lines represent micelles; solid line represents a control experiment).

(D) The precursor is consumed faster with micelles (dashed line) than without them (solid line).

Reprinted with permission from Morrow et al.<sup>59</sup> Copyright 2019 Springer.

Interestingly, the catalytic reaction cycle can be autocatalytic under the right circumstances. Since the product forms micelles, it can aid the solubilization of the 1-octanethiol, which is a reactant in the activation. The autocatalytic behavior leads to a



**Figure 15. The Formation of Dynamic Vesicles Driven by the Hydrolysis of ATP**

(A) The chemical reaction cycle that forms dissipative vesicles by hydrolyzing ATP.

(B) Cryogenic transmission electron microscopy (cryo-TEM) micrographs of a vesicle (scale bar: 50 nm).

(C) Aromatic nucleophilic substitution carried out in the presence of the vesicles.

(D) The yield of the reaction depicted in (C) as a function of fuel (ATP) added.

Reprinted with permission from Maiti et al.<sup>72</sup> Copyright 2019 Springer Nature.

faster decrease of precursor and a faster formation of the product (Figures 14C and 14D). Thus, the presence of the micelles increases the local concentration, thereby increasing the rate of activation. The autocatalytic reaction cycle is a rare and well-designed example of a system in which the assemblies and the kinetics of the reaction cycles are reciprocally coupled and exert feedback on one another, which



means that the assembly will form as a result of the reaction cycle, and the reaction cycle will operate faster as a result of the assemblies.

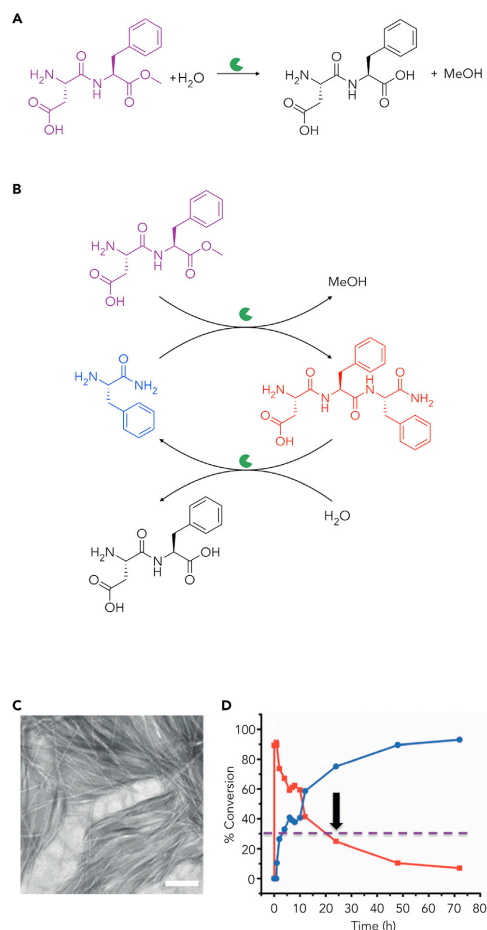
Prins and co-workers explored the strategy that combines a soluble precursor with a soluble fuel to form self-assembled vesicles through dissipative self-assembly. The assembly is driven by a chemical reaction cycle fueled by ATP. ATP plays a double role in the cycle, as it both the fuel and an amphiphilic headgroup that forms a complex with three surfactant tails ( $C_{16}TACN \cdot Zn^{2+}$  in Figure 15A).<sup>72</sup> Because of the combination of the molecules, the resulting complex is able to self-assemble into vesicles as evidenced by confocal microscopy and cryo-electron microscopy (Figure 15B). With the help of the enzyme potato apyrase, the ATP hydrolyzes to ADP, and the vesicles disassemble to their precursor state. The lifetime of the emerging vesicles can be tuned by the amount of ATP added or by the amount of the enzyme in the system. Interestingly, the authors used the dissipative vesicles as transient nanoreactors for reactions that will usually not occur at high rates in water (Figure 15C). For example, the temporary vesicles are used to compartmentalize two hydrophobic reactants 1-octanethiol and NBD-Cl (4-chloro-7-nitrobenzofurazan). In the presence of the vesicles, the aromatic nucleophilic substitution between the two reagents occurred with higher yields compared to without vesicles (Figure 15D).

Ulijn and co-workers explored the design strategy to combine two well-soluble segments in the activation reaction to form a product that self-assembles into fibers.<sup>73,74</sup> They used a chemical reaction cycle that is driven by the energy obtained from the hydrolysis of aspartame—specifically, the hydrolysis of the methyl ester of aspartame (Figure 16A). In the activation reaction, the methylated C terminus of the peptide aspartame is reacted with the N terminus of phenylalanine amide (F-NH<sub>2</sub>, precursor) to yield the tripeptide product DFF-NH<sub>2</sub> (Figure 16B). That reaction is not spontaneous but is catalyzed by the enzyme chymotrypsin. Chymotrypsin also catalyzes the subsequent hydrolysis of the peptide product, yielding the original precursor and the demethylated aspartame as waste. The resulting cycle is thus driven by the hydrolysis of aspartame into aspartate as fuel releasing the demethylated fuel and methanol as waste products. The approach cleverly uses only one enzyme to catalyze multiple reactions, which negates the need for orthogonal conditions (buffer, temperature, and pH) to suit the need of multiple enzymes.

While both the fuel and precursor were well soluble in water, the product was able to self-assemble into fibers due to its extended peptide backbone. The product (DFF-NH<sub>2</sub>) self-assembles into an entangled fiber network with fibers around 5 μm (Figure 16C). The maximum conversion to the product could be observed after roughly 30 min by HPLC. After 24 h, the tripeptide DFF-NH<sub>2</sub> concentration falls below the critical aggregation concentration due to the hydrolysis of the product (dashed line, Figure 16D). The reaction cycle cycles can be refueled up to three times, but with a loss in conversion to the corresponding tripeptide, due to the accumulation of waste products of the deactivation reaction.

### Conformational Changes to Induce Self-Assembly upon Activation

The final design strategy to induce self-assembly driven by the chemical reaction cycles we discuss involves changing the conformation of the precursor, such that it becomes able to self-assemble. This strategy is the most similar to the ATP-driven self-assembly of the actin filaments that we discussed above. In that example, the binding of ATP induces a conformational change of the actin monomer that allows it to bind to other activated monomers. However, this strategy has been



**Figure 16. Transient Hydrogel Formation Driven by the Hydrolysis of Aspartame**

(A) The energy to drive the chemical reaction cycle is obtained from the hydrolysis of aspartame.

(B) The chemical reaction cycle hydrolyzes aspartame and yields the transient tripeptide product (red).

(C) TEM image of the gel formed by DFF-NH<sub>2</sub> after 5 min (scale bar: 500 nm).

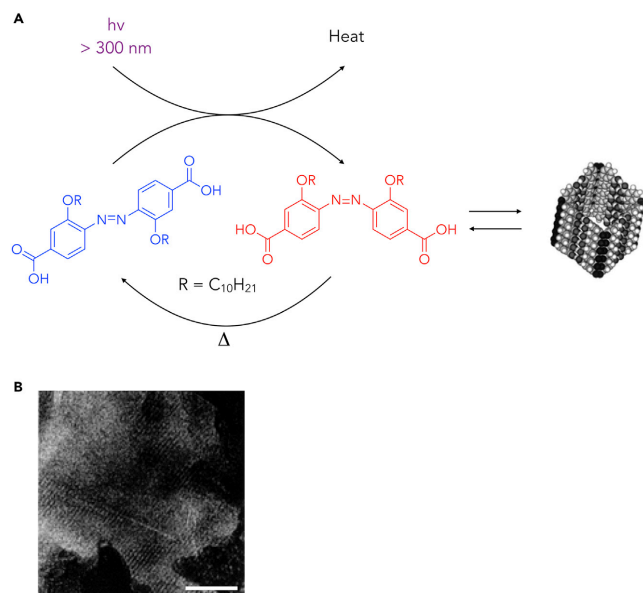
(D) HPLC analysis of the chemical reaction network shows the emergence and decay of product (red).

Reprinted with permission from Pappas et al.<sup>74</sup> Copyright 2015 Wiley-VCH.

underexplored when it comes to synthetic dissipative self-assembly, i.e., the number of examples that use conformational changes to induce self-assembly remains limited.

Photo-isomerization reactions are ideal chemical reactions to induce a change in the conformation of a molecule. For example, the photo-induced isomerization of azobenzene or stilbene from their (Z) to (E) conformation results in a relatively large





**Figure 17. Dissipative Self-Assembly Driven by UV Light**

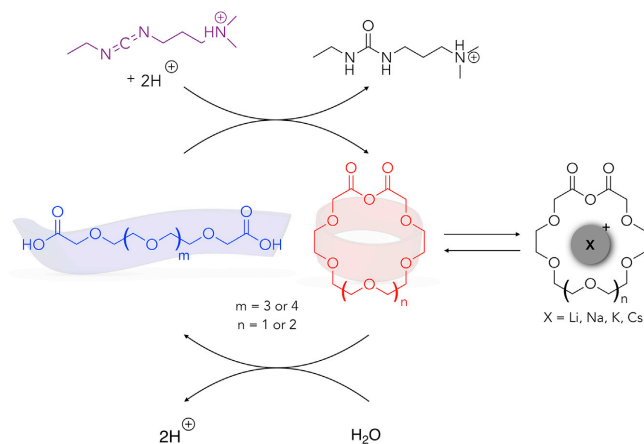
(A) The chemical reaction cycle that forms rod-like structures driven by UV light.

(B) TEM of directly deposited films of the product of the CRN (scale bar: 50 nm).

Reprinted with permission from Rakotonradany et al.<sup>52</sup> Copyright 2003 Wiley-VCH.

conformational change, which has been described to induce self-assembly<sup>75,76</sup> as well as disassembly.<sup>75,77</sup> Other examples of light-switchable derivatives to control assemblies include hydrazine-based switches<sup>78</sup> and the previously discussed diarylethene-based switches.<sup>57</sup>

Indeed, photoisomerization reactions have been used to induce a conformational change of a precursor molecule that drives dissipative self-assembly.<sup>57,79</sup> An early example by Sleiman and co-workers<sup>52</sup> demonstrates the design strategy well. The authors used an azobenzene derivative as a precursor in the chemical reaction cycle. The precursor is able to photo-isomerize from its thermodynamically favored *trans* conformation to the *cis* conformation by irradiation with UV light, which constitutes the activation reaction (Figure 17A). Because the *cis* state is thermodynamically not favored, it spontaneously isomerizes back to its *trans* state. Consequently, a dynamic reaction cycle in which molecules reach a photostationary state can be reached with continuous light irradiation. In the *trans* configuration, the precursor can self-assemble and form linear tapes, which can subsequently organize into larger, higher-ordered structures (Figure 17B). However, upon UV-light irradiation, the *cis* configuration is dynamically formed, which leads to a morphological transition. Evidenced by X-ray powder diffraction, the authors demonstrate the cyclic structures formed in the *cis* configuration results rod- or bundles of rod-like assemblies, which constitutes the first example of dissipative self-assembly driven by a conformation change in the precursor.



**Figure 18. Dissipative Formation of Crown Ethers Driven by the Hydrolysis of Carbodiimide Fuels**

The chemical reaction cycle driven by the hydrolysis of carbodiimides that forms dissipative crown ethers that can host cations. The reaction cycle is adapted from Kariyawasam and Hartley.<sup>45</sup>

The final example of a chemical reaction cycle that induces a conformational change in a precursor which drives assembly was recently described by Hartley et al.<sup>45</sup> The work relies on the chemical reaction cycle that is driven by the hydrolysis of carbodiimides and forms transient anhydride as we discussed above. The precursor in the cycle is based on oligo(ethylene glycol) that is functionalized with a carboxylic acid on each of its extremities (Figure 18). The carbodiimide-driven activation ring closes the precursor and forms the corresponding cyclic anhydride. The conformational change from an extended oligomer to a macrocycle affects the affinity to bind metal. In this particular example, two precursors are used that, in their product state, mirror the design of the crown ethers 18-crown-6<sup>80</sup> and 21-crown-7<sup>81</sup> (Figure 18). The behavior of the crown ethers was tested with four different metal ions: lithium, sodium, potassium, and cesium. The presence of the ions had a negative templating effect that is somewhat counterintuitive. That means the authors found lower concentrations of the transient macrocyclic product, when the matching ion was present in solution, yet more product with an ion that was not exactly matching the size of the cavity of the macrocycles.

### CONCLUSION AND OUTLOOK

In the past decades, the field of supramolecular chemistry has focused on creating structures beyond the molecule, using non-covalent interaction, as opposed to covalent bonds, in order to create molecular constructs with ever-increasing size and complexity.<sup>82</sup> Because biology uses a similar approach toward complexity, this strategy led us leaps forward toward life-like behavior in synthetic structures. Moreover, the combination with systems chemistry resulted in emergent behavior from libraries of simple components.<sup>83</sup> However, the use of supramolecular chemistry at equilibrium is not sufficient to create living systems. If we want to create molecular assemblies as complex and functional as the molecular assemblies in living systems, we should develop these assemblies out of equilibrium. Out of equilibrium, we can find complex behavior such as pattern formation, self-replication,<sup>84</sup> molecular evolution,<sup>85,86</sup> motion,<sup>87,88</sup> the exertion of forces,<sup>89</sup> and oscillations.<sup>51</sup> These synthetic



assemblies with complex behavior can be ideal model systems for biological assemblies and teach us the fundamentals of molecular self-assembly in living systems. Fundamental knowledge of these assemblies will also serve as stepping stones toward synthetic life.

In this work, we have set out several strategies to synthesize molecular assemblies driven by chemical reaction cycles. For the reaction cycle, we have identified two possible energy carriers, i.e., energy harvested from the conversion of fuel into waste or energy harvested from the conversion of photons into heat. The first type of reaction cycle is, in fact, a catalytic reaction cycle in which precursor molecules catalyze the conversion of fuel into waste. While doing so, some of the energy is used to form transient dynamic structures. To couple these energy-consuming reaction cycles to the formation of dissipative assemblies, we identified three strategies, i.e., the reaction cycle can transiently negate an ionic charge on the precursor, the reaction cycle can transiently couple two non-assembling blocks, or the reaction cycle can transiently change the conformation of the precursor. By identifying these strategies, we have set out preliminary design rules for dissipative self-assembly.

Despite the progress in the field, there is still work to do. We believe that the number of successful chemical reaction cycles to drive dissipative assembly remains rather limited. Given the enormous number of chemical reactions that chemists have at their disposal, we foresee many new reaction cycles that can drive dissipative self-assembly. The challenge is, however, to find an activation and deactivation reaction that operates under one set of reaction conditions. Another challenge is the accumulating amount of waste as the reaction cycle proceeds. Using a waste product that precipitates or escapes as gas could be a solution. Alternatively, a third chemical reaction that reverts the waste into fuel would be ideal.

We believe that the use of dissipative assemblies to perform a function is unexplored. Biology assembles microtubules in the spindle apparatus to assist during cell division, while the actin network is assembled used to generate force in our muscles. In these examples, the energy harvested from the chemical reaction cycles is used to perform a function, while the assembly serves as a tool. In the coming years, we anticipate seeing more examples of the use of the kinetically controlled assembly as a tool. For example, calculations have shown that droplets can spontaneously divide as a result of chemical fluxes of building blocks,<sup>90</sup> and other work has shown that chemical fuels can regulate transport through a membrane.<sup>91</sup>

Finally, the time is now ripe to further focus on the fundamental questions of dissipative self-assembly. For example, our lab is interested in how kinetic parameters, like the half-life of the product or the order of a chemical reaction, affect the behavior of the dissipative assembly. Such fundamental insights would support or oppose theoretical predictions. Moreover, fundamental knowledge could offer valuable insights into biological systems, which can be too complex to study individually. Particularly exciting in these future reaction cycles is to engineer autocatalytic or self-inhibiting reactions within these cycles. When coupled to assemblies, we can expect self-replication and competitive behavior between assemblies, which would truly be the first step toward synthetic life. These future developments will be the first step toward synthetic life from the bottom up.

## ACKNOWLEDGMENTS

J.B. is grateful for funding by the Technical University of Munich-Institute for Advanced Study, funded by the German Excellence Initiative and the European Union Seventh Framework Programme under grant no. 291763. B.R. is grateful for funding by the Deutsche Forschungsgemeinschaft (DFG, German Research Foundation) via the Collaborative Research center SFB 863 project B11. R.K.G. thanks the DFG for funding (project no. 245845833) within International Research Training Group IRTG 2022 – the Alberta Technical University of Munich School for Functional Hybrid Materials (ATUMS). Support within TUM IGSSSE is greatly appreciated.

## REFERENCES AND NOTES

- Amabilino, D.B., Smith, D.K., and Steed, J.W. (2017). Supramolecular materials. *Chem. Soc. Rev.* 46, 2404–2420.
- Zhang, S. (2003). Building from the bottom up. *Mater. Today* 6, 20–27.
- Yokoi, H., Kinoshita, T., and Zhang, S. (2005). Dynamic reassembly of peptide RADA16 nanofiber scaffold. *Proc. Natl. Acad. Sci. USA* 102, 8414–8419.
- Hartgerink, J.D., Beniash, E., and Stupp, S.I. (2001). Self-assembly and mineralization of peptide-amphiphile nanofibers. *Science* 294, 1684–1688.
- Kitamura, T., Nakaso, S., Mizoshita, N., Tochigi, Y., Shimomura, T., Moriyama, M., Ito, K., and Kato, T. (2005). Electroactive supramolecular self-assembled fibers comprised of doped tetrathiafulvalene-based gelators. *J. Am. Chem. Soc.* 127, 14769–14775.
- Scheibel, T., Parthasarathy, R., Sawicki, G., Lin, X.M., Jaeger, H., and Lindquist, S.L. (2003). Conducting nanowires built by controlled self-assembly of amyloid fibers and selective metal deposition. *Proc. Natl. Acad. Sci. USA* 100, 4527–4532.
- Korevaar, P.A., George, S.J., Markvoort, A.J., Smulders, M.M., Hilbers, P.A., Schenning, A.P., De Greef, T.F., and Meijer, E.W. (2012). Pathway complexity in supramolecular polymerization. *Nature* 481, 492–496.
- Vauthey, S., Santos, S., Gong, H., Watson, N., and Zhang, S. (2002). Molecular self-assembly of surfactant-like peptides to form nanotubes and nanovesicles. *Proc. Natl. Acad. Sci. USA* 99, 5355–5360.
- Ghadiri, M.R., Granja, J.R., Milligan, R.A., McRee, D.E., and Khazanovich, N. (1993). Self-assembling organic nanotubes based on a cyclic peptide architecture. *Nature* 366, 324–327.
- Yan, D., Zhou, Y., and Hou, J. (2004). Supramolecular self-assembly of macroscopic tubes. *Science* 303, 65–67.
- Reches, M., and Gazit, E. (2003). Casting metal nanowires within discrete self-assembled peptide nanotubes. *Science* 300, 625–627.
- Lewandowska, U., Zajaczkowski, W., Corra, S., Tanabe, J., Börrmann, R., Benetti, E.M., Stappert, S., Watanabe, K., Ochs, N.A.K., Schaeublin, R., et al. (2017). A triaxial supramolecular weave. *Nat. Chem.* 9, 1068–1072.
- Holowka, E.P., Pochan, D.J., and Deming, T.J. (2005). Charged polypeptide vesicles with controllable diameter. *J. Am. Chem. Soc.* 127, 12423–12428.
- Blanazs, A., Armes, S.P., and Ryan, A.J. (2009). Self-assembled block copolymer aggregates: from micelles to vesicles and their biological applications. *Macromol. Rapid Commun.* 30, 267–277.
- Rizzuto, F.J., von Krbek, L.K.S., and Nitschke, J.R. (2019). Strategies for binding multiple guests in metal–organic cages. *Nat. Rev. Chem.* 3, 204–222.
- Datta, S., Saha, M.L., and Stang, P.J. (2018). Hierarchical assemblies of supramolecular coordination complexes. *Acc. Chem. Res.* 51, 2047–2063.
- Glover, D.J., and Clark, D.S. (2016). Protein calligraphy: a new concept begins to take shape. *ACS Cent. Sci.* 2, 438–444.
- Gao, J., Zhan, J., and Yang, Z. (2019). Enzyme-instructed self-assembly (EISA) and hydrogelation of peptides. *Adv. Mater.* e1805798.
- Seeman, N.C., and Sleiman, H.F. (2018). DNA nanotechnology. *Nat. Rev. Mater.* 3, 17068.
- Draper, E.R., and Adams, D.J. (2017). Low-molecular-weight gels: the state of the art. *Chem* 3, 390–410.
- Savyasachi, A.J., Kotova, O., Shanmugaraju, S., Bradberry, S.J., O'Maille, G.M., and Gunlaugsson, T. (2017). Supramolecular chemistry: a toolkit for soft functional materials and organic particles. *Chem* 3, 764–811.
- Kim, Y., and Tamaoki, N. (2014). A photoresponsive planar chiral azobenzene dopant with high helical twisting power. *J. Mater. Chem. C* 2, 9258–9264.
- Hegmann, T., Qi, H., and Marx, V.M. (2007). Nanoparticles in liquid crystals: synthesis, self-assembly, defect formation and potential applications. *J. Inorg. Organomet. Polym. Mater.* 17, 483–508.
- Greaves, T.L., and Drummond, C.J. (2008). Ionic liquids as amphiphile self-assembly media. *Chem. Soc. Rev.* 37, 1709–1726.
- McConney, M.E., Rumi, M., Godman, N.P., Tohgha, U.N., and Bunning, T.J. (2019). Photoresponsive structural color in liquid crystalline materials. *Adv. Opt. Mater.*
- Grimaldi, N., Andrade, F., Segovia, N., Ferrer-Tasies, L., Sala, S., Veciana, J., and Ventosa, N. (2016). Lipid-based nanovesicles for nanomedicine. *Chem. Soc. Rev.* 45, 6520–6545.
- Freeman, R., Han, M., Álvarez, Z., Lewis, J.A., Wester, J.R., Stephanopoulos, N., McClendon, M.T., Lynsky, C., Godbe, J.M., Sangji, H., et al. (2018). Reversible self-assembly of superstructured networks. *Science* 362, 808–813.
- Du, X., Zhou, J., Shi, J., and Xu, B. (2015). Supramolecular hydrogelators and hydrogels: from soft matter to molecular biomaterials. *Chem. Rev.* 115, 13165–13307.
- Mart, R.J., Osborne, R.D., Stevens, M.M., and Ulijn, R.V. (2006). Peptide-based stimuli-responsive biomaterials. *Soft Matter* 2, 822–835.
- Tantakitti, F., Boekhoven, J., Wang, X., Kazantsev, R.V., Yu, T., Li, J., Zhuang, E., Zandi, R., Ortony, J.H., Newcomb, C.J., et al. (2016). Energy landscapes and functions of supramolecular systems. *Nat. Mater.* 15, 469–476.
- Whitesides, G.M., and Grzybowski, B. (2002). Self-assembly at all scales. *Science* 295, 2418–2421.
- Lancia, F., Ryabchun, A., and Katsonis, N. (2019). Life-like motion driven by artificial molecular machines. *Nat. Rev. Chem.* 3, 536–551.
- Needleman, D., and Dogic, Z. (2017). Active matter at the interface between materials science and cell biology. *Nat. Rev. Mater.* 2, 17048.
- Pollard, T.D., Blanchoin, L., and Mullins, R.D. (2000). Molecular mechanisms controlling actin filament dynamics in nonmuscle cells. *Annu. Rev. Biophys. Biomol. Struct.* 29, 545–576.
- Hennessey, E.S., Drummond, D.R., and Sparrow, J.C. (1993). Molecular Genetics of actin function. *Biochem. J.* 291, 657–671.
- Pantaloni, D., Le Clairinche, C., and Carlier, M.F. (2001). Mechanism of actin-based motility. *Science* 292, 1502–1506.
- Merindol, R., and Walther, A. (2017). Materials learning from life: concepts for active, adaptive and autonomous molecular systems. *Chem. Soc. Rev.* 46, 5588–5619.
- Rieß, B., and Boekhoven, J. (2018). Applications of dissipative supramolecular materials with a tunable lifetime. *ChemNanoMat* 4, 710–719.

39. Klajn, R., Wesson, P.J., Bishop, K.J., and Grzybowski, B.A. (2009). Writing self-erasing images using metastable nanoparticle "inks". *Angew. Chem. Int. Ed. Engl.* 48, 7035–7039.
40. Boekhoven, J., Hendriksen, W.E., Koper, G.J., Eelkema, R., and van Esch, J.H. (2015). Transient assembly of active materials fueled by a chemical reaction. *Science* 349, 1075–1079.
41. Boekhoven, J., Brizard, A.M., Kowligi, K.N., Koper, G.J., Eelkema, R., and van Esch, J.H. (2010). Dissipative self-assembly of a molecular gelator by using a chemical fuel. *Angew. Chem. Int. Ed. Engl.* 49, 4825–4828.
42. Tena-Solsona, M., Wanzke, C., Riess, B., Bausch, A.R., and Boekhoven, J. (2018). Self-selection of dissipative assemblies driven by primitive chemical reaction networks. *Nat. Commun.* 9, 2044.
43. Rieß, B., Wanzke, C., Tena-Solsona, M., Grötsch, R.K., Maity, C., and Boekhoven, J. (2018). Dissipative assemblies that inhibit their deactivation. *Soft Matter* 14, 4852–4859.
44. Tena-Solsona, M., Rieß, B., Grötsch, R.K., Löhrer, F.C., Wanzke, C., Käs Dorf, B., Bausch, A.R., Müller-Buschbaum, P., Lielie, O., and Boekhoven, J. (2017). Non-equilibrium dissipative supramolecular materials with a tunable lifetime. *Nat. Commun.* 8, 15895.
45. Kariyawasam, L.S., and Hartley, C.S. (2017). Dissipative assembly of aqueous carboxylic acid anhydrides fueled by carbodiimides. *J. Am. Chem. Soc.* 139, 11949–11955.
46. Kariyawasam, L.K.J., Jiang, R., Sommer, A., and Hartley, S. (2019). Structure–property effects in the generation of transient aqueous benzoic acid anhydrides by carbodiimide fuels. *ChemRxiv*. <https://doi.org/10.26434/chemrxiv.9941627>.
47. Grötsch, R.K., Wanzke, C., Speckbacher, M., Angi, A., Rieger, B., and Boekhoven, J. (2019). Pathway dependence in the fuel-driven dissipative self-assembly of nanoparticles. *J. Am. Chem. Soc.* 141, 9872–9878.
48. Grötsch, R.K., Angi, A., Mideksa, Y.G., Wanzke, C., Tena-Solsona, M., Feige, M.J., Rieger, B., and Boekhoven, J. (2018). Dissipative self-assembly of photoluminescent silicon nanocrystals. *Angew. Chem. Int. Ed. Engl.* 57, 14608–14612.
49. Bal, S., Das, K., Ahmed, S., and Das, D. (2019). Chemically fueled dissipative self-assembly that exploits cooperative catalysis. *Angew. Chem.* 131, 250–253.
50. Sorrenti, A., Leira-Iglesias, J., Sato, A., and Hermans, T.M. (2017). Non-equilibrium steady states in supramolecular polymerization. *Nat. Commun.* 8, 15899.
51. Leira-Iglesias, J., Tassoni, A., Adachi, T., Stich, M., and Hermans, T.M. (2018). Oscillations, travelling fronts and patterns in a supramolecular system. *Nat. Nanotechnol.* 13, 1021–1027.
52. Rakotonradany, F., Whitehead, M.A., Lebuis, A.M., and Sleiman, H.F. (2003). Photoresponsive supramolecular systems: self-assembly of azobenzonic acid linear tapes and cyclic tetramers. *Chemistry* 9, 4771–4780.
53. Prasad, S.K., Nair, G.G., and Hegde, G. (2005). Dynamic self-assembly of the liquid-crystalline smectic A phase. *Adv. Mater.* 17, 2086–2091.
54. Ikegami, T., Kageyama, Y., Obara, K., and Takeda, S. (2016). Dissipative and autonomous square-wave self-oscillation of a macroscopic hybrid self-assembly under continuous light irradiation. *Angew. Chem. Int. Ed. Engl.* 55, 8239–8243.
55. Geng, S., Wang, Y., Wang, L., Kouyama, T., Gotoh, T., Wada, S., and Wang, J.Y. (2017). A light-responsive self-assembly formed by a cationic azobenzene derivative and SDS as a drug delivery system. *Sci. Rep.* 7, 39202.
56. de Jong, J.J., Hania, P.R., Pugzlys, A., Lucas, L.N., de Loos, M., Kellogg, R.M., Feringa, B.L., Duppen, K., and van Esch, J.H. (2005). Light-driven dynamic pattern formation. *Angew. Chem. Int. Ed. Engl.* 44, 2373–2376.
57. de Jong, J.J., Lucas, L.N., Kellogg, R.M., van Esch, J.H., and Feringa, B.L. (2004). Reversible optical transcription of supramolecular chirality into molecular chirality. *Science* 304, 278–281.
58. Pu, S.-Z., Sun, Q., Fan, C.-B., Wang, R.-J., and Liu, G. (2016). Recent advances in diarylethene-based multi-responsive molecular switches. *J. Mater. Chem. C* 4, 3075–3093.
59. Morrow, S.M., Colomer, I., and Fletcher, S.P. (2019). A chemically fuelled self-replicator. *Nat. Commun.* 10, 1011.
60. Ghosh, A., Haverick, M., Stump, K., Yang, X., Tweedle, M.F., and Goldberger, J.E. (2012). Fine-tuning the pH trigger of self-assembly. *J. Am. Chem. Soc.* 134, 3647–3650.
61. Grzelczak, M., Liz-Marzán, L.M., and Klajn, R. (2019). Stimuli-responsive self-assembly of nanoparticles. *Chem. Soc. Rev.* 48, 1342–1361.
62. Kakuta, T., Yamagishi, T.A., and Ogoshi, T. (2018). Stimuli-responsive supramolecular assemblies constructed from Pillar[n]arenes. *Acc. Chem. Res.* 51, 1656–1666.
63. Kundu, P.K., Samanta, D., Leizrowice, R., Margulis, B., Zhao, H., Börner, M., Udayabhaskararao, T., Manna, D., and Klajn, R. (2015). Light-controlled self-assembly of non-photoresponsive nanoparticles. *Nat. Chem.* 7, 646–652.
64. Heuser, T., Weyand, E., and Walther, A. (2015). Biocatalytic feedback-driven temporal programming of self-regulating peptide hydrogels. *Angew. Chem. Int. Ed. Engl.* 54, 13258–13262.
65. Heinen, L., and Walther, A. (2017). Temporal control of i-motif switch lifetimes for autonomous operation of transient DNA nanostructures. *Chem. Sci.* 8, 4100–4107.
66. Menger, F.M., and Caran, K.L. (2000). Anatomy of a gel. Amino acid derivatives that rigidify water at submillimolar concentrations. *J. Am. Chem. Soc.* 122, 11679–11691.
67. Smith, A.M., Williams, R.J., Tang, C., Coppo, P., Collins, R.F., Turner, M.L., Saiani, A., Uljin, R.V., and Self, F.-D. (2008). Assembles to a hydrogel via a novel architecture based on  $\pi$ - $\pi$  interlocked  $\beta$ -sheets. *Adv. Mater.* 20, 37–41.
68. Jayawarna, V., Ali, M., Jowitt, T.A., Miller, A.F., Saiani, A., Gough, J.E., and Uljin, R.V. (2006). Nanostructured hydrogels for three-dimensional cell culture through self-assembly of fluorenylmethoxycarbonyl-dipeptides. *Adv. Mater.* 18, 611–614.
69. Leira-Iglesias, J., Sorrenti, A., Sato, A., Dunne, P.A., and Hermans, T.M. (2016). Supramolecular pathway selection of perylene diimides mediated by chemical fuels. *Chem. Commun. (Camb.)* 52, 9009–9012.
70. Hao, X., Chen, L., Sang, W., and Yan, Q. (2018). Periodically self-pulsating microcapsule as programmed microseparator via ATP-regulated energy dissipation. *Adv. Sci.* 5, 1700591.
71. Zhang, B., Jayalath, I.M., Ke, J., Sparks, J.L., Hartley, C.S., and Konkolewicz, D. (2019). Chemically fueled covalent crosslinking of polymer materials. *Chem. Commun. (Camb.)* 55, 2086–2089.
72. Maiti, S., Fortunati, I., Ferrante, C., Scrimin, P., and Prins, L.J. (2016). Dissipative self-assembly of vesicular nanoreactors. *Nat. Chem.* 8, 725–731.
73. Debnath, S., Roy, S., and Uljin, R.V. (2013). Peptide nanofibers with dynamic instability through nonequilibrium biocatalytic assembly. *J. Am. Chem. Soc.* 135, 16789–16792.
74. Pappas, C.G., Sasselli, I.R., and Uljin, R.V. (2015). Biocatalytic pathway selection in transient tripeptide nanostructures. *Angew. Chem. Int. Ed. Engl.* 54, 8119–8123.
75. Draper, E.R., Eden, E.G., McDonald, T.O., and Adams, D.J. (2015). Spatially resolved multicomponent gels. *Nat. Chem.* 7, 848–852.
76. Ogawa, Y., Yoshiyama, C., and Kitaoka, T. (2012). Helical assembly of azobenzene-conjugated carbohydrate hydrogelators with specific affinity for lectins. *Langmuir* 28, 4404–4412.
77. Frey, J.W., Méndez-Ardoy, A., Kwangmettata, S., Boichchio, D., Matt, B., Stuart, M.C.A., Huskens, J., Katsonis, N., Pavan, G.M., and Kudernac, T. (2017). Molecular photoswitches mediating the strain-driven disassembly of supramolecular tubules. *Proc. Natl. Acad. Sci. USA* 114, 11850–11855.
78. Ryabchun, A., Li, Q., Lancia, F., Aprahamian, I., and Katsonis, N. (2019). Shape-persistent actuators from hydrazone photoswitches. *J. Am. Chem. Soc.* 141, 1196–1200.
79. Jalani, K., Dhiman, S., Jain, A., and George, S.J. (2017). Temporal switching of an amphiphilic self-assembly by a chemical fuel-driven conformational response. *Chem. Sci.* 8, 6030–6036.
80. Gokel, G.W., Cram, D.J., Liotta, C.L., Harris, H.P., and Cook, F.L. (1974). Preparation and purification of 18-crown-6[1,4,7,10,13,16-hexaoxacyclooctadecane]. *J. Org. Chem.* 39, 2445–2446.
81. Frensdorff, H.K. (1971). Stability constants of cyclic polyether complexes with univalent cations. *J. Am. Chem. Soc.* 93, 600–606.
82. Vantomme, G., and Meijer, E.W. (2019). The construction of supramolecular systems. *Science* 363, 1396–1397.



83. Mattia, E., and Otto, S. (2015). Supramolecular systems chemistry. *Nat. Nanotechnol.* *10*, 111–119.
84. Carnall, J.M., Waudby, C.A., Belenguer, A.M., Stuart, M.C., Peyralans, J.J., and Otto, S. (2010). Mechanosensitive self-replication driven by self-organization. *Science* *327*, 1502–1506.
85. Altay, Y., Tezcan, M., and Otto, S. (2017). Emergence of a new self-replicator from a dynamic combinatorial library requires a specific pre-existing replicator. *J. Am. Chem. Soc.* *139*, 13612–13615.
86. Altay, M., Altay, Y., and Otto, S. (2018). Parasitic behavior of self-replicating molecules. *Angew. Chem. Int. Ed. Engl.* *57*, 10564–10568.
87. Wu, K.T., Hishamunda, J.B., Chen, D.T., DeCamp, S.J., Chang, Y.W., Fernández-Nieves, A., Fraden, S., and Dogic, Z. (2017). Transition from turbulent to coherent flows in confined three-dimensional active fluids. *Science* *355*, eaal1979.
88. Jia, Y., and Li, J. (2019). Molecular assembly of rotary and linear motor proteins. *Acc. Chem. Res.* *52*, 1623–1631.
89. Keber, F.C., Loiseau, E., Sanchez, T., DeCamp, S.J., Giomi, L., Bowick, M.J., Marchetti, M.C., Dogic, Z., and Bausch, A.R. (2014). Topology and dynamics of active nematic vesicles. *Science* *345*, 1135–1139.
90. Zwicker, D., Seyboldt, R., Weber, C.A., Hyman, A.A., and Jülicher, F. (2017). Growth and division of active droplets provides a model for protocells. *Nat. Phys.* *13*, 408–413.
91. Dambeniaks, A.K., Vu, P.H.Q., and Fyles, T.M. (2014). Dissipative assembly of a membrane transport system. *Chem. Sci.* *5*, 3396–3403.

## 8. Acknowledgments

First, I want to thank Prof. Job Boekhoven for giving me the opportunity to work in his lab and on such a fascinating topic. I really enjoyed working on the topic of dissipative supramolecular chemistry and learned a lot of new techniques and skills. I started the thesis with a quote from Ben Feringa: "Universities should be playgrounds" and I think that is what Job established here, a playground for his coworkers. Job's door was always open, and he gave me the freedom to develop new ideas and also helped me with all kinds of topics, from scientific discussions to bikes. Thank you!

Next, I want to thank Marta and Raphael for accepting me in your small group. The two already did a great job in setting up the lab. Marta did a great job as postdoc and I really enjoyed working with you! Raphael, it was a pleasure to share a lab with you. It was fun working, party and shooting pipette tips or nerf darts through the lab with you! After Raphael left the group, the "BoekhovenRacing Team" has just two members, and now just Job is left. I hope that somebody is following Raphael's and my spirit and takes the bike to work! Besides Marta and Raphael, Caren is one of the old guys in the BoekhovenLab. Thank you for going on conferences, your scientific inputs, and Schafkopf skills.

Also, I want to thank Carsten Troll, who always helped us out with every technical problem we had.

Now it is time for the new generation to take over and show what they have learned from the old guys or not. I am sure they, Schnitti, Patrick aka Fetti 2, Carsten, Kun what Dai, Michi, Laura, Alexander, Jennifer, Xiaoyao, Brigitte, Christine, Spabi, Michele, will do a great job (the order does not mean anything, or does it?).

I also want to thank my interns, Sebastian, Laura, Erika, Christine, Steffen, for her interest in supramolecular chemistry and helping me on various projects. What can I do more than pressing ok?!? Hope you learned more than that.

Thanks to the Canadian guys, especially Any & Chris, who joined the group and brought new ideas and concepts to the group. It was a pleasure having you here. I

also wanted to thank Prof. Mathias Feige, for letting me use his fluorescence microscope for hours and hours. Unfortunately, we had to end the project without any paper of nice moving droplets.

I also want to thank the Mittagsbiter for checking out different food locations at the campus and talk a science and bullshit.

Thanks to Max and Leo for joining me last summer on an awesome bike trip to France. Am Ende möchte ich meinen Eltern, Gudrun und Georg, danken, ohne sie wäre ein das alles nicht möglich gewesen. Danke, dass ihr mir in jeder Lebenslage den Rücken gestärkt habt. Auch meinem Bruder Simon möchte ich danken für seine Unterstützung, den nötigen Ausgleich oder die ein andere Diskussion über vegane Ernährung, die vielleicht doch irgendwo zu diesem Schritt hin zum Veganer beigetragen haben.

Marie, danke dass es dich gibt. Und du mich so akzeptierst und liebst wie ich bin, egal ob ich gestresst, müde oder genervt von der Arbeit war oder ich wieder mit dem Fahrrad irgendwo hinfahren will. Du bist immer für mich da. Mau!



## 9. References

1. D. B. Amabilino; D. K. Smith; J. W. Steed, Supramolecular Materials. *Chem. Soc. Rev.* **2017**, *46* (9), 2404-2420.
2. R. K. Grötsch; J. Boekhoven, Unique Properties of Supramolecular Biomaterials through Nonequilibrium Self-Assembly. In *Self-Assembling Biomaterials*, Helena S., A.; Ricardo M. P., d. S., Eds. Woodhead Publishing: 2018; pp 235-250.
3. A. Sorrenti; J. Leira-Iglesias; A. J. Markvoort; T. F. A. de Greef; T. M. Hermans, Non-Equilibrium Supramolecular Polymerization. *Chem. Soc. Rev.* **2017**, *46* (18), 5476-5490.
4. S. A. P. van Rossum; M. Tena-Solsona; J. H. van Esch; R. Eelkema; J. Boekhoven, Dissipative out-of-Equilibrium Assembly of Man-Made Supramolecular Materials. *Chem. Soc. Rev.* **2017**, *46* (18), 5519-5535.
5. J. D. Hartgerink; E. Beniash; S. I. Stupp, Self-Assembly and Mineralization of Peptide-Amphiphile Nanofibers. *Science* **2001**, *294* (5547), 1684-8.
6. T. Kitamura; S. Nakaso; N. Mizoshita; Y. Tochigi; T. Shimomura; M. Moriyama; K. Ito; T. Kato, Electroactive Supramolecular Self-Assembled Fibers Comprised of Doped Tetrathiafulvalene-Based Gelators. *J. Am. Chem. Soc.* **2005**, *127* (42), 14769-75.
7. T. Scheibel; R. Parthasarathy; G. Sawicki; X. M. Lin; H. Jaeger; S. L. Lindquist, Conducting Nanowires Built by Controlled Self-Assembly of Amyloid Fibers and Selective Metal Deposition. *Proc Natl Acad Sci U S A* **2003**, *100* (8), 4527-32.
8. P. A. Korevaar; S. J. George; A. J. Markvoort; M. M. Smulders; P. A. Hilbers; A. P. Schenning; T. F. De Greef; E. W. Meijer, Pathway Complexity in Supramolecular Polymerization. *Nature* **2012**, *481* (7382), 492-6.
9. S. Vauthey; S. Santoso; H. Gong; N. Watson; S. Zhang, Molecular Self-Assembly of Surfactant-Like Peptides to Form Nanotubes and Nanovesicles. *Proc Natl Acad Sci U S A* **2002**, *99* (8), 5355-60.
10. M. R. Ghadiri; J. R. Granja; R. A. Milligan; D. E. McRee; N. Khazanovich, Self-Assembling Organic Nanotubes Based on a Cyclic Peptide Architecture. *Nature* **1993**, *366* (6453), 324-7.
11. D. Yan; Y. Zhou; J. Hou, Supramolecular Self-Assembly of Macroscopic Tubes. *Science* **2004**, *303* (5654), 65-7.

12. M. Reches; E. Gazit, Casting Metal Nanowires within Discrete Self-Assembled Peptide Nanotubes. *Science* **2003**, *300* (5619), 625-7.
13. U. Lewandowska; W. Zajaczkowski; S. Corra; J. Tanabe; R. Borrmann; E. M. Benetti; S. Stappert; K. Watanabe; N. A. K. Ochs; R. Schaeublin; C. Li; E. Yashima; W. Pisula; K. Mullen; H. Wennemers, A Triaxial Supramolecular Weave. *Nat Chem* **2017**, *9* (11), 1068-1072.
14. E. P. Holowka; D. J. Pochan; T. J. Deming, Charged Polypeptide Vesicles with Controllable Diameter. *J. Am. Chem. Soc.* **2005**, *127* (35), 12423-8.
15. A. Blanazs; S. P. Armes; A. J. Ryan, Self-Assembled Block Copolymer Aggregates: From Micelles to Vesicles and Their Biological Applications. *Macromol. Rapid Commun.* **2009**, *30* (4-5), 267-77.
16. Y. Kim; N. Tamaoki, A Photoresponsive Planar Chiral Azobenzene Dopant with High Helical Twisting Power. *J. Mater. Chem. C* **2014**, *2* (43), 9258-9264.
17. T. Hegmann; H. Qi; V. M. Marx, Nanoparticles in Liquid Crystals: Synthesis, Self-Assembly, Defect Formation and Potential Applications. *J. Inorg. Organomet. Polym.* **2007**, *17* (3), 483-508.
18. T. L. Greaves; C. J. Drummond, Ionic Liquids as Amphiphile Self-Assembly Media. *Chem. Soc. Rev.* **2008**, *37* (8), 1709-26.
19. M. E. McConney; M. Rumi; N. P. Godman; U. N. Tohgha; T. J. Bunning, Photoresponsive Structural Color in Liquid Crystalline Materials. *Adv Opt Mater* **2019**, *7* (16).
20. N. Grimaldi; F. Andrade; N. Segovia; L. Ferrer-Tasies; S. Sala; J. Veciana; N. Ventosa, Lipid-Based Nanovesicles for Nanomedicine. *Chem. Soc. Rev.* **2016**, *45* (23), 6520-6545.
21. R. Freeman; M. Han; Z. Alvarez; J. A. Lewis; J. R. Wester; N. Stephanopoulos; M. T. McClendon; C. Lynsky; J. M. Godbe; H. Sangji; E. Luijten; S. I. Stupp, Reversible Self-Assembly of Superstructured Networks. *Science* **2018**, *362* (6416), 808-813.
22. X. Du; J. Zhou; J. Shi; B. Xu, Supramolecular Hydrogelators and Hydrogels: From Soft Matter to Molecular Biomaterials. *Chem Rev* **2015**, *115* (24), 13165-307.
23. G. M. Whitesides; M. Boncheva, Beyond Molecules: Self-Assembly of Mesoscopic and Macroscopic Components. *Proc Natl Acad Sci U S A* **2002**, *99* (8), 4769-74.
24. F. Tantakitti; J. Boekhoven; X. Wang; R. V. Kazantsev; T. Yu; J. Li; E. Zhuang; R. Zandi; J. H. Ortony; C. J. Newcomb; L. C. Palmer; G. S. Shekhawat; M. O. de la Cruz;

- 
- G. C. Schatz; S. I. Stupp, Energy Landscapes and Functions of Supramolecular Systems. *Nat Mater* **2016**, 15 (4), 469-76.
25. T. Fukui; S. Kawai; S. Fujinuma; Y. Matsushita; T. Yasuda; T. Sakurai; S. Seki; M. Takeuchi; K. Sugiyasu, Control over Differentiation of a Metastable Supramolecular Assembly in One and Two Dimensions. *Nat Chem* **2017**, 9 (5), 493-499.
26. P. Jonkheijm; P. van der Schoot; A. P. Schenning; E. W. Meijer, Probing the Solvent-Assisted Nucleation Pathway in Chemical Self-Assembly. *Science* **2006**, 313 (5783), 80-3.
27. Y. Yan; J. Huang; B. Z. Tang, Kinetic Trapping - a Strategy for Directing the Self-Assembly of Unique Functional Nanostructures. *Chem Commun (Camb)* **2016**, 52 (80), 11870-84.
28. A. R. Hirst; S. Roy; M. Arora; A. K. Das; N. Hodson; P. Murray; S. Marshall; N. Javid; J. Sefcik; J. Boekhoven; J. H. van Esch; S. Santabarbara; N. T. Hunt; R. V. Ulijn, Biocatalytic Induction of Supramolecular Order. *Nat Chem* **2010**, 2 (12), 1089-94.
29. T. D. Pollard; L. Blanchoin; R. D. Mullins, Molecular Mechanisms Controlling Actin Filament Dynamics in Nonmuscle Cells. *Annu. Rev. Biophys. Biomol. Struct.* **2000**, 29, 545-76.
30. E. S. Hennessey; D. R. Drummond; J. C. Sparrow, Molecular Genetics of Actin Function. *Biochem J* **1993**, 291 ( Pt 3), 657-71.
31. L. Spinardi; W. Witke, Gelsolin and Diseases. *Subcell Biochem* **2007**, 45, 55-69.
32. S. De; R. Klajn, Dissipative Self-Assembly Driven by the Consumption of Chemical Fuels. *Adv. Mater.* **2018**, 30 (41), e1706750.
33. S. Dhiman; A. Sarkar; S. J. George, Bioinspired Temporal Supramolecular Polymerization. *RSC Advances* **2018**, 8 (34), 18913-18925.
34. G. Ragazzon; L. J. Prins, Energy Consumption in Chemical Fuel-Driven Self-Assembly. *Nat Nanotechnol* **2018**, 13 (10), 882-889.
35. G. J. M. Koper; J. Boekhoven; W. E. Hendriksen; J. H. van Esch; R. Eelkema; I. Pagonabarraga; J. M. Rubí; D. Bedeaux, The Lost Work in Dissipative Self-Assembly. *Int. J. Thermophys.* **2013**, 34 (7), 1229-1238.
36. E. Mattia; S. Otto, Supramolecular Systems Chemistry. *Nat Nanotechnol* **2015**, 10 (2), 111-9.
37. G. M. Cooper; R. E. Hausman, *The Cell: A Molecular Approach*. Sinauer Associates, Incorporated, Publishers: 2016.

- 
38. S. Roychowdhury; M. M. Rasenick, Tubulin-G Protein Association Stabilizes Gtp Binding and Activates Gtpase: Cytoskeletal Participation in Neuronal Signal Transduction. *Biochemistry* **1994**, 33 (32), 9800-5.
39. N. Singh; G. J. M. Formon; S. De Piccoli; T. M. Hermans, Devising Synthetic Reaction Cycles for Dissipative Nonequilibrium Self-Assembly. *Adv. Mater.* **2020**, e1906834.
40. M. Tena-Solsona; J. Boekhoven, Dissipative Self-Assembly of Peptides. *Isr. J. Chem.* **2019**, 59 (10), 898-905.
41. L. Heinen; A. Walther, Celebrating Soft Matter's 10th Anniversary: Approaches to Program the Time Domain of Self-Assemblies. *Soft Matter* **2015**, 11 (40), 7857-66.
42. R. Merindol; A. Walther, Materials Learning from Life: Concepts for Active, Adaptive and Autonomous Molecular Systems. *Chem. Soc. Rev.* **2017**, 46 (18), 5588-5619.
43. A. Walther, Viewpoint: From Responsive to Adaptive and Interactive Materials and Materials Systems: A Roadmap. *Adv. Mater.* **2019**, e1905111.
44. G. Wang; S. Liu, Strategies to Construct a Chemical-Fuel-Driven Self-Assembly. *ChemSystemsChem* **2020**.
45. J. Boekhoven; W. E. Hendriksen; G. J. Koper; R. Eelkema; J. H. van Esch, Transient Assembly of Active Materials Fueled by a Chemical Reaction. *Science* **2015**, 349 (6252), 1075-9.
46. J. Boekhoven; A. M. Brizard; K. N. Kowlgi; G. J. Koper; R. Eelkema; J. H. van Esch, Dissipative Self-Assembly of a Molecular Gelator by Using a Chemical Fuel. *Angew. Chem. Int. Ed. Engl.* **2010**, 49 (28), 4825-8.
47. The Nobel Prize in Chemistry 1997, Nobelprize.Org, Nobel Media Ab 2020. <https://www.nobelprize.org/prizes/chemistry/1997/9175-lifes-energy-currency-atp/> Accessed 10.04.2020.
48. A. J. B. Alberts, J. Lewis, et al., *Molecular Biology of the Cell Vol. 4*. Garland Science New York: 2002.
49. B. Rad; S. C. Kowalczykowski, Efficient Coupling of Atp Hydrolysis to Translocation by Recq Helicase. *Proc Natl Acad Sci U S A* **2012**, 109 (5), 1443-8.
50. K. Beginnen; G. Karp; S. Vogel; S. Kuhlmann-Krieg, *Molekulare Zellbiologie*. Springer Berlin Heidelberg: 2005.
51. M. Orlosky; H. O. Smith, Action of Atp-Dependent Dnase from Hemophilus Influenzae on Cross-Linked DNA Molecules. *J. Biol. Chem.* **1976**, 251 (19), 6117-21.

- 
52. A. Sorrenti; J. Leira-Iglesias; A. Sato; T. M. Hermans, Non-Equilibrium Steady States in Supramolecular Polymerization. *Nat Commun* **2017**, *8*, 15899.
53. J. Leira-Iglesias; A. Tassoni; T. Adachi; M. Stich; T. M. Hermans, Oscillations, Travelling Fronts and Patterns in a Supramolecular System. *Nat Nanotechnol* **2018**, *13* (11), 1021-1027.
54. S. M. Morrow; I. Colomer; S. P. Fletcher, A Chemically Fuelled Self-Replicator. *Nat Commun* **2019**, *10* (1), 1011.
55. F. Rakotondradany; M. A. Whitehead; A. M. Lehuis; H. F. Sleiman, Photoresponsive Supramolecular Systems: Self-Assembly of Azodibenzoic Acid Linear Tapes and Cyclic Tetramers. *Chemistry* **2003**, *9* (19), 4771-80.
56. S. K. Prasad; G. G. Nair; G. Hegde, Dynamic Self-Assembly of the Liquid-Crystalline Smectic a Phase. *Adv. Mater.* **2005**, *17* (17), 2086-2091.
57. T. Ikegami; Y. Kageyama; K. Obara; S. Takeda, Dissipative and Autonomous Square-Wave Self-Oscillation of a Macroscopic Hybrid Self-Assembly under Continuous Light Irradiation. *Angew. Chem. Int. Ed. Engl.* **2016**, *55* (29), 8239-43.
58. S. Geng; Y. Wang; L. Wang; T. Kouyama; T. Gotoh; S. Wada; J. Y. Wang, A Light-Responsive Self-Assembly Formed by a Cationic Azobenzene Derivative and Sds as a Drug Delivery System. *Sci Rep* **2017**, *7*, 39202.
59. T. Bian; Z. Chu; R. Klajn, The Many Ways to Assemble Nanoparticles Using Light. *Adv. Mater.* **2019**, e1905866.
60. K. Jalani; S. Dhiman; A. Jain; S. J. George, Temporal Switching of an Amphiphilic Self-Assembly by a Chemical Fuel-Driven Conformational Response. *Chem Sci* **2017**, *8* (9), 6030-6036.
61. A. Ryabchun; Q. Li; F. Lancia; I. Aprahamian; N. Katsonis, Shape-Persistent Actuators from Hydrazone Photoswitches. *J. Am. Chem. Soc.* **2019**, *141* (3), 1196-1200.
62. J. J. de Jong; P. R. Hania; A. Pugzlys; L. N. Lucas; M. de Loos; R. M. Kellogg; B. L. Feringa; K. Duppen; J. H. van Esch, Light-Driven Dynamic Pattern Formation. *Angew. Chem. Int. Ed. Engl.* **2005**, *44* (16), 2373-6.
63. J. J. de Jong; L. N. Lucas; R. M. Kellogg; J. H. van Esch; B. L. Feringa, Reversible Optical Transcription of Supramolecular Chirality into Molecular Chirality. *Science* **2004**, *304* (5668), 278-81.

- 
64. S.-Z. Pu; Q. Sun; C.-B. Fan; R.-J. Wang; G. Liu, Recent Advances in Diarylethene-Based Multi-Responsive Molecular Switches. *J. Mater. Chem. C* **2016**, *4* (15), 3075-3093.
65. W. Hordijk, Evolution of Autocatalytic Sets in Computational Models of Chemical Reaction Networks. *Orig Life Evol Biosph* **2016**, *46* (2-3), 233-45.
66. M. D. Bajczyk; P. Dittwald; A. Wołos; S. Szymkuć; B. A. Grzybowski, Discovery and Enumeration of Organic-Chemical and Biomimetic Reaction Cycles within the Network of Chemistry. *Angew. Chem.* **2018**, *130* (9), 2391-2395.
67. D. Zwicker; R. Seyboldt; C. A. Weber; A. A. Hyman; F. Jülicher, Growth and Division of Active Droplets Provides a Model for Protocells. *Nature Physics* **2016**, *13* (4), 408-413.
68. A. Ghosh; M. Haverick; K. Stump; X. Yang; M. F. Tweedle; J. E. Goldberger, Fine-Tuning the Ph Trigger of Self-Assembly. *J. Am. Chem. Soc.* **2012**, *134* (8), 3647-50.
69. M. Grzelczak; L. M. Liz-Marzan; R. Klajn, Stimuli-Responsive Self-Assembly of Nanoparticles. *Chem. Soc. Rev.* **2019**, *48* (5), 1342-1361.
70. T. Kakuta; T. A. Yamagishi; T. Ogoshi, Stimuli-Responsive Supramolecular Assemblies Constructed from Pillar[*N*]Arenes. *Acc. Chem. Res.* **2018**, *51* (7), 1656-1666.
71. P. K. Kundu; D. Samanta; R. Leizrowice; B. Margulis; H. Zhao; M. Borner; T. Udayabhaskararao; D. Manna; R. Klajn, Light-Controlled Self-Assembly of Non-Photoresponsive Nanoparticles. *Nat Chem* **2015**, *7* (8), 646-52.
72. T. Heuser; E. Weyandt; A. Walther, Biocatalytic Feedback-Driven Temporal Programming of Self-Regulating Peptide Hydrogels. *Angew. Chem. Int. Ed.* **2015**, *54* (45), 13258-62.
73. L. Heinen; A. Walther, Temporal Control of I-Motif Switch Lifetimes for Autonomous Operation of Transient DNA Nanostructures. *Chem Sci* **2017**, *8* (5), 4100-4107.
74. F. M. Menger; K. L. Caran, Anatomy of a Gel. Amino Acid Derivatives That Rigidify Water at Submillimolar Concentrations. *J. Am. Chem. Soc.* **2000**, *122* (47), 11679-11691.
75. J. Leira-Iglesias; A. Sorrenti; A. Sato; P. A. Dunne; T. M. Hermans, Supramolecular Pathway Selection of Perylenediimides Mediated by Chemical Fuels. *Chem Commun (Camb)* **2016**, *52* (58), 9009-12.

76. X. Hao; L. Chen; W. Sang; Q. Yan, Periodically Self-Pulsating Microcapsule as Programmed Microseparator Via Atp-Regulated Energy Dissipation. *Adv Sci (Weinh)* **2018**, 5 (3), 1700591.
77. B. Zhang; I. M. Jayalath; J. Ke; J. L. Sparks; C. S. Hartley; D. Konkolewicz, Chemically Fueled Covalent Crosslinking of Polymer Materials. *Chem Commun (Camb)* **2019**, 55 (14), 2086-2089.
78. J. Deng; D. Bezold; H. Jessen; A. Walther, Multiple Light Control Mechanisms in Atp-Fueled Non-Equilibrium DNA Systems. *Angew. Chem. Int. Ed.* **2020**.
79. C. G. Pappas; I. R. Sasselli; R. V. Ulijn, Biocatalytic Pathway Selection in Transient Tripeptide Nanostructures. *Angew. Chem. Int. Ed.* **2015**, 54 (28), 8119-23.
80. S. Debnath; S. Roy; R. V. Ulijn, Peptide Nanofibers with Dynamic Instability through Nonequilibrium Biocatalytic Assembly. *J. Am. Chem. Soc.* **2013**, 135 (45), 16789-92.
81. S. Espinoza-Sanchez; L. A. Metskas; S. Z. Chou; E. Rhoades; T. D. Pollard, Conformational Changes in Arp2/3 Complex Induced by Atp, Wasp-Vca, and Actin Filaments. *Proc Natl Acad Sci U S A* **2018**, 115 (37), E8642-E8651.
82. E. R. Draper; E. G. Eden; T. O. McDonald; D. J. Adams, Spatially Resolved Multicomponent Gels. *Nat Chem* **2015**, 7 (10), 848-52.
83. Y. Ogawa; C. Yoshiyama; T. Kitaoka, Helical Assembly of Azobenzene-Conjugated Carbohydrate Hydrogelators with Specific Affinity for Lectins. *Langmuir* **2012**, 28 (9), 4404-12.
84. J. W. Freedy; A. Mendez-Ardoy; S. Kwangmettata; D. Bochicchio; B. Matt; M. C. A. Stuart; J. Huskens; N. Katsonis; G. M. Pavan; T. Kudernac, Molecular Photoswitches Mediating the Strain-Driven Disassembly of Supramolecular Tubules. *Proc Natl Acad Sci U S A* **2017**, 114 (45), 11850-11855.
85. L. S. Kariyawasam; C. S. Hartley, Dissipative Assembly of Aqueous Carboxylic Acid Anhydrides Fueled by Carbodiimides. *J. Am. Chem. Soc.* **2017**, 139 (34), 11949-11955.
86. G. W. Gokel; D. J. Cram; C. L. Liotta; H. P. Harris; F. L. Cook, Preparation and Purification of 18-Crown-6[1,4,7,10,13,16-Hexaoxacyclooctadecane]. *J. Org. Chem.* **1974**, 39 (16), 2445-2446.
87. H. K. Frensdorff, Stability Constants of Cyclic Polyether Complexes with Univalent Cations. *J. Am. Chem. Soc.* **1971**, 93 (3), 600-606.

- 
88. R. Klajn; P. J. Wesson; K. J. Bishop; B. A. Grzybowski, Writing Self-Erasing Images Using Metastable Nanoparticle "Inks". *Angew. Chem. Int. Ed. Engl.* **2009**, *48* (38), 7035-9.
89. M. Fialkowski; K. J. Bishop; R. Klajn; S. K. Smoukov; C. J. Campbell; B. A. Grzybowski, Principles and Implementations of Dissipative (Dynamic) Self-Assembly. *J. Phys. Chem. B* **2006**, *110* (6), 2482-96.
90. H. Hess; J. L. Ross, Non-Equilibrium Assembly of Microtubules: From Molecules to Autonomous Chemical Robots. *Chem. Soc. Rev.* **2017**, *46* (18), 5570-5587.
91. J. M. Carnall; C. A. Waudby; A. M. Belenguer; M. C. Stuart; J. J. Peyralans; S. Otto, Mechanosensitive Self-Replication Driven by Self-Organization. *Science* **2010**, *327* (5972), 1502-6.
92. M. Tena-Solsona; C. Wanzke; B. Riess; A. R. Bausch; J. Boekhoven, Self-Selection of Dissipative Assemblies Driven by Primitive Chemical Reaction Networks. *Nat Commun* **2018**, *9* (1), 2044.
93. K. T. Wu; J. B. Hishamunda; D. T. Chen; S. J. DeCamp; Y. W. Chang; A. Fernandez-Nieves; S. Fraden; Z. Dogic, Transition from Turbulent to Coherent Flows in Confined Three-Dimensional Active Fluids. *Science* **2017**, *355* (6331).
94. Y. Jia; J. Li, Molecular Assembly of Rotary and Linear Motor Proteins. *Acc. Chem. Res.* **2019**, *52* (6), 1623-1631.
95. Y. Altay; M. Tezcan; S. Otto, Emergence of a New Self-Replicator from a Dynamic Combinatorial Library Requires a Specific Pre-Existing Replicator. *J. Am. Chem. Soc.* **2017**, *139* (39), 13612-13615.
96. M. Altay; Y. Altay; S. Otto, Parasitic Behavior of Self-Replicating Molecules. *Angew. Chem. Int. Ed. Engl.* **2018**, *57* (33), 10564-10568.
97. F. C. Keber; E. Loiseau; T. Sanchez; S. J. DeCamp; L. Giomi; M. J. Bowick; M. C. Marchetti; Z. Dogic; A. R. Bausch, Topology and Dynamics of Active Nematic Vesicles. *Science* **2014**, *345* (6201), 1135-9.